TABLE OF CONTENTS

List of Figures

List of Tables

1.0 INTRODUCTION

In the physical processing stage of material recovery from end-of-life printed circuit boards (eol PCB), metallic and non-metallic values on the boards are separated into different materials fractions through a series of stage-wise comminution-separations. Various separation technologies are employed in processing the diverse mixture of materials that the comminution operations produce at different stages. These include magnetic separation, eddy current separation, electrostatic separation, air tables, gravity air classifiers, air cyclones and shape screens, among others (Goosey and Kellner, 2003; Li *et al.*, 2004; Kang and Schoenung, 2005; Hamos GmbH).

As expected, each separation operation gives optimum efficiencies at specific size ranges. At smaller sizes, below 2mm, electrostatic separation has been mostly applied for copper recovery from the grinding mix (Zhang and Forssberg, 1997; Iuga *et al.*, 1998; Li *et al*, 2004, Hamos GmbH; Kang and Schoenung, 2005). From classical mineral processing, application of electrostatic separation is known to give poor separation efficiencies at −100 µm fine sizes (Wills, 1997). Zhao *et al*. (2004) demonstrated the application of a type of column air separator compared to an electrostatic separator. For the −75 µm fractions, copper recoveries of 27.83 % at a grade of 26.8 % were obtained from the pneumatic separator while separation from the electrostatics at that size was declared poor and not reported. The low recovery implies valuable metal loss at this size range, while such poor grade implies product contamination, thereby complicating the finishing recovery processes. Overall improvement to the physical processing stage, in order to produce cleaner fractions, has been emphasized (Goosey and Kellner, 2003).

In the cited instance (Zhao *et al*., 2004), more than 20 % of the product of the hammer mill grinding from 30 mm feed top size reported to the -75 µm fraction, assaying almost 2.9 % copper. Less than half copper recovery from this fraction implies that more than 0.29 % of the total grinding product by weight, ~2.9 kg/ton of copper, will be lost. In NEC corporation recycling operation, at -300 + 100 µm (Yokoyama and Iji, 1997; Iji and Yokoyama, 1997),

copper rich powder (82%Cu, at >90% recovery) was produced from the electrostatic separation, with the non-conducting fraction containing 64 % glass fibre, 34 % epoxy resin, 2.1 % Cu, and solders. Some end-use applications, such as filler for epoxy resin polymer products, were investigated for the glass fibre-resin fraction. However, at 2.1 % copper content, the fibre glass-resin non-conducting fraction assays higher than many natural porphyry copper deposits that are being mined and economically processed (Wills, 1997). It therefore deserves further beneficiation. Moreover, as precious metals are coated to a few microns in the printed circuit board (PCB) sockets and slots, and on the edge connectors, abrasion in the event of comminution is likely to make this precious metal report to this fine fraction also. With the poor separation efficiencies of electrostatic separation at -100 μm, these precious metal fraction will mostly report to the non-conducting fraction (Kelly and Spottiswood, 1989), representing a major loss to the economic drive of the whole operation. Traces of noble metal anti-etch materials used during the printed copper circuit production (Li *et al*., 2004) should also be present on the copper traces; copper particles not recovered carry such to waste. All these underscore the point that the fine fraction from PCB grinding presents the challenges of low separation efficiency and contamination of product fractions, while contributing a drop to the overall physical processing recovery relative to coarser size fractions.

The inefficiency of electrostatic separation in processing the fine fraction has been tolerated by recycling operations, possibly because of preference for keeping the operations dry. Wet processes are avoided in most recycling operations, to avoid wash water circuit and treatment costs, among other reasons (Kellerwessel, 1993). Given the diverse material make-up of printed circuit boards (PCB), chances of hazardous leaching during wet processing may also be contemplated. However, at this stage of PCB physical processing, the operation need not be restricted to dry. Wet processing, and especially froth flotation, appears very promising. Success in this direction can be a pointer to improved processing approach and overall improvement in PCB physical processing. Density-based applications for wet table and centrifugal separations have been reported (Galbraith and Devereux, 2002; Xuefeng *et al*., 2005). Froth flotation exploits distinct surface property of individual particles and it appears very promising for detailed investigation, more so that there has not been any effort to conduct empirical research into its applicability. Froth flotation is well explored in minerals and, to some extent, in waste processing. Outstanding features of froth flotation are its selectivity, flexibility, throughput and

handling of relatively fine sizes. These make it very relevant to this application. Froth flotation has been used for beneficiation of ore bearing native metals and oxides minerals, among others. Flotation of plastics has also been applied in municipal solid waste treatment (Shent *et al*., 1999; Alter, 2005). PCB fines consist of a mixture of metals, alloys, ceramics and plastics with distinct surface properties that should enable selective wetting and make froth flotation separation possible. This is a broad hypothesis upon which froth flotation can be expected to be applicable for the beneficiation of this material mixture. However, if co-occurrence of three minerals such as chalcopyrite, pyrite and galena is recognised as complex in conventional minerals processing (Wills, 1997), then this sample is really complex. It will present an interesting challenge to the versatility of flotation technique.

The general objective of this research is, therefore, to investigate froth flotation for beneficiation of this material mixture, with the aim of being able to conclude on the applicability. In this connection, characterisation relevant to flotation investigation of the sample will first have to be done. From the peculiarities of the sample based on the characterisation, along with general literature survey, and with pointers from trial investigations, logical flotation schemes will be drawn for the investigations. Toward these ends, a general background literature review is first presented. This is followed by a more focused literature-based discourse aimed at drawing the flotation schemes, and at stating more specific objectives, and approaches to, the investigation.

2.0 BACKGROUND – PCB PHYSICAL PROCESSING

2.1 INTRODUCTION

Physical processing is admitted to be the most environmentally-friendly approach among others such as pyrometallurgical and hydrometallurgical processes for materials recovery from end-of-life (eol) printed circuit boards (PCB), and general waste in electrical and electronic equipment (WEEE). Table 2.1 summarises the basics of the different techniques.

Table 2.1: A comparison of general e-waste treatment approaches

Treatment Approach	Operation	Merits	Demerits
Landfilling	Direct dumping of classified wastes in landfills	A means of disposal; at least removes physical junks	Leaching of hazardous constituents; wasteful disposal of otherwise huge material resources.
Hydro-metallurgy	A secondary processing, entailing leaching and winning.	Gives high purity product; can handle small tonnages of feed supply	Preconcentration is important on complexity of the leaching and winning. Treatment of secondary effluent streams
Pyro-metallurgy	Smelting in furnaces, giving three products: noble metals report to molten metal phase, metal with more stable oxides report to slag phase, while metals with high vapor pressure will be collected from the vapor phase. Each product further treated separately.	Little feed preparation: sizing, removal of hazardous components - mercury bearing, capacitors.	Require consistent high grade and quantity of feed; dedicated plant highly capital intensive; feasible where there are existing facilities which accepts e-waste as secondary feed materials; recovers zero value for plastic constituents; off-gas treatment; facilities not available in many parts of the world.
Physical Processing	Applied mineral processing: comminution and separation of constituent materials by exploring variations in physical properties.	Already relevant in feed preparation for hydro or pyro routes; handling of varying feed constituents; amenable for low or high scale operation; least impact on the environment.	Dust handling in aggressive grinding for total liberation; possible precious metal losses; noise; not very clean fractions.

Major demerits of the physical processing option include product fractions that remain largely unsorted to have best end-values as separate material fractions (Lee *et al.*, 2004). This makes pyrometallurgical follow-up processing indispensable and extensive (Lee *et al.*, 2004; Shuey, *et al.*, 2006). This points to the need for cleaner fractions from the physical processing stage.

A background review of PCB physical processing will help to place the various aspects of the operation into perspective. A characterisation to appraise the huge material resource and the diversity in the material stream will be informative. This is followed by a review of the physical processing operations in almost three decade of this endeavor. This will clarify how improvement in the beneficiation of the comminution fines can contribute to improving the operation.

2.2 PCB CHARACTERISATION

2.2.1 Occurrence and Reserve

Printed circuit board (PCBs) mechanically support and electrically connect electronic components by using conductive pathways, or traces, etched from copper sheets laminated onto a non-conductive substrate (Wikipedia). Alternative names are printed wiring board (PWB), etched wiring board (EWB). Populated PCBs have mounted components, while unpopulated ones comprise of only reinforced resin and printed copper wiring laminate. PCBs are found in almost all electronic applications, spanning personal computers, telecommunication equipment, hospital equipment, cellphones and various consumer electronics. Continuing and rapid advances in technological innovations result in a high rate of obsolescence of this equipment, leading to large tonnages of PCB going into the WEEE stream.

In the United States of America (USA), for personal computers (PC) alone, 63 million units was estimated to be obsolete in 2005 (Figure 2.1; Kang and Schoenung, 2005). At about 0.75 kg PCB per PC unit or 2.75 % by weight, and one PC unit with monitor weighing about 27.5kg (Shuey *et al.*, 2006), the huge tonnage of materials this translates to can be appreciated. In the UK, about 50 000 tons of waste PCBs are generated *per annum* (Goosey and Kellner, 2003). Of these, about 40 000 tons are populated PCBs, and 10 000 tons are unpopulated or associated boards

manufacturing scrap. The estimate for 2006 is 100500 tons (Shuey *et al.*, 2006). A year 2000 review in Taiwan claims about 300 000 scrap PC units *per annum* (Lee *et al.*, 2000), and this had risen to 700 000 by 2004 (Lee *et al.*, 2004). With generally few statistics for South Africa, more than 500 000 PC units are reported dumped per year. Intel South Africa, an original equipment manufacturer (OEM), has been in business for 35 years and has sold more than one billion CPUs. This implies a lot of PCs out somewhere (Mackay, 2004). Large undocumented accumulation, or scatters, of PCBs occur around the world, much due to shipment of used PC to developing countries. A 2005 British Broadcasting Corporation (BBC) report, focused on Nigeria, claimed that about 400 000 used computers are imported to Nigeria monthly. Almost 75 % of these cannot be used, cannot be repaired economically or resold. The situation is typical of many developing countries (Laurie, 2005).

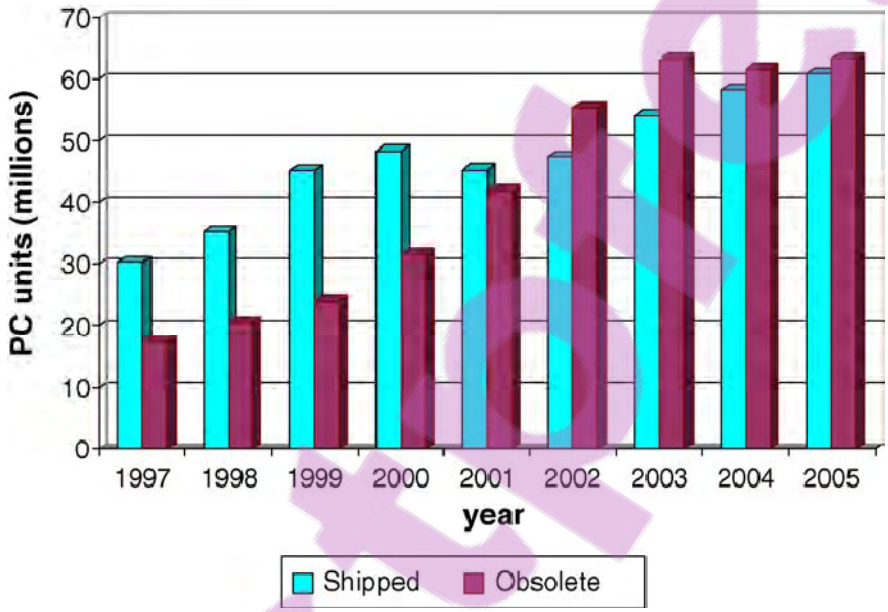

Figure 2.1: Personal computer shipments and obsolescence in the United States (Kang and Schoenung, 2005)

Taking PCBs as a highly valuable polymetallic resource, the foregoing has been an attempt to present its occurrence and 'reserve'. Recognizing the material values it contains (see Section 2.2.3), eol PCB stream can be referred to as a type of ore, rather than a waste stream. Though not containing specific minerals with definite chemical composition, according to the classical

definition of an ore, the stream contains many of the metallic elements in the periodic table, in proportions greater than many natural deposits of such metals. It therefore deserves better recognition as a resource stock. PCB processing yields concentrates that feed into metal production, just like run-of-mines. On this basis, PCBs and other end-of-life electronic equipment can regarded as a type ore – industrial ores (Castro *et al.*, 2005). This distinguishes PCBs from natural ore from the mine, because this material stream is from the industry after a service life. In the broad view of cyclic material use, WEEE is essentially a transit title.

2.2.2 PCB Structure

PCB structures have varied with technological advances over time. Earlier boards were single-sided with large components on one side of the board and the soldering for mechanical support on the order side. Etched copper wiring makes electrical connections from the soldering side (see Figure 2.2). All the components had terminals dipping through the board. The top side and the bottom side were therefore referred to as the component side and the solder side, respectively (Holm, 2001). This type of boards was used in very primitive circuits.

Figure 2.2: Single sided boards

Double-sided boards are more recent boards having conductor patterns on both sides of the board with interconnecting electrical 'bridges' called vias. Vias (singular: via) are holes in the PCB that are filled or plated with metal and touch the conductor pattern on both sides. Since the surface available for the conductor pattern is twice as large compared to single-side boards, and wiring can now cross the sides, double-sided PCBs are for more complex circuits than the single-sided ones: the wiring is thinner and much denser, and the components are usually surface-mounted chips without leads (see Figure 2.3).

Figure 2.3: Double-sided PCBs – top (left) and bottom (right) views

Multilayered boards are developments on the double-sided boards and are formed by bonding together separately etched thin boards such that these boards have trace (wiring) layers inside the compact board. Two, four, eight, twelve and sixteen layers boards have been produced (Vinod and Sanjay, 2005; Wikipedia). The conducting traces are connected through vias. Either the holes are electroplated or small rivets are inserted. Such high-density PCBs have blind vias, which are visible only on one surface, or buried vias, connecting the interlayer, and so not visible on either surfaces. In 2005, multilayered boards accounted for about 20 % of total PCB production (Vinod and Sanjay, 2005), and manufacturers are confident this will become the dominant type of board. Rigid flex and flexible printed circuits are other types of boards found in specialised applications like printers and communication equipment.

Sockets and edge connectors are common features on the PCBs. The sockets serve to connect removable components such as memory units to the PCB. Figure 2.4 shows a zero insertion force (ZIF) socket for mounting a processor. Edge connectors, consisting of small uncovered pads of copper located along one side of the PCB (see Figure 2.4), are used to connect the circuit on one board to another board (for example, sound or graphic card to the motherboard). Edge connectors and sockets are usually plated with precious metals to ensure least junction resistance.

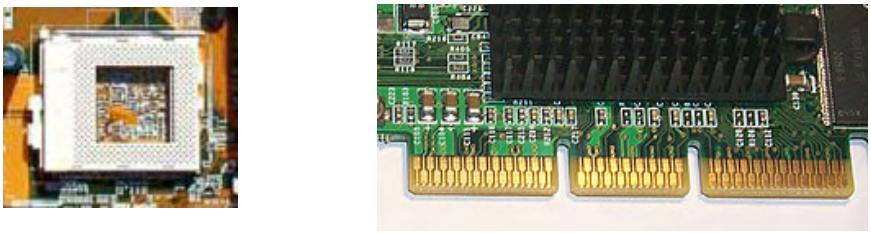

Figure 2.4: ZIF socket (left) and edge connector (right)

2.2.3 PCB Material Make-Up

The materials make-up of PCB is very diverse. Populated PCBs are reported to contain most of the elements in the periodic table (Li *et al.*, 2004). Unpopulated boards consists of conducting copper traces and non-conducting substrate. During production of the printed wiring by etching, thin film of metals such as nickel, silver, tin, tin-lead and gold are used as etch-resistant materials to protect part of the copper layer which will represent the wiring from the etchant. The substrate is a composite material. It originally consisted of woven glass fibre impregnated with an epoxy resin matrix containing bromine additive as flame retardant.

The matrix material called FR4 was the industry standard for many years until environmental concern started protesting against the use of the material because of its hazardous brominated flame retardant (BFR) content (Directive 2002/95/EC; D'Silva, 2004). This led to the development of various halogen-free materials. Phosphorus and antimony additives have been used for flame retardants. Up to five types of halogen free epoxy resins have been tested qualified for use in PCB production. These include epoxy resin cross linked with aminophenyl phosphate (Ehrler, 2002; Mauerer, 2005). There have also been developments toward improving the Tg (glass transition temperature) of the board material using epoxy resin blends and alternative resin materials. From the PCB materials development efforts, quite a number of plastic materials can now be found in waste PCB (Ehrler, 2002). These include:

- The conventional FR-4.
- Higher Tg FR-4, with a higher content of tetra- or multifunctional epoxy resins in the formulation to give greater cross-linking density in the cured material.
- Cyanate ester (CE) resin based, also with a relatively high Tg.
- GETEK^{R}/MEGTRON resin, a blend of 70/30 high Tg epoxy and thermoplastic polyphenylene oxide (PPO), developed by General Electric.
- Bismaleimide-triazine (BT) based material, developed by Mitsubishi Gas Chemical.
- Hydrocarbon resin filled with fine grained ceramics, designed for high frequency high speed applications by Rogers.
- A-PPE resin, in which polyphenylene oxide has been modified into a thermosetting resin

- Thermount[R] reinforced materials: a para-aramyd polymer fibre reinforced material developed by Thermount[R] DuPont Advance Fibre Systems.

Alternative reinforcement materials to glass fibres have also been developed. The paper-like para-aramid polymer fibre called Kevlar[R] for Thermount[R] is an example. Details about the thermomechanical and electrical properties significant for PCB applications, such as the dielectric constants, dissipation factor, through hole reliability, copper peel strength, z-axis expansion, volume resistivity and solder shock laminate, are available in literature (Roesch and Ehrler, 1997; Ehrler, 2002).

Populated boards have components put in place on them. It is expected to find resistors, chips, aluminium heat sinks, batteries, switches, capacitors, inductors, transistors (triodes, diodes and thyristors), fan units, connector terminals/slots, cables, transformers, solders, screws and rivet fittings, among others. The different components have different material compositions. Many metals, alloys, ceramics and plastics are used in these components and fittings. For the solders, more than 100 solder alloys are known (MatWeb). Table 2.2 shows some of these solders and their compositions.

Table 2.2: Representative solders: Composition, melting point and density (MatWeb) (The number in front of the elements is the mass percent in the alloy)

Solders	Composition (mass, %)	Melting Point (^{O}C)	Specific Gravity
Pb-Sn Eutectic (ASTM B 32 Grade Sn63)	37Pb 60Sn 3(Ag, Al, As, Zn, Sb, Cd, Cu, Fe)	183	8.4
95Sn-5Ag (ASTM B 32 Grade Sn95)	95Sn 4.4-4.8Ag, (Al, As, Zn, Sb, Cd, Cu, Fe)	221 - 245	7.5
95Sn-5Sb, ASTM B 32 Grade S65	95Sn, 4.5Sb, (Al, As, Zn, Sb, Cd, Cu, Fe)	234 - 240	7.25
AIM47 Fusible alloy	22.6Pb, 44.7Bi, 5.3Cd, 19.1In 8.3Sn	47	8.86
WS363 Lead Free	98.65Au 3.15Si	363	15.7
WS305 Lead Free	78Au 22Sn	280 - 305	14.81
WS238A	97Sn 3Sb	232 - 238	9.28
Indalloy[R] 281 Bi-Sn	58Bi 42Sn	138	8.56
Indalloy[R] 227 Sn-In-Ag	77.2Sn 20In 2.8Ag	175 - 187	7.25

Leaded solders are expected in earlier boards, while more recent boards may use unleaded solders. Base metals such as iron (in screws, transformers, electromagnets and rivets), copper (in inductors, transformers and cables), aluminium (in heat sinks, foils and wrappings) and tin, can be found in fair bulk sizes on PCBs. Rare metals, such as tantalum, are found in high performance capacitors. Noble metals, such as gold, silver and palladium, occur in sockets and edge connector plating and in some high performance components. Gallium and other platinum group elements can also be found. Lead, cadmium, chromium and mercury are usually concentrated in batteries. Mercury is also found in relays and switches, while cadmium is found in some surface-mounted chip resistors, infrared detectors and semiconductors. Ceramics, used in bridges and slots on the boards, include alumina and beryllium oxide. Silica, other alkaline earth oxides, mica and barium titanate are also found. Chip components contain elements such as Ga, In, Ti, Si, Ge, As, Sb, Se and Te, while semiconductors contain Ge, Si, Se, Ga and other elements in small quantities.

Apart from the board resins, other plastics generally found in populated boards are polyvinyl chloride (PVC), acrylonitrile butadiene styrene (ABS) and polystyrene (PS). Varying amounts of these plastics may be found on the PCB depending on the socket, slots and cable coating materials used. Varieties of plastics that can be found in the populated PCB materials streams, including density and critical surface tension of some of the plastics, are presented in Table 2.3.

In general, there are a number of overall material compositions reported for the PCB. Some of these compositions, as well as one determined in this work, are contained in Table 2.4. The data for each element can be seen to vary across the different compositions. This is expected as PCBs material make-up continues to change with technology over time. This makes quantitative analysis of the stream really difficult, and a ‘typical’ PCB composition may not be presented rigidly. Unfortunately, the OEMs are not of help in this context: more than one manufacturer is responsible for one populated PCB, while components are ordered according to electronic functions and not by materials composition. PCB manufacturers therefore do not have complete information regarding the material composition (Li *et al.*, 2004). The bulk comes back to the materials processor to determine a composition upon which resource recovery analysis can be based. There are other implications of PCB material make-up on its physical processing.

Table 2.3: Plastics obtainable from PCB materials streams

Plastics	Specific Gravity	γ_c, critical surface tension
Polyethylene (PE)		31
Polyethylene terephthalate (PET)	1.33 – 1.37	43
Polyvinylchloride (PVC)	1.16 – 1.38	39
Polytetrafluorethane (PTFE)	2.3 – 2.32	18
Nylon	1.1 – 1.35	
Polypropylene (PP)		
Acrylonitrile butadiene styrene – ABS	1.04	35
Fibre reinforced ABS (Acrylonitrile butadiene styrene)	1.286 - 1.45	
Polystrene (PS)	1.04	33
Cyanate Ester (CE) Resin		
Polyphenylene oxides (PPO)Resin		
Polyphenylene ether (PPE)		
Bismaleimide-Triazine (BT) Resin		
FR-4 Epoxy resin	1.8-2	47
FR-2 Phenolic resin based		
Para-aramid polymer fibre		

2.2.4 Physical Processing Implications

The material make-up of PCB has implication both on the comminution and the separation operations in the physical processing. The PCB structure presented shows that classical mineral processing comminution equipment such as gyratory/jaw crushers and tumbling mills will not apply because brittle cleavage or shatter fracture may not be expected from PCBs. This was demonstrated by trial comminution in a laboratory ball mill with 35 mm steel balls. The fragments were only rubbed and beaten smooth after twenty minutes of operation (Ogunniyi, 2006). Shear shredders, which can be considered as a modification of toothed roll crushers, are used mostly for primary crushing, while hammer mills, which employ impact and shear, are mostly used for the grinding operation (Taylor, 2002; Goosey and Kellner, 2003; Hamos GmbH; Sander *et al*., 2004, Schubert and Bernotat, 2004). Grinding in impact equipment with cryogenic conditioning to enhance the brittleness of the polymer matrix has also been reported (Kravchencko *et al*., 1983; Goosey and Kellner, 2002). It should be noted that PCB comminution

need not seek to obtain a characteristic breakage function. For instance, single-sided older generation boards with a high proportion of fibre glass and low density of the copper trace will be expected to show more overall brittle tendency compared to recent high density multilayereded boards with poly-aramid reinforcement. Populated boards will present more varied characteristics.

Table 2.4: Material Compositions of PCB (Weight %)

Materials		% [1]	%[2]	%[3]	%[4] *	%[5]	%[6]	%[7]
Metals (Max. 40%)[1]	Cu	20	26.8	10	15.6	22	17.85	23.47
	Al	2	4.7	7	--	--	4.78	1.33
	Pb	2	--	1.2	1.35	1.55	4.19	0.99
	Zn	1	1.5	1.6	0.16	--	2.17	1.51
	Ni	2	0.47	0.85	0.28	0.32	1.63	2.35
	Fe	8	5.3	--	1.4	3.6	2.0	1.22
	Sn	4	1.0	--	3.24	2.6	5.28	1.54
	Sb	0.4	0.06	--	--	--	--	--
	Au/ppm	1000	80	280	420	350	350	570
	Pt/ppm	-	-	-	-	--	4.6	30
	Ag/ppm	2000	3300	110	1240	--	1300	3301
	Pd/ppm	50	-	-	10	--	250	294
Ceramics (Max 30%)[1]	SiO_2	15	15		41.86	30		--
	Al_2O_3	6	--	--	6.97	--		
	Alkaline and Alkaline earth oxides	6	--	--	CaO 9.95 MgO 0.48	--	--	
	Titanates, Mica, etc	3	--	--	--	--	--	--
Plastics (Max 30%)[1]	Polyethylene	9.9	--	--		16	--	--
	Polypropylene	4.8						
	Polyesters	4.8						
	Epoxies	4.8						
	Polyvinyl-chloride	2.4						
	Polytetra-flouroethane	2.4						
	Nylon	0.9						

[1]Shuey *et al.*, 2006 from Sum, 1991; [2]Zhao *et al.*, 2004 from Lehner, 1998; [3]Cui, 2005 from Zhang and Forssberg, 1997; [4]Kim *et al.*, 2004, *Incinerated PCB Product; [5]Iji and Yokoyama, 1997; [6]Patent Application, 2006; [7]ICPOES analysis of cellphone PCBs

Another consequence of the diversity of valued constituents on PCBs is the complexity of beneficiation into clean material fractions. Target metallic values range from percentages to ppm proportions, in various forms of man-made 'occurrences' or 'dissemination'. Among the valuables are hazardous contents. Lead, mercury, cadmium, hexavalent chromium and polychlorinated biphenyl (pcb) are among the six materials declared hazardous in the RoHS (Restriction on Hazardous Substances) directives (Directive 2002/95/EC). Polychlorinated biphenyl is found in some capacitors, while batteries contain cadmium, mercury, lead and chromium. These components must not be ground along with others, but must be removed for separate treatment (see section 2.2.3). This is why physical processing has to be in stages of comminution-separation, decongesting the stream as comminution progresses to finer sizes, and different values are being liberated. In this manner, the materials variety would have been significantly reduced before final grinding to liberate the values within the laminates.

2.3 PCB PHYSICAL PROCESSING OPERATIONS

In the 1970s the predominant method of recovery of metals from electronic scrap was via the blast furnace in conjunction with secondary copper/lead smelter (Sum, 1991). Details about physical processing effort were rare until the early 1980s. Figure 2.5 is a typical flowchart of earlier physical processing of scrap from multi-component REE – radio-electronics equipment (Kravchenko *et al*., 1983). Scrap REE has now taken on the WEEE nomenclature. Features of this processing included differentiated disassembly (more recently referred to as selective disassembly), cryogenic cooling and crushing, airflow classification, stages of magnetic separations and, finally, magneto-hydrostatic separation (MHS). The magneto-hydrostatic separation density was first set to 2000 kg/m^3 (2 g/cm^3), then to 3000 kg/m^3. This will cause non-metallic stuff to be floated first, followed by aluminum in the second stage, while copper, lead and tin were in the sink product.

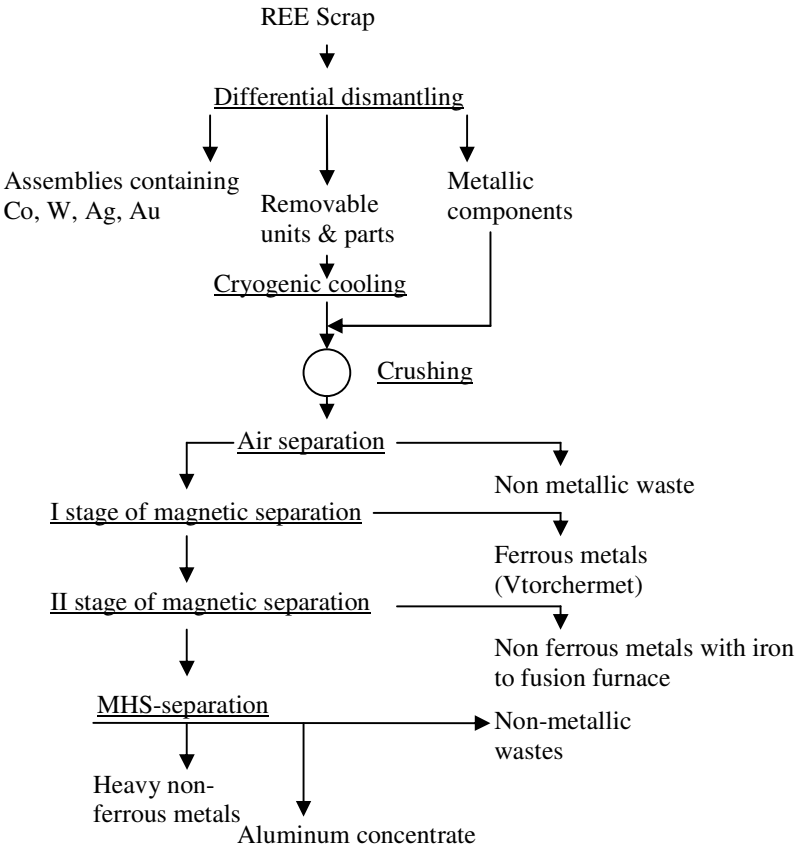

Figure 2.5: Flowsheet for reprocessing of multicomponent REE scrap (Kravchencko *et al.*, 1983 - Redrawn)

Magneto-hydrostatic separation, also called ferro-hydrostatic separation (FHS), is a technology that uses colloidally stable and magnetizable fluids. It dates back a few decades, with reported application for municipal solid waste processing (Khalafalla, 1973, 1976; Zhan and Shenton, 1980; Vesilind and Rimer, 1981). More recently, Debeers group reported efforts to apply it to mineral processing (Svoboda, 2000). A suspension of nanosized magnetic particles (often in kerosene) forms the ferrofluid whose apparent density can be varied by its surrounding magnetic field; the apparent density increases with increasing field strength. Under the influence of the field, the nanoparticles tend to align in space inside the ferrofluid and become stationary. This tends to make the fluid rigid so that particles sink through it with greater resistance, making the density appear higher. In application, the apparent density can be varied up to a specific gravity

above 20 in fine steps, making it possible to achieve sink float separation of a mix to tenths of specific gravity.

In later operations, electrostatic separation was broadly used in place of the FHS for treating the fine fractions. Low throughput, high electricity costs for the field electromagnets in scale-up and optimal feed size, identified as limitations of the FHS (Kruger, 2006), could have been some of the reasons for this trend. By the 1990s, emphases were on the disassembly stage before crushing. The recovered component would be tested, refurbished and then resold in some second user specialist marketplace. Design for easy disassembly became an issue for the original equipment manufacturers (OEMs), and many works were towards automated disassembly, for components recycling (Feldmann and Sheller, 1995; Stennett and Whalley, 1999).

Figure 2.6 shows the flowchart of the recycling operation of NEC Corporation, Japan (Yokoyama and Iji, 1997). The operation entails first stage components and solders removal by heating, impacting and shearing (Yokoyama and Iji, 1997). The evacuated board then goes through pulverising and separation stages. The pulverising stage is considered critical to liberating copper in multi layered boards. Two types of equipment are used for crushing and fine pulverising. The first employs a cutting and shearing force for size reduction to 10 mm. The second employs a pulverizing roller on a table to apply compressive and shearing forces. The operation has a notable feature of liberating the copper more coarse than the glass fibre and the resin, due to differences in brittleness, see Figure 2.7 (Higashiyama and Asano, 1998). A gravimetric separator, based on density, is used on the product to produce a 23 wt % copper-rich residue. This is followed by a rotor-type electrostatic separator, producing recovery and grade of more than 90 % and 60 %, respectively, on the 100 – 300 µm size fraction.

Prior manual disassembly of precious metal bearing parts on the PCB was employed at Noell Abfall, Germany, and Energietechnik in their 21000 tonnes *per annum* plant in 1996 (Goosey and Kellner 2002). The plant was specifically intended for redundant telecomunication scrap and eol PCBs were also treated. The overall methodology deploys a three-stage liberation and sequential separation route with ferromagnetic removal via overhead permanent magnets and eddy current techniques, because of the effectiveness of the eddy current separation force on the fractions in the 5 mm to 200 mm particle size range. Air table techniques were used to separate

particulate fractions in the 5 mm to 10 mm, 2 mm to 5 mm and less than 2 mm ranges respectively.

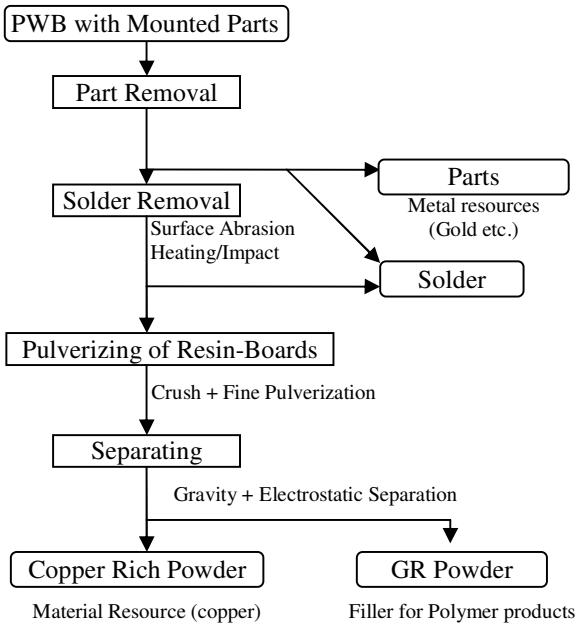

Figure 2.6: Flowchart of the NEC's recycling process (Yokoyama and Iji, 1997)

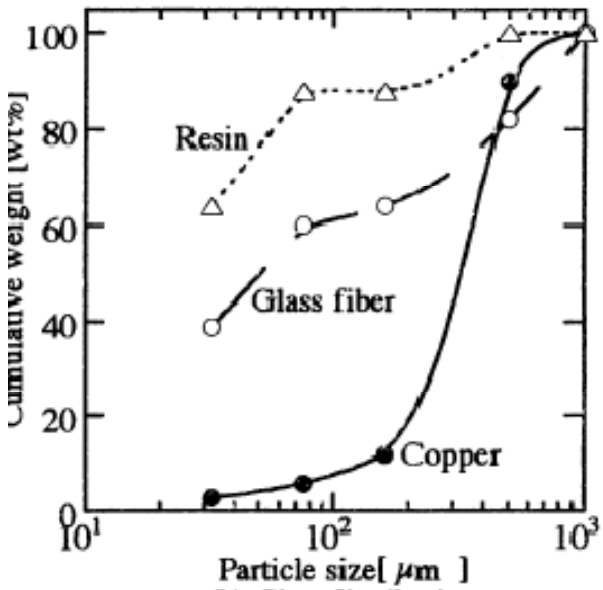

Figure 2.7: Size distribution of the NEC Corp comminution product (Higashiyama and Asano, 1998)

Cost effective automated disassembly, either by 'look and pick' or 'evacuate and sort', is a specialised technology on its own. It requires a data-intensive object-image recognition information system for sorting after evacuation; special numerically controlled jaw grippers for through-hole-device disassembly; vacuum grippers for surface-mounted devices; chemical or electrochemical dissolution of solders with specialised etchants, among other features (Feldmann and Scheller, 1995; Stennett and Whalley, 1999; Jianzhi *et al.*, 2004).

Although robotic technology operating on a cost effective component identification and disassembly was reported in the USA (Goosey and Kellner, 2002), this automation suffered setbacks in case of old 'orphan' boards with no existing database. Another strong factor against component recycling is the rapid advancement in production and materials technology. This makes components obsolete too quickly, not reusable, and new ones much cheaper. More recently, emphases for selective disassembly reduced greatly (Taylor, 2002). Total feed comminution in shredders, followed by separation, now substitutes disassembly devices in many operations. Although some extent of manual dismantling, to single out hazardous component, can be judged as indispensable because of the complex nature of the stream (www.desco.co.za), efforts to further disassembly expertise still continue (Elif and Surendra, 2006).

In Taiwan, all capacitors on the boards (possibly containing polychlorinated biphenyl) that have diameters greater than one centimetre and a height larger than two centimeters are usually removed manually from the board before comminution (Lee *et al.*, 2004). Products from integrated circuit (IC) boards in computer recycling plants are generally classified into three groups: ferrous, non-ferrous and non-metals – and each fraction sells at minimum of US$ 57, US$ 743, and US$ 43 per ton respectively. The Huei-Chia-Dien Company (Taiwan) has a dedicated flowsheet for physical processing of scrap IC boards, Figure 2.8 (Lee *et al.*, 2004). Iron, plastics, fibre glass and resin, aluminium and copper fractions are obtained. Except for the ferrous fraction, the other metallic fractions is usually a mixture of metals and are sold to smelters.

VOGT Electronic FUBA, Germany, runs a recycle centre for unmounted PCBs and material scrap, with 5000 tons per year capacity, adjacent to its PCB manufacturing plant (Goosey and Kellner, 2002; Gold and Dietz, 2003). The operation is fully mechanical and dry (see Figure 2.9).

Hammer mills convert the scrap feed into fairly liberated small pieces of particles or fragments for separation, while material separation uses the different specific gravities and electrical conductivities of the metal, glass and resin. The products obtained consist of copper metal and two plastic products – fibrous and powdery. The recovered copper is returned to metal smelters. The glass fibre and resin fraction finds most successful use in production of pallets for underground mining and storage. This product takes advantage of the flame retardant property of the resin fraction (Goosey and Kellner, 2002). A block diagram of the operation is shown in Figure 2.9.

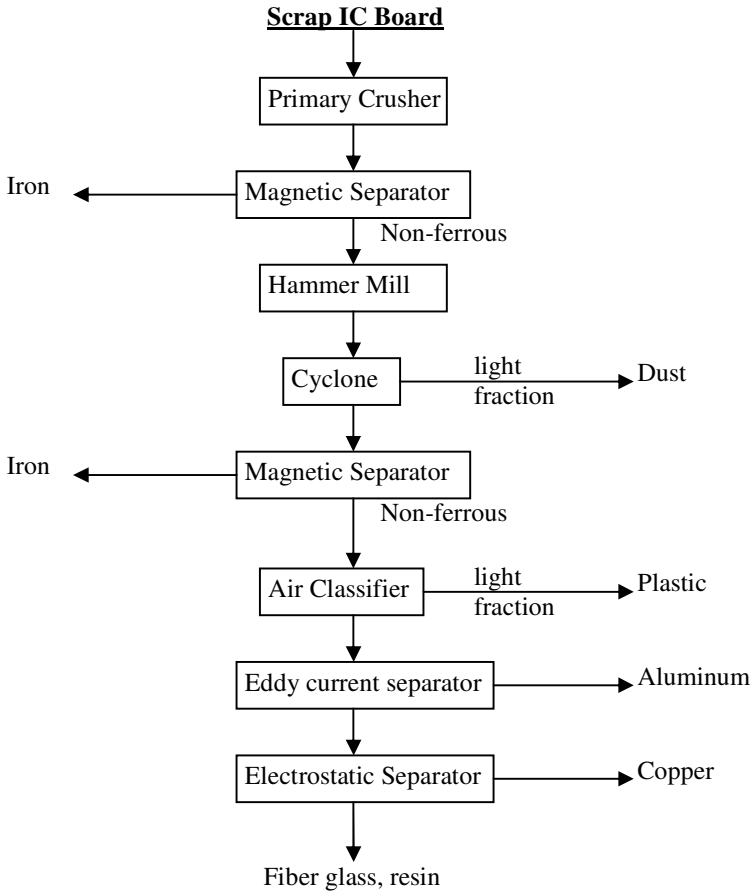

Figure 2.8: Huei-Chia-Dien Company's physical separation flowsheet for recycling of scrap IC boards (Lee *et al*., 2004).

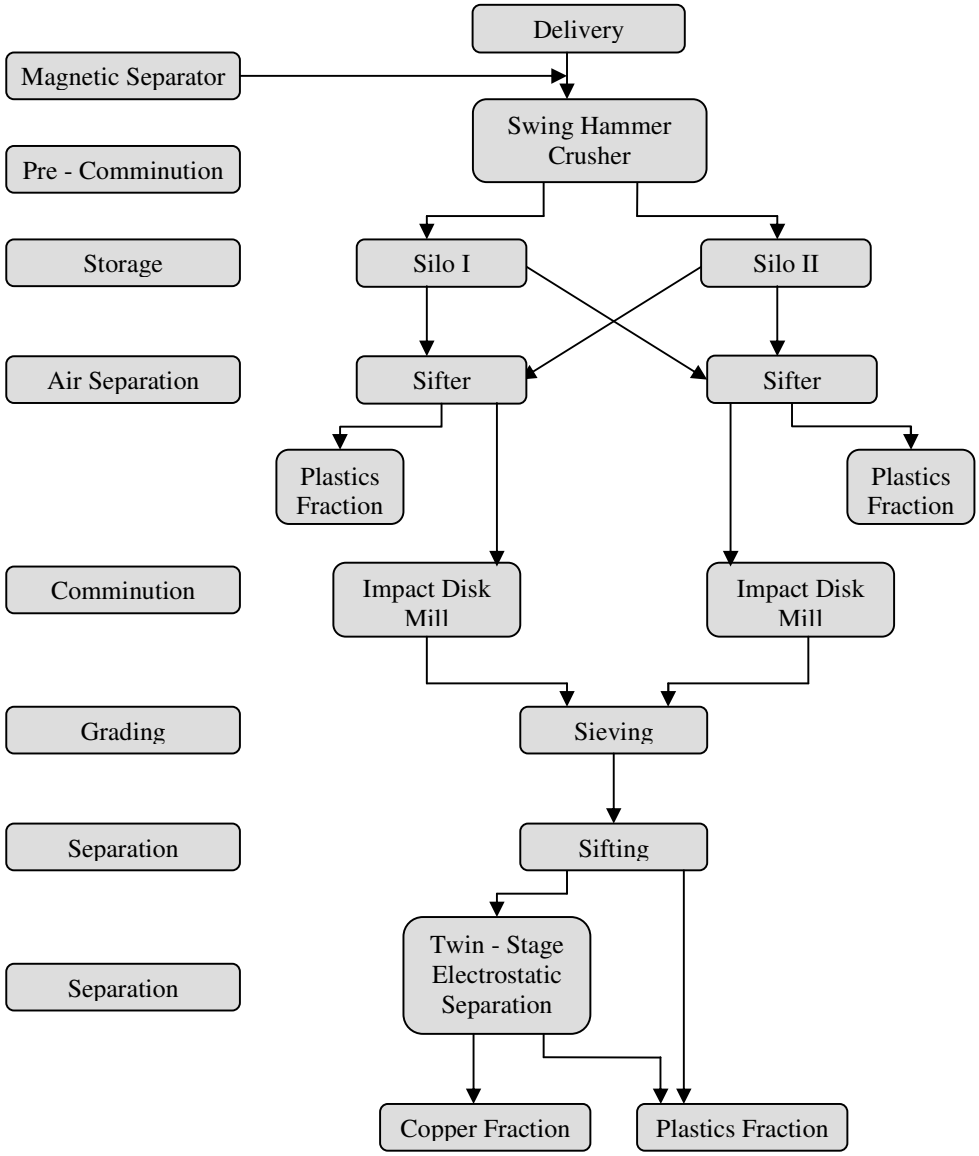

Figure 2.9: Block diagram of PCB recycling operation at FUBA, GmbH (Goosey and Kellner, 2002)

A commercial turnkey electronic recycling plant (ERP) for a wide range of electronic scraps, including populated PCBs, was developed by Hamos recycling and separation technologies, Germany (Hamos GmbH, Germany). It is an automated and integrated mechanical system, Figure 2.10, producing three products: a ferrous metal fraction, a mixture of non-ferrous metals and a mixed fraction of plastics and ceramics. The major stages of the operations involve pre-comminution for a coarse liberation; magnetic and eddy-current separation of coarse ferrous and non-ferrous metals; liberation of non-ferrous metals; classification for improved separation; electrostatic separation of the metal fraction; subsequent comminution of unliberated materials; dust extraction; and optional gravity or eddy-current separation of coarse metal fractions (Hamos GmbH, Germany).

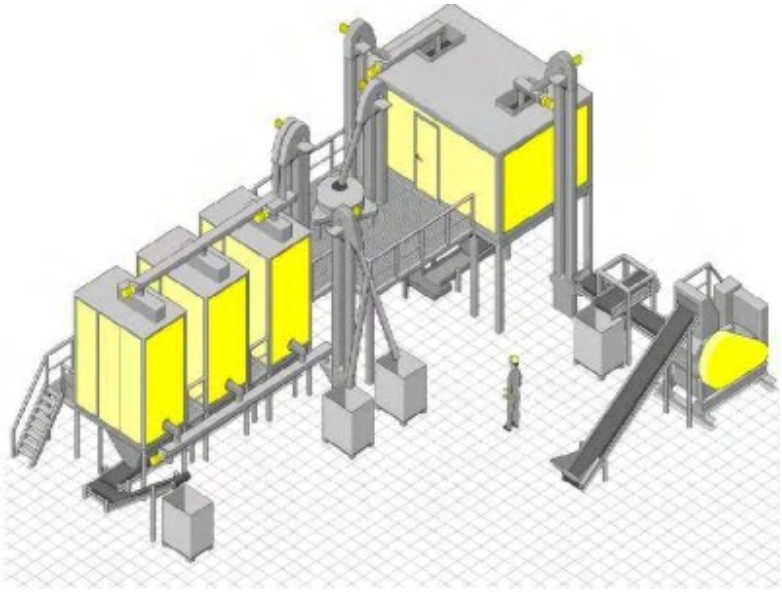

Figure 2.10: Hamos GmbH ERP – electronic recycling plant

Noranda Recycling Inc. operates in USA, Canada and Asia. The firm has established smelting operations and uses mechanical processing to upgrade general electronic wastes for smelting the feed (Shuey, 2006). Hazardous components are first removed manually before introducing the handpicked waste into a series of shredders that reduces the junk to five centimetre-sized pieces. Separation technologies, such as magnetic and eddy current, are used. In this way, the electronic scrap is separated into various commodity streams which are sent to different Noranda

operations. Fractions rich in copper and precious metals, copper-plastic mixed fraction and circuit boards are sent to the copper smelting operations to recover copper, silver, gold, platinum, palladium, selenium, tellurium, cadmium and nickel. The steel output from the mechanical processing goes directly to the steel foundry, while the aluminium fraction goes to an aluminium smelter. As Noranda's products are dedicated to established smelters, the mechanical processing does not try to achieve the best clean material fractions possible.

In the USA, physical processing is generally applied to electronics waste at MRFs (material recovery facilities) to produce three fractions of ferrous metals, non-ferrous metals and plastics. The unit operations, Figure 2.11, usually involve physical sorting, comminution, screening, and magnetic, eddy current and density separations (Kang and Schoenung, 2005). The fractions are then forwarded to appropriate material processing plants.

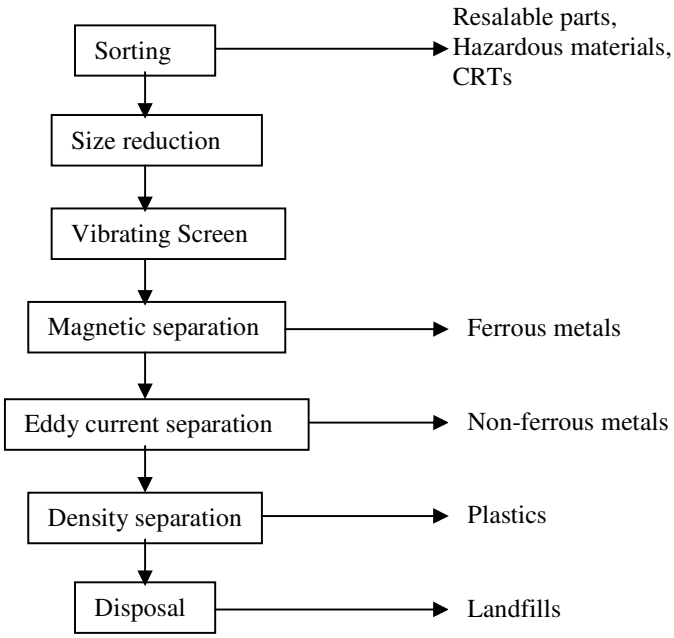

Figure 2.11: Simplified flowsheet at a materials recovery facility, MRF (Kang and Schoenung, 2005)

Researchers at Daimler Benz in Germany developed a process comprising initial size reduction to ~2 cm x 2 cm and magnetic separation. Then cryogenic grinding was done by passing –196 ^{o}C liquid nitrogen through a hammer mill. This imparts brittleness to the feed, effects process cooling, and provides inert atmosphere which prevents oxidation by-products such as dioxins

and furans. Sieving and electrostatic separation is applied for material separation of the milled product (Goosey and Kellner, 2002).

In South Africa, two major recyclers – Desco Electronic Recyclers and Universal Recycling Company – are known in the e-waste recycling industry. Of these, only Desco Electronic Recyclers is reported to have dedicated PCB processing operation (eWaste Guide, 2006; Finlay, 2005). Another establishment, Reclaim, is considered to be the largest recycling organisation in South Africa. It also accepts e-waste, but passes it onto Universal Recycling (Finlay, 2005). Other minor players basically serve as collectors and pass on the general e-waste to any of the two major establishments. African Sky, who also accepts e-waste, carries out very minimal processing or value addition before exporting the stock virtually as-received to Citiraya waste recycling company in Singapore (Finlay, 2005). Citiraya, which now operates as Centillion Environment and Recycling UK Limited (www.centillion-er.com; www.researchandmarkets.com), is considered to be one of the world biggest processor of corporate e-waste and deals with multinationals such as Nokia and HP (Finlay, 2005; eWaste Guide, 2006).

Desco Electronic Recyclers is reported to process about 400 tons of PCBs along with about 2000 tons of other electronic waste annually (eWaste Guide, 2006). Desco strips the feed manually, disassembles and sorts it into separate specific components and material types. Materials for recycling are not thrown into the shredder as whole units. This prevents a mixture of plastics, ferrous and non-ferrous materials being shredded together (www.desco.co.za). Plastics are separated from the PCBs, producing a relatively clean plastic fraction for the final plastic recycler clients. The boards are then shredded, followed by pulverisation, and separation stages. The machinery used is designed and built by Desco, and the details are proprietary.

The operation at Universal Recycling is fully mechanised, without any hand sorting. The stock is conveyed via belts between different operations. These include shredding, heavy media separation, eddy current separation, sorting, milling, granulation and rotary magnetic separation (www.urc.co.za). The heavy media separates the comminution products, based on densities in stages, giving product fractions of plastics, glasses and metals. The water for the heavy media separation is fully recycled (Finlay, 2005). The operation, however, handles the feed as a mixed

load with no specific provision for e-waste or PCBs. Electronics are simply considered along with non-ferrous materials. Components such as nickel-cadmium batteries, bearing hazardous constituents all go through the shredder, but somehow along the line, they are separated (Finlay, 2005). The final products from these operations are sold mostly to Rand refineries, South Africa, as non-ferrous fraction from waste recycling.

All these operations are basically preparatory to finishing recovery via smelting. Consequently, clean fractions are not paramount. Except for ferrous fractions which can be achieved at fairly high grade and recovery, optimum reports for copper, for instance, include 60 % copper grade and 90 % recovery in 100 – 300 µm fraction (Yokoyama and Iji, 1997). FUBA operation reports 92 % copper grade from unpopulated boards, which is a less complex feed. Product grades from many operations are rare in reports. Zhang and other workers conducted various investigations on PCB and WEEE physical processing (Zhang *et al*., 1997; Zhang and Forssberg, 1997). Using air table separation, optimum result reported 72 % grade and 76 % recovery for copper in the 1 mm to 0.6 mm mill fraction (Zhang and Forssberg, 1997).

Compared to typical assay figures in conventional minerals processing, the copper assays in the product fractions appear satisfactory. Chalcopyrite ($CuFeS_2$), for instance, is the main ore mineral of copper, and the best copper assay from its processing is 34.7 %. Such chalcopyrite concentrate is amenable to straightforward matte smelting chemistry, oxidizing iron sulphide to the slag phase and sulphur to the gas phase, leaving metallic (blister) copper (Rosenqvist, 1988). In contrast, for PCB non-ferrous copper rich separation products, at much higher assays, the smelting and refining processes are much more extensive. This is because for a fraction assaying, say, 90 % copper, the 10% complementary matter will not be from a single mineral element (such as sulphur alone with copper in chalcocite) or a few definite co-occurring elements, but a lot of contaminants. This is to say that, while poor separation efficiencies are obtained at non-optimal size fractions, even the products with best grades still need improving.

From what commonly obtains at present: (i) returns to the independent physical processing plant are not maximized (some prices are cited for Taiwan); (ii) overall recycling ratio is low (as secondary use of unsorted fraction is limited); and (iii) secondary smelting for metallic value recovery requires extensive facilities. Such a smelting facility, Pb-Cu smelter, is cost intensive

and not available in many parts of the world where PCB and general electronics waste recycling has to be done. In fact the more complex Pb-Cu-Zn smelters with facilities for recovery of metals such as zinc from volatiles are the most appropriate. Constructing such a capital-intensive metallurgical plant specifically for e-waste processing will require a more integrated collection and shipping infrastructure of the waste stream. Although the pyrometallurgical follow-up route may not be avoided outright, the downstream processing chemistry can be simplified considerably by cleaner fractions from the physical processing.

Improving eol PCBs beneficiation demands that the material complexity involved is recognised and an effective beneficiation operation is developed to match. While ores containing three target minerals are considered complex in classical minerals processing, with extensive beneficiation operation, common eol PCBs beneficiation flowsheet, are generally too brief for the task.

2.4 IMPROVING PCB PHYSICAL PROCESSING: FINES BENEFICIATION

It can be seen from the review of PCB physical processing presented that, for the −2 mm comminution products, electrostatic separation is the technology been employed. In conventional mineral processing, it is known that separation efficiency of corona or high tension electrostatics separator drops rapidly below 75 µm feed sizes (Wills, 1997; Kelly and Spottiswood, 1989).

Zhao *et al*. (2004) compared a type of column air separator to electrostatic separator for recovery of metal values from PCB hammer mill grinding products (Tables 2.5 and 2.6). More than 20 % of the product of the hammer mill grinding from 30 mm feed size reported to the −75 µm fraction, assaying almost 2.9 % copper. Copper recoveries of 27.83 % at a grade of 26.8 wt. % were obtained from the pneumatic separator. Separation from the electrostatics at that size was not reported, probably because it was too poor. The work concluded that below 75 µm, electrostatic separation efficiency is poor for PCB grinding fines.

In the NEC's operation (Yokoyama and Iji, 1997; Iji and Yokoyama, 1997), at −300 + 100 µm, copper-rich powder (82 % Cu, at less than 90 % recovery) was produced. The non-conducting fraction from the electrostatics separation contained 64 % glass fibre, 34 % epoxy resin, 2.1 % copper and solders. Some end-use applications, such as filler for epoxy resin polymer product, were investigated for the glass fibre-resin fraction. But at 2.1 % copper content, the fibre glass-

resin fraction assays higher than many natural deposits being mined and processed economically. It therefore deserves further beneficiation.

Table 2.5: PCB Grinding Size Distribution (Zhao *et al.*, 2004)

Size Range (mm)	Weight (%)	
	Open Circuit Hammer Mill Grinding	*1mm Closed Circuit Hammer Mill Grinding*
+1	15.86	0
−1 + 0.5	35.26	40.87
−0.5 + 0.25	10.10	11.73
−0.25 + 0.125	12.86	15.23
−0.125 + 0.075	4.70	5.54
−0.075	21.22	26.73

Table 2.6: Copper recovery and grade versus size range and separation technology (Zhao *et al.*, 2004)

Size Range	Pneumatic Separation (Air Classifier)		Electrostatic (Corona)	
	Recovery	*Grade*	*Recovery*	*Grade*
−1.0 + 0.5 mm	70.11	49.08	97.65	53.75
−500 + 250µm	66.42	54.66	97.88	71.61
−250 + 125µm	90.76	49.54	43.78	90.62
−125 + 75µm	80.35	29.98	37.57	90.90
−75µm	27.83	26.81	--	--

Precious metals are usually coated in a couple of microns in the PCB sockets and slots, and on the edge connectors. Abrasion in the event of comminution is therefore likely to make them report to the −75 µm fraction. With electrostatics separation, these fine metallic particle will be poor recovered (Kelly and Spottiswood, 1989), representing a major loss to the economic drive of the whole operation. Traces of noble metals used as anti-etch materials during the printed copper circuit production (Li *et al.*, 2004) can also be present on the copper particles. Unrecovered copper therefore carries such to waste.

The inefficiency of electrostatics separation with PCB grinding fines could have been tolerated because (i) the relatively higher assays and better recoveries from the coarser fractions (Yokoyama and Iji, 1997; Zhao *et al.*, 2004) pay for the operation profitably well; (ii) the metallic products of PCB physical separation are generally being destined to pyrometallurgical operations (Shuey *et al.*, 2006; Lee *et al.*, 2004), and (iii) dry operations are preferred for handling the PCBs.

Only the last point can make the tolerance understandable. Wet processes are avoided in most recycling operations to avoid wash water circuit and treatment costs, among other reasons (Kellerwessel, 1993). In particular, because PCBs contains such a wide diversity of materials, leaching and oxidation behaviours cannot be absolutely predicted in a wet process. Also, at the coarse fractions of the comminution-separation operation (with particles of all sorts of shapes) particle flow will not be good. But at finer sizes, slurry flow is much better. The issue of hazardous leaching or material oxidation still remains. It could, however, be much reduced at the fine sizes, as many materials from many components, particularly components bearing hazardous substances, have being removed. Materials expected will be mostly chippings from metallic particles, copper from the traces, solder remains, ceramics used in small resistors and chips, resin materials like epoxy, remains of plastics used in slots and reinforcement material such as glass fibre.

At this stage of PCB physical processing, the operation need not be restricted to dry. Froth flotation is a specific wet processing technique that appears very promising for beneficiation of the fine fraction. Froth flotation, exploits distinct surface properties of individual particles; it is particularly effective in the −75 μm range; and it can be executed via different schemes toward enhancing selectivity. The prospect therefore deserves detailed investigations. An overview of how froth flotation can be applied to this material stream will be presented in the next chapter in order to set out a detailed methodology for the investigation.

2.5 CONCLUSION

Physical processing of PCB dates to about three decades now - not totally a new area of endeavor, yet not fully developed. Essentially, it remains a stage-wise comminution-separation

operation. Given the peculiar material composition of the printed circuit boards, shear shredders can be taken as the industry standard comminution equipment used. Separation technologies employed in the industry include magnetic, eddy-current, electrostatic, dense-medium and air-classification. Product material fractions are ferrous, non-ferrous, plastics and ceramics, with different degrees of cross contamination depending on particle liberation and the size at which the material fraction was obtained. The non-ferrous fraction mostly serves as secondary feed at established smelters having requisite extensive facilities. Hydrometallurgical follow-up route to the physical processing has relative advantages over the pyrometallurgical routes, but it requires much cleaner material fractions to simplify process chemistry. The −75 μm fine fraction in the comminution products has been observed to contribute a drop to the overall recovery and separation efficiencies. Loss of precious metals to the fine fraction is also possible, representing a major economic loss to the operation. Froth flotation appears very promising for investigation into its applicability for beneficiation of the metallic values deported to this fine size fraction.

3.0 FROTH FLOTATION FOR THE BENEFICIATION OF PCB FINES

3.1 INTRODUCTION

As presented in Chapter 2, the material constituents of the comminution fines will be quite diverse. This will include copper from the traces; solder remains; precious metals – gold, palladium, platinum – relatively in trace proportions; chipped or torn particles of various alloys; synthetic or natural ceramics used in certain resistors, semiconductors, glazed components and chips; resin materials like epoxy; particles of plastics used in slots; and board reinforcement material such as glass fiber. It follows that flotation of native metals, plastics, and ceramics (oxides, conventional minerals) are all of relevance towards evolving logical flotation schemes for the sample. These and other relevant concepts are reviewed in this chapter. The concepts are used to advance probable schemes, and to make more specific objective statements for the investigation. As this application will traverse a broad spectrum of surfactants, a brief on surfactants are presented first.

3.2 SURFACE ACTIVE AGENTS

Surface active agents (surfactants) are organic compounds with a heteropolar molecular structure. The non-polar hydrocarbon chain group of the molecule prefers to attach to air, while the polar functional groups prefer aqueous phase. The surface activity derives from this property. They can therefore adsorb (accumulate) at air-water, air-mineral and/or water-mineral interfaces. The specific application of a surfactant is determined by the properties of the polar functional group, which can be ionic – cationic or anionic, or non-ionic. Ionic surfactants are electrolytes. They can adsorb at mineral-water interfaces, electrostatically and/or chemically. This makes them useful as collectors. Non ionic surfactants are non-electrolytes, and they adsorb majorly at air-water interface. Table 3.1 shows some common surfactants compounds. The adsorption at air-water interface lowers the surface tension of the solution. This makes thin films of the solution metastable and therefore supports frothing. It also creates wetting effects, lowering overall surface energy and tension.

Table 3.1: Some common surfactant and applications

Classification		Example	Major Application
Ionic	Salts of organic acid	Carboxylate salts	Soap
		Sodium alkly sulphonate	Wetting and Detergency
		Alkyl phosphate salt	Wetting and Detergency
	Amine Salts	Primary Amine	Collectors
	Sulphydryl	Dithiocarbonates	
		Trithiocarbonates	
		Dithiophosphates	
Non-ionic	Alcohols	Methyl IsoButyl Carbinol	Neutral Frothers
		Pine Oil	
	Hydroxylated polyglycol ethers	Polypropylene glycol methyl ether	
		Tripolypropylene glycol methyl ether	
		Nonylphenol polyglycol ether.	
	Alkoxy substituted Parafins $(R`OH)_xH$	Multi ethoxylated butane (1,1,3 Tri ethoxy butane)	

The reduction in the surface tension of the aqueous solution is towards that of the surfactant in proportion to the concentration of the surfactant molecules adsorbed at the interface. This can be described by the Gibb's adsorption equation in the form:

$$d\gamma = -S_S dT - \sum_i \Gamma_i d\mu_i \quad . \quad . \quad . \quad . \quad . \quad . \quad . \quad 3.1$$

where dγ, S_S, T, Γ_i and μ_i are the changes in surface tension, surface entropy, temperature of the system, adsorption density of specie *i* and the chemical potential of specie *i*, respectively, at constant pressure (Fuerstenau, 1982). Defining i = 1 for the solvent specie, then $\Gamma_1 = 0$ as the solvent does not adsorb in itself. Since, $d\mu_i = RTd \ln a_i$, at constant temperature, as in flotation process, it follows that:

$$d\gamma = -RT\sum_{i=2}\Gamma_i^1 d\ln a_i \cong -RT\sum_{i=2}\Gamma_i^1 d\ln C_i \quad . \quad . \quad . \quad . \quad 3.2$$

where Γ_i^1 refers to the surface excess (adsorption density) of specie i relative to the solvent at the interface, and a_i is the activity of i, which approximates the concentration of i, C_i, in very dilute solutions.

However, Eq. 3.2 is not a continuous function. The surface tension decreases towards a limiting value which is that of the surfactant, and C_i is defined within the solubility range of the surfactant, beyond which micelle or droplet formation (phase separation) commences. With further increase in concentration such droplet will act as antifoamer in frothing application (Pugh, 2007). The selective wetting achievable by surface tension control is the basis for gamma flotation separation of plastics (see Section 3.4).

3.3 FLOTATION OF METALS AND ALLOYS FOR PCB FINES APPLICATION

Many studies have shown that metallic particles can be rendered hydrophobic and floated. With higher surface energies (than plastics), metallic particles can react with collector molecules (chemisorption) forming hydrophobic surfaces. Woods (1996) included the adsorption of xanthates on gold, platinum, silver and copper in a detailed review of chemisorption of thiols on metals and metal sulphides. For platinum and gold, voltamogramms of their electrodes in ethyl xanthate indicate anodic peaks at the region of the reversible potentials of the ethyl xanthate/dixanthogen couple:

$$2C_2H_5OCS_2^- \rightleftharpoons (C_2H_5OCS_2)_2 + 2é \quad . \quad . \quad . \quad . \quad . \quad . \quad 3.4$$

Peaks corresponding to the cathodic reduction of the anodic oxidation product can also be observed on the reverse potential scan. It was inferred that anodic oxidation of ethyl xanthate to dixanthogen and adsorption of the latter occurs on the metals. Tafel slope for the anodic oxidation, however, indicate that the oxidation to the dimer can proceed via an initial chemisorption step:

$$2C_2H_5OCS_2^- \rightleftharpoons 2(C_2H_5OCS_2)ads + 2é = (C_2H_5OCS_2)_2 + 2é \quad . \quad . \quad 3.5$$

Lins and Adamian (1993) used amyl xanthate as a collector to study the effects of some physical variables on gold flotation. Good recoveries were obtained for gold from a synthetic mixture of silica and gold particles over 0.16 mm – 0.71 mm size ranges. About 90 % recovery and 5 kg/ton gold grade in the float was achieved from a 167 g/ton feed with 0.16 mm d_A sample at 18% pulp density (Figure 3.1). The work of Lins and Adamian is notable considering the good flotation of 0.71 mm gold particles that was claimed.

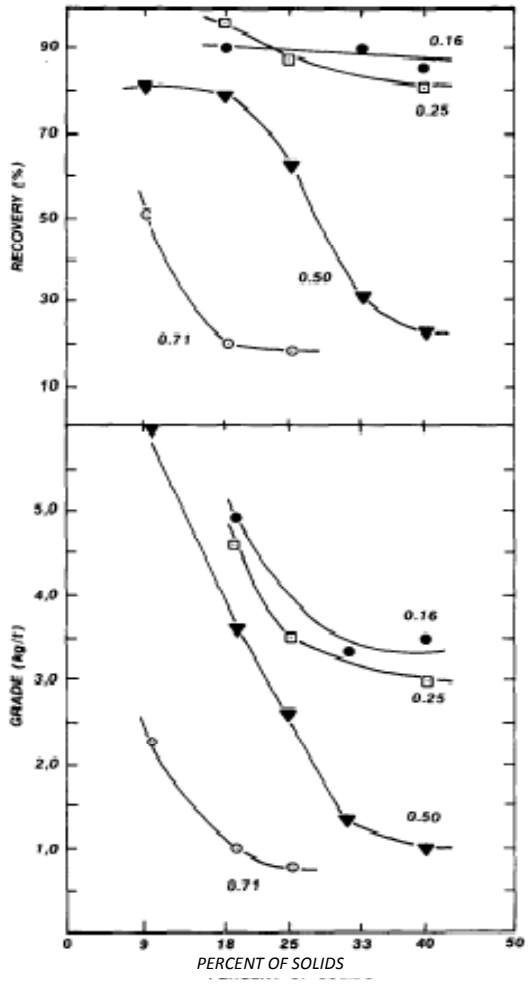

Figure 3.1: Recovery and grade of gold in concentrate as a function of solids present and gold size (mm): 3.6 lpm of air, 1200rpm, 167g Au/t feed (Lins and Adamian, 1993).

Dicresyl monothiophosphate (DCMTP) was used to achieve recovery of native gold against sulphides at a pH above 7 in some specific ores (Nagaraj *et al*., 1991). Basilio *et al*. (1992)

suggested that DCMTP does not have effect on the floatability of pure gold as such, and infra red spectroscopic measurement confirming this. The improved gold recovery was linked to silver-DCMTP interaction in further studies (Nagaraj *et al.*, 1992). It was shown by X-ray photoelectron spectroscopy (XPS) that more DCMTP was adsorbed, and higher recovery observed, when the percentage of silver alloyed with the native gold was higher. Hence, only silver-bearing native gold will respond to DCMTP. The interesting context here is that adsorption on the alloy surface is synergistic. It can therefore be projected that alloys in the PCB mixture will respond to a collector as much as one of its constituent elements interacts with that collector.

Forrest *et al.* (2001) using a range of collectors (Table 3.2) at varying pH on a free-gold bearing copper-pyrite ore, obtained free gold recovery from the sulphides at d_{90} of 106 µm. While chalcopyrite recovery was almost independent of pH in the range 8 – 13, and pyrite recovery drop with increasing pH over the range (see Figure 3.2), gold grade shot up above pH 11.5 (Figure 3.3) for aeroflot 7249 and aeroflot 208. Selectivity for free gold by these collectors was concluded for the gold grade increase at pH above 11.5, since pyrite was depressed and chalcopyrite recovery remained almost the same over the pH range.

Table 3.2: Collector reagents in Forrest *et al.* (2001)

Reagents	Chemical Family
S-5688	Dicresyl monothiophosphate
Aero 7249	Di-isobutyldithiophosphate/ di-isobutylmonothiophospahte blend
Aerofloat 208	Dithiophosphate
Aero 6697	Di-isobutylmonothiophosphate
PAX	Potassium amly xanthate

Although reports on flotation of metals have concentrated more on those that occur in native forms which are the real situations in flotation operations, many metals and alloys in the PCB fines that do not naturally occur in native forms can also be expected to respond to collectors. Auger electron spectroscopy (AES) and XPS studies of the chemisorbed xanthate monolayer on chalcocite and galena showed the same chemical environment for the metal atoms in the substrate and the monolayer xanthate (Buckley and Woods, 1990, 1991; Shchukarev *et al.*, 1994). This indicates direct interaction with the metal atoms in a substrate, and implies that

under adequate conditions, the metals will interact with collectors and float. However, the potentials at which a collector compound will form on a pure metal and on its mineral compound are expectedly different (Woods, 1996).

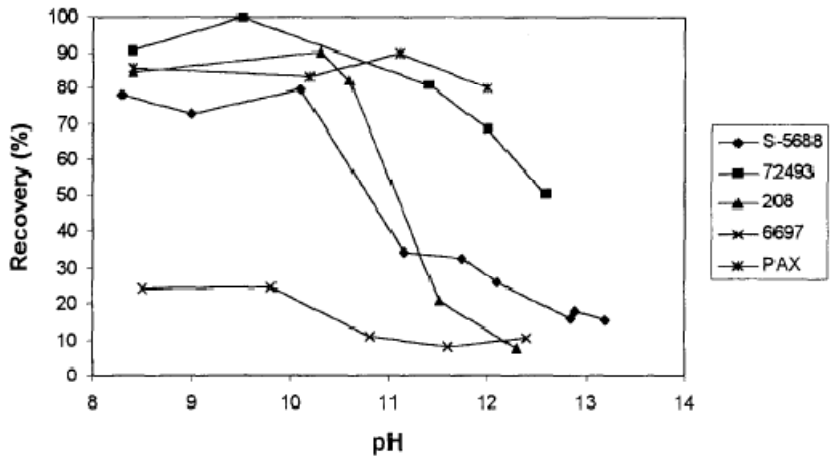

Figure 3.2: Effect of pH on pyrite recovery (Forrest *et al.*, 2001)

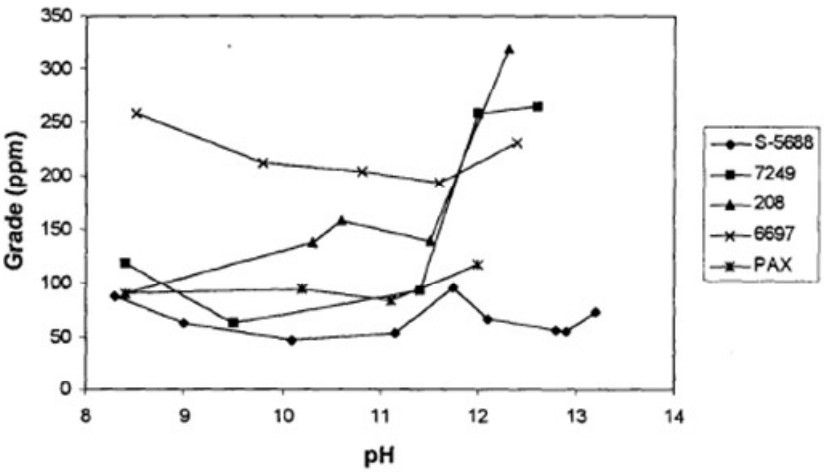

Figure 3.3: Effect of pH on gold concentrate grade (Forrest *et al.*, 2001)

As in conventional mineral processing, activation with $CuSO_4$ should also apply for particles (such as of zinc) whose collector-metal compounds have fairly high K_{eq} (dissociation constant) which makes their surface product fairly soluble and unstable. Possibility of unselective activation can be very important in a pulp with such diverse constituent. Mercaptans, such as

sodium mercaptobenzothiazole (SMBT), are a selective collector of native copper (Wills, 1997) and it can be expected that this can be applied in obtaining a selective metal fraction.

In the event of certain alloy particles having tarnished or oxidised surface layer, sulphidation activation should be applicable as with conventional minerals to make such particle interact better with sulphydryl collectors. By addition of sodium sulphide (Na_2S), hydrolysis to sodium hydroxide and hydrogen sulphide occur (Wills, 1997). The hydrogen sulphide dissociates giving hydrosulphide ions (HS^-). These adsorb and dissociate at the surface of the particle, causing sulphur ions to pass into the crystal lattices:

$$Na_2S + 2H_2O \rightleftharpoons 2NaOH + H_2S \quad . \quad . \quad . \quad . \quad . \quad 3.6a$$

$$H_2S \rightleftharpoons H^+ + HS^- \quad . \quad . \quad . \quad . \quad . \quad . \quad . \quad 3.6b$$

$$HS^- \rightleftharpoons H^+ + S^{2-} \quad . \quad . \quad . \quad . \quad . \quad . \quad . \quad 3.6c$$

This gives a pseudo insoluble sulphide surface, allowing interaction with sulphydryl collectors. Careful dosage of this sulphidisers is very important because excess HS^- ion at a surface gives the particle a high negative surface charge. This prevents adsorption of anionic collectors, causing depression, while too little dosage will not maximize the conditioning effect desired (Wills, 1997; Lee *et al*., 1998). The dosage required for a system will depend on the pulp pH. At high pH values, equation 3.6b and 3.6c proceed farther to the right, generating the depressant ions. Because of the possibility of altering (increasing) pulp alkanility due to NaOH dissociation from Equation 3.6a, sodium hydrogen sulphide (NaHS) is preferred to sodium sulphide for sulphidation.

In the event of comminution, it is possible that the particle surfaces will be tarnished or oxidised. In this regard, SMBT has been found effective collector for oxidized copper and tarnished ores (Wills, 1997). Also, from general flotation of oxide and silicate minerals, collectors that mainly physisorbs (interacts electrostatically), such as amines and sulphonates can be used.

Flotation of glass fiber can also be conceived, considering the flotation of quartz from heamatite. A reverse flotation of heamatite employs amine at pH 6-7. The amine adsorb on the negatively charged quartz particle to float, leaving the heamatite particles that are relatively neutral at that pH range (Fuerstanau and Healy, 1972).

Another approach floats quartz activated with calcium ion at pH 11-12 with a soap collector, while using starch to depress heamatite. Soap application which can also have the effect of gamma depression (see Section 3.5.2.4) is notable here, but isolating the activity or interactions may not be easy in this very diverse material mixture: depression is already involved, and influences on other particles exist. Interwoven and complicated reagent effects are not unexpected in a sample of this type.

As addressed above, different collectors used with native metal and alloys, and tarnished ores, in conventional minerals processing and in various investigations, can be expected to interact with the metals and alloys in the PCB mixture – xanthates, amines, SMBT are all candidate collectors. However, appropriate pH is critical to reagent-surface interaction.

3.3.1 Selectivity by pH Control

Pure water has a dissociation constant of 10^{-14} in which $-\log [OH^-] = -\log [H^+] = 7$, the pH of neutral water. The concentrations of OH^- and H^+ vary in proportion to maintain the equilibrium constant at other pH values. In aqueous medium, OH^- and H^+ are potential determining ions for particles of oxide minerals and those with bases in their dissociation products, such as carbonates (Kelly and Spottiswood, 1989). The pH of the medium therefore determines the surface charges or neutrality (point of zero charge, or PZC) of the suspended particles. Response to ionic collectors is a function of surface charge condition, and hence a function of pH. This is a basis of selectivity by pH control.

Hydration of the surface and the stable surface species similarly depends on the pH. With iron, for example, the Eh-pH diagram for Fe-O-H system indicates $Fe(OH)_3$ as the stable specie for most of the positive potentials at alkaline pH (see Figure 3.4). This frustrates formation of the less stable metal-collector compound with xanthate collectors at high pH values. Pyrite, for example, will therefore float under xanthate only at pH around 4 or below (Wills, 1997). With

lead, the lead-xanthate compound prevails till about pH 8, above which the stable lead-H_2O specie predominates and lead or the lead compound, say galena, get depressed.

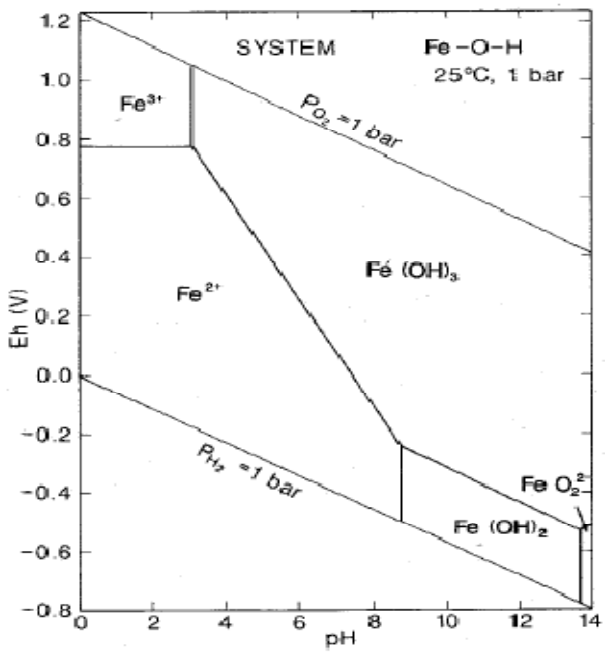

Figure 3.4: Fe-O-H potential-pH diagram (Douglas, 1988)

Parallel bases for selectivity by pH variation can be expected for the corresponding metallic alloys in the PCB mixture. Surface specie as a function of pH of metallic elements should be as in the various Eh-pH diagrams. Differences in the systems are, however, notable. The actual Eh-pH-species diagram that will apply in this multicomponent system will not be the ones for the single metal-water system. Diagrams or data for a ten-element or more system as the PCB mixture analysis will require are scarce in literature. This will be a major challenge to the easy prediction of surface species. However, the window of stability of certain species in the general aqueous system at natural potentials and room temperature is fairly wide to allow some projection. The presence of heavy metals, which can activate particles that should not float at certain pH, remains another source of possible complication in making projections based on pH.

Pulp pH can be varied by the adding acids, bases or salts. Acids are neutral molecules, such as HCl, H_2SO_4, H_2S, CH_3COOH, which dissociate in aqueous solutions giving H^+ cations. Bases are crystalline solids such as NaOH, KOH, $Ca(OH)_2$, $Ba(OH)_2$, whose anion is OH^-, or neutral

molecules such as NH_3, and CH_3NH_2 that forms proton acceptors and causes increase in the OH^- proportion, when dissolved in water. Salts are generally electrolytes whose ions are neither H^+ nor OH^-, but there are acid or basic salts whose aqueous solution is not neutral because they cause proton concentration increase or decrease, respectively, on dissolution. NH_4Cl, for example, is an acid salt, with NH_4^+ cation, which is a proton donor in water:

$$NH_4^+ + H_2O \rightleftharpoons NH_3 + H_3O^+ \quad . \quad . \quad . \quad . \quad . \quad . \quad . \quad . \quad 3.7$$

Also Na_2CO_3 in aqueous solution gives CO_3^{2-} which is a weak base – a reluctant proton acceptor in water:

$$CO_3^{2-} + H_2O \rightleftharpoons HCO_3^- + OH^- \quad . \quad . \quad . \quad . \quad . \quad . \quad 3.8$$

In flotation practice, sulphuric acid [H_2SO_4] and lime [$Ca(OH)_2$] are cheap and effective reagents used to increase acidity and alkalinity, respectively, in pulps. When the depressant effect of lime at high pH can be consequential, Na_2CO_3 is also used instead. Collector stability, as a function of pH is also of importance in pH control and pH may not be varied unilaterally. In regulating pH of PCB fines pulp with acids or bases, it is necessary to first establish the natural pulp pH and to observe its stability with time. Varying pH with time, or buffering when trying to regulate the fines pulp pH from the natural pH, is not impossible in such a complex mixture.

3.4 SELECTIVE WETTING OF PLASTICS FOR PCB FINES FLOTATION APPLICATION: GAMMA FLOTATION

Plastics are naturally hydrophobic. Selective wetting to effect separation of plastics by flotation has been demonstrated under four methods (Shent *et al.*, 1999):

(i) physical conditioning, in which hydrophilic functionalities such as =O, –OH and –COOH, are grafted into polymer chains at the surface usually by plasma treatment;

(ii) selective adsorption of wetting agents or chemical conditioning;

(iii) selective hydrophobic modification, also a chemical conditioning, in which a surface conditioning agent is selectively solubilised in the plastics so that it penetrate to a shallow depth on the surface of some plastics; and

(iv) gamma flotation.

Gamma flotation is the most applied of the four methods and still best understood. It is based on the critical surface tension of wetting of the solids (Buchan and Yarar, 1995), similar to the original Zisman's critical surface tension concept (Zisman, 1964) described by Alter (2005). The critical surface tension of wetting for a solid (γ_C) is the minimum surface tension of a liquid that will not wet the solid. That is, pure liquids or liquid solutions with surface tensions below this value will wet the solid. Hence, by reducing the surface tension of a liquid (γ_{LV}), such as water, to a value between the critical surface tension values of two plastic particles in a mix, say, γ_{C1} and γ_{C2}, so that:

$$\gamma_{C1} < \gamma_{LV} < \gamma_{C2}, \quad . \quad . \quad . \quad . \quad . \quad . \quad . \quad 3.9$$

the particles of the plastic with $\gamma_C = \gamma_{C2}$ become wetted, while the particles of the other plastic, with $\gamma_C = \gamma_{C1}$, remain hydrophobic and float with air bubbles. Buchan and Yarar (1995), using 190 ppm methyl isobutyl carbinol (MIBC) as frother, 20 % methanol and 80 % H_2O, achieved an aqueous solution with surface tension of 40.8 dynes/cm, to effect the flotation separation of PVC (γ_C = 39 dynes/cm) from PET (γ_C = 43 dyne/cm) which was wetted and sank. At the pulp density of 1.0 % and pH 11, PET recovery to float was 0 %, while the recovery of PVC reached 92 %.

Shen *et al*. (2002) demonstrated the adsorption mechanism. Methyl cellulose was used for selective chemical conditioning of the surface of seven plastics. Separation into three groups of plastics was achieved. Van der Walls attraction-based physisorption between the numerous polar groups in methyl cellulose and some of the plastics was used to explain the selective adsorption and wetting, as the polar groups in some of the plastics were oriented towards the aqueous phase. Surface tension effect was ruled out as methyl cellulose cannot reduce the surface tension of water to the critical surface tension of wetting, γ_C, of the plastics wetted (see Figure 3.5). The conclusions of the explanation may be debated given that a surface conditioning depressant having hydrophobic non-polar group can as well impart flotation (Alter, 2005).

The work by Fraunholcz *et al.* (1997a, 1997b) is an extensive fundamental research on plastics flotation involving five classes of reagents, as shown in Table 3.3. The work concluded that the effect of non-ionic surfactant on plastic wettability appears to be governed mainly by gamma flotation. It stated further that the inorganic reagents did not affect plastic flotation, while the low molecular weight complex compounds also do not adsorb sufficiently to effect depression. Cations (including Na^{+}, Ca^{2+}, Mg^{2+}, Fe^{2+}, Fe^{3+} and H^{+}) were said to have significant effect on the adsorption of the non-ionic weak acid and the anionic macromolecular depressants. Due to the low reactivity of plastics, the influence of pH over the range of 5-12 on plastic flotation was reported to be insignificant (Shibata *et al*., 1996).

For the plastics in PCB grinding mixture, non-ionic surfactants based gamma flotation appears more straightforward and clearer to apply. The surface tension of the pulp is simply reduced below the critical surface tension of wetting for some of the plastic constituents (see Table 2.3). The non-ionic surfactants can also contribute to frothing. As it is necessary to be able to delineate the effect of reagents addition in a sample, the other physical and chemical conditioning methods are not straightforward for a complex mix of this sort. As mentioned, the effects of ionic and weak acid macromolecular depressants depend on many cationic species in the pulp. These effects will be difficult to isolate in a complex pulp such as the pulp of PCB comminution fines, and can even impair flotation of the metallic values afterward.

Equations 3.2 and 3.3 indicate that selective wetting of the plastic particles requires careful choice and dosage of the non-ionic surfactants. Some surfactant can depress surface tension so much that the bulk becomes difficult to float. Also, the surfactant type should be such that desired wetting is achieved with moderate dosage. In the work of Buchan and Yara (1995), 20 % methanol in water was used to reduce the surface tension to 40.8 dyne/cm. This will represent a significant reagent load and consumption. Moreover, the pulp density of 1.0 % used is too dilute and reagent dosage may still shoot up at real industrial pulp densities. With methyl isobutyl carbinol, MIBC, about 200 ppm reduces surface tension to 50 dynes/cm (Buchan and Yara, 1995). Figure 3.5 shows Tergitol 15-S-7 to be more effective in reducing the surface tension below 35 dynes/cm at 20 ppm. Such can, therefore, be a better candidate reagent.

Table 3.3: Reagent investigated by Fraunholcz *et al.* (1997)

Class	Names	**Abbreviation**
1. Non-ionic surfactants (frothers)	Diacetone alcohol	DAL
	Methyl isobutyl carbinol	MIBC
	Tripolypropylene glycol methyl ether	PPG3
	Iso-octanol	IOL
	Pine oil (a-Terpineol)	POIL
	Polyethylene glycol dodecyl	$C_{11}EO_8$
	Nonylphenol polyglycol ether.10EO	$C_{9+6}EO_{10}$
2. Electrolytes	Na_2CO_3	
	NaCl	
	$NaNO_3$	
	$MgCl_2$	
	$CaCl_2$	
	$FeCl_2$	
	$FeCl_3$	
	HCl	
3. Inorganic depressants	Sodium disulphite	NaDS
	Sodium hexa meta phosphate	NaPh
	Sodium silicate	NaSi
4. Low-molecular-weight complex compounds	Malic acid	MAC
	Tartaric acid	TAC
	Citric acid	CAC
	1,2,3-trihydroxy benzene	THB
	2,4,6-trihydroxy benzoic acid	THBA
5. Macromolecular wetting agents	Arabicum gum, composition: m:n:p:q_1:1:3:3	ARG
	Na-carboxymethyl cellulose	NaCMC
	Na-lignin sulfonate	NaLS
	Potato starch	PST
	Quebracho	QUE
	Tannic acid	TNA
	Polyvinyl alcohol	PVA
	Na-polyacrylic acid	NaPAA
	Polyacrylamide	PAM
	Polyethylene oxide	PEO

Different surfactants have been marketed under the trade name Tergitol by Union Carbide Corporation and Dow^R. Dow^R produces nonylphenol ethoxylates (NPEs) and secondary alcohol ethoxylates (SAEs) as Tergitol NP and Tergitol 15-S series, respectively, and ethylene oxide/propylene oxide (EO/PO) copolymers as Tergitol L, XD, XJ and XH series (Dow^R Surfactants). Union Carbide Corporation has other codes and series for similar products, such as TERGITOL® X-series for the EO/PO (TERGITOL® XDLW). In case of availability and cost constraints, these products are generically nonionic surfactants. Other products of these generic

constituents, such as Betamin 127A and Betamin 65 of Betachem (Pty) Ltd., South Africa, are good candidate materials for investigation. From Betachem material safety and data sheet (Betachem MSDS, 2007), Betamin 127A is ethoxy nonyl phenol, while Betamin 65 is triethoxy tetradecane (a multiethoxylated alcohol, i.e. an alkoxy substituted paraffin). Common soaps (carboxylate salts) and detergents (alkyl phosphates, etc) will also achieve wetting, with cost advantages, but this are ionic surfactants, and physisorption effect can compound the response.

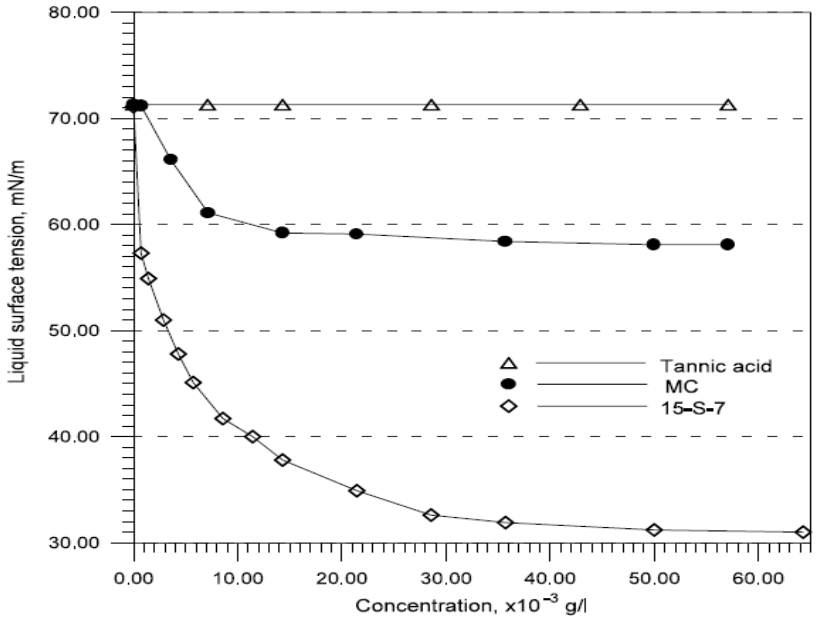

Figure 3.5: Surface tension versus concentration of three reagent solutions: Tannic acid, MC – Methyl Cellulose, Tergitol-15-S-7; 29.4 mg/l MIBC; pH 9.2; 25^{o}C (Shen *et al.*, 2002)

3.5 PROBABLE FLOTATION SCHEMES

From the foregoing previews, probable flotation schemes in this application can be divided into two: natural hydrophobic response and chemical conditioning schemes. These are described as follows.

3.5.1 Natural Hydrophobic Response (NHR) Schemes

The particles in the PCB fines sample being so diverse, it can be expected that some should exhibit natural hydrophobicity while some will be naturally hydrophilic. This is the hypothesis

upon which a collectorless flotation can be proposed as a starting scheme for the flotation of this sample. Relative to water's surface tension, plastics have lower energy surfaces and it can be projected that the plastics along with other relatively low free surface energy (LFSE) particles will be hydrophobic and should report to the float, while metals with other high free surface energy (HFSE) particles will be wetted (Gupta and Yan, 2006), and report to the sink. The scheme will therefore represent a reverse flotation in respect of the metallic values. It will essentially separate the HFSE from the LFSE particles. Table 3.4 shows representative surface tension values of some materials.

Table 3.4: Approximate surface tension of some materials at room temperature (Adamson, 1990)

Material	γ (N/m)*
Paraffin	0.025
Graphite	0.110
Halite (NaCl)	0.230
Flourite	0.450
Magnesia (MgO)	1.000
Gold	1.800
Alumina	1.900
Diamond	5.600
Water	0.072

*1000 N/m = dynes/cm.

3.5.2 Chemical Conditioning Schemes

3.5.2.1 Bulk metallic flotation (BMF)

Based on the recognized interaction of xanthates with metal surface, the projection here is to condition the pulp with bulk collector, such as butyl or amyl xanthate, to achieve a float of all the metallic particles into a float fraction. Depending on the extent of recovery observed from the natural hydrophobic response, this scheme can be applied directly on the bulk sample or after the NHR scheme.

3.5.2.2 Sulphidation activation

There is the possibility that metallic particles surfaces can be tarnished or oxidised in the event of comminution. The extent of metallic response obtained from the bulk metallic flotation can be indicative of this. In this case, sulfidation is a conceivable approach to activate such particles to xanthates. Sulfidation is discussed in Section 3.3 and NaHS can be considered as the reagent of choice.

3.5.2.3 Selective metallic flotation (SMF)

Depending on clarity of the response to reagent, some selective metallic flotation can be projected based on reagents known to be selective of certain metallic values. Mercaptobenzothiazole (MBT) is recognized as a selective collector in flotation of tarnished or oxidized lead and copper minerals (Fuerstenau and Raghavan, 1986; Numata *et al.*, 1998). The copper and lead particles in the PCB comminution fines can also be conceived as tarnished (a basis for sulfidation as explained above). The proportions of copper and lead in the PCB comminution fines sample are relatively high. These are good rationales upon which to try selective flotation with MBT. However, the selectivity will depend on the extent of the natural hydrophobic response. This will determine the order of implementing the selective schemes. The selective conditioning may have to be carried out on the sink of the NHR or on the float of the bulk metallic flotation. Careful choice and use of depressant may also be needed to enhance the selectivity. NHR particles, or residuals thereof, may need to be depressed to prevent contamination of intended metallic fraction. Choice of depressant in this type of system will also demand some careful experimentation.

3.5.2.4 Macromolecular and gamma depression

Achieving selectivity often demands selective depression. Generally, depressants selection takes note of the particles in the system versus collector suite. In classical mineral processing, chemical depressants such as cyanide and dichromate solubilise collector-particle surface compound and frustrate air attachment (Wills, 1997). This will not regulate particles floating under their natural hydrophobicity. Besides, the pulp here is complex enough and reagent addition must be carefully regulated so that more active reagents are not added to the system if it can be avoided.

Organic macromolecular depressants, such as starch, tannin and quebracho are non-ionic and can be regarded as less chemically reactive as they tend to smear and cover particles physically, as in slime coating, to insulate them from reagent activation (Wills, 1997). Along this line, the impression will be that these reagents will be bulk depressants. However, selective chemisorption has been observed, such as in starch depression of heamatite from quartz activated to soap collector by calcium ions at pH 11 – 12 (Fuerstenau and Fuerstenau, 1982). Without the starch, heamatite would also float under this condition.

The work of Shent *et al.* (1999) mentioned in Section 3.4, showed the selective adsorption of methyl cellulose (anionic) on some plastics. The explanation was based on physisorption by Vander der wall attraction between the numerous polar groups in methyl cellulose and some of the plastics. Broad acid-base interaction is becoming more convincing in explaining polysaccharides adsorption (Laskowski *et al.*, 2007). In depression of floatable carbonate and silicate gangues in sulphide flotation, anionic organics, such as carboxymethyl cellulose (CMC) are mostly used. Non-ionic ones are also used but high dosage levels are required, thereby depressing the sulphide (Bulatovic, 1999). For possibility of effectiveness at moderate dosage, without causing bulk depression, CMC can be considered as a probable macromolecular depressant in this investigation.

From the idea of gamma flotation in plastics (Section 3.4), reduction in surface tension can be used to achieve depression in the PCB comminution fines pulp. This surface tension (γ) based depression concept can be succinctly described as gamma depression. By lowering the surface tension of the pulp with appropriate surfactants, wetting becomes more favorable; the higher the dosage, the lower the surface tension (Equation 3.2), and the higher the overall depression. This will easily regulate natural hydrophobic flotation. For this purpose, non ionic surfactants (Table 3.2) can be used. This will give the advantage of no further addition of ions into the pulp. Depression alternatives for the PCB comminution fine pulp may therefore be within these two options – macromolecular and gamma depression.

Before this proposition is closed, gamma depression appears to oppose particle-bubble attachment in the same pulp. Gamma depression requires reduction of surface tension of the

aqueous medium to effect wetting of some of the particles, whereas bubble attachment is also desired to effect flotation of some particles. The condition for wetting is:

$$\gamma_{LG} + \gamma_{SL} < \gamma_{SG} \quad . \quad . \quad . \quad . \quad . \quad . \quad . \quad . \quad 3.10$$

The opposite is the condition for bubble attachment:

$$\gamma_{LG} + \gamma_{SL} > \gamma_{SG} \quad . \quad . \quad . \quad . \quad . \quad . \quad . \quad . \quad 3.11$$

where, γ_{LG}, γ_{SL} and γ_{SG} are the liquid-gas, solid-liquid and solid-gas interfacial tensions.

It appears that lowering of the medium's surface tension γ_{LG} to achieve wetting is to forfeit bubble attachment, as it becomes difficult for the sum of γ_{LG} and γ_{SL} to exceed γ_{SG} again. Some clarification is required to sustain the prospect of the projected process.

Plastics generally have low γ_{SG}, lower than that of water. This easily satisfies Equation 3.11, so that they hardly wet. However, the magnitudes of γ_{SG} and γ_{SL} for plastics are such that Equation 3.11 can be easily reversed by halving the γ_{LG} for water with surfactants. This will satisfy the conditions of Equation 3.10.

For metallic particles and minerals, with much stronger interatomic bonds than plastics, the γ_{SG} is orders of magnitude greater than γ_{LG} of water. Compare gold to water in Table 3.4 which shows figures of surface tensions of some materials. Equation 3.10 is therefore easily satisfied and they normally wet. The value of γ_{LG} for water is relatively insignificant in this case, regulating it by the absence or presence of surfactant will not reverse Equation 3.10 to make such particles hydrophobic. This is why hydrophobicity is imparted on high energy surfaces by directly modifying such surfaces rather than the surface tension of the medium. This is what the collectors do. By chemically reacting with the high energy surface, or electrostatically attaching to it, a pseudo hydrocarbon surface is formed with γ_{SG} below that of the medium. This prevents wetting.

The application to gamma depression is that bubble attachment will still occur as long as the surfactant dosage does not lower γ_{LG} of the medium so much that it is impossible for the

hydrophobic species adsorbed on the particles to meet the condition of equation 3.11. A useful but scarce data to regulate the dosage will be surface tension values (γ_{SG}) of the surface-collector species to allow a projection of the minimum γ_{LG} of the medium for a specific collector. However, the non-polar hydrocarbon chains are hydrophobic. Hence, moderate reduction of γ_{LG} of the pulp will still accommodate flotation of particles on which such surfactants are adsorbed, or particles that are of sufficiently low surface tension values (γ_{SG}). Surfactants (collectors, frothers) have always caused some reduction in medium surface tension, anyway. Yet, particle bubble attachment still occurs in flotation pulps.

3.5.2.5 Cationic conditioning

At a given pH, particles in a pulp develop positive or negative charges or remain neutral (at their point of zero charge). Cationic collectors can therefore be expected to achieve a bulk collection based on surface charges, adsorbing on the negatively charged particles to float. This scheme can be conceived in further beneficiation of the NHR sink. Generally physisorption-based conditioning is considered not to be as selective as those based on chemisorption.

However, given the diversity of particles in this sample, any logical scheme is worth a trial. An obvious variable here is the system pH, which can help improve selectivity. Amines are the popular collector of choice, but with pH considered as a variable, the choice can be restricted to quaternary amines. The fact is that the ionization of primary, secondary and tertiary amines varies with pH so that the same dosage of this class of amines will show varying activity as pH varies, thereby complicating the basis for comparing the response based on pH variation. Quaternary amines, on the other hand, ionize completely at all pH values. Since the hydrophobicity imparted by these heteropolar organic compounds increases with increasing hydrocarbon chain length, the choice can be narrowed down to tetrabutlyammonium chloride, with the long chain butyl groups.

3.6 APPLICABLE RANGE OF KINETIC PARAMETERS AND SAMPLE CHARACTERISATION

The variety of the schemes presented underscores the unconventional flotation system this sample will present. Flotation variables are many – kinetics, reagent types and dosages. In

conventional mineral flotation investigations, there are known favorable operating regimes. This helps to narrow down the variables. However, this usual range may not be invoked for this application. Success of any of the schemes therefore depends on appropriate kinetics being established first.

In flotation kinetics, the determinants of rate of particle removal by bubbles in a flotation cell include gas flow rate, bubble diameter, cell volume, turbulence dissipation energy, fluid and particle densities, kinematic viscosity, efficiency of collection (which consists of efficiency of collision, attachment, and stability subprocesses), and of course the quantity of the particles to be removed that are present at a time (Pyke *et al*., 2003).

Fortunately, these variables are not all mutually exclusive, so that not all these need to be investigated. For a broad characterisation or description of the kinetic regime that will be appropriate for this system and the projected schemes, it will suffice to use three basic independent variables of air flow rate, impeller speed and pulp density. Other variables such as bubble size, pulp viscosity, and turbulent dissipation energy are functions of these basic variables. Other specific (material) characterisation that will be necessary here is in respect of liberation and chemical composition analysis of the sample.

Particle liberation in PCB CF reported in literature can be summarized as very good; 100 % below 600 µm, 500 µm, and 250 µm, as reported by various workers (Zhang and Forssberg, 1997; Wen *et al.*, 2005; Zhao *et al.*, 2004). The easy conclusion then is that -75 µm fraction will consist of sole material particles. This arouses suspicion about the figures quoted in literature, moreso that various authors differ. A basic liberation investigation of the fines will easily confirm if liberation is total or not in the fines, and provides a working evidence in this application. On the other hand, chemical composition characterisation is necessary to justify a method of choice for assay analysis in this work.

Background fact here is that analytical procedure for this sample are lacking in standard references (ASTM; ASTM, 2007; ISO). Studies and reviews have recommended and applied various analytical techniques, such as XRF, XRD, FTIR, Raman spectroscopy, thermogravimetry, wet assaying and fire assaying (Li et al 2004). While all of these techniques may not be applicable to this sample, wet spectroscopic techniques appear to be quite relevant

for the quantitative work that beneficiation recovery analyses demand. Assays from wet techniques are known to depend on the extent of the recovery of the target constituent to the leach liquor. Given the constitution of PCB fines, 100 % recovery of analytes may be difficult. When little experience is available with respect to the digestion of a matrix, comparison of a number of digestion techniques is recommended (Henryk, 2003). An investigation of comparative digestion techniques can be informative for the assaying requirements in this investigation.

3.7 INVESTIGATION OBJECTIVES

From the foregoing discourse, specific objectives towards this investigation are to:

i. Carry out qualitative liberation analysis of the −75 µm PCB comminution fines to establish if the constituent particles are sole material particles or if composite particles still persist at this size range of PCB comminution product.
ii. Carry out comparative wet digestion analysis to establish the effect of relevant digestion techniques on the wet assay values of PCB comminution fines.
iii. Carry out trial and full experiments to establish favourable range of flotation kinetic parameters applicable in the prospect of PCB comminution fines flotation.
iv. Investigate applicability of flotation for the beneficiation of PCB comminution fines by employing logically probable flotation schemes that are based on expected differences in natural hydrophobicity of particles in the fines sample and on responses to certain chemical conditioning.

Essentially, the third objective must be pursued simultaneously with the fourth as the kinetics must be observed under a scheme. This is the rationale for the preliminary trials, which will have to set out from uncertain kinetic regime under unproven scheme. Some ancillary investigations that may ensue in the course of these investigations, towards understanding the behaviour of the system better, will be attended to, while not deviating too much from the set objectives.

In summary, the investigation will offer material and kinetic characterisation insights relevant to PCB CF flotation prospects. It will establish how the sample responds to the reasonable flotation schemes based on general froth flotation understanding. It will surely provide a basis for pursing

further interests in this direction. Detailed work approach towards realising these objectives, as well as secondary investigation objectives that ensued, are presented in the following chapter.

4.0 MATERIALS AND METHODS

4.1 INTRODUCTION

On the basis of the reviews and objectives presented in the previous chapters, the materials and methods for this investigation are presented in this chapter. Other investigations that are relevant, consequent upon or supplementary to the primary investigations are also presented.

4.2 PCB COMMINUTION FINES GENERATION

About 250 kg of assorted of eol populated printed circuit boards from PCs, cellphones, radio equipment and switchboards were obtained. The boards mostly spanned the period 1989 to 2002, PI to PIV and different makes such as Cyrix, Intel Celeron, IBM, Octek, and Socket 3, 7 and 8. Most of the boards are multilayered (with maximum of four layers), with few older single-sided types. Components such as capacitors, liquid crystal displays and batteries which are usually rich in hazardous substances (Cui and Forssberg, 2003; EU, 2003) were first removed from the boards before comminution.

The boards were first cut with a bench guillotine (employing a shearing action as in shear shredders) into roughly 4 cm x 6 cm fragments appropriate for the choke of the swing hammer mill (Eriez magnetics MACSA Pedestal Type, Model 300) used for the fine crushing and grinding. The comminution was basically the result of impact, with shear, compression and abrasion, until a particle get below the screen size in at least two of its dimensions and favourably oriented to pass through. The size reduction was done in stages, starting from 20 mm closed fine crushing. Product from this stage was screened into size classes. The −13200 µm + 1180 µm fraction was removed from the stream as it consisted of sufficiently liberated metallic and plastic pieces that are amenable to eddy current separation, gravity air classifier and magnetic separation.

The +13200 µm fraction, containing almost bare board fragments go through closed comminution again at 8 mm, 5 mm and 2 mm screens to liberate the copper traces, solders still locked in the board vias, pin insertions, board fibres and resins. The −1180 µm fraction from the first stage was mixed with the final product from the 2 mm grinding, and the −75 µm fraction was screened from the final −2 mm fraction. Hazards associated with this operation were well appreciated, and adequate personal protective equipment was used. A documentary of the sample generation is shown in Appendix 1.

The total sample obtained was split with vibratory rotary splitters to 12 subsamples of average mass 5.6 kg (relative standard deviation = 4 %). These batches were split further down as required for each investigation.

4.3 SAMPLE CHARACTERISATION

4.3.1 Particle Size Distribution and Density

With a set of sieves of 105 µm, 75 µm, 53 µm and 38 µm aperture diameters, about 200g true split samples were shaken using Electrolab Electromagnetic sieve shaker, Model EMS-8, at the maximum power setting of 20. After every ten minutes of shaking, the sieve set was dissembled to confirm when all the sample has passed through the 105 µm. In this manner a period of 120 minutes was concluded as the proper screening period for this sample at that power setting. Repeat batch sieving was therefore done over this period to obtain a good representation of the particle size distribution (PSD) of the sample generated. This also gave fractions with narrower PSDs of −75+53 µm, −75 µm +38 µm, −53+38 µm, and −38 µm, for other investigations.

A column of PCB CF was observed to compact on vibration. The apparent volume therefore depends on how packed the volume is. Densities of the generated sample were therefore determined as true density, also as ‘loose bulk density’ and ‘tapped bulk density’ after the procedure for solids that compact, such as powdered milk (Svarosky, 1987; Niro A/S, 2009). Loose bulk density is based on a given volume loosely and gently filled with the sample and weighed, while tapped bulk density is based on volume compacted by gentle impacts on hard surface until height in a beaker remains constant. Tapped density is also quoted as ‘1000 tapped

density', although for the PCB CF, the height of the column stabilise well before tapping 100 times.

A milliliter-graduated 100 ml cylinder was gently filled with sample to the 100 ml mark. The volume mark of this sample was obtained after tapping 200 times, and the weight of the sample finally obtained. For the true density, the true volume of a known mass of sample was obtained as displaced liquid volume. Samples of 20 g and 10 g were made into suspensions in a milliliter-graduated (100 ml) narrow cylinder, using water from a known volume in graduated cylinder. The density determinations were done in triplicates.

4.3.2 Liberation Assessment and Particle Shape Characterization

Qualitative liberation assessment of the fines was done by examining polished sections of the sample in two size ranges of −75+38 µm and −38 µm. Complementary observations were done with a Nikon Eclipse ME600 light microscope and a Jeol JSM 6300 scanning electron microscope. The electron microscope was operated at 30 keV to generate all useful lines under energy dispersive X-ray spectroscopy mode. To improve contrast between organic particles in the sample and the mounting medium in secondary and back-scattered electron modes, iodoform was embedded in the mounting resin. This increases the electron density of the mounting medium compared to the plastic particles.

The iodoform, 10 % by weight of resin plus hardener (Gomez *et al.*, 1984), was first dissolved in the resin before adding the hardener. The resin and hardener used – Eli-CAST FRF 676 – are cold setting combination products of Elite chemicals. This resin system was selected as it uses a slow hardener to prevent vigorous exothermic reaction with iodoform that was observed when faster hardener systems were first used. Another polished section was obtained from a sample mounted in clear setting resin to enhance natural colour contrast under light optical microscope. A micrograph from the clear mounting medium was used for circularity shape factor analysis of the particles, using ImageJ (version 1.42q). ImageJ is a public domain Java-based image processing program developed at the US National Institutes of Health (NIH, 2009).

4.3.3 Comparative Wet Spectroscopic Analysis

The total fines sample generated was split down in stages with rotary vibratory splitters. Approximately 50 g true split sample was taken, from which, after thorough mixing, samples for all the investigations were finally taken. This was done to eliminate sampling error as much as possible. A combination of reagent and environment to achieve total digestion was first sought. Hot aqua regia, and two other aggressive combinations were considered: HNO_3 + HF + microwave radiation and sodium peroxide fusion followed by HCl dissolution. The three conditions were designated as AR, HHM and SPF respectively.

1g sample was taken for AR and HHM digestion. The recipe for SPF is 0.5 g sample with 3.0 g sodium peroxide plus 1.5 g sodium carbonate. The mixture was heated over a gas flame in a zirconium crucible. This gives a vigorous exothermic reaction, charring red with a momentary flame, before it fuses into a liquid. The whole crucible was then immersed in concentrated HCl solution (25 ml of 32 % analytical grade HCl added to 100 ml deionised H_2O) to digest the fused sample totally.

For aqua regia digestion, 50 ml acid was added and the sample heated until the brown nitrous fume ceased and the fume became faint white (steam). The content was evaporated down slightly. About a total of another 30 ml acid was added and the heating cycle repeated. Heating to incipient fusion, as in recommended procedures (Babara, 2003; Henryk, 2003) was not done, because this produces fused particles that will not disperse on further addition of acid.

Digestion for each condition was done in duplicate. When necessary, undigested residue was filtered to obtain the analysis liquor. Inductively-coupled plasma-optical emission spectroscopy readings were done for each solution in triplicate and averaged. Inductively-coupled plasma-mass spectroscopy was used to analyse for Au, Ag, Pt and Pd separately with solutions from AR and HHM only. Averages of triplicate readings over duplicate samples were calculated. The SPF solution was not analysed for the precious metals, reasons expanded in Chapter 5. All the analyses were done with UIS Analytical Services, South Africa.

4.3.4 Thermogravimetric Analyses for Organic Constituents

Thermogravimetry (TG), along with other thermal techniques such as differential thermal analysis (DTA), has being reported as applicable to PCB composition analysis (Li *et al.*, 2004). The extent of applicability may be debated because of the diversity of the constituents. Many reactions can occur simultaneously and obtaining precise inflexions to enable useful characterisation of constituents may be difficult. However, being well established techniques, an exploration may be worthwhile. This investigation will thus serve a first purpose of clarifying the applicability of TG for PCB comminution fines characterisation, upon which it can be adopted in characterisation of any of the constituents in this sample. A contrary conclusion will still be useful, so that PCB characterisation efforts will be aware of the techniques that are not applicable even if such have been well established for other types of samples.

The thermogravimetric analysis was performed both in air and nitrogen, from room temperature to 800 ^{o}C, in steps of 10 ^{o}C/min. The plots were presented together with the derivative plots. The analysis was done using a Mettler Toledo thermal analyzer with the STARe software, and sample size of 20 mg.

4.4 PRELIMINARY MICROFLOTATION INVESTIGATION

A 6 g sample from a small true-split sample was used for microflotation. This is larger than about 2 g often used in conventional mineral microflotation experiments (Bradshaw and O'Connor, 1996) to ensure representative sampling of a sample with such wide variety of material particles. Pulping was meticulously done in a small volume, as the sample tends to form globules (see section 5.2 and 6.3.1), before transferring the sample into the microflotation cell. Natural pulp pH was measured over time in a separate pulp every 5 minutes until 60 minutes, and then at 120, 240 and 360 minutes.

The Orion 3-Star Plus benchtop pH meter of Thermo Scientific was used for the pH measurement. The cell volume was 250 cm^3 and distilled water was used. The peristaltic pump setting was started at 130 rpm, (Bradshaw and O'Connor, 1996), but the particle turbulence observed was too high. The pumping setting was reduced to 100 rpm (Martinovic *et al.*, 2004). It was further reduced in stages to between 8 rpm and 40 rmp, equivalent to a pulp circulation rate

of 190 ml/min to 1350 ml/min respectively, according to the pumping rate calibration of the pump settings. Figure A.2 in Appendix I shows a picture of the microflotation cell employed. Air was used as the flotation gas at a rotameter setting of 4.5, which is 10 cm^3/min (Martinovic *et al.*, 2004), according to the flow rate calibration of the rotameter settings. Preliminary sodium isobutyl xanthate (SIBX) flotation at 50, 100 and 200 g/ton was performed. This was followed by collectorless flotation and another conditioning step using SIBX with 0.1 g detergent (sodium sulphonate active constituent) as wetting agent. Froth was collected at 90, 300 and 720 seconds of aeration. Inferences for detailed investigations were made based on visual and cumulative mass pull data.

4.5 APPLICABLE KINETIC REGIME AND THE NATURAL HYDROPHOBIC RESPONSE (NHR) FLOTATION SCHEME

With the backgrounds presented in Sections 3.5.1, 3.6 and 3.7, investigation of favourable kinetics in the prospect of froth flotation beneficiation of PCB comminution fines was pursued along with that of the feasibility of the natural hydrophobic response (NHR) scheme. The kinetic parameters of interest were narrowed to air flow rate, impeller speed and pulp density. The interaction of these factors influences other factors such as bubble sizes, pulp viscosity and turbulent dissipation energy, so that all the parameters need not be individually investigated to establish useful regimes.

A 3.5 *l* Leeds cell (supplied by University of Cape Town) was used for experimental reproducibility. The picture of the cell is shown in Figure A.3 (in the Appendix I). From the density characterisation result, a 600 g batch sample was chosen, but the response observed necessitated smaller sample size of 300 g (Section 6.3.2). Each true split batch sample from the total sample generated (see Section 4.2) was split down to subsamples of about 500 g and 50 g, followed by splits and combinations, so that each batch flotation sample were true split as much as possible. Reconstituted assays with regard to the target constituent elements of the flotation fractions from the investigations (Section 6.3.4, Table 6.2) give good indication of the representativeness of the batch samples obtained from the splitting.

Using distilled water, flotation pulps containing 300 g and 600 g sample were prepared per batch. This gave pulp solid concentrations of 9 and 18 wt. % respectively. The pulping was done by first forming a paste of the sample, introducing the paste into the cell, before filling up with water. This procedure was adopted because the sample floats if it is poured on water, while water simply displaces it if water is poured over it. This observation is linked to and the rationales explained in Sections 5.2 (density) and 6.3.1 (surface property). No collector was used.

It also turned out that no frother was needed (see Section 6.3.2). Air flow rates were varied over 500 and 1000 ml/min and impeller speeds over 300, 400 and 500 rpm for the 300 g. Only one condition was experimented for the 600 g pulp due to experimental observations (Section 6.3.2). Designations of the combinations of the experimental conditions are summarized in Table 4.1. Compared to natural mineral investigations with values such as 1200 rpm impeller speed and 1.8 to 5.4 *l*/min and higher aeration (Lins and Adamian, 1993; Forrest *et al.*, 2001; Miller *et al.*, 2006), the low regimes chosen for these parameters is based on initial microflotation (Section 6.2) and Leeds cell trials.

Table 4.1: Designations of experimental conditions for kinetic and natural hydrophobic response investigation.

Designation	Solid concentration (wt %)	Aeration (ml/min)	Agitation Speed (rpm)
E11A	18	500	300
E21A	9	500	300
E21B	9	500	400
E21C	9	500	500
E22A	9	1000	300
E22B	9	1000	400
E22C	9	1000	500

Above the range of 500 rpm agitation and 1000 ml/min aeration, the turbulence was too high. The quiescent zone was destroyed and the pulp surface swirled. The natural pulp pH was measured in the pulps, for record. Each experimental condition was run in duplicate and mass pulls were collected at one, four, 10, 18 and 30 minutes. Scraping was done every 30 seconds for the first four minutes, every minute from the fourth to the eighteenth minute, and every two minutes from the eighteenth to the thirtieth minute.

Filtration of the recovered fractions was not done to avoid loss of trace values to porous filter medium. Instead, floats were collected in stainless steel bowls while sinks were flushed into buckets, allowed to settle down (usually overnight), decanted and the sink fraction recovered. Float and sink fractions were oven dried, and the weight of fractions obtained thereafter. All the mass pulls were confirmed to repeat within 5 – 10 %. Repeats that fell outside this range, due to procedural imprecision, were rerun to ensure all the data conformed to this level of repeatability. The concentrate mass percent (the fraction of the feed remaining in the sink) was calculated as an inverse indication of the ratio of concentration for the reverse flotation. For a first check of the conformity of the response to flotation behaviour, the cumulative mass fraction recovered to float for all conditions was fitted to the classical first-order kinetics model in the form (Kelly and Spottiswood, 1989; Polat and Chander, 2000):

$$ln\left(\frac{R_m}{R_m - R}\right) = kt \quad . \quad . \quad . \quad . \quad . \quad . \quad . \quad . \quad 4.1$$

where R_m (%) is the maximum cumulative recovery, k (min^{-1}) is the rate constant, and R is recovery at time, t, in minutes.

Samples of the fractions were digested in hot aqua regia among other possible digestion routes (based on the comparative digestion analysis, Section 5.4). After thorough mixing, for the digestion, a 2 g sample was taken for every 50 g float fraction weight, or parts thereof. 1 g analysis sample was used for fractions that are well below 10 g in mass. The variation in quantity of sample taken for digestion is to account for variations in the total quantity, so as to ensure representative sampling of each float fraction. Undigested residue was filtered and weighed, while the final digestion liquor was made up to 250 ml with deionized water and about 5ml aqua regia. A quick assessment of the enrichment of metallic values into the sink was first done using the fractions of each sink sample digested as an indication of total metallic assay. Indication of recoveries was also computed based on this. Assays of selected elements were analyzed from the leach liquor with ICP-OES for a better indication of the deportments (concentrations) of the elements in each float fraction. The ppm assay of the leach liquor was converted to actual assay in percentages of the individual float fraction by using a divisor factor of 40, 80, 160 and 240 for

every 1 g, 2 g, 4 g and 6 g digested sample, respectively. The factors derive from the constant 250 ml final volume after digestion (see Appendix 1.3).

Specifically Ag, Al, Au, Ca, Cu, Fe, Mg, Ni, Pb, Pd, Pt, Si, Sn, Ti and Zn were assayed. The analysis was done on Perkin Elmer instruments with UIS Analytical Services, Centurion, South Africa. Elemental assays, enrichment ratios (ratio of the reverse flotation concentrate assay to feed assay) and recoveries over time into sink were computed from these data. Although batch feeds were obtained as true split samples, to eliminate error that may be due to any sample assay variation, the computations were based on reconstituted feed assays of each run.

4.5.1 Possibility of Formation of NHR Froth by Inherent Surfactant in the Sample

Based on the result from the NHR scheme, it was expedient to investigate the possibility of inherent presence of surfactant in the sample. Comparison of the dynamic froth stability of the pulp itself and that of filtrate from the pulp will indicate any frothing effect due to surfactant presence in the pulp liquid. Pulp filtrate surface tension measurement was also considered a necessary complement.

The dynamic froth stability tests were done using a Betachem modified Bikerman test rig (Bikerman, 1973; Betachem (Pty) Ltd., South Africa). The test unit uses a Watson Marlow peristaltic pump with about 30 mm (external diameter) pipe pumping capacity. The froth column is marked at a 5 *l* level for reference pulp or solution height before aeration. A picture of the test rig is shown in Appendix 1, Figure A1.6. A pulp containing 425 g sample in total volume of 5000 ml (the same solid concentration as investigated for the NHR 300 g scheme) and a clear filtrate from a pulp of the same solid concentration were used for the test. The aeration rate and the peristaltic pump setting were kept constant when measuring the frothing of the pulp and the filtrate. The dynamic froth height measurements were done at the constant rotameter setting of 20 (equivalent to about 4 *l*/min, as calibrated) and peristaltic pump setting of 30 on the test rig. The tests and measurements were repeated three times using different pulp filtrates.

The surface tension of the pulp filtrate was measured using the pendant drop technique in an automated contact angle goniometer with RHI 2001 imaging software (Rame-Hart Inc., 1999). Figure A1.7 (Appendix I) shows the goniometer stand. Instances of pendant drop of the filtrate

almost detaching from the accessory needle were created in front of the camera. The live image display around reference lines helped to ensure the needle was exactly vertical. At hydrostatic and interfacial equilibrium, the imaging software determines the profile of the pendant drop and, with the liquid type information provided, generates the surface energy value. The procedure, being straight forward, was repeated 10 times. Results from these approaches suffice for necessary concrete inferences. Higher precision surface tension analysis, such as capillary rise method, was therefore unnecessary.

4.5.2 Improving the Performance of the NHR Scheme

Based on observed recoveries and enrichment ratios from the NHR scheme, the possibility of improving on the performance was investigated. The material bulk density being low, the projection is to reduce turbulence in the pulp by variation or modification of some kinetic parameters. This is expected to reduce entrainment and entrapment of sink particles thereby improving recovery without compromising enrichment.

On this basis, effect of pulp solid concentration on mass pull was studied by varying pulp solid concentration of 300 g down to 50 g at the same aeration rate and impeller speed as under E21C condition (see Table 4.1). From this, a 150 g sample size was chosen, as there was indication that lower solid content minimises turbulence, but to another extreme lowers overall mass pull unacceptably. The impeller speed was kept at the low speed of 300 rpm, and aeration rate at 0.5 *l*pm. As this setting, the bubble sizes resulting from this impeller speed were large, with short residence time, visually bursting through the froth zone.

The aeration pipe of the impeller system was therefore modified as shown in Figure 4.1 to achieve bubble size reduction at the same aeration rate and impeller speed. The pipe diameter at the air outlet was reduced from 8 mm in the single aeration pipe to about 4 mm in four smaller outlet pipes, keeping total outlet area and in turn the exit air velocity effectively the same at constant aeration rate. Using the two aeration pipes, frozen frames of the resulting bubbles as they rise through clean water were taken for a visual indication of the effect of the modification on bubble sizes. The frames were taken using Sony digital camera DSC W55 at ISO 1000.

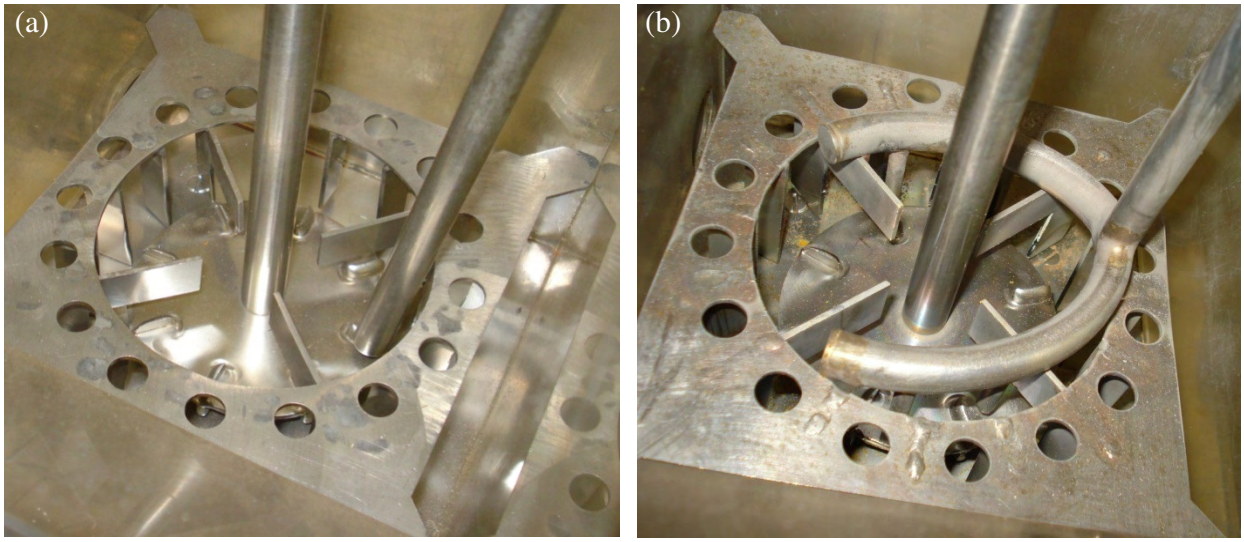

Figure 4.1: Impeller system of the Leeds cell used before (a) and after modification (b).

As trial runs indicated, the resulting kinetics with the modified impeller system achieved moderate turbulence but resulted in low mass pull rates. Further investigations were therefore carried out for a flotation period of 48 minutes, collecting float fractions F1, F2 and F3 at 18, 30 and 48 minutes respectively. The impeller speed was increased to 350 rpm after 18 minutes of flotation to improve efficiency of collision after a significant fraction has been pulled and mass pull became very slow with time.

This NHR improvement investigation and procedure is designated XNHR for ease of reference. At this kinetics (impeller speed and aeration rate), natural hydrophobic flotation over narrower PSDs of −38 µm, +38−75 µm and +75−106 µm were done. The necessary data for computing water recovery for each fraction were obtained following a careful procedure (see Appendix 1.3). This investigation was used to compare water recovery at varying particle sizes and to conclude on contribution of particle entrainment in water to the flotation response observed. The investigation also shows the size fraction most favoured by this kinetics. It also explores the possibility of applying froth flotation to larger size fraction (−106 + 75 µm) of PCB comminution product.

4.6 CHEMICAL CONDITIONING SCHEMES

The rationales for some of the specifics of the chemical conditioning investigations described below follow from the results and observations from previous investigations, which are discussed in Chapter 5 and 6. The following procedure applies to all the chemical conditioning schemes, except for Section 4.6.1, or when otherwise stated.

A sample mass of 150 g, and aeration rate of 0.5 *l*pm was used. 30 minutes of natural hydrophobic flotation was first performed before chemical conditioning of the residual sink. During the natural hydrophobic flotation, the impeller speed was 300 rpm for the first 18 minutes, and 350 rpm for the period 18 to 30 minutes. This is the condition used for the XNHR investigations. It is to maximize reverse recovery of the metallic particles before reagent conditioning. Conditioning time after each collector addition was five minutes, and when frother is added, another two minutes of conditioning was allowed to elapsed before aeration (Forrest *et al.*, 2001; Bravo *et al.*, 2004; Martinovic *et al.*, 2004), to ensure that the response was not impeded due to short conditioning time.

After conditioning, the impeller speed of 350 rpm was maintained and flotation continued for another 18 minutes. Skimming was done every one minute or every two minutes as mass pull rate changes; one minute for the first 8 minutes, and two minutes for the last 10 minutes of the scheme. Data to compute water recovery for each fraction were obtained as before. The floats from conditioned sinks were collected in one fraction as only the bulk recovery and the assay were of interest.

Trial runs were performed extensively to observe the response to each reagent added. Dosage levels that did not show distinct effects as projected were discarded. The experiments were run mostly in triplicate. Fractions recovered were oven dried and masses of fractions obtained, as under the NHR scheme. Mass pull was computed based on the mass of float obtained after conditioning and the final sink fraction. These reconstitute the mass just before conditioning.

Aqua regia digestion for chemical composition analysis, as described, was also done for the float and sink fractions. The target analytes were Ag, Al, Au, Ca, Cr, Cu, Fe, Mg, Ni, Pb, Pd, Pt, Sn, Ti, V and Zn. For this purpose, inductively-coupled plasma optical emission spectroscopy

(ICPOES), and supplementary mass spectroscopy (MS) were used for the elements in relative trace proportions, particularly to have more accurate information on the Pt response. Based on the assay and mass of the fractions, assay of the residual sink after the NHR stage were computed to obtain enrichment ratio and recovery of metallic values to the float fractions obtained from sinks conditioned with reagents.

4.6.1 Macromolecular versus Gamma Depression

Two reagents were investigated for the selective depression of the sample: sodium carboxyl methyl cellulose, NaCMC (obtained from Cellulose Derivatives Property Ltd., SA) as a macromolecular depressant, and Betamin 127A (see Section 3.4) supplied by Betachem (Pty) Ltd., South Africa, for the gamma depression concept (see Section 3.5.2.4).

The depressants were studied against the natural hydrophobic response at the kinetic conditions of E21C (500 rpm impeller speed at 0.5 *l*pm aeration). Starting at 200 g/ton and increasing to 2 kg/t and above, increasing dosages of NaCMC were used to observe achievable depressions of the NHR in the bulk sample. Dosages of 10 and 30 wt. % were eventually used for reported experiments (see Section 7.2.1). For gamma depression, 0, 20, 60, 100 and 150 ppm dosages of B127A were first used on the bulk sample.

A second set of treatments was intended to establish an effective depressant for residual natural hydrophobic particles after 30 minutes of NHR flotation – as can be done before collector conditioning. A NaCMC dosage of 3.3 wt. % was used with a conditioning time of five minutes before aerating for 18 minutes.

For Betamin 127A, a 30 ppm dosage was used with one minute conditioning before aeration for 18 minutes. Inductively-coupled plasma optical emission spectroscopy and inductively-coupled plasma mass spectroscopy were combined for assaying of selected elements in the resulting fractions. The assays were compared and discussed.

4.6.2 Bulk Metallic Flotation (BMF)

The NHR residual sink was conditioned with PAX (potassium amly xanthate) using two dosages of 100 g/t and 400 g/ton. The choice of PAX is intended to achieve maximum bulk collection

(Section 3.5.2). Other trial dosages were used but these two will suffice in reporting the effects observed.

These dosages were chosen as the response tends to be negligible at the usual lower dosages. Collector consumption in excess of 200 g/ton is known in operating plants, specifically those that treat tarnished sulphides (Bulatovic, 2003). The PAX was obtained from Betachem (Pty) Ltd., South Africa. It was always freshly purified before use by dissolving it in chemically pure acetone (minimum 98 %, from Merck), followed by filtration and extraction from the filtrate by adding petroleum ether (AR, from Merck, University of Pretoria) as a desolvent, to precipitate the xanthate as fine faint yellow solid (Rao, 1971).

4.6.3 Sulfidation Activation

Analytical grade sodium hydrogen sulfide (NaSH), supplied by Sigma Aldrich (Cat. #: 161527) was used for the sulfidation scheme. Given the natural pulp pH of the system, which is alkaline (see Section 6.2), equations 3.6 b and 3.6 c will tend to favour generation of the depressant ions (see Section 3.3). A minimal dose is appropriate to avoid the depression effect. Hence, a dosage of 500 g/t was used. This is moderate compared to the 1575 g/ton used in controlled potential sulfidation by Lee *et al.* (2009). The pulp was conditioned for three minutes before adding PAX at 400 g/t. The pulp was conditioned again for another five minutes before aeration. No frother was used.

4.6.4 Depression followed by PAX Activation

In an attempt to take advantage of observations from various treatments, a scheme intended to achieve a clean metallic fraction was conceived.

A prolong NHR flotation of 48 minutes was run to exhaust the natural hydrophobic response as much as possible. Impeller speed was maintained at 350 rpm for the extended 30 – 48 minutes. Betamin 127A was then added to the pulp in 2 ppm increments, with trial aeration in between to observe bubble loading. In this manner, 10 ppm dosage was obtained after which the bubbles were no longer loaded, the bulk of the NH particle being pulled already.

Hence, 10 ppm Betamin 127A was added after 48 minutes of NHR. This was followed by 400 g/t of PAX, five minutes conditioning, 50 ppm methyl isobutyl carbinol (MIBC) as frother, a further two minutes of conditioning and aeration for 18 minutes. Designations and a summary of all the treatments using PAX are presented in Table 4.2.

Table 4.2: Designation and description for treatments involving PAX

Designation	*Description*
PAX1	Bulk metallic flotation scheme with 100 g/ton PAX
PAX2	Bulk metallic flotation scheme with 400 g/ton PAX
SPAX	Bulk metallic flotation with sulphidation; 400 g/ton PAX+500 g/ton NaHS
DPAX	Depressant followed by PAX conditioning, then frother: 10 ppm B127A, 400 g/ton PAX, 50 ppm MIBC

4.6.5 Cationic conditioning

Cationic conditioning, as explained in Section 3.5.2, was investigated using tetrabutyl ammominum chloride. The quaternary amine was chosen to ensure that pH variation, which is considered to be a deciding variable in exploring particle surface potential, does not affect the collector activity (dissociation). The butyl hydrocarbon was used to ensure impartation of higher hydrophobicity compare to shorter alkyl groups. Three pH levels – natural pulp pH (about 8), pH 4 and pH 10 – were used for the preliminary runs.

Approximately 0.02 M (1.8385×10^{-2} M) acid solution, used to lower the pulp pH, was made by adding 1 cm^3 of 98 % concentrated sulphuric acid (oil of aerosol, SG 1.98, 18.385 M) supplied by Merck (University of Pretoria) to 1 *l* of distilled water. After addition of appropriate volumetric proportions, and monitoring with Orion pH meter, the pulp showed a gradual rise in pH. More acid solution was needed to drag the pH down to desired value.

Anhydrous sodium hydroxide pellet (supplied by Merck, University of Pretoria) was used for preparing the basic solution to regulate the pulp pH to 10. Tetrabutylammonium chloride (AR), obtained from Merck, SA, was used at 100 g/t dosage. Judging from the preliminary trials (see Section 7.5), the pH 4 condition was dropped from further investigation and frother addition was

considered necessary for this scheme. Thus, 50 ppm MIBC was added and the pulp conditioned for two minutes before aeration.

4.6.6 Selective Metallic Flotation

As noted in Section 3.5.2, sodium mercaptobenzothiazole (SMBT), supplied by Betachem (Pty) Ltd., SA, was used for the selective metal flotation investigation. SMBT is a selective collector of tarnished or oxidised lead and copper minerals (Fuerstenau and Raghavan, 1986). The copper and lead particles in this sample can be conceived as tarnished. This is because the particles are from end-use alloys that have been exposed to the atmosphere all their service lives. Outcropped native metals in mineral deposits tarnish simply by being exposed to the atmosphere.

A dosage of 200 g/t SMBT was used for the reported flotation. A very selective flotation was expected. The natural hydrophobic flotation was therefore carried out for 48 minutes before the conditioning. The impeller speed was set at 300 rpm for the first 18 minutes, then at 350 rpm for the last 30 minutes of the NHR flotation. After conditioning, it was maintained at 350 rpm for the 18 minutes of aeration. Skimming was done every two minutes after the conditioning. Fractions were recovered and analyses done for selected elements as described above.

4.7 FOLLOW UP INVESTIGATION FROM THE CHEMICAL CONDITITONING SCHEME

The following investigations were carried out in attempt to substantiate the probable causatives advanced (in Section 7.6) for explaining the responses observed from the various chemical conditioning schemes.

4.7.1 Calcium Dissemination in PCB CF

Direct observation of particles of the sample was done in JOEL JSM 3600 scanning electron microscope in the Industrial Minerals and Materials Research Institute (IMMRI) in the Materials Science and Metallurgical Engineering department, University of Pretoria. A dispersed layer of the sample was made on carbon tape and the layer was coated by carbon deposition. The particles were observed in both backscattered electron and secondary electron modes to enhance

composition contrasts and achievable resolution of surface features. Clearly defined phases and morphologies were focused by the electron beam. The energy dispersive X-ray spectra of the phases were observed to identify-calcium bearing particles. Representative spectra of the particles in the sample were also taken.

4.7.2 Calcium Presence in Process Water

For the process water composition study, filtrates of the flotation pulp were obtained and trace element ICP-MS scan of the filtrate was done to establish the elements that leach into the filtrate. The scan was for a total of 68 elements: Ag, Al, As, Au, B, Ba, Be, Bi, Ca, Cd, Ce, Co, Cr, Cs, Cu, Dy, Er, Eu, Fe, Ga, Gd, Ge, Hf, Hg, Ho, In, Ir, K, La, Li, Lu, Mg, Mn, Mo, Na, Nb, Nd, Ni, Os, P, Pb, Pd, Pr, Pt, Rb, Re, Ru, Sb, Sc, Se, Si, Sm, Sn, Sr, Ta, Tb, Te, Th, Ti, Tl, Tm, U, V, W, Y, Yb, Zn and Zr. This investigation can also serve to assess hazardous contamination with elements such as Pb, Cr, Hg and Cd during PCB CF wet processing.

4.7.3 Investigation of Particle Surfaces

High resolution observation of the surface of copper trace particles, picked from the fine sample and mounted on carbon tape, at 1 kV electron energy was done. The Carl Zeiss Field Emission Scanning Electron Microscope (FESEM) at the Electron Microscopy facilities of the University of Pretoria, was used for this investigation. Auger electron spectroscopic investigation for information about the surface make up of metal particles in the sample was also done.

For this investigation, a survey of auger kinetic energies on each surface was first taken, then profiled for 40 minutes. Surveys were taking every five minutes of profiling. The primary electron beam was kept at a landing voltage of 5 kV and a 10 nA beam current. The argon ion gun was operated at 2 kV, 2 µA, giving about 85 Å sputter depth per minute (as characterised for SiO_2)**.** The auger electron kinetic energy surveys for all the surfaces spanned 0 – 2400 eV, to be a comprehensive search for all possible elements. The PHI 700 Scanning Auger Nanoprobe of the Department of Physics, University of Free State, Bloemfontein, South Africa, was used for this study.

A total of eight particle surfaces were studied. Three were from assorted particles in the conducting fraction from corona electrostatic separation of +212 – 300 µm size fraction of PCB

comminution product. This conducting fraction is very rich in copper particles so that a copper surface can be easily picked up from the fraction when inside the microscope. Most of the particles in the actual −75 µm fine fraction were not metallic particles of interest for the surface investigation. Searching out the actual metallic particles for observation from such a sample will involve time-consuming surveys. Moreover, the bulk in the fine fraction is non-conducting and the majority of the particles will be charging profusely. This is why grains of the actual −75 µm fraction were not used for this purpose. The metallic particles surfaces in the +212 – 300 µm fraction can be taken to represent that of metallic particles in the –75 µm fraction, since they are screened from product of the same comminution stage. The particles from the coarser fraction were therefore used. The five other particles were elongated (fibre) particles. These were easily distinguishable in and selected from the –75µm fraction.

A portion of the assorted particles (electrostatic conducting fraction) was taken and rinsed in distilled water, drained and allowed to dry in the open laboratory room temperature for four hours. Another portion was rinsed in the PCB CF pulp filtrate and a third portion was untreated. The fibres were also given similar treatments. Table 4.3 summarised the designation and description of the surfaces.

A few grains from each portion of the assorted particles were carefully placed on separate carbon tape with a clean spatula. The tape was then blown by pure nitrogen gas to remove particles lying on top of others and not directly adhering to the tape. This gave a dispersed almost monolayer of the particles on the tape. The fibres were also carefully placed on the carbon tape, ensuring that the particles do not roll on the tape in the process.

4.8 STATISCAL ANALYSES AND ERRORS

Although detailed data for some repeat runs are presented as appendix data, some are reported directly as averages. For an indication of the scatter of the actual values for the averaged data, when considered necessary, relative standard deviations of the mean (δ_r,%) were computed as:

$$\delta_r, \% = 100.\delta/\bar{x} = 100\sqrt{\frac{(x-\bar{x})^2}{n}}\ /\ \bar{x} \quad . \quad . \quad . \quad . \quad . \quad . \quad 4.2$$

where δ is the standard deviation of the averaged data, n is the number of runs averaged, $(x - \bar{x})$ is the difference between each data value and the averaged value. This is tabulated with such averaged data. The associated errors with the averages were computed as the standard error of mean (ε) for such data points as:

$$\varepsilon = {}^{\delta}/_{\sqrt{n}} \quad . \quad . \quad . \quad . \quad . \quad . \quad . \quad . \quad . \quad 4.3$$

The standard errors are indicated as negative and positive error bars when plots are made from averaged data.

Table 4.3: Designation and description of particles surfaces studied by Auger Electron Spectroscopy

Designation	Description and Surface condition
P1	From assorted particles as taken.
P2	From assorted particles soaked in process water (PCB pulp filtrate) and dried in open laboratory air.
P3	From assorted particles soaked in distilled water and dried in open laboratory air.
F1	Copper trace fibre particle soaked in process water and dried in open laboratory air.
F2	Copper trace fibre particle soaked in distilled water and dried in open laboratory air.
F3	Copper trace fibre particle as taken from the PCB CF sample.
F4	A more brownish (possibly copper) fibre particle as taken from the PCB CF sample.
F5	A whitish fibre particle as taken from the PCB CF sample.

5.0 CHARACTERIZATION OF PCB COMMINUTION FINES FOR FROTH FLOTATION INVESTIGATION

5.1 INTRODUCTION

The total printed circuit board comminution fines (PCB CF) sample generated weighed about 70 kg (see Appendix 1). Results and discussion of the relevant characterization investigations on the sample towards the flotation investigations are presented in this chapter. It covers particle size distribution, sample density, liberation and comparative chemical composition analysis.

5.2 DENSITY AND PARTICLE SIZE DISTRIBUTION

Table 5.1 (detailed data is given in Appendix 2) shows the density figures obtained for the PCB CF sample. The small deviations are from systemic errors resulting from imprecision in repeatedly filling the fixed volume with exactly the same mass of sample. The values show that the fines sample is not very dense, as the loose and tapped bulk density values indicate in particular. An implication of this property value on flotation is that the sample will pour unto water and not into water during pulping. That is, the bulk sample can float on water. Water can as well simply displace the sample when poured over it in a cell. This, in fact, was the experience during the preliminary microflotation trials (see Section 4.4), after which the density determination was carried out. Sample pulping hence has to be done by first forming a paste of the sample with a small quantity of water. The paste is then dispersed under water. This is what was done when determining the true density.

Table 5.1: Density values for the PCB CF sample

Description	Value (g/cm^3)	Relative Std. Dev, % (triplicate test)
Loose bulk density	0.54	1.4
Tapped bulk density	0.90	0.7
True density	2.9	2.3

The true density value of 2.9 g/cm^3 shows that the actual particles are generally much denser than what the bulk density (0.9 g/cm^3) indicates. This shows that packing even after 200 tappings is not perfect, and porosity in the column accounts for the bulk volume. Poor packing is indicative of very diverse particle morphology (shape) and is clearly confirmed in the liberation study below.

Figure 5.1 shows the particles size distribution obtained from the –75 to +38 µm sieving analysis (data for the figure is shown in Appendix 2). This plot is only an indication of the size distribution, as sub-sieve analyses were not done because of the particle morphology and material diversity constraints. These are addressed below (see Section 5.3).

However, the data generally indicate that a large proportion (66.7 %) passed 38 µm. It follows that certain PCB components break selectively into very fine particle sizes. Metallic particles are ductile and cannot be expected to crumble into fines. Instead, grinding into powder can be expected with brittle comminution of glassy particles, ceramics glazing on certain resistors, semiconductor diode valves, chips, insulating ceramics (such as mica) and components with brittle thermosets (see Section 2.3).

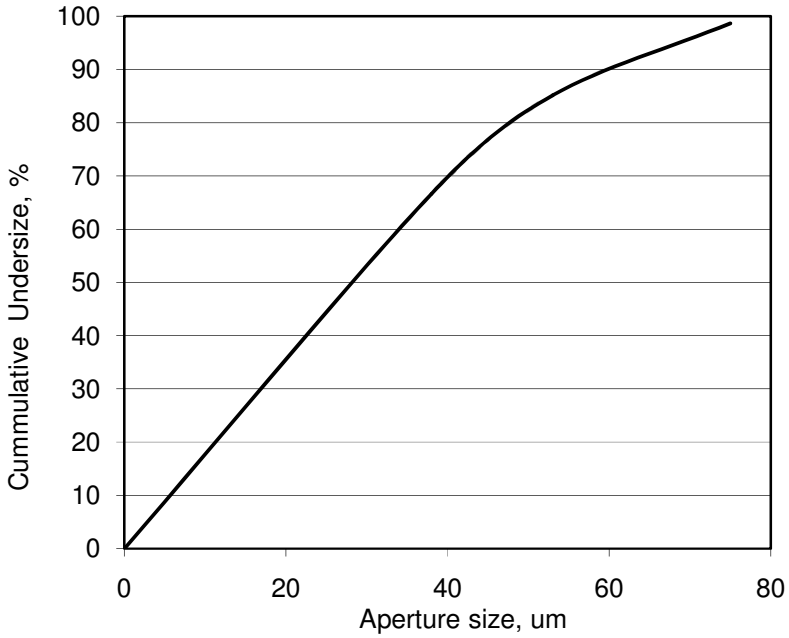

Figure 5.1: Particle size distribution of PCB CF

Given the peculiarities of fines in flotation behavior (Pease *et al*., 2005), a major influence of fine particles on the flotation response can be expected (see Section 6.3.1). Sub-sieve analysis also appears necessary, but the liberation assessment gave important constraints discussed below.

5.3 MORPHOLOGY AND LIBERATION ASSESSMENT

Figure 5.2 (a – d) shows the optical micrographs of polished sections of the printed circuit boards comminution fines. Dark field, compared to bright field, illumination was used for these images to enhance colour and relief contrasts in the sample (Murphy, 2001). On a conservative analysis, the white particles are the more reflective metallic particles, the black patches include organic particles, and glass fibres remain distinctly fibrous. Judging from the reflectivity, the metallic particles are in much smaller proportion, while the fibrous particles are the most common. The general morphology shows that the particles are present in very random shapes – fibrous, angular, subangular, partially rounded, and almost cubical.

Leaving the distinctly fibrous glass particles out, the circularity shape factors of the other particle were obtained from the binarised image shown in Figure 5.3. This image is from an optical micrograph of a polished section (in clear, non-iodised, resin) shown in Figure A2.1, while Table A2.3 (both in Appendix A) shows the shape analysis data for a total particle count of 116. Small pixel-sized specks of particles up to 50 pixel square in area (approximately 16 μm^2 from pixel size to scale bar ratio of image) were left out to avoid erroneous circularity of 1, which will be caused by poor boundary and aspect ratio definitions in small particles.

The average circularity was found to be 0.63, while average solidity was 0.85. These conform to the visible diverse particle morphology in the sections. It is indicative of material diversity, as well as various shear, tensile, impact and complex forces under which the comminution of the particles was achieved. The glass fibres, on the other hand, produce particles with length well above the sieve aperture diameter (d_A) of 75 µm, as easily seen in the sections.

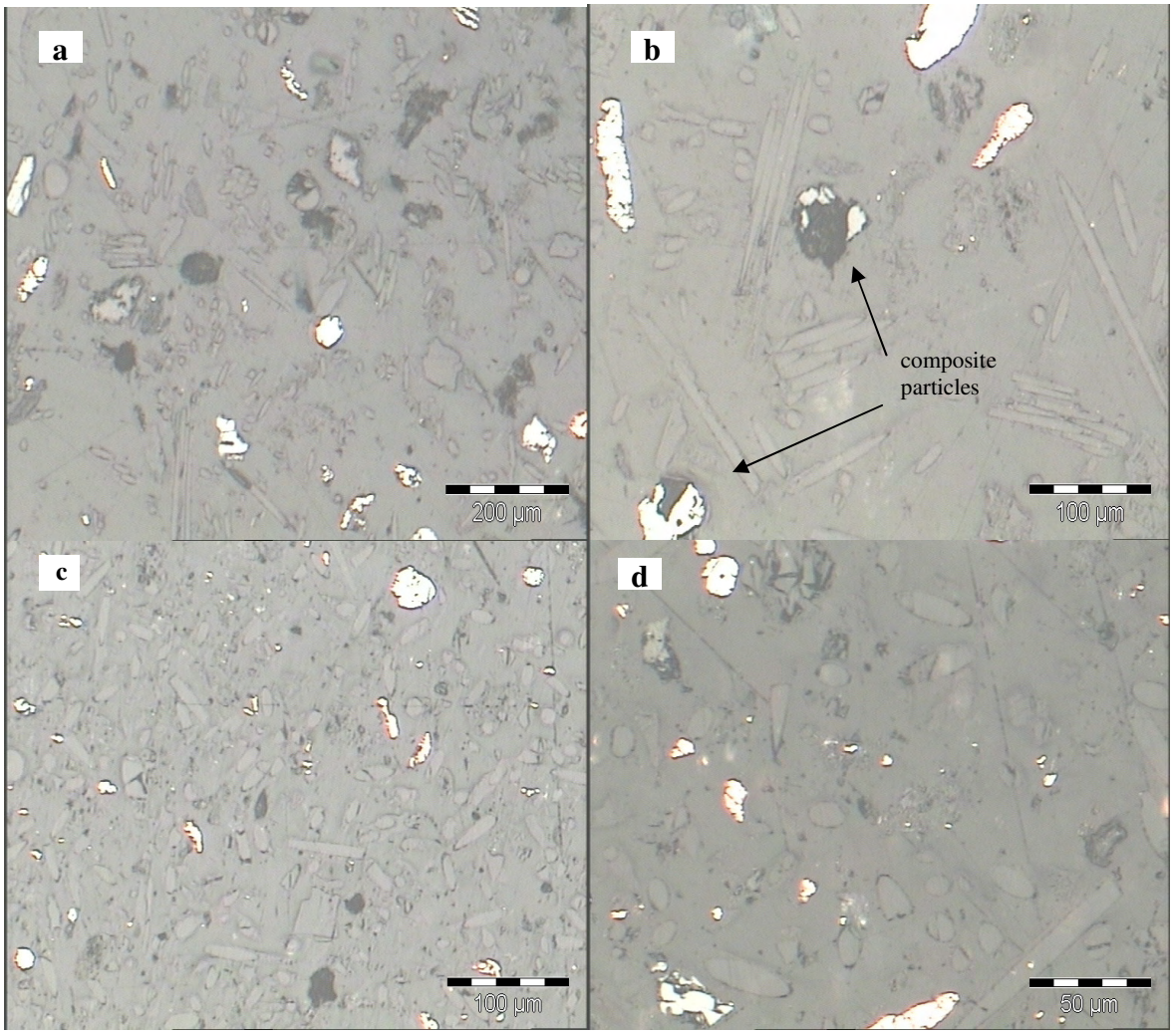

Figure 5.2: Optical micrographs of PCB comminution fines polished sections:
a. −75+38 µm, 50 x magnification; b. −75+38 µm, 100 x magnification; c. -38 µm, 100 x magnification; d. −38 µm, 200 x magnification. *Micrograph clearly shows diverse particle shapes*.

This diverse particle morphology explains why screening time was so prolonged (see Section 4.3.1), despite the maximum amplitude (vibration energy) used. Some particles have to tumble a number of times before assuming favorable orientation to pass through the screen. Another implication of this morphology is its limitation on the effectiveness or applicability of some common techniques for sub-sieve analysis. Although the classification can still easily go a step further down with finer cloth screen in 25 µm sieve, the challenge is to do a detailed analysis down to a micron. For example, the result of analysis from the volume-based laser diffraction technique using the Malvern's Mastersizer (Rawle, Malvern Instruments) may not be precisely

interpreted. A glass fibre particle in the −38 µm fraction from a mesh sieve analysis certainly has two dimensions below the d_A of 38 µm. If a fibre particle is about 35 µm in diameter, and about 150 µm long (as is common in Figures 5.2b and A2.1), its equivalent sphere diameter (d_S) on the Mastersizer will be returned as 65 µm. This follows from equating the volume of a cylindrical particle to that of its volume equivalent sphere as:

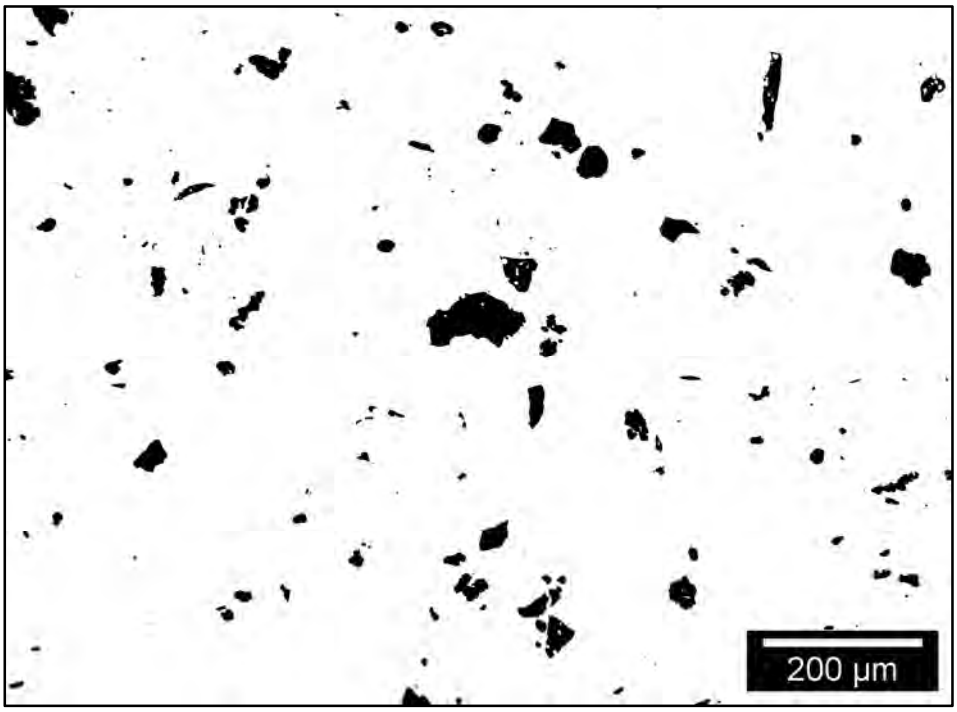

Figure 5.3: Binarised image for circularity shape factor analysis of the metal particles.

$$\frac{1}{4}\pi {d_A}^2 h = \frac{1}{6}\pi {d_s}^3 \quad . \quad . \quad . \quad . \quad 5.1$$

where h is the length and d_A is the aperture diameter of a cylindrical particle, while d_S is the diameter of the sphere of the same volume. Then,

$$d_s = \sqrt[3]{\frac{3}{2}}\left({d_A}^2 h\right) \quad . \quad . \quad . \quad . \quad 5.2$$

d_A and h are then substituted as 35 µm and 150 µm respectively. With such diverse particle morphology, a PSD based on d_S may therefore not make much sense.

The cyclosizer is another good subsieve device. It separates base on mass effect under centrifugal force. For a sample containing particles of the same material (density), variation in particle mass is also variation in particle size, and the mass-based separation therefore gives size classification. With assorted materials, particles of the same size can have very different masses, and therefore separate to different size classes or generally give poor partition. The assorted material constituents and the diverse particle morphology observed in the PCB CF therefore present major constraints for its sub-sieve size classification.

As an indication of the composition of the fines sample, it can be observed that the bright metallic particles have a low proportion compared to the less reflective phases. It was mentioned that metals are ductile and will not preferentially report to the fines. A low metallic assay of the fines may therefore be expected.

With regard to liberation, Figure 5.2a shows almost total liberation of all the particles in the −75+38 µm range. However, the close-up in Figure 5.2b (at 100x magnification) shows that some composite particles can still be found. For -38 µm size particles, such composite particles could not be found on (four) polished sections at 100 and 200 times magnification (Figure 5.2 c and d).

The scanning electron microscope (SEM) observation provided a more qualitative assessment of the sections. Although almost all the metallic particles in the sections as observed with the SEM are unlocked, unliberated particles could still be found (Figure 5.4a). A close up on such composite particle is shown in Figure 5.4b. Table 5.2, shows the energy dispersive X-ray analysis data of the two distinct phases of this particle. From the image and the composition data, this particle appears to be a copper trace unliberated from solder.

Averaged point counts of such composites relative to totally liberated particles on a number of sections gives a ratio of 1 to 194, implying a degree of liberation above 99 %. As the polished section may not be considered as being accurately representative of the particles' relative

abundance in the sample, this value may be taken as an instance only. The primary purpose here is to establish whether or not unliberated particles still exist at −75 µm.

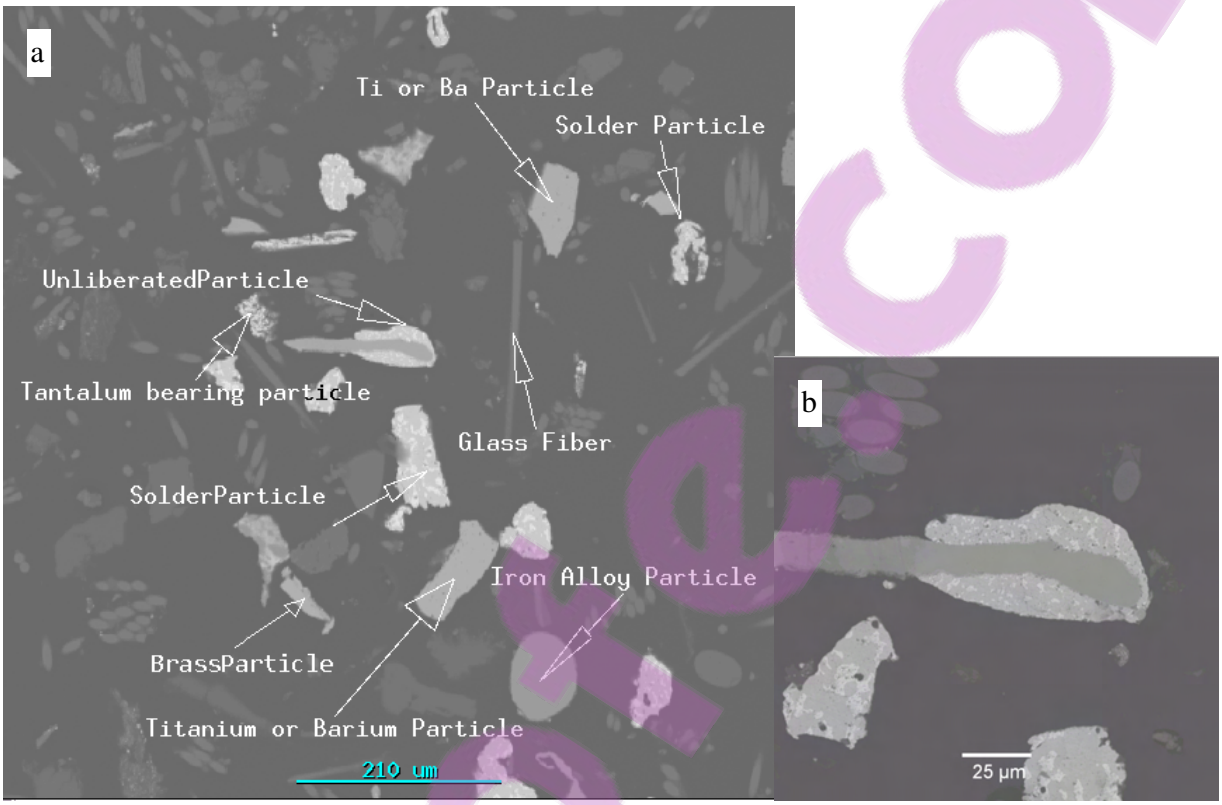

Figure 5.4: SEM back scattered electron images of −75+38 µm printed circuit boards comminution fines section (a), and a close-up of an unliberated particle (b).

On another note, although this degree of liberation can be taken as almost total (as it will be readily taken in conventional mineral processing), in a sample where compositions of the various constituents range from percentages to ppm (see Section 5.4), the small balance can be critical. In clearer perspective, a balance of 0.5 % in the degree of liberation (as the actual computation will roughly give) is equivalent to about 5000 composites per million particles. Assuming a constituent with total assay of 200 ppm is concentrated in the 5000 composite particles, the response of such constituents will grossly deviate from normal expectations in a flotation scheme.

Table 5.2: Energy Dispersive X-ray composition analysis of phases in -75+38 µm printed circuit boards comminution fines polished section.

Phases	Elemental Lines	Atom %	Element wt %
Composite particle outer (Figure 5.2b)	Al-K	1.2	0.3
	Sn-L	82.1	77.0
	Ca-K	0.9	0.3
	Cu-K	1.9	1.0
	Zn-K	1.3	0.7
	Pb-L	12.7	20.8
Composite particle inner (Figure 5.2b)	Sn – L	0.5	1.0
	Ca – K	0.2	0.1
	Cu – K	64.2	63.3
	Zn – K	35.1	35.6
Ti - Barium particle (Figure 5.2a)	Co-L	2.2	1.4
	Al-K	0.7	0.2
	Si-K	0.7	0.2
	Ca-K	2.3	1.0
	Ba-L	43.6	67.3
	Ti-K	44.5	24.0
	Zn-K	1.2	0.9
	Zr-K	4.8	4.9
Fe-alloy particle (Figure 5.2a)	Al-K	0.3	0.2
	Si-K	23.2	13.2
	Mn-K	0.7	0.8
	Fe-K	75.8	85.8
Brass particle (Figure 5.2a)	Sn-L	48.2	63.6
	Fe-K	0.8	0.5
	Cu-K	50.5	35.6
	Zn-K	0.4	0.3

Apart from the existence of composite particles, the EDS analysis of individual particles also showed the liberated particles are made up of alloys. The material make up of liberated particles certainly will have important implications for beneficiation planning. Table 5.2 shows the chemical compositions of some of the particles annotated in Figure 5.4. This implies that beneficiating this sample will, at best, produce fractions that are not cleaner than the alloys. For example, in a solder particle, lead would be inseparable from either zinc or tin. A realistic

objective in flotation will be to recover as much as possible of the metallic values into a bulk product fraction. This is the motivation for the bulk metallic flotation proposal (see Sections 3.5.2 and 4.6.2). It was also noted that collector adsorption on alloy surface is synergistic: a collector will interact with an alloy as much as one of its constituent elements interacts with that collector (see Section 3.3). This should assist the response of the alloys to bulk collectors.

5.4 COMPARATIVE WET SPECTROSCOPIC ANALYSIS

Of the three digestion systems employed, only SPF (sodium peroxide (Na_2O_2) fusion followed by HCl dissolution), achieved total digestion of the sample. Aqua regia (AR) and HHM ($HF + HNO_3$ plus microwave radiation) gave only partial digestions. Various elements dissolve to different extents under the partial digestions as the assays indicate. Table 5.3 shows the assay values for 42 elements from the three digestion conditions. Elements not detected under a digestion condition are entered as ND. These assays are averages for duplicate digestions. The repeatability was within 95% for most elements, but 90% was also noted for some. Notably Pd was observed to give best repeats, about 1.5 % relative standard deviation, while silicon and silver gave about 10 %. This is considered acceptable recognizing that a perfect replicate sample from such highly heterogeneous stock may be unrealistic.

Detailed analysis of sampling variance, element by element, over reasonably large population of samples, while using a single digestion technique, can be informative in this connection. However, this is outside the present scope. Bearing the possibility of sampling variance in mind, only assay differences above 10% are considered significant when comparing the effectiveness of the digestion techniques in recovering a particular element into analysis liquor.

Table 5.3: Assay values from ICP OES and ICP MS analyses of printed circuit boards comminution fines from different digestion conditions (mg/Kg)

Element	AR: Aqua regia	HHM: HNO_3 + HF + Microwave	SPF: Na_2O_2 Fusion + HCl dissolution
Ag	849	18.9	--
Al	32900	32890	32922
As	32.5	N.D.*	--
Au	220	124	--
B	10800	9170	--
Ba	7590	8120	8140
Bi	319	237	--
Ca	63400	64500	75400
Cd	17	11.2	--
Ce	72	48	--
Co	92.2	90.6	--
Cr	160.0	323	416
Cu	42700	43200	42800
Fe	26800	32300	33630
Hf	10.4	N.D.*	--
K	717	737	--
La	91.5	19.9	--
Li	40.3	39.7	--
Mg	2180	2130	2150
Mn	1200	1230	1457
Mo	53.7	40.1	138
Na	2120	2050	--
Ni	1900	2110	2512
P	1120	1110	--
Pb	23100	22300	23530
Pd	158	137	--
Pt	1.7	5.3	--
S	555	2750	--
Sb	2620	3180	--
Se	N.D.*	N.D.*	--
Si	4070	11600	139300
Sn	29100	29800	--
Sr	785	686	780
Te	N.D.*	N.D.*	--
Th	6.0	2.4	--
Ti	3340	4070	4168
Tl	N.D.	N.D.*	--
U	1.9	1.9	--
V	26.3	30.0	30
Y	9.65	5.80	--
Zn	4890	5510	6212
Zr	245	297	--

It should be noted that the assays in Table 5.3 are for printed circuit boards comminution fines and do not represent a complete board analysis as in Table 2.4. In general, metallic value deportment to the finer fractions in the comminution operation is lower than that to the coarser fractions, because metallic materials are generally ductile and do not shatter into fines during comminution. It will also be noted that many elements (including Au, Ag, Pd, Sb, Sn, and Zr) were not read from the total digestion solution from SPF treatment. This is because of possible pronounced matrix effect on these elements under the optical emission spectroscopy (Willard *et al.*, 1988). Hence, only solutions from AR and HHM digestions were analysed for all the 42 elements.

From the data, Si gave values that were more than 10 times higher with SPF digestion compared to AR and HHM digestions. These result from the digestion of glass fibres. It is expected that SPF, which gave total digestion, should give the highest assays, and this is true for almost all of the elements. Some exceptions are for Cu and Mg, which returned highest values from HHM and AR respectively. However, the values are significantly close for all the three conditions that it may not be said that the recovery of Cu and Mg are lesser under SPF digestion. Au, Ag, Pd gave higher assays with AR than with HHM. Ag, in particular, is sparingly digesting under HHM digestion with only 18.9 ppm dissolved, compared to 849 ppm in AR. For Pt, HHM digestion appears to give a better digestion recovery (higher assay), compared to AR digestion. For other elements, the assays from AR and HHM treatments are comparably close and within the range of sampling variations.

These observations confirm that (i) printed circuit boards comminution fines wet assaying will depend very much on the digestion condition, and (ii) a single digestion condition cannot give best assays for all the elements combined. While SPF treatments resulted in complete digestion, many elements could not be analysed from the resulting solution. Readings from AR and HHM treatments also did not clearly give one condition as better than the other for all the elements. This reflects the heterogeneity of the sample, as different chemical elements exhibit different activities at the chemical potential of a digestion system.

In this context, the digestion condition that gives the maximum assay value for a particular element can be considered as ideal for that element, and the assay obtained from that condition

can be taken as most indicative of the absolute assay for that element in the fines sample. Assays from other digestion conditions will only be fractions of this absolute value. For elements such as Au, Ag, Pd and Ti, the AR condition – hot aqua regia digestion – gives the absolute assay, while for Ni, Fe, Sb and Pt, for instance, the absolute assay is from the HHM treatment.

An implication of these observations for a standard approach to eol printed circuit board composition analysis is that absolute or actual assays of the constituent metallic elements will have to be combined from more than one digestion condition. It may be mentioned that the routine of obtaining the absolute assay may be unnecessary except in analyses for hazardous constituents as in environmental concerns. It may be noted here that no standard procedure yet exist for PCB chemical composition analysis (ASTM; ASTM, 2007; ISO).

In beneficiation investigations, valid inferences can be made based on relative assays of product fractions obtained from one digestion condition, whether absolute assays were obtained for all target values or not. It follows that, the final choice for a particular PCB comminution fines analysis depends on the target elements and the analytical objective, whether for comparative or absolute assaying. This implies that printed circuit boards wet analysis reports need to specify the digestion condition used. This will help data interpretation and inferences.

In any case, when the data from the three digestion conditions are compared, hot aqua regia digestion appears to be the best for general purpose analysis. It is able to give analysis liquor for all the elements. The procedure is also less hazardous compared to using HF in the HHM treatment. Hence, for analysis of flotation performances for the present investigation, hot aqua regia digestion will be used. It gives good assays for major target values such as Au, Pd and Cu.

5.5 THERMOGRAVIMETRIC ANALYSIS FOR ORGANIC CONSTITUENTS

Figure 5.5 shows the result of the thermogravimetric analysis. The top plots show the percentage change in mass with temperature for the air and the nitrogen environment (distinguished by colour). The lower plots show the derivatives (rate of change of mass with temperature) in an attempt to accentuate the inflection points.

The result shows final mass in air as 75.62 %. The analytical question is to determine what constituent fraction the 24.38 % mass loss represent. Certainly there are organics that will be expected to burn off and contribute to the mass loss. However, the drop in mass was continuous over the whole temperature range, indicating continuous reactions that cannot be attributed to a specific organic constituent in the composition. To make the distinction less obvious, the sample contains solder particles that could have developed relatively high vapour pressure as temperatures rose, with consequent volatilisation loss. This is further complicated by the possibility of metallic particles oxidising with weight gain. The overall mass loss may, therefore, not be taken as total but only as net from loss and gain. The mass drop in the air environment may therefore not quantify any particular constituent in the sample.

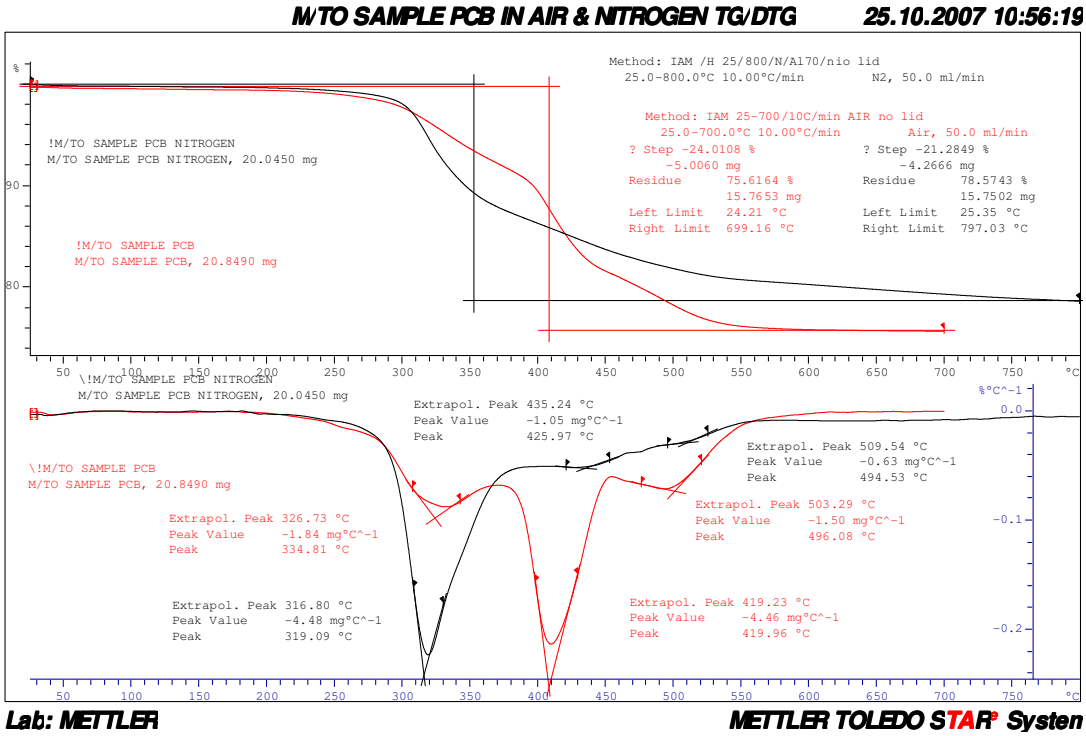

Figure 5.5: Plots of thermogravimetric analysis and the derivatives for PCB CF sample under air and nitrogen.

The nitrogen atmosphere is considered relatively more inert, and some reactions will be expected to be absent so that some distinctions in the trend can be expected. The residue in the nitrogen environment is 78.57 %, implying that combustion loss was lesser than it was in air. The nitrogen plot lying below that of air between 300 ^{o}C and 420 ^{o}C actually confirms that some

weight gain was compensating for the weight loss in air. The weight loss sloped faster under nitrogen, when oxidation weight gain was absent. After this interval, as temperature rose, combustion losses appear higher under air and the mass dropped quickly to stabilise around 600 ^{o}C. This was not happening under nitrogen and, as the negative slope reduced, the rate of mass loss became very low. This continued slowly and did not stabilise even at 800 ^{o}C.

The comparison shows that combustion loss under air was pronounced in the sample and can be taken as responsible for much of the higher weight loss under air. However, the nitrogen atmosphere either did not characterise any specific constituent in the sample. Early into the heating program, from about 50 ^{o}C, mass loss commenced, and continued with a slope all through. Again, no position over the whole temperature range gave zero derivative of mass with temperature (dM/dT = 0), to characterise a constituent distinctly.

This results show that thermogravimetry may not be recommended for PCB composition analysis. No concrete qualitative or quantitative information may be extracted for characterising a given constituent. It appears that more than one reaction or event was occurring simultaneously over the whole temperature range. This can be attributed to the very diverse material constituent of the sample.

5.6 CONCLUSION

Characteristics of PCB CF observed under the characterisation investigation were interesting and peculiar. Without the basic understanding of these material characteristics – the density, PSD, liberation and the chemical composition – and the implications all of these will have on flotation, investigating the prospects of flotation application may not be possible.

It was found that the PCB CF loose bulk density is lighter than the density of water. This, coupled with other peculiar surface properties of the bulk sample, necessitates the careful pulping procedure that had to be adopted in the flotation investigations (see Sections 6.2 and 6.3.1).

The wet assaying of the sample was found to be very dependent on the digestion condition. From the result it was inferred that determining the absolute assays of all constituent elements will require comparing data from more than one digestion condition. However, if the analytical objective is a comparative assaying of samples from beneficiation treatments, aqua regia digestion can be recommended for most of the constituents. The procedure is less hazardous compared to HF, microwave and HNO_3 treatment. It also gives analysis liquor from which all the elements can be analysed, compared to that obtained from the Na_2O_2 fusion + HCl total digestion. Ironically, total digestion has a demerit here due to the complexity of the sample. The sample complexity also posed a limitation when applying the thermal analyses technique. The thermogravimetry analysis gave no distinct inflexion point to characterise any constituent.

Particle liberation in the sample was found to be very high. It may almost be taken as fully liberated, as reported in the literature, except that micrographic evidence obtained to the contrary is too vivid to be ignored. The unliberated fraction can be put at about 5000 particles per million. The particle morphology was observed to be very diverse and this, coupled with the material diversity, is a major constraint to sub-sieve PSD analysis.

Based on the mesh sieve analysis, 67 % of the sample generated was found to be below 38 µm. Pronounced effect of fines on the flotation response of the sample should therefore be expected. The liberated particles themselves contain more than one chemical elements, being alloys. Beneficiation operations therefore cannot attempt to separate these particles into constituent elements: realistic schemes can aim only at achieving some bulk collection of metallic values into a concentrate.

6.0 NATURAL HYDROPHOBIC RESPONSE SCHEME AND FAVORABLE KINETICS FOR PCB CF FROTH FLOTATION

6.1 INTRODUCTION

Results of the investigations based on the natural hydrophobic response scheme are presented and discussed in this chapter. Useful inferences made from the preliminary microflotation are mentioned first. The variations in response – mass pull, extent of fit to first order kinetic, assay and recovery – with the kinetic regimes employed serve both to: assess a favourable kinetic regime for PCB fines flotation; as well as for drawing a conclusion on the applicability of froth flotation, and the natural hydrophobic response scheme, in particular, in concentrating the PCB comminution fines.

6.2 PRELIMINARY MICROFLOTATION

During the microflotation experiments, it was observed that 130 rpm (1.8 lpm) peristaltic pump setting, commonly used for mineral microflotation investigations (Bradshaw and O'Connor, 1996), produced high turbulence in the cell column. The particles were carried through to the top of the suspension and the quiescent zone could not be observed. The pump setting had to be lowered to 40 rpm. It was observed that even 10 rpm would still maintain suspension of the pulp after aeration. This low energy input required to keep the particles in suspension is understandable, given the low bulk density of the sample and the large -38 µm proportion (Section 5.2). This observation informed the choice of the low range of initial impeller speeds used for the flotation investigation in the Leeds cells (see Section 4.5).

The detailed observation of the pulp pH over time is shown in Figure 6.1, which indicated that the natural pulp pH averages around 8.00. It also shows that the natural pulp pH is acceptably stable with time and a variation of pH over the flotation period will not occur. This observation and clarification is necessary given the diversity of the sample constituents, where the possibility of slow dissolution of acids or bases may not be ruled out without a definite confirmation.

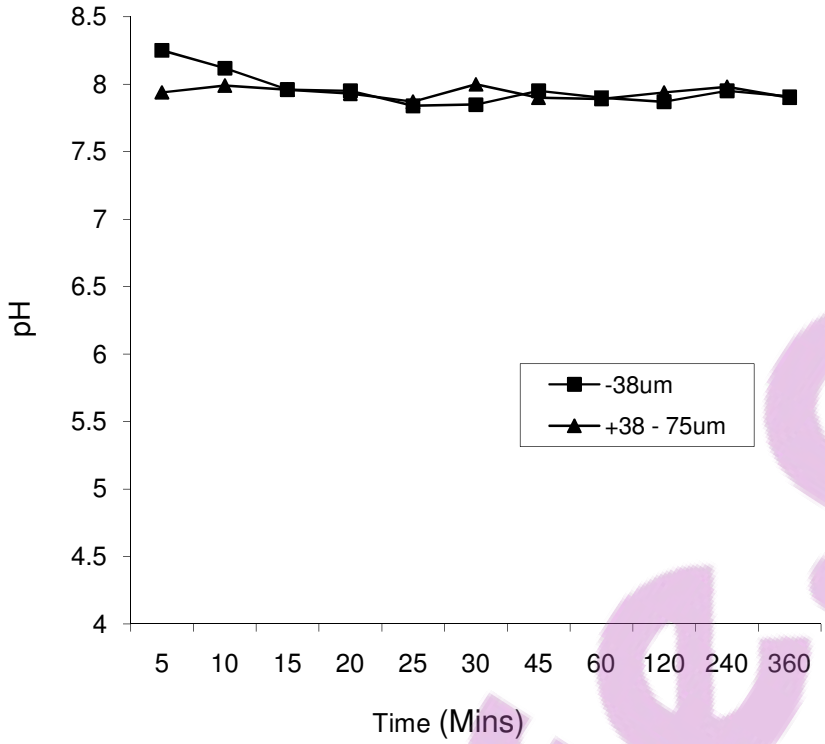

Figure 6.1: Natural pulp pH with time for two size fractions

Figure 6.2 shows mass pull data that summarises major observation from the microflotation treatments. The initial treatment using a collector pulled a fraction of the sample well above 50 wt %. This fraction being so high reinforced the idea of particles floating under natural hydrophobic response. This was confirmed, as flotation without any treatment also gave high mass pulls. A further observation was that mass pull does not tend to be higher when a collector is used compared to when it is not. At 200 g/ton dosage, the mass pull even appeared to be lowered (Figure 6.2). When a collector was used with detergent as a wetting agent (designated CWA in Figure 6.2), a remarkable drop in the mass pull was observed.

Basically, the detergent acted as an ionic surfactant and lowered the surface tension of the pulp. It follows that the collectorless mass pull is due to particles floating under their natural hydrophobicity, and that when the pulp surface tension was reduced certain particles were wetted and remained in the sink. Collectors as surfactants also generally contribute some decrease in the liquid surface tension (Section 3.2). This may explain some decrease in the mass pull that seems to accompany the SIBX conditioning compared to the collectorless flotation. The distinct

collectorless response observed encouraged detailed investigations into the prospect of the natural hydrophobic response described in Section 3.5.1. The scheme was simultaneously used for studying the favorable kinetics for PCB CF flotation.

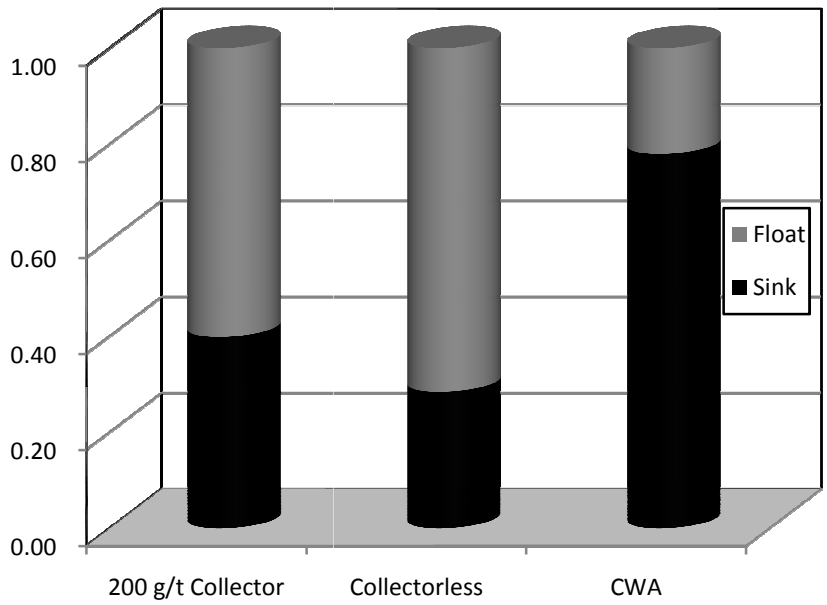

Figure 6.2: Microflotation float and sink fractions represented in stacked columns scaled to a total of 1.

6.3 THE NATURAL HYDROPHOBIC RESPONSE SCHEME

6.3.1 The Natural Hydrophobic Froth

As observed previously, without the addition of any reagent, the pulp pH measurements in the Leeds cell averaged 8.00 (δr = 1.6%) for measurement in 14 different pulps. Also, for all the kinetic conditions investigated, and without any frother addition, stable froths formed in the cell. Figure 6.3 shows a picture of the froth build-up inside the cell (see also Appendix 2.2). This distinctly shows that the natural hydrophobic response exists. The observed mass pull was also generally high, above 50% in most conditions (see Section 6.3.2).

Figure 6.3: PCB CF froth in the flotation cell under natural hydrophobic response

This immediately clarifies the difficulty experienced in pulping the sample. Despite the fact that the true density should sink the particles, the bulk hydrophobic behaviour kept water out, so that the sample formed into globules covered by a skin of water. The particles inside the globules remained dry, retaining the loose bulk density (see Section 5.2). The globules thus easily floated on top of the pulp. Intense agitation simply broke the globules into smaller sizes, while aerating the pulp at the same time. A scum thus formed on top of the pulp, even before commencement of flotation. This is a frustration of the operation, as the scum contains tiny globules with trapped dry sample inside, which does not allow separation of the sink constituent. The way around this was to form a paste of the sample first, introduce it to the cell, cover the paste with water and then break the paste under the water with the impeller. This is summarised as a peculiarity of this sample which demands that pulping must be done under water.

Considering the extent of frothing observed as indicated in Figure 6.3, another issue that needs to be addressed is the origin of this froth. A possible assumption is for an inherent frothing constituent in the heterogeneous sample. Exploring this assumption, an inventory of organics present in the sample shows that none of the thermoplastic constituents, PVC, ABS, PET, etc., (see Table 2.3) are water soluble. Considering the flame retardant additives in the resins, most

congeners in this broad class are reported as not being water soluble (D'Silva, 2004). However, tetrabromobisphenol-A (TBBPA), which is a principal epoxy resin used in PCBs, is reported to show low water solubility (Chemtura, 2005). This makes the analysis more interesting, and this is the basis for investigations detailed in Section 4.5.1.

The froth stability tests with the pulp of the sample gave a dynamic froth stability height of 5 cm, whilst the filtrate of the pulp of the same solid concentration gave no stable froth that could be measured. The surface tension measurement of the pulp filtrate also gave averages around 72 dynes/cm – similar to that of deionised water. These two observations tend to indicate that the observed frothing is due to something else, other than a soluble heteropolar organic compound in the sample. This is further substantiated by the fact that the actual solubility of the suspect compound (TTBPA) is 0.148 mg/l (Chemtura, 2005); a value about one-hundredth of typical surfactants dosages (Crozier and Klimpel, 1989). Hence it can be safely inferred that the observed frothing is not due to inherent surfactant constituents in the sample.

Another possibility is that this froth resulted from fine particle stabilisation. In this context, it may be necessary to first address some basics of the frothing phenomena. Froth is formed on aerating a solution or a suspension if trapping of air (or gas) bubbles by the liquid film can be achieved. Froth is therefore a dispersed system; it will want to break down spontaneously to lower overall surface and energy (Harris, 1982). This is to say, froth is essentially unstable. Stability of the froth film is, therefore, the major issue in achieving a tangible froth.

In surfactant solutions, overall surface tension is lowered by the surfactant (Section 3.2). This also lowers the free energy difference accompanying surface area reduction. This reduces the spontaneity of breakdown, giving a metastable two-phase froth. In pulps of surfactant solution (as in mineral processing), it is recognised that the stability of the three-phase froth is increased or decreased by solid particles in the pulp – particle size, concentration, shape and degree of hydrophobicity of the solid particles being the interacting factors (Klassen and Mokrousov, 1963; Harris, 1982, Feng and Aldrich, 1999, Pease *et al.*, 2005). With particles of low hydrophobicity, froth stabilisation occurs when a closed packed monolayer of particles is formed in the froth film (Harris, 1982). In this case, the particles attached to the interfaces cannot be

forced out of the film and the two interfaces are kept apart. Flocculation of particles also prevents coalescence of bubbles in the froth (Harris, 1982). This sort of reinforces the film wall.

The other extreme that also exists is stability of froth solely by fine particles in surfactant free pulps. Molecular solutions of compounds such as diacetone alcohol and ethyl acetal (compounds that do not alter solutions surface tension) have been shown to produce adequate froth with fine coal (hydrophobic) particles (Lekki and Laskowski, 1975). Three phase froth has also been generated by aerating a suspension of clean nanosized hydrophilic silica particles in distilled water (Bindal *et al*., 2002). It was submitted that the foaminess observed was directly proportional to particle concentration, inversely proportional to particle size, and the self organization of the colloidal particles into a layered structure between gas bubbles provided a barrier against coalescence, thereby stabilising the foam lamella (Bindal *et al*., 2002).

This brief about froth phenomena is provided to submit that, hydrophilic and hydrophobic particles have been observed to stabilise froth; appropriate particle size is what matters. In a two-phase froth system, lowering of surface tension is a prerequisite, while this is not compulsory to achieve a tangible three phase froth – fine particle stabilisation will suffice. From this standpoint, it is easy to see the possibility of the observed froth resulting from fine particle stabilisation. The sample contains about 65 % passing 38 µm. It was pointed out that the bulk of the finer constituents will be the brittle glass fiber and thermoset (epoxy resin) constituents (see Section 5.2). A close-packed layer of fine hydrophobic particles enveloping gas bubbles in the froth lamella is the major mechanism that can be inferred for stabilisation of the froth. Such stable bubbles floating around at the pulp froth interface are easily seen from the side of the cell. The thick bubble interstices seen in the froth (as in Figure 6.3) also suggest flocculation of particles, thereby reinforcing the bubble walls.

Considering the high mass pull observed (above 50% in most cases, see Figure 6.4), it is also possible to expect that total froth may not result from true flotation due to natural hydrophobicity of some particles alone. Other effects, such as entrainment and entrapment occur in flotation (George *et al*., 2004), and can be expected under such high mass pulls. Fine particles can easily entrain with water, even if not hydrophobic. Strands of copper particles from the PCB traces could also be found in the float fraction, while glass fibers abounds (See Appendix 2).

Entrapment within bubble-particle agglomerates under bulk upward mass transfer will be enhanced by the elongated morphology of such fibrous copper trace and glass particles. For the glass fibers, it will be recalled that in PCB production, the fibers were impregnated with the resin until it sets in place on the fiber. Strong adhesion between the reinforcement and the matrix is a quality requirement in composites. Hence, flotation due to air bubble attachment to the resin impregnated pseudo-hydrophobic surface can be another strong reason for the glass fibers transport to the froth. The various kinetic regimes will be expected to promote the true flotation and other effects differently. This can reflect in how well the responses under each regime fit the first order kinetics.

6.3.2 Kinetic Response

Figure 6.4 shows the cumulative mass pull with time under varying kinetic regimes. The error bars were plotted as the standard error of the mean of the duplicate values for each data point on the plot. The markers tend to eclipse the bars for some points, the standard errors being very small. Data details for the figure and the error analysis are provided in Appendix 2. The E11A condition (see Table 4.1) shows that at the 18 wt. % solid concentration, the proportion of froth-phase bound particles in the cell appeared to be too high that mass pull did not stabilise with time - even after 30 minutes. Driving the rate higher with higher hydrodynamics will simply worsen entrainment and compromise selectivity. The high proportion of the glass fiber particles and its tendency to increase viscosity due to the elongated morphology will also aid this. The lower solid concentration was therefore used in subsequent experiments.

With increasing combinations of the kinetic parameters, the mass pull rate can be seen to increase until the mass recovery curves show definite asymptotes at the experimental conditions of E21C, E22B and E22C. As projected (in Section 6.2), it is notable that this prevailing kinetic condition, which suffice to keep the particles in suspension, corresponds to impeller energy and aeration rate much lower than what is found in conventional flotation of ores that also liberate in this fines size range. This can be connected to the much lower aggregate density of this sample.

As expected, the observed mass pull rate varied over time for the different regimes. Considering the regimes with fully defined responses under the time interval (with asymptotes in Figure 6.4),

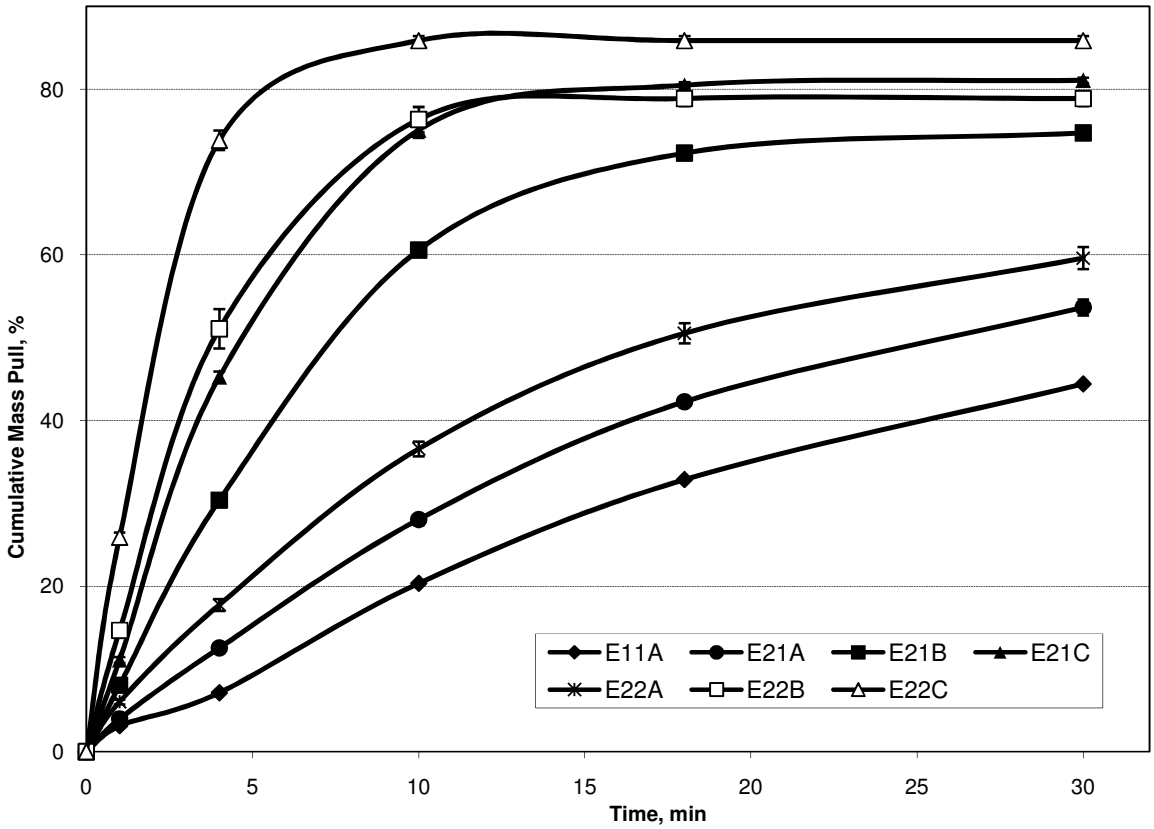

Figure 6.4: Cumulative mass pull with time under natural hydrophobic response and varying kinetic parameters.

mass pull under E21C became very faint in the last 18 to 30 minutes; under E22B, mass pull stopped at around 12 minutes of flotation. For E22C, mass pull ended under 10 minutes (Appendix A2: Table A2.4). The extent of fit of the responses to the classical first order model (Equation 4.1) is shown in Figure 6.5. Detail of the fitting data is shown in Table A2.6. E22B clearly shows overall higher kinetics compared to E21C, whereas the cumulative plots for the two regimes give competing performances in Figure 6.4. The higher correlation coefficient shows E21C conforms more to the first order trend in Figure 6.4. Although the responses under E22B and E22C regimes ended earlier due to the higher prevailing kinetics, so that the fits are fully described with fewer points, yet the responses fit well while they last. In general, all the conditions gave good correlation, and this indicates that the observed responses conform to describable froth flotation phenomena. However, the reverse enrichment of the desired metallic values into the sinks will give surer basis for assessing the performance of the scheme.

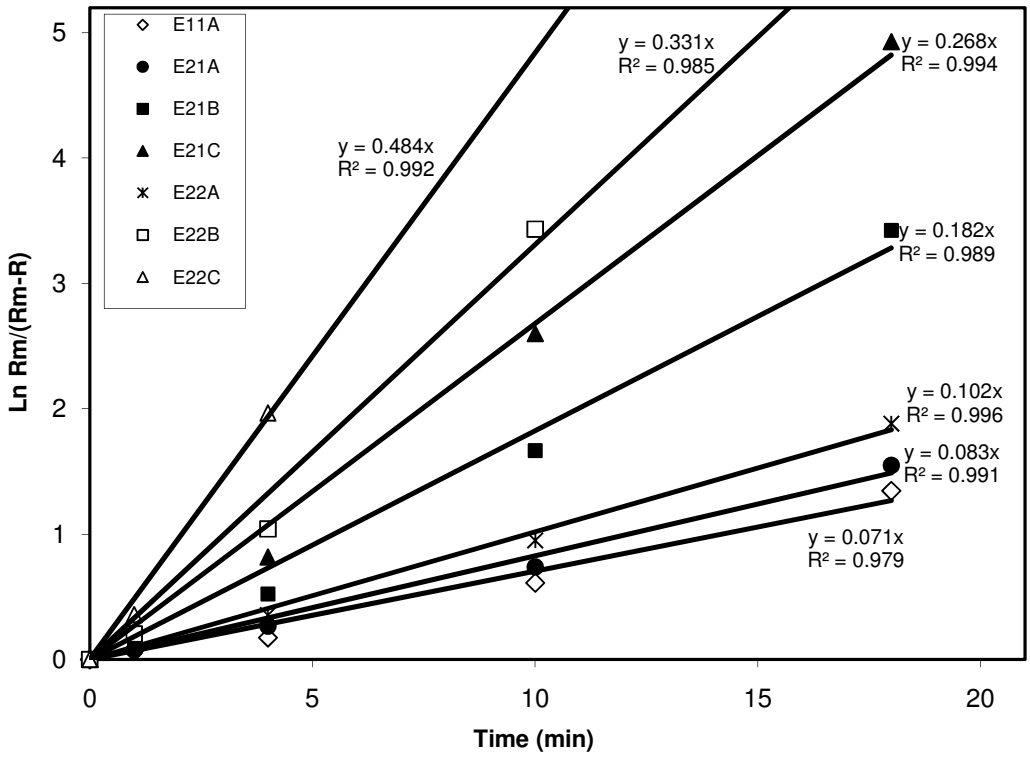

Figure 6.5: First order fitting of PCB comminution fines NHR under various kinetic regimes

6.3.3 Sink Enrichment: Digested Total Metallic Content

Figure 6.6 summarises the sinks' enrichment based on the fractional digestion data, as described in Section 4.5. Relevant data and computation details for the figure are shown in Appendix A2. The general trend shows assay-recovery tradeoff typical of beneficiation operations. The low enrichment levels (assays) indicated for E11A and E21A confirms the inadequate pulp density and kinetics noted for these conditions. The highest recovery in E11A merely indicates that the bulk of the feed (concentrate mass being 55% of feed) still remains in the sink; 100 % recovery to sink can as well be achieved by carrying out no beneficiation. E22C gave indication of the best metallic assay as being 43 %, but with the worst compromise on recovery. E21C and E22B with close performances based on kinetic assessment, appear to give the best combinations of assay and recovery, with 42 % and 38 % assays and recoveries of 39% and 41% respectively.

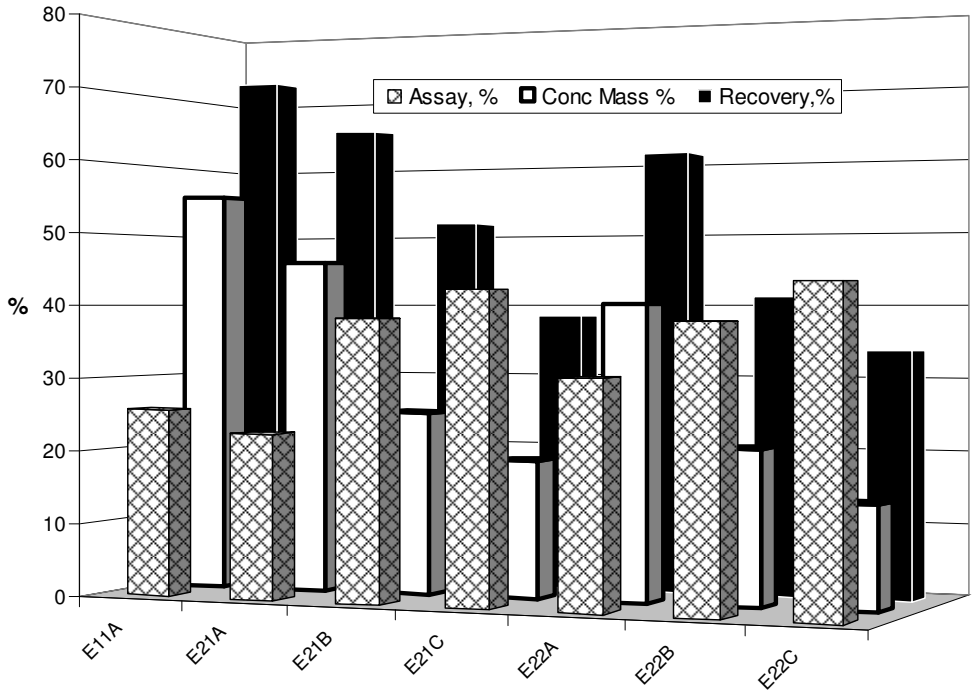

Figure 6.6: Indications of enrichment of metallic values into the sink fraction. *(Metallic assay inferred from total fraction digested. Concentrate mass percent is the proportion of final sink to feed and recovery of metallic values to sink based on the indicated assay value)*

As these responses are based on the natural hydrophobic response, with no collector or frother and no treatment to alter hydrophobicity, the responses must be explained from the kinetic parameters variation. From the flotation cell operation, higher impeller speeds, at constant aeration, produce finer bubbles. The figures in Appendix A2.5 show frozen frames that give visual indications of sizes at the various kinetic regimes. Finer bubbles at constant aeration imply higher bubble surface area, lower buoyancy and increased bubble residence time. Increased turbulent dissipation energy is also a direct effect of higher impeller speed. All these factors increase the efficiency of particle bubble collision (Duan *et al*., 2003; Pyke *et al*., 2003). With favourable surface conditions for attachment, higher collision efficiency in turn gives higher collection efficiency.

Taken to the extreme, this condition (increasing impeller speed and consequently lower bubble sizes) can also increase turbulent carry-over and entrainment at the expense of the reverse recovery. Froth interstices, which are conduits for entrainment, increase. Resultant upward momentum also increases resistance to sinking for otherwise sink-fraction particles. Hence,

higher mass pull (lower sink concentrate mass) was observed from increasing impeller speeds, as can be seen in Figures 6.4 and 6.6, when comparing E22A, E22B and E22C, or E21A, E21B and E21C. It follows that a lower concentrate mass resulted in a lower reverse recovery; this implies target value loss to the high mass pull. Conversely, assay increased with a lower concentrate mass and a lower reverse recovery as more froth phase particle could rise at the higher mass pull, leaving a smaller but richer sink.

The performance across the category can also be resolved on this basis. Studying the response under E21C and E22B regimes, the result reflects the interplay of superficial gas velocity (J_g, cm/s), the superficial surface area flux (S_b, s^{-1}) of bubbles and the actual bubble sizes (d_b, cm) on the observed recovery and rate. S_b is a function of J_g, which is a function of aeration rate (Q), but S_b is also dependent on d_b (Vera *et al.*, 1999; Schwarz and Alexander, 2006):

$$S_b = {}^{6J_g}/_{d_b} \quad . \quad . \quad . \quad . \quad . \quad . \quad . \quad . \quad . \quad 6.1$$

while,

$$J_g = {}^{Q}/_{A} \quad . \quad . \quad . \quad . \quad . \quad . \quad . \quad . \quad . \quad 6.2$$

where A is the cross-section area of the cell.

It follows that increasing Q increases J_g and vice versa. However, if such operation alters d_b simultaneously, S_b will not change proportionately. Under the regimes in focus, in moving from E21C to E22B, bubble size was increased both by increasing Q and lowering the impeller speed. Table 6.1 gives ratios of these parameters under these regimes at the constant cell cross-sectional area and based on the estimates of d_b in Appendix A2.6.

Table 6.1: Ratio of some kinetic parameters under E21C and E22B regimes

Parameters	Ratio of parameters under regimes	
	E21C Regime	E22B Regime
Aeration rate, Q	1	2
Superficial gas velocity, J	1	2
Bubble diameter, d_b	1	2.5
Superficial surface area flux, S_b	1.25	1

Connecting this to what was observed, the higher buoyancy of the larger bubbles under E22B, and the larger flow rate reflected in the higher rate constant. But with a lower residence time of the much larger bubbles, particle-bubble collision probability became so low after substantial mass was pulled that mass pull ended around 12 minutes (see Figure 6.4). Under E21C, on the other hand, the higher residence time of the finer bubbles (at higher impeller speed), with the high surface area of bubbles flowing through, maintained collision efficiency such that mass pull persisted after 18 minutes. The E21C regime thus compensated for half the air flow rate and achieved overall higher mass pull over time compared to E22B. However, this extra pull turned out to be a disadvantage based on the elemental analysis of sink enrichment with time.

6.3.4 Sink Enrichment: Elemental Analysis

Table 6.2 shows reconstituted feed assays of selected elements from the float and sink fractions from the batch samples for each investigation, averaged with assay of a direct feed sample. This gives a total of 14 assays averaged for each element. The relative standard deviation for each element in the table gives an indication of how the assays compare in all the batch samples. It shows that the batch samples were generally representative of the bulk, most of the relative standard deviations being under 5%.

Obvious extremes are Pt and Ag, showing that the reasons may be more than sampling variation. Pt reflects the analytical limitation of ICPOES for trace quantities. Ideally, ICP MS is supposed to complement ICP OES with respect to the trace quantities. The analysis at this stage of the investigation being voluminous, with 135 leach solutions, only ICPOES was used because of cost constraints. Silver (Ag) showed peculiar analytical challenges possibly due to light sensitivity of the element and the effects of this on its emission spectra. Ag would have been

better analysed individually using AAS (atomic absorption spectroscopy) rather than multi-element analysis. Again, the constraint is the same. However, to account for any possible variation in feed assays, reconstituted assay for each batch flotation feed was used in all the recovery analyses.

Table 6.2: Reconstituted feed assay of select elements

Element	Average Assay (ppm)	Relative Std. Dev. (%)
Ag	662	19.99
Al	34 864	0.81
Au	202	5.68
Ca	70 078	2.92
Cu	36 783	2.63
Fe	27 656	1.20
Mg	2 001	1.88
Ni	2 195	2.85
Pb	26 007	1.19
Pd	162	1.64
Pt	2	100.8
Si	280	12.79
Sn	36 855	2.25
Ti	2 748	2.38
V	33	2.14
Zn	5 975	3.77

Table 6.3 summarises the recoveries and enrichment ratios of specific elements for all the sinks, while separate plots of the enrichment ratio (ER) versus reverse recovery in the sinks over time for some selected elements under the different kinetics are shown in Figures 6.7 to 6.13. Analytical data and computation details for the figures are presented in Appendix 3. Enrichment ratio (ratio of concentrate to feed assays) has been used to give a uniform basis for comparison as the assays range from ppm to percentage levels for the different elements. In addition, with the assay scale, a response can lie above another, even at t = 0 (that is, before any enrichment), due to feed sample assay variations in such heterogeneous stock. Feed sample assays for gold, for instance, in this analysis ranged, from 190 to 219 ppm, while the range for Pd was 160 – 165 ppm.

Considering the response of gold, the best recovery of 79% was obtained at the lowest ER of 1.72 under E12A conditions. The best ER of 3.65 was achieved with a recovery of 51% under E22C experimental condition (Table 6.3). A combination of 64% recovery and 3.05 ER was obtained under the E22B condition. This can be considered optimum relative to E21C, which gave a recovery of 58% at almost the same ER of 3.08. This is an actual assay of 626 ppm at 58% recovery in the case of E21C, with an equivalent concentration of 622 ppm at 64% recovery for E22B. Trading off such little enrichment for a 6 % higher recovery is a good economic judgment for precious metals. The picture is made clear in Figure 6.7 which shows the E22B plot lying well ahead (higher recovery) that of E21C.

For palladium, the E22B plot (see Figure 6.8) also lies clearly ahead and above (higher enrichment) that of E21C showing a notably better performance, with the final assay being 456 ppm at 58 % recovery under E22B. Ni and Zn are other elements for which E22B can be taken as giving the best performance (see Table 6.3), with actual assays of 5562 ppm and 1.43%, respectively.

Table 6.3: Recoveries (Rec) to and Enrichment Ratios (ER) in the sinks for specific elements

Elements	E21A		E21B		E21C		E22A		E22B		E22C	
	Rec, %	ER	Rec, %	ER	Rec, %	ER	Rec, %	ER	Rec, %	ER	Rec, %	ER
Ag	42	0.93	24	0.80	19	1.04	32	0.79	18	0.87	17	1.18
Al	46	0.99	22	0.74	16	0.83	39	0.96	18	0.88	12	0.88
Au	79	1.72	68	2.52	58	3.08	77	1.90	64	3.05	51	3.65
Ca	42	0.92	19	0.63	12	0.66	35	0.87	15	0.72	10	0.67
Cu	66	1.44	47	1.70	38	2.04	61	1.53	41	1.93	31	2.21
Fe	61	1.35	42	1.51	33	1.76	56	1.38	35	1.65	27	1.93
Mg	45	0.98	23	0.79	17	0.90	39	0.96	20	0.93	14	1.02
Ni	76	1.65	60	2.21	50	2.66	72	1.78	54	2.56	42	2.97
Pb	74	1.60	55	2.02	45	2.37	67	1.68	46	2.20	34	2.40
Pd	80	1.74	64	2.37	52	2.74	77	1.91	58	2.76	46	3.23
Si	37	0.82	27	0.93	30	1.57	45	1.11	31	1.47	32	2.23
Sn	70	1.53	51	1.84	40	2.12	64	1.58	42	1.98	30	2.09
Ti	81	1.77	72	2.70	66	3.52	79	1.96	67	3.21	61	4.31
Zn	73	1.58	56	2.05	47	2.50	68	1.70	51	2.44	43	3.05

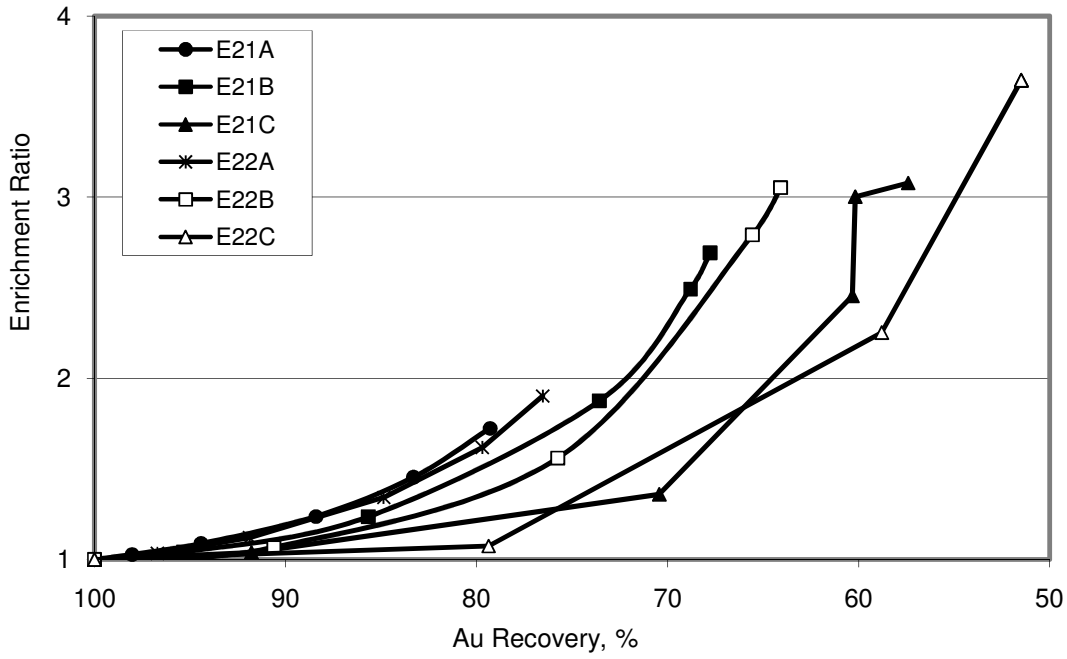

Figure 6.7: Enrichment ratio vs. recovery of Au to sinks under varying kinetic regimes.

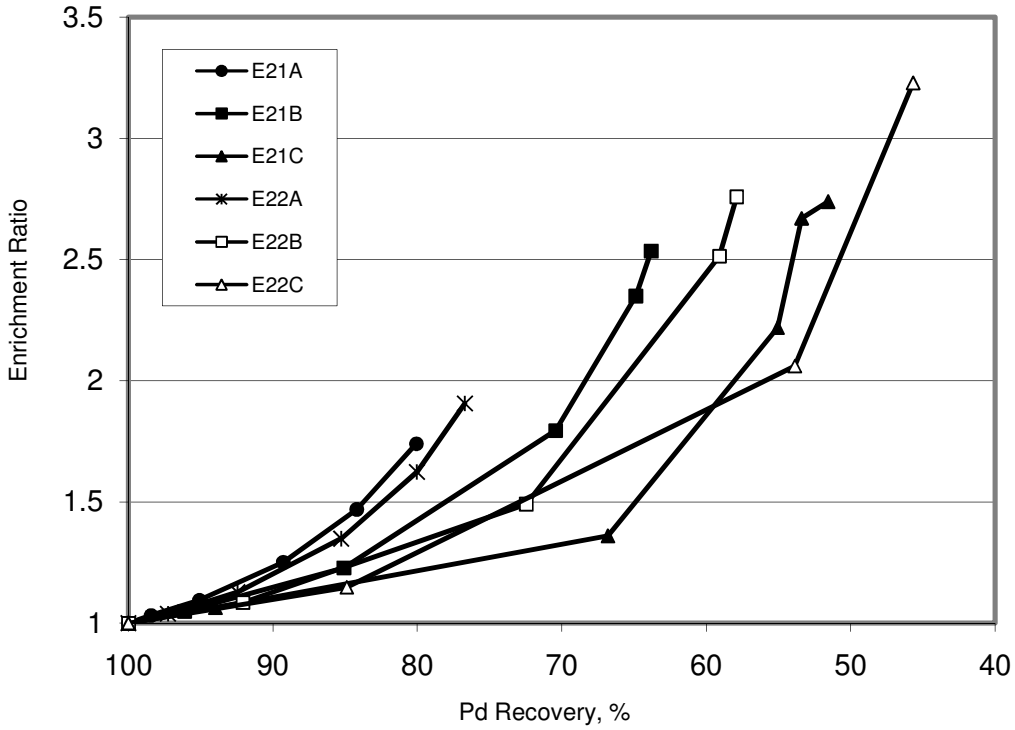

Figure 6.8: Enrichment ratio vs. recovery of Pd to sinks under varying kinetic regimes.

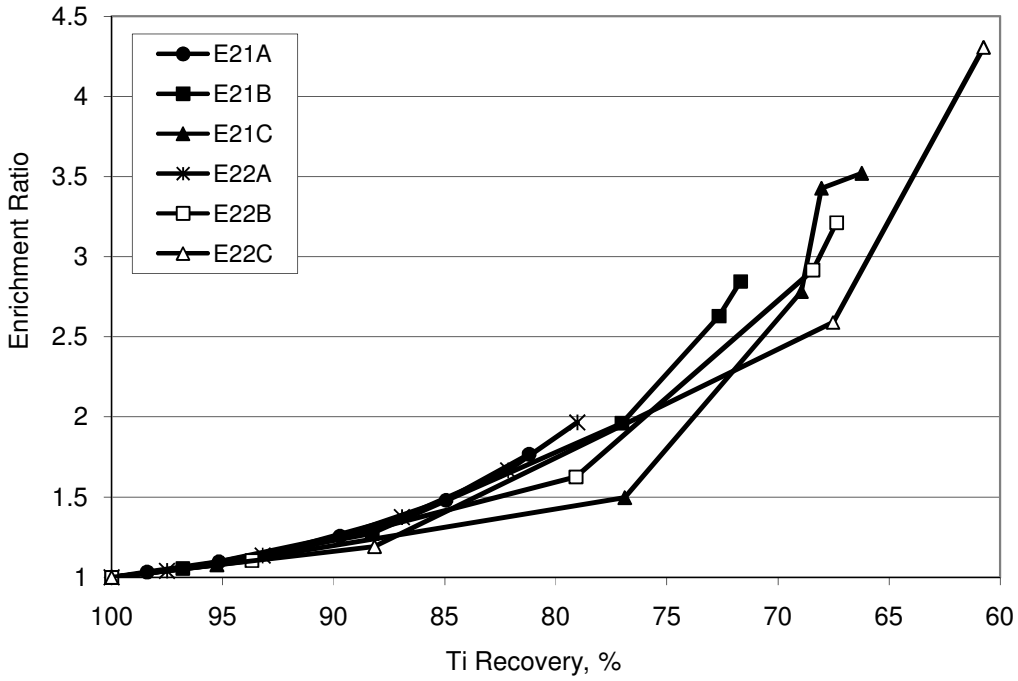

Figure 6.9: Enrichment ratio vs. recovery of Ti to sinks under varying kinetic regimes.

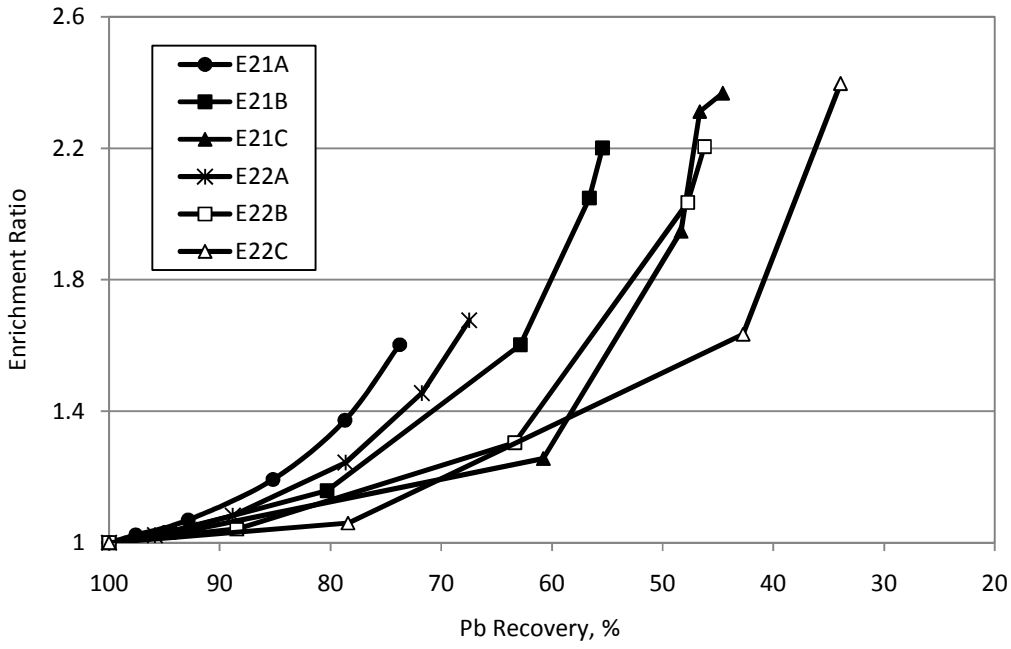

Figure 6.10: Enrichment ratio vs. recovery of Pb to sinks under varying kinetic regimes.

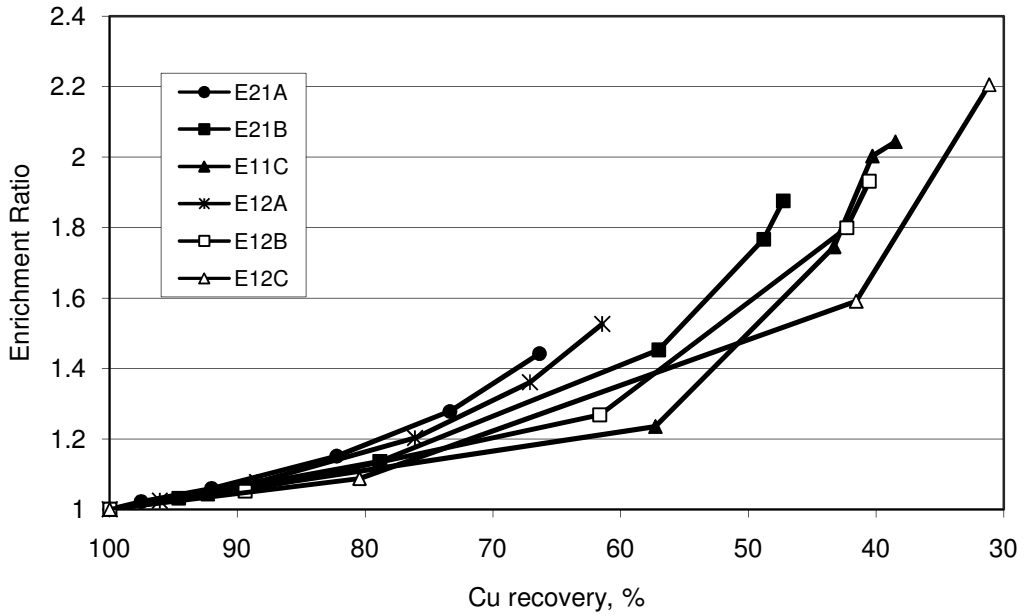

Figure 6.11: Enrichment ratio vs. recovery of Cu to sinks under varying kinetic regimes.

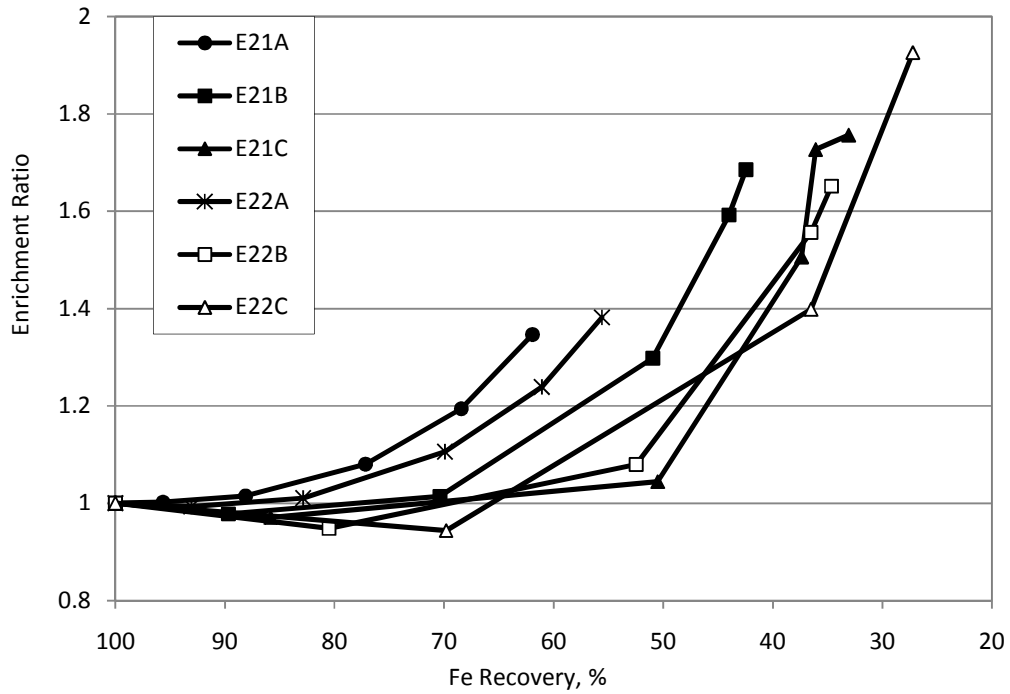

Figure 6.12: Enrichment ratio vs. recovery of Fe to sinks under varying kinetic regimes.

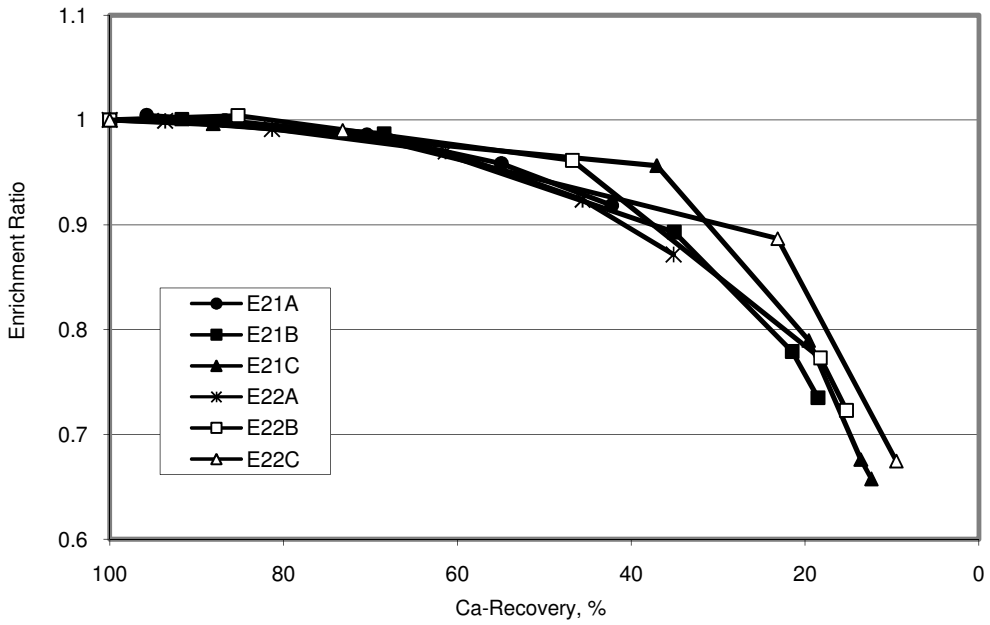

Figure 6.13: Enrichment ratio vs. recovery of Ca to sinks under varying kinetic regimes.

For Ti and Pb, a careful observation of the responses in Figures 6.9 and 6.10 shows that E21C gave a better performance than E22B. Before 18 minutes of flotation, mass pull under E22B conditions stopped (Figure 6.4), while under E12C condition, little mass pull still continued until the 30th minute of flotation. In this last interval, a disproportionate drop in recovery versus ER in all the E21C plots in Figures 6.7 to 6.12 can be observed. Plots of Sn and Zn (not shown) also show the same trend. Comparing the two kinetic regimes at the end of 18 minutes, E21C gave better enrichment ratios and better or almost equal recoveries when compared with E22B. This implies that E21C operating parameters should have run for 18 minutes, as for E22B, in order to result in better ER and recovery for these elements.

The response for Fe (Figure 6.12) also shows best performance under E21C, though with high compromise on recovery, dropping down to 37 % at 18 minutes. With E22B and E22C condition, a worse performance of negative enrichment could even be observed at some stages in the pulp. This negative enrichment is more pronounced with Ag, Mg and Al (Table 6.3), showing that these elements prefer the froth phase. Recoveries dropped below 20 % at ER of 0.9 under E21C for Mg, for instance. Ca is of special interest due to its significant proportion ~7 % by mass in the feed (Table 6.2). Consistent reduction in Ca assays in the sink fractions over time

(negative ER) for all the kinetic regimes can be seen in Figure 6.13, giving less than 15 % residual recovery in the sink for E21C. Platinum assays were too low – a few ppm – for purposes of reliable analytical figures (see relative standard deviation of Pt assay in Table 6.2).

To explain these responses, it is expected that metallic particles reports to the sink. Metallic particles will have a high surface energy, be hydrophilic (Gupta and Yan, 2006) and therefore prefer the sink. Density advantage is also expected here to enhance the separation between denser hydrophilic metallic particles and lighter hydrophobic plastic particles. The questions then will be: Why is recovery to sink not 100% for such metals, and why do some metallic elements preferentially report to the froth?

It is necessary to appreciate that the elements are contained in particles occurring as some end-use alloy or compounds. These particles are present in diverse shapes, and can still be part of a composite particle. Considering the fact that composite particles still exist in this sample (see Section 5.2), the response of elements occurring in such particles would not be expected to be perfect. Comminution of ductile metallic materials generally produces particles with random shapes (Section 5.2), including flattened pieces that will have a tendency to float around in the pulp, particularly in this size range. Gold flakes float for this reason in conventional minerals flotation circuits (Allan and Woodcock, 2001).

The split of Cu to the float and sink stream is another example that can be readily attributed to shape influence. Copper particles from the PCB traces remain in elongated forms (Figure A2.5) that can be easily carried over into the froth by rising masses and bubbles. Hence, short strands of the PCB copper trace were found in the float, as noted previously (see Section 6.3.1). On the other hand, those from copper nuts, edges, etc., which could have chipped into a more cubical particle, can resist the upward current and report better to the sinks.

For metals preferring the froth phase, probable reasons could also be the size and shape in which particles occur. For instance, Al, Ca, Mg from the oxides (see Table 2.4) will occur more in the finer sizes from comminution of the ceramics. Separate elemental analysis of −38 µm and −75+38 µm size fractions of the fines sample (see Table A2.11 and Appendix 2) show all the metals have higher assays in the coarser fraction (allowing for a minimum 10% difference for significance), except Al and Ca. The brittle ceramics containing Al and Ca would have

undergone more selective pulverization relative to the ductile metallic alloys. The much finer particles will be entrained with water at the prevailing kinetic condition more easily than the relatively larger particles. It is expected that favourable kinetics will differ among particles in the whole -75 µm size range (Pease *et al*., 2005). However, fine Al bearing particles can also occur as flattened chips from the ductile alloy. Chances are that the flat or foil mini-chips, coupled with low density of aluminum, can be carried under bulk upward mass transfer of the glass fibers. The same shape factor can be expected to influence Mg, being even lighter than Al.

From the foregoing discussions, it follows that the interacting mechanisms that could be responsible for the responses observed include: natural hydrophobic response to float and hydrophilic preference for the sink; presence of hydrophobic material on an otherwise hydrophilic surface; particle morphology (shape) enhanced carryover under bulk upward mass transfer; and fine particle entrainment in water to froth. The kinetic regimes investigated were seen to promote these factors differently as the responses vary with kinetic conditions. To one extreme of kinetics, recovery can be extremely compromised, and to the other, enrichment.

The actual range of values at which the kinetic parameters will give the most favorable regime to optimize the performance will of course vary to some extent among cells (O'Connor *et al*., 1987). In the present observation, the favorable range is 400 rpm impeller speed with 1000 ml/min aeration to 500 rpm with 500 ml/min aeration (the range for E21C and E22B regimes). This gives an indication of the low energy (turbulence) requirement of this sample relative to conventional mineral flotation. The analysis also shows that the interactions of the various factors favor enrichment and recovery of Au and Pd to the sink. The response from these precious metals, which are the economic drivers for PCB resource recovery, shows the scheme can indeed be prescribed for PCB comminution fines beneficiation.

6.3.5 Improving the Performance of the Natural Hydrophobic Response Scheme

With the recovery values across the elements from the NHR scheme, performance improvement is conceivable. The observed float fraction being so high, it was projected that the kinetics of the operation should be slowed down to reduce mass pull rate. The intention was that lower mass pull rate would allow true flotation to be more pronounced, while entrainment and entrapment would be minimized. With about 65% passing 38 µm in this sample, and recognising that the

same kinetic regime cannot favour all the particles in the -75 µm range (Pease *et al.*, 2005), a narrower size distribution was also probable for better performance. Investigations in this regard are detailed in Section 4.5.2.

The impeller modification indeed gave glaringly smaller bubble sizes at the 300 rpm impeller speed, compared to what was obtained before modification (see figures in Section A2.5, Appendix 2). Coupled with the sample size of 150 g, the turbulence in the cell is much more moderate. After 18 minutes, mass pull rate at 300 rpm was observed to become very slow in the initial trial runs, and the impeller speed had to be increased to 350 rpm to increase particle bubble collision and sustain the pull. Investigations with this kinetic regime was designated XNHR. Table 6.4 shows the averaged cumulative mass pull for triplicate experiments. The raw data is contained Section A2.7, Appendix 2. Compared to the initial responses, shown in Figure 6.4, it can be observed that the prevailing kinetics after the impeller modification gave generally lower cumulative mass pulls. The response was closest to what was obtained under E21A conditions (see Table 6.3). In these two regimes (E21A and XNHR), the effect of smaller bubble size on the kinetics compensated for lower solid concentration (collision frequency), such that the cumulative mass pull in the same time interval was comparable.

Table 6.4: Cumulative mass pull after impeller modification

Time (minutes)	Cum Mass Pull (%)	Standard Deviation
18	41.2	1.8
30	52.5	1.2
48	57.7	0.4

In the final analysis, the intention was to achieve an: increase in recovery of metallic values to the sink without compromising the enrichment level obtained; increase in enrichment while maintaining recovery levels; or increase in both. Table 6.5 shows the enrichment ratio and recovery levels in the prevailing kinetics compared to what was obtained in some of the previous conditions. Based on this elemental analysis, the performance is again almost the same as in the E21A regime and a remarkable improvement may not be inferred. This could show that equivalent cumulative mass pull over a given time is effectively an indication of similar kinetic regimes. A more definite difference in performance can therefore be expected if equivalent mass pull is obtained over a different time interval. On this basis, the performance after 48 minutes can

be compared to what was obtained in E22A, which gave a comparable cumulative mass pull of 59% after 30 minutes. Still a drastic improvement may not be inferred, because the little increase in recovery appeared to be due to the sink fraction being a bit larger and ER dropped off a little for the increase.

Table 6.5: Comparison of reverse metallic recovery (Rec) versus enrichment ratio (ER) before and after impeller modification

	XNHR - 18 mins		XNHR - 30 mins		XNHR - 48 mins		E21A - 30 min		E22A - 30 min	
Element	**Rec, %**	**ER**	**Rec, %**	**ER**	**Rec, %**	**ER**	**Rec, %**	**ER**	**Rec, %**	**ER**
Ag	59.1	1.01	46.1	0.98	40.8	0.97	41.9	0.93	31.76	0.79
Al	57.6	0.98	45.3	0.96	40.1	0.95	45.7	0.99	38.81	0.96
Au	85.4	1.46	80.2	1.70	78.2	1.86	79.3	1.72	76.53	1.90
Ca	56.1	0.96	43.0	0.91	37.4	0.89	42.3	0.92	35.11	0.87
Cr	63.5	1.08	53.3	1.13	48.3	1.15	-	-	-	-
Cu	74.8	1.27	68.1	1.44	64.7	1.54	66.4	1.44	61.42	1.53
Fe	65.2	1.11	55.2	1.17	51.6	1.23	61.9	1.35	55.59	1.38
Mg	59.5	1.01	47.3	1.00	41.4	0.99	44.9	0.98	38.78	0.96
Ni	80.1	1.36	73.9	1.57	71.2	1.70	76.1	1.65	71.57	1.78
Pb	77.2	1.32	69.9	1.48	67.0	1.60	73.7	1.60	67.47	1.68
Pt	82.5	1.41	77.4	1.64	75.1	1.79	-	-	-	-
Pd	84.0	1.43	78.3	1.66	76.0	1.81	80.1	1.74	76.71	1.91
Sn	75.0	1.28	67.0	1.42	64.0	1.52	70.4	1.53	63.76	1.58
Ti	86.7	1.48	82.2	1.74	80.0	1.90	81.2	1.77	79.02	1.96
V	62.2	1.06	51.3	1.09	46.5	1.11	53.6	1.17	46.61	1.16
Zn	81.1	1.38	75.5	1.60	72.6	1.73	72.9	1.58	68.44	1.70

The summary observation, therefore, is that if the kinetics is slowed down too much, in an attempt to pull slowly over time, particle bubble collision gets too much compromised and even the natural hydrophobic particles recover poorly. This is what was observed when the impeller speed had to be increased to 350 rpm under XNHR, otherwise a bulky sink would be obtained with minimal enrichment. If the kinetics is also to the extreme, the froth phase particle can be pulled more effectively, leaving a cleaner sink but grossly compromising the reverse recovery. At the reduced kinetics, when comparing achieved reverse recovery and enrichment, the idea of minimizing turbulence and a slower mass pull rate does not appear to improve selectivity. The bulk flotation behavior of the sample basically remains the same: the higher the mass pull, the

lower the reverse recovery and the higher the reverse enrichment. In other words, at the lower kinetics, reverse recovery loss to float still occurs in proportion to the mass pull. The investigation over narrower PSDs provides useful insight to reconcile this.

Figure 6.14 shows cumulative pulls over 30 minutes at narrower and varying sample PSDs. Comparing the mass pulls, the −38 µm fraction gave the highest mass pull, while the −106 + 75 µm fraction gave the least. At the same sample mass of 150 g, the actual number of particles in the samples for each of the size classes certainly differed widely. This translates into a major difference in the kinetics of particle bubble mass removal, which reflected in clear differences in the cumulative mass pulls. This again shows that cumulative mass pull over a given time is a major indicator for effectively different kinetic regimes. Also, the responses further support the submission on fine particle stabilisation of the NHR froth, as the coarsest size fraction pulled least mass. With less stable froth, bubbles lose part of their particle load back to the pulp.

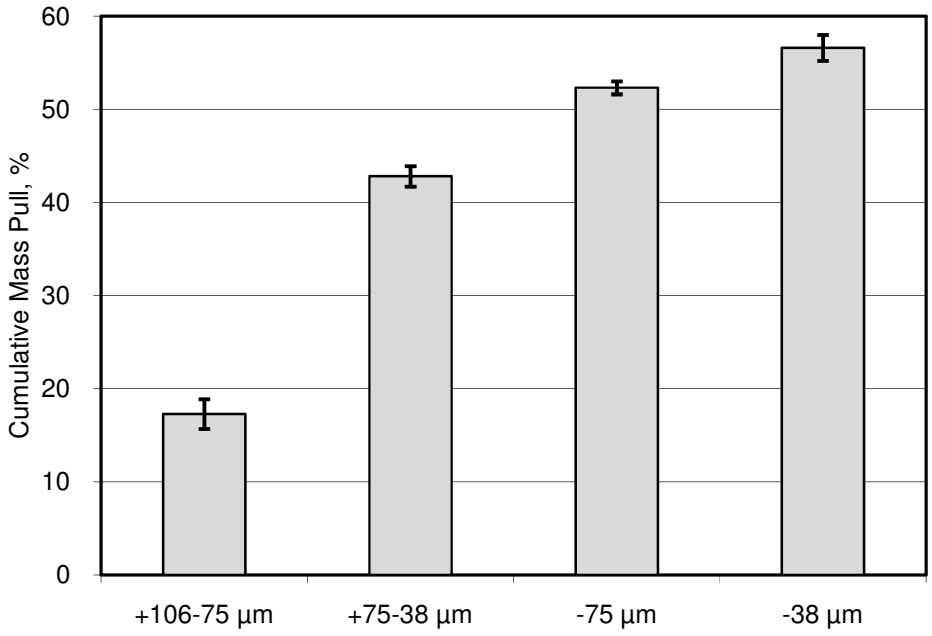

Figure 6.14: Cumulative mass pulls after 30 minutes for varying sample PSDs

Table 6.6 shows the recovery and enrichment ratios obtained from the fraction assays, while Figure 6.15 shows a comparison of the performance for specific elements – Au, Pd and Cu –

over the different size ranges. Comparing – 75+38 µm and –38 µm fractions, the coarser size clearly shows better recoveries and enrichment ratios. For Au, Pd and Cu for instance (see Figure 6.15), recoveries were 91.2%, 92.8% and 86.3%, with enrichment ratios of 1.6, 1.62 and 1.51 respectively for –75+38 µm. For the same elements, recoveries were 64.9 %, 66.5 %, 62.7 % and enrichment ratios 1.44, 1.48 and 1.39, respectively for –38 µm fraction. The prevailing (XNHR) kinetics obviously favours the coarser fraction. This implies that operating at narrower PSD and favourable kinetics for each size fraction will achieve better performance from the NHR scheme, compared to processing wide PSDs, such as the –75 µm fraction. As can be seen, the recoveries from the –75+38 µm are clearly higher than for the –38 µm fraction, without compromising the enrichment ratios.

Table 6.6: Comparison of reverse recoveries and enrichment ratios for varying sample PSD

Element	Recovery, %				Enrichment Ratio			
	105-75µm	-75 µm	75-38 µm	-38 µm	+106-75µm	-75 µm	75-38 µm	-38 µm
Ag	93.3	46.1	63.0	29.3	1.14	0.98	1.10	0.65
Al	79.8	45.3	47.6	44.7	0.97	0.96	0.83	0.99
Au	97.6	80.2	91.2	64.9	1.19	1.70	1.60	1.44
Ca	75.0	43.0	42.3	43.2	0.91	0.91	0.74	0.96
Cr	93.2	53.3	67.3	50.2	1.14	1.13	1.18	1.12
Cu	97.7	68.1	86.3	62.7	1.19	1.44	1.51	1.39
Fe	95.6	55.2	69.8	54.0	1.17	1.17	1.22	1.20
Mg	80.7	47.3	49.3	45.8	0.98	1.00	0.86	1.02
Ni	98.4	73.9	88.5	68.4	1.20	1.57	1.55	1.52
Pb	98.5	69.9	88.2	61.6	1.20	1.48	1.54	1.37
Pt	98.2	77.4	93.1	68.9	1.20	1.64	1.63	1.53
Pd	99.0	78.3	92.8	66.5	1.21	1.66	1.62	1.48
Sn	98.3	67.0	86.5	60.4	1.20	1.42	1.51	1.34
Ti	98.6	82.2	92.9	78.0	1.20	1.73	1.74	1.63
V	90.3	51.3	58.6	51.2	1.10	1.09	1.03	1.14
Zn	97.8	75.5	89.5	70.0	1.19	1.60	1.57	1.55

This result shows that the higher mass pull at –38 µm fraction compared to the –75+38 µm fraction resulted in a lowering of enrichment. This would either be due to non-selective entrainment of sink values with water at the higher mass pull or to pure entrapment and carry-over under heavier upward mass transfer. The water recoveries observed over the different size classes is shown in Figure 6.16. The figure shows cumulative mass recoveries to froth versus

cumulative water recoveries over 30 minutes of flotation. The result shows that the finer size fractions recovered less water per unit mass pull compared to the other sizes, as the slopes in the figure indicate. This tallies with observation during the experiment, as the froth from the finer fractions was well drained and drier, with a high dynamic froth height; the coarser fraction was more like a muddy scum and wet (see Appendix 2.7). It is notable here that stability of the froth in the finer fraction does not rely on low surface tension liquid film, hence the air bubbles enveloped by fine hydrophobic particles rising to the froth in the finer size fraction can be expected to entrain less water. The froth from the coarse fraction, on the other hand, being less stable, collapses into a mud that does not allow effective drainage of water trapped within it.

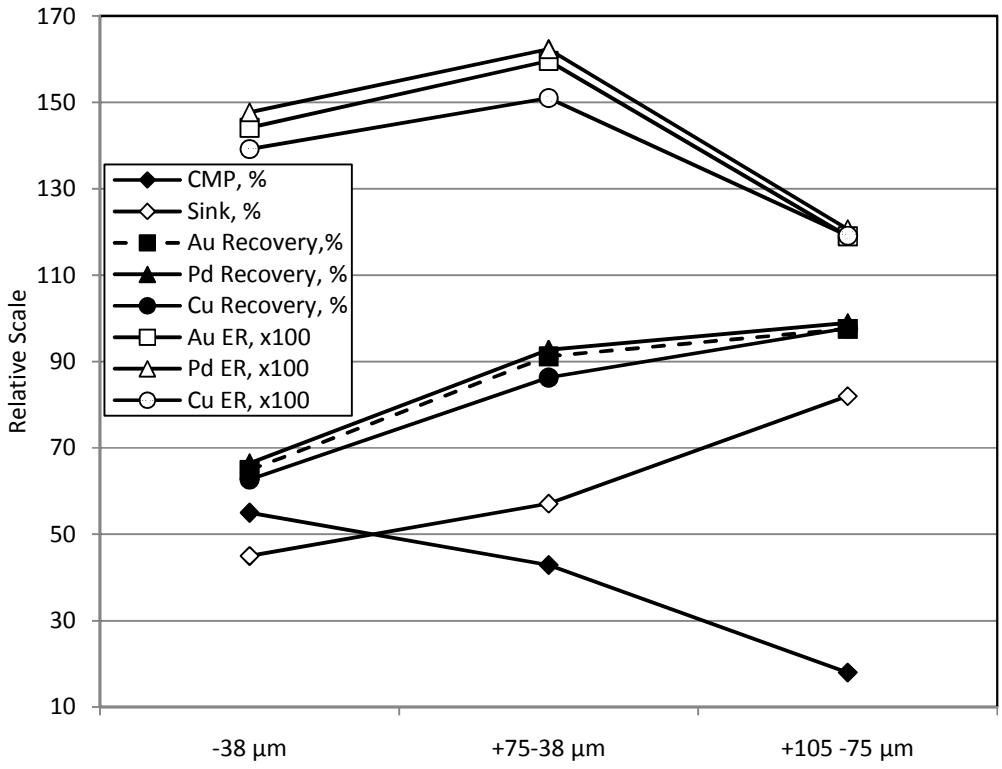

Figure 6.15: Comparison of NHR performance with varying particle size range *The y-axis is a numerical scale to indicate percentages for the cumulative mass pull (CMP) and recovery data, as well as the enrichment ratios (ER) multiplied by a factor of 100 (to accentuate the differences).*

The interpretation that follows from this is that reverse recovery loss due to water entrainment in the finer fraction should be lower, as this fraction recovers less water per unit mass to froth. The higher loss of value to the froth in the finer fraction, which occurs at higher mass pull, should

therefore be due to non-selective transport of sink particles to the froth phase by carry-over under the heavier upward mass transport and entrapment in the froth phase. This effect will be significant in this flotation system where it is the bulk that is responding under natural hydrophobicity and the particles being entrapped constitute a very small proportion.

It will also be noted that the particles rising to the froth also consisted of glass fibers in the bulk. Such particles make the flow more viscous and thus tinier particles are easily dragged along. It follows that the observed bulk NHR response of the sample will be difficult to reverse in favour of the metallic particles that are in a much smaller proportion, hence a recovery versus assay tradeoff occurs readily, as observed when comparing the treatments. The poorest enrichment at the coarsest fraction that recovers the largest amount of water per unit mass pull is understandably due to generally low upgrading, as the bulk remains in the sink and may not be taken as entrainment of the coarse particles with water. The fact that observed recovery at the coarsest fraction is so high (discussed below) shows that the relatively high water pull per unit mass was not entraining values.

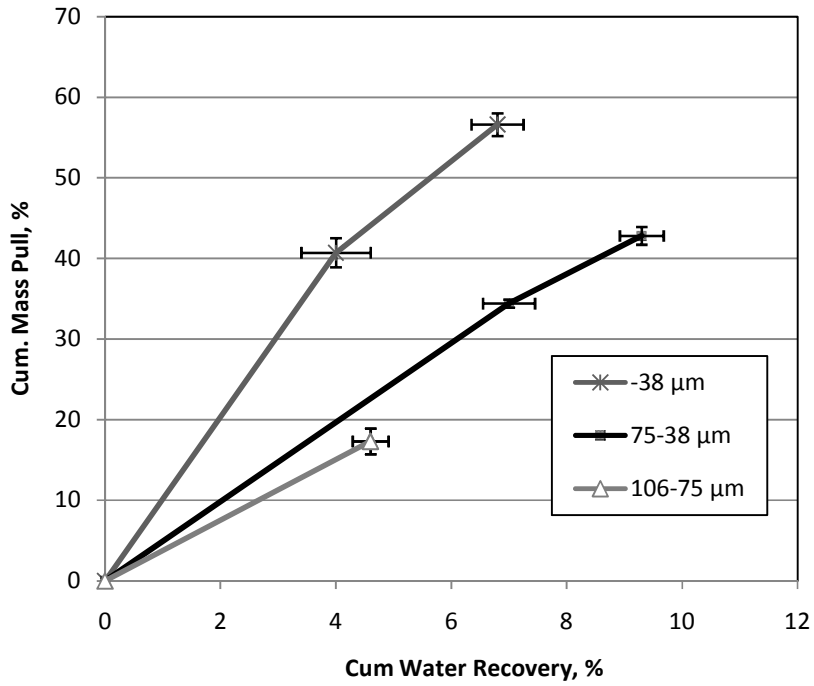

Figure 6.16: Cumulative mass pull versus cumulative water recovery under NHR of samples of varying PSDs.

On another note, this investigation shows that the natural hydrophobic response could still be observed at the coarser size of +75 −106 µm. From Figures 6.14 mass pull can be seen to be least at this size fraction. The total number of particles was much less and particle bubble collision efficiency was very low, so that mass pull stagnated after a little pull (18%).

Although the coarser size fraction also showed natural hydrophobic response, the absence of the fines required to stabilise the froth was obvious. The dynamic froth stability was much lower relative to the finer sizes, as indicated by the froth height in the cell (compare Figure A2.2 to Figure A2.7 in Appendix 2). The lower pull and the heavier coarser sizes also minimised entrapment (as mentioned) and coarser particles would also be more difficult to drag along. Only froth phase particles would, therefore, have best chances of making it to the launder. This gave rise to the high reverse recovery observed: Pd gave a notable recovery of 99 %. Many other metals gave between 98 and 97. However, enrichment was minimal, as the bulk of the feed was still left over as the concentrate under the prevailing kinetics. Using different kinetics to enhance higher mass pull will achieve a cleaner sink. The tradeoff in recovery will depend on how favourable the kinetics regime will be. In all, it can be said that this scheme will work, even for this larger size fraction.

6.4 CONCLUSION

It was projected that the particles in the PCB, being so diverse, some should exhibit natural hydrophobicity and this could be exploitable for a froth flotation scheme. The natural hydrophobic response was first observed under microflotation and then investigated in detail with the Leeds cell as reverse flotation with respect to the metallic values. It was also projected that enrichment versus recovery to the sink under this scheme could be optimised with variation in the operating kinetic regimes. The range of kinetic parameters appropriate for flotation application with this sample was observed. Most of the target metallic values wet and preferentially remained in the sink, justifying the reverse flotation approach. Au and Pd, which are the major economic drivers of PCB processing, were among the elements best enriched into the sink at optima of 64% for Au at an enrichment ratio above three. Ti achieved an even better performance. For these metals, which show preference for the sink, recovery loss to the float was observed to increase with mass pull, and not water recovery, when flotation results over varying

PSDs were compared. Such loss will therefore be due more to carry-over under bulk upward mass transfer and entrapment in the froth. Flotation over narrower size distribution still shows improvement in the performance obtained for the −75+38 µm size fraction, compared to the −75 µm wider PSD.

The results provide the basis to consider froth flotation as applicable for PCB CF beneficiation, and the natural hydrophobic response scheme to be effective in this regard.

7.0 INVESTIGATION OF CHEMICAL CONDITIONING SCHEMES FOR FROTH FLOTATION OF PCB CF

7.1 INTRODUCTION

The investigations into the chemical conditioning schemes are presented and discussed in this chapter. As outlined in Section 4.6, the collectors used were PAX, SMBT and TBAC; the depressants were sodium carboxyl methyl cellulose and Betamin 127A, respectively abbreviated as CMC and B127A hereafter. Investigations with PAX, described separately in Sections 4.6.2 to 4.6.4, are presented together herein for ease of comparison of the treatments.

7.2 MACROMOLECULAR VERSUS GAMMA DEPRESSION

7.2.1 Bulk Depression

As a result of the high response observed under the NHR scheme, application of depressant appears very relevant in PCB CF flotation. Bulk depression was therefore considered first to determine wether the high natural hydrophobic pull could be suppressed, prior to chemical conditioning for selective flotation. Considerations for depressant selection and probable depressants for this type of sample were discussed in Section 3.5.2. As detailed in Section 4.6.1, CMC and B127 were employed for this investigation. With CMC, preliminary dosages from 200 g/ton in steps up to 2 kg/ton did not show any remarkable depression. At these dosages, steady froth built and cumulative mass pull remained high. The high mass pull to be suppressed was blamed. Much higher dosages continued to be used, but frothing and high mass pull continued up to very high dosages used. At 10 mass percent (100 kg/ton) CMC, mass pull of 19.5% was still obtained. At a profuse dosage of 30 mass percent CMC, a 5.7 % mass pull was still obtained. At this dosage, the pulp viscosity had increased noticeably.

A dosage of 500 g/t normally would suffice for effect in normal mineral applications (Bulatovic, 1999). That mass pulls persist at these extreme dosages basically implies that depression of the NHR response with CMC is ineffective. Only physical coating of particles, as in slime coating, appears to be occurring. The froth-phase-bound particles are in a very high proportion, with the

bulk of this at −38 µm. It implies that, without definite chemisorbtion, physical coating with hydrophilic molecules will require a very large dosage for a remarkable drop in mass pull to be observed in this system. The idea of total depression, therefore, appears not feasible within practical CMC dosages.

B127A, on the other hand, shows observable suppression of the natural hydrophobic froth, however, frothing entrainment sets in. Before aeration, the pulp surface shows evidence of wetting as faint traces of natural hydrophobic particles that is normally on the pulp surface was totally absent, being wetted and sank. Froth loading visibly dropped with increasing dosage, as the froth changed to a faintly loaded dirty white and eventually to a clearly unloaded white froth. On skimming, the froth released entrained particles to give a high mass pull, as Figure 7.1 shows. Relative standard deviations (δ_R, %) of the duplicate CMP data in Table A2.12 (Appendix II) all show acceptable spread: the higher spread in the first few minutes of flotation can be allude to imprecision in float skimming between repeats due to higher mass pull rate in this time interval.

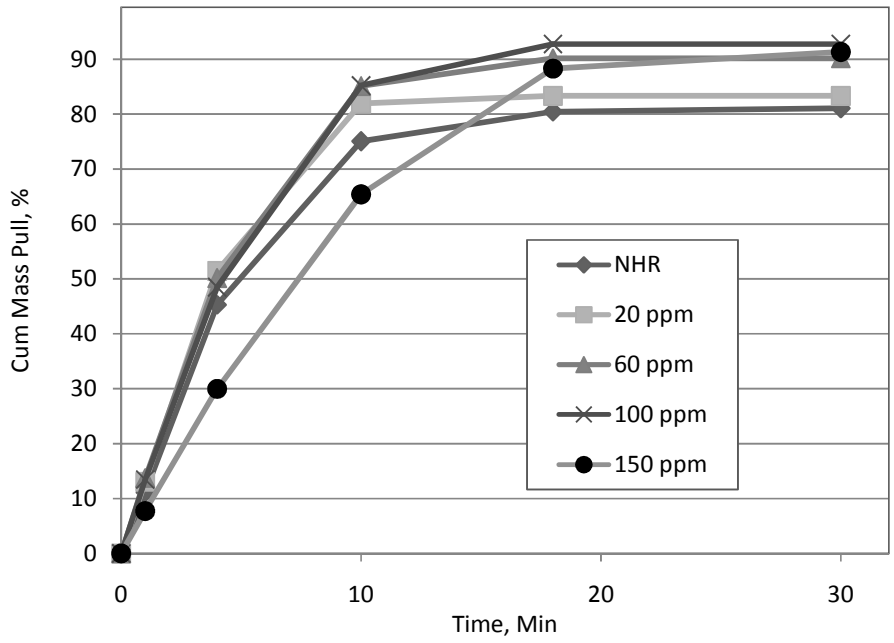

Figure 7.1: Mass pull over time in PBC comminution fine flotation with Betamin 127A as depressant at various dosages.

Generally, the response shows the ease with which the pulp particles entrain readily with water after wetting. The low density and fine size of much of the pulp particles also aid this. As can be observed from Figure 7.1, mass pull increased with dosage, indicating increasing contribution of entrainment. Lower surface tension at higher surfactant concentration (see Equation 3.2) led to easier frothing, smaller bubble sizes, higher froth volume and more froth interstitials (Harris, 1982; Pugh, 2007), all of which promote entrainment. At 150 ppm, the mass pull rate was noticeably slower, indicating that extensive wetting of the particles had occurred; natural hydrophobic response was fully depressed and entrainment was about the only means of particle transport to froth. The run gave a cumulative water recovery of 10.5 %. The plot (Figure 7.1) shows the deviation from classical first order response towards linearity with time until 10 minutes (first four data points for the 150 ppm plot). The entrainment slowed down only after pulp particles neared exhaustion.

Table 7.1: Reverse recovery and sink enrichment ratio for select metallic values at different Betamin 127A depressant dosages (NHR condition implies 0ppm depressant dosage)

	NHR		20 ppm		150 ppm	
Element	Recovery, %	ER, %	Recovery, %	ER, %	Recovery, %	ER, %
Ag	19	1.04	14	0.84	12	1.44
Al	16	0.83	15	0.90	7	0.77
Au	58	3.08	55	3.32	48	5.61
Ca	12	0.66	12	0.73	5	0.59
Cu	38	2.04	31	1.85	18	2.11
Fe	33	1.76	26	1.55	20	2.29
Mg	17	0.90	16	0.95	7	0.86
Ni	50	2.66	39	2.36	22	2.55
Pb	45	2.37	34	2.07	22	2.56
Pd	52	2.74	42	2.54	22	2.51
Si	30	1.57	19	1.16	12	1.42
Sn	40	2.12	30	1.83	21	2.42
Ti	66	3.52	52	3.15	22	2.55
V	25	1.33	21	1.29	12	1.35
Zn	47	2.50	36	2.19	21	2.41

It follows that while trying to subdue one effect of direct mass pull, due mostly to natural hydrophobicity, another major effect of froth entrainment after wetting was setting in. Table 7.1 shows elemental recovery and enrichment ratios at the extreme dosages of B127A used (20 and 150 ppm) and at 0 ppm. The 0 ppm dosage corresponds to the E21C NHR condition. A consistent drop in recovery upon the wetting agent being added can be observed across all the elements. The higher the dosage, the more the values entrained. Wetting increased at the reduced surface tension, depressing natural hydrophobicity; but more froth also formed, with more interstices until entrainment predominated. By 150 ppm, reverse recovery of metallic values compared to that under NHR showed a sharp decrease.

The assays also showed a consistent decrease for some of the elements, such as Pd, Pb, Ti. Only Au appeared to show a remarkable assay increase in compensation for the recovery drop, as shown in Figure 7.2. Cu, also shown in Figure 7.2, shows a minimal assay increase for more than 50% recovery loss compared to recovery at 0 ppm (as in Table 7.1). In general, the observation and analysis show unselective entrainment of otherwise sink phase particles after wetting. Perhaps a lower dosage of B127 would have reduced the frothing and entrainment as the high natural hydrophobic pull to be suppressed demands the high dosages used.

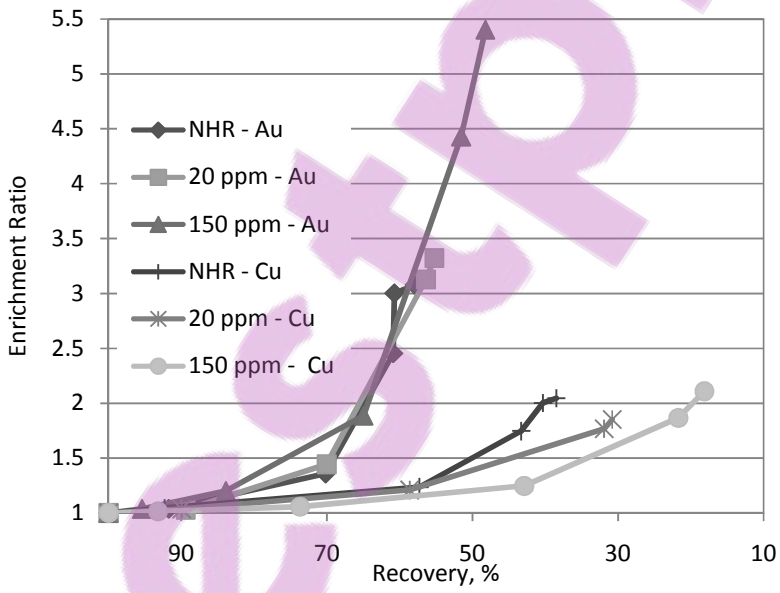

Figure 7.2: Enrichment ratio versus recovery for Au and Cu at varying Betamin 127A dosages

From these observations, attempting to suppress the natural hydrophobic response to allow for direct chemical conditioning of the sample is not advisable. Given the bulk proportion that wants to report to the froth on natural hydrophobicity, it is rational to allow and exhaust this natural response before conditioning. Perhaps a moderate dosage of the depressants will then be effective to subdue any little residual natural hydrophobic particles.

7.2.2 Depression of Residual NHR

After allowing NHR for 30 minutes, a moderate depressant dosage was investigated to suppress any residual natural response. The idea was to ensure a clean undiluted response after chemical conditioning. After conditioning with the depressants, 30 ppm B127A and 3.3% CMC (Section 4.6.1), the responses obtained further reinforced observation made from the depression of the bulk sample. With CMC conditioning after 30 minutes of NHR, froth still formed as when NHR is subsiding. It was lightly loaded, with the particle stabilised froth building up slowly over time. The total sample recovered over the 18 minutes of aeration was 3.8 g, which is 4.7 % of the sink mass before the conditioning (i.e. after the NHR pull).

The B127A conditioning, on the other hand, gave unloaded white froth with small froth bubble sizes, also building slowly up over time. On skimming, the unloaded froth collapsed to release entrained particles giving, a total of 4.5 g mass pull. This is 5.7 % of the sink mass before the conditioning. Under XNHR, in this time interval, the F3 fraction pulled 10.9 wt. % of the residual sink (see Section 6.3.5). Table 7.2 shows the assays of select elements from these fractions with averaged assays of the XNHR F3 (30 to 48 minutes) fraction for comparison. The assays tend to show that when CMC is compared to NHR, it will slightly lower value pull from the residual NHR pulp, in the 30 – 48 minutes of flotation. Given that Ag and Al follow trends opposite to other metallic values in NHR, B127A generally tends to entrain a little more value into the froth. As explained above, the increased wetting in the bulk causes easy entrainment, carrying target metallic values along. This same wetting and entrainment effect was still observed at the 30 ppm dosage in the residual NHR pulp.

Based on the mass pull, some depression of the NHR response can be inferred, but a definite recommendation needs careful consideration. It is notable that CMC dosage was 3.3 % (33kg/ton). A depressant requiring this dosage level is obviously ineffective and cannot be

recommended for application. B127A, on the other hand, suppresses particle bubble attachment, giving clearly unloaded froth. In any case, the overall mass pull difference, with or without these depressants, after pulling the bulk NHR particles, may not amount to too much contamination of a float fraction after collector conditioning. The final decision to use a depressant along with a collector, therefore, depends on how the system responds to conditioning with the collector alone.

Table 7.2: Elemental assays (ppm) of fractions after NHR and depressant treatments

Elements	B127A	CMC	XNHR - F3
Ag	504	431	513
Al	24 250	20 688	23 000
Au	68	61	81
Ca	76 375	63 000	74 250
Cr	117	115	137
Cu	16 263	15 013	18 900
Fe	17 700	13 463	15 900
Mg	2 103	1 764	2 340
Ni	890	713	1 065
Pb	11 925	10 063	13 175
Pd	60	40	67
Sn	18 713	16 500	20 550
Ti	818	570	845
V	28	23	28
Zn	2 160	1 745	2 525

7.3 PAX CONDITIONING SCHEMES

PAX conditioning of NHR sink was considered probable for achieving a bulk metallic float fraction (see Section 3.5.2). The treatments include consideration for activation with NaHS, as well as depression with B127A. For ease of reference, Table 7.3 provides the description and designation of treatments employing PAX (see Sections 4.6.2 to 4.6.5). After conditioning, mass pull showed a slight increase above that from XNHR in the 30 – 48 minutes. The pulp generally gave a moderate froth, compared to ordinary NHR in this time interval.

Figure 7.3 shows the mass pulls (%) obtained under the different PAX treatments. Understanding that the figures are mass percentages pulled from residual NHR sinks, it shows that the actual masses pulled were not large. The small masses were obtained with relatively high water to mass

recovery ratios. These factors may be responsible for the large spread in these data compared to the NHR mass pulls such as in Figure (6.14). Increased mass pull with PAX dosage can be seen with the 100 and 400 g/ton dosages. Sulfidation also showed an increase in mass pull at the PAX dosage of 400 g/ton. Judging from the visual observation of the float fraction during flotation and after drying, the response did not appear to be strictly selective of metallic particles only. Fibre particles were obvious in the fractions. The elemental assay analysis gave a recovery and enrichment ratio from the treatments as shown in Table 7.4. Recovery here is with respect to the float and not the sink fraction, as for the NHR reverse flotation analysis. The enrichment ratio was calculated as elemental assay of the float fraction divided by respective elemental assay of the sink before conditioning (see Section 4.6).

Table 7.3: Designation and description of treatments involving PAX conditioning (Section 4.6.2).

Designation	*Description*
PAX1	Bulk metallic flotation scheme with 100 g/ton PAX
PAX2	Bulk metallic flotation scheme with 400 g/ton PAX
SPAX	Bulk metallic flotation with sulfidation; 400g/ton PAX+500g/ton NaHS
DPAX	Depressant followed by PAX conditioning and frother: 10 ppm B127A, 400 g/ton PAX, 50 ppm MIBC

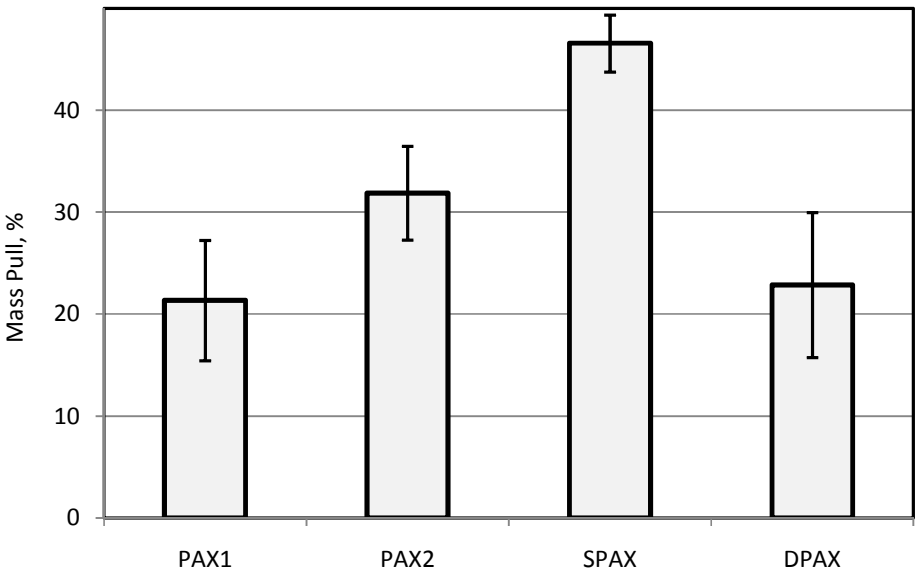

Figure 7.3: Mass pull under different PAX treatments.

A general overview of the recovery data shows that the target metallic values did not preferentially report to the float after the PAX conditioning and the bulk values remained in the sink. The understanding is that the initial 30 minutes of natural hydrophobic pull at the XNHR condition is towards maximizing reverse recovery, so that some natural hydrophobic particles are still left in the sink. The NHR scheme (see Section 6.3.2) showed mass pulls up to 80 % compared to about 52 % obtained at the XNHR condition for 30 minutes (see Table 6.3). Increasing the impeller speed, for instance, would have increased particle bubble collision efficiency and caused further pull. By keeping the kinetics constant after the 30 minutes and conditioning the system with xanthate, only metallic particles are expected to start floating, since natural hydrophobic response had already subsided at the prevailing kinetics. The float is, therefore expected to contain more of the targeted conditioned metallic values.

Table 7.4: Recovery and Enrichment Ratio for fractions from the different PAX treatments (described in Table 7.3)

Elements	Recovery, %				Enrichment Ratio			
	PAX1	PAX2	SPAX	DPAX	PAX1	PAX2	SPAX	DPAX
Ag	30	41	34	38	1.41	1.30	0.74	1.68
Al	22	38	45	31	1.05	1.18	0.96	1.36
Au	7	12	21	7	0.31	0.37	0.45	0.29
Ca	25	40	47	34	1.15	1.25	1.02	1.49
Cr	20	30	42	21	0.92	0.95	0.90	0.91
Cu	12	22	50	18	0.56	0.70	1.07	0.78
Fe	16	25	35	16	0.75	0.79	0.74	0.71
Mg	23	37	44	30	1.08	1.15	0.94	1.32
Ni	9	16	32	11	0.41	0.49	0.68	0.50
Pb	11	19	29	12	0.53	0.61	0.62	0.54
Pt	7	16	29	12	0.34	0.51	0.61	0.53
Pd	9	17	30	12	0.41	0.55	0.64	0.54
Sn	12	20	28	13	0.57	0.64	0.60	0.57
Ti	6	11	16	10	0.27	0.35	0.35	0.44
V	19	30	35	24	0.89	0.95	0.75	1.04
Zn	9	17	36	15	0.44	0.53	0.76	0.64

The recoveries analysis however did not show this. The enrichment ratios obtained were also below 1 (except for Ag, Al, and Ca, Mg which always tend to show reverse trends to other metals from the NHR scheme). This shows that the float is even poorer in the metallic values when compared to the pulp at the beginning of conditioning, i.e.: the resulting sinks have

actually been enriched after the treatment. This implies that although the mass pull increased with an increasing dosage of PAX, as well as on sulfidation, the conditioning appeared to influence other pulp particles even more than the metallic particles. This increased the floatability of otherwise natural hydrophobic particles at supposedly unfavorable prevailing kinetics.

However, studying the recovery and assay data closely shows assays and recovery increase together with increasing dosage of PAX, i.e. the response does not show assay-recovery compromise. Sulfidation also gave higher recoveries and assays, except for Ag, Ca, Al, Mg (noted for opposite responses). This shows that PAX was actually interacting with the metallic particles as projected, and that sulfidation was also achieving activation of the surface to xanthates. Increase in enrichment and recovery as dosage increases shows that these reagents target these particles somehow. The problem therefore appears to be that other particles were activated along with, and even ahead of, the target metallic particles, giving the overall low recovery and enrichment. Since the other particles are in higher proportion in the float, it shows that certain mechanism favours flotation of such particles over the target metal particles.

Xanthate conditioning is well studied and understood at least for metals that occur in native forms (Lins and Adamian, 1993; Woods, 1996; Forrest *et al.*, 2001). Formation of metal xanthates, chemisorption, and/or dixanthogen adsorption on such metallic particles and activation, as a result, were therefore expected (see Section 3.3). But for the plastics and glass fibres, study of adsorption of xanthates on these surfaces is very scarce. Nevertheless, given the low reactivity of plastics, or the negative surface charges of quartz at this pH, xanthate activation would not be expected for these materials.

A probable explanation for the competing activation of other particles could be modification of the frothing behavior of the pulp by the xanthate, which assists in stabilizing the froth of the natural hydrophobic particles when fine particle stabilization has subsided at the prevailing kinetics. Residual natural hydrophobic particles in the pulp would still float if the kinetics changed favourably. For instance, increased bubble surface areas available at higher impeller speeds and/or aeration rate would maintain particle bubble collision efficiency for effective transport to the froth phase. At the prevailing kinetics, the surfactant addition could amount to an

alteration of the physical chemistry of the pulp and compensate for the slower kinetics. Xanthates, though dedicated collectors (see Table 3.1), are heteropolar and in essence will have air-water interface activity, no matter how little relative to dedicated frothers. This could be particularly true of PAX, with the long chain amyl hydrocarbon: the higher the hydrocarbon length, the more the surfactant effect. Any such little surfactant activity could be effective here, given that the competing particles are naturally hydrophobic in the first place, needing only the stabilisation of bubble-particle agglomerates.

Another possible explanation for the response is traceable to the noticeably high proportion of calcium in the PCB CF sample, and in the NHR float fractions. Lime addition for pH increase is known to have a depressant effect in normal mineral flotation, resulting from Ca^{2+} adsorption or calcium precipitation products (see Section 3.3.1). $CaSO_4$ or $CaCO_3$ can precipitate on particle surfaces (Wills, 1997). In pyrite flotation, when lime is used for pH regulation instead of KOH or K_2CO_3, electrostatic adsorption of calcium ion (on negatively charged pyrite at pH > 7) is known for pyrite depression (Fuerstenau, 1982). If the metallic particles in the PCB CF pulp are oxidised, as increased recovery due to sulfidation tends to show, the oxide could have negative surface charges at the natural pulp pH on which Ca^{2+} could physisorb, preventing collector interaction.

This explanation appears plausible, given that gold surface in aqueous solutions shows negative surface potentials down to an isoelectric point at pH 2 (Thompson and Collins, 1992). Judging from dependence of electrophoretic mobility of the gold particles on pH, coupled with other reactive inferences, the charge development was attributed to surface oxidation and not simple (chemically less stable) adsorption of OH^-/H+ species. Other less noble metals would therefore be expected to oxidize (even if only up to a few monolayers) and carry negative surface potentials by the same surface oxide charging mechanism at the prevailing natural alkaline pH of the PCB CF pulp.

The idea of using a starvation dosage of B127A, just sufficient for depression of residual NHR, stemmed from this observation, with a target to subdue any competing natural hydrophobic response to ensure that only conditioned metallic surfaces were pulled to the froth. After the 30 minutes pull before conditioning with xanthates, 10 ppm B127A was found to suffice to subdue

residual natural hydrophobic loading of bubbles (see Section 4.6.4). At this dosage, stable froth was not forming. The dosage barely sufficed to achieve the depression without causing too much reduction in the pulp surface tension, which would lead to stable frothing, and hindering of bubble-particle attachment in the pulp. MIBC was added as frother to assist in stabilising any pull after conditioning. having observed that MIBC does not depress the natural hydrophobic response and does not promote two phase frothing significantly. Trials without MIBC in this depressant plus collector scheme did not actually form stable froth. No froth loading was also shown at 30 ppm dosage of B127A.

After conditioning, the froth loading was light and the froth built up slowly over time. The froth still did not appear metal selective, and glass fibres could still be seen in the fraction after drying. The resulting mass pull (see Figure 7.3), showed a drop compared to the PAX2 condition, with the same 400 g/ton PAX dosage. This was expected as the projection was to have a smaller, cleaner froth. The recovery and enrichment data, provided in Table 7.4, however, indicate the response did not show targeted selectivity. The recovery dropped below that obtained under PAX2 for all the elements. So also is the enrichment for some of the elements. Other particles, apart from the targeted metallic values, still reported to the small mass pull. It generally appears, as earlier explained, that the natural hydrophobic particles and some other particles that entrain more readily will always compete to report to any froth phase that will be formed in this pulp. Perhaps sulfidising the depressed pulp could achieve some improvement in the response of the metallic values; but judging from the data range from these treatments, the response will still be a far cry from a remarkable improvement.

7.4 SMBT CONDITIONING

After aeration, faintly loaded watery froth was collected. The total mass pull was 9 %. This is a total average of 6.3 g mass pulled out of a residual NHR sink of 69.7 g before conditioning. The mass pull was accompanied with 85 g of water (2.4% water recovery) in this interval; i.e. more than 12 g of water per gram mass pull.

Table 7.5 shows the recovery and enrichment ratio for the select elements from the analysis of the float fraction resulting from this conditioning scheme. The result shows overall poor recovery and enrichment. Even the primary target elements here (Cu and Pb) were poorly recovered.

SMBT is a recognized selective collector of tarnished or oxidized lead and copper minerals (Wills, 1997). The response observed here may be explained by reactivity difference between a natural mineral and end use alloy particles. The natural pulp pH or potential might not favor the interaction with the alloyed surface. The calcium depression mentioned above also remains a possibility here. Since sulfidation appeared to show improvement, which tends to indicate oxidation / tarnishing of the metallic values, SMBT conditioning would be expected to give improved recovery. That this was not observed shows a major depressant presence may have limited the response. The high dosages of PAX and NaHS used are an indication that a constraint needed to be overcome for the projected response to be observed.

Table 7.5: Recovery and Enrichment Ratio of select elements after SMBT conditioning.

Elements	Recovery (%)	Enrichment Ratio
Ag	8.2	1.04
Al	7.2	1.01
Au	1.7	0.24
Ca	7.8	1.09
Cr	6.0	0.82
Cu	4.2	0.58
Fe	4.4	0.59
Mg	7.2	1.01
Ni	2.7	0.36
Pb	3.4	0.48
Pt	2.9	0.42
Pd	2.8	0.40
Sn	3.6	0.51
Ti	1.7	0.23
V	5.8	0.84
Zn	3.0	0.42

7.5 TBAC CONDITIONING

The first observation to be noted here is about regulating the pulp pH. Three pH levels were to be used (see Section 4.6.5). The basic pH of 10 was easy to achieve and it remained stable; but reducing to pH 4 was difficult. The pulp showed a strong buffering against lowering the pH. On

addition of acid, while maintaining agitation, the pulp pH dropped and rose again, unlike the steady natural pH the pulp showed over time (see Figure 6.1). Buffering over more than one pH unit easily occurred within a minute or two, pushing the pH back to higher values. Since the pH was easy to increase to 10, the pulp was not acting strictly as a buffer system, containing an acid-base conjugate pair (Kotz and Treichel, 1999). Rather, it represents a system with a high weak base reserve, so that a shift in the pH downwards drives the activity of the base. Acid solution had to be added well in excess of the normal dilution ratio to drag the pH down to 4. During aeration, it still rose close to 5. Continuous compensation for the pH was not done, as no mass pull was being observed at this acidic pH range.

Figure 7.4 shows the mass pull at the various pH levels. At the natural pH, a mass pull of about 16 % was observed, which was a bit lower when compared to that under PAX1, despite the fact that MIBC was used to assist frothing here. XNHR gave an increase of about 5 % in cumulative mass pull in this time interval (see Table 6.3), which is equivalent to about 12% of the residual NHR sink. At the more basic pH 10, increase in this pull was observed. Tetra butyl ammonium ions were expected to physisorb on negatively charged particles, and the higher the negative surface potential, the higher the adsorption expected.

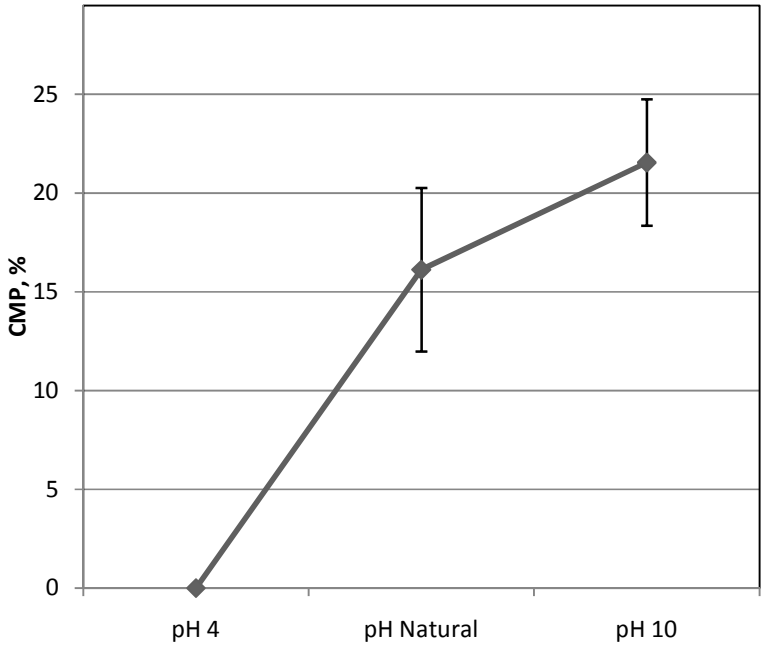

Figure 7.4: Cumulative mass pull under TBAC conditioning with varying pH

Particles with negative surface potentials were expected to be in higher proportion in this pulp and the overall mass pull level was expected to be higher. Surface hydration, hydroxylation and/or oxidation with development of general negative charges by the particles were expected at the higher pH level. Silica (glass fibre) particles were in high proportion and these would be at negative surface potential over this pH range (Fuerstenau and Fuerstenau, 1982). Many other oxides were also expected to be present. Metallic particles would be expected to show some surface hydroxylation/oxidation and acquire negative surface potentials at higher pH values.

Based on these projections, the chance of this scheme achieving good selectivity was considered to be better towards acidic pH. The projection at the acidic or natural pulp pH was that a very high mass pull of the silica particles for instance would be obtained, leaving a richer, more metallic sink. At the basic pH, a higher but less selective pull was expected. It turned out that the basic pH showed little pull, which increased from the natural pulp pH 8 to the pH 10 condition, while low (acidic) pH 4 achieved no pull.

Considering this low response to TBAC, the presence of calcium in the sample is still probable, coupled with the fact that calcium has been showing high recovery to the NHR float. Calcium ion activation of quartz surface for soap (anionic) collector is an effective scheme in heamatite-quartz flotation; heamatite in the scheme being depressed by chemisorbtion of starch (Fuerstenau and Fuerstenau, 1982). The silica particles in the PCB comminution fine pulp could, therefore, have been conditioned by calcium ions, giving them a positive surface potential, which hindered adsorption of the butyl ammonium ions. This reasoning is the basis for the investigations into calcium dissemination in the sample and its presence in the process water, detailed in Section 4.7.2. The results are discussed separately in Section 7.6.

Analysis of the float fractions from the natural pH and the pH 10 treatments gave recoveries and enrichment ratios shown in Table 7.6. The data shows that the recovery of metallic value to the froth after the conditioning was generally low; lower at neutral pH, with a little increase at pH 10, which obviously derives from the higher mass pull. The enrichment ratios also show broadly low levels. These indicate that the metallic values were selectively rejected to the sink. The slight increase in recovery from the natural pH to pH 10 was accompanied by some increase in enrichment (see Table 7.6). As explained, at the higher pH levels, development of negative

surface charges by the particles was expected. A higher proportion of OH^-, which is a potential determining ion for oxides, would promote this. It follows that the metallic values developed more negative surface charges and hence the increase in their relative response at the higher pH.

Table 7.6: Recovery and enrichment ratio of elements under the TBAC condition scheme

Elements	Recovery (%)		Enrichment Ratio	
	Natural pH	pH 10	Natural pH	pH 10
Ag	28.0	23.3	1.69	0.96
Al	24.8	26.8	1.50	1.11
Au	3.1	4.8	0.19	0.20
Ca	27.8	32.9	1.68	1.36
Cr	14.3	20.1	0.87	0.83
Cu	7.5	10.1	0.45	0.42
Fe	10.8	16.1	0.65	0.66
Mg	24.3	27.9	1.47	1.15
Ni	5.9	10.5	0.35	0.43
Pb	6.0	10.8	0.36	0.45
Pt	4.4	7.4	0.27	0.31
Pd	5.0	8.5	0.30	0.35
Sn	6.1	12.0	0.37	0.50
Ti	4.4	5.2	0.27	0.22
V	16.4	22.9	0.99	0.94
Zn	6.4	9.2	0.38	0.38

Assessing the performance of the TBAC conditioning from the viewpoint of enriching the NHR sink further with metallic values, the natural pH condition achieved about 16% mass pull, that is, 16% mass reduction of the NHR sink (see Figure 7.4), with about 3% compromise of gold content in sink, Pd 5 %, Pt 4 % and Cu 4 %. The pH 10 condition showed a higher loss to the float at 21% reduction of the sink mass. The natural or lower pH therefore appear better for selective rejection of the metallic values to the sink, except that higher mass pull would still be desired, given the relative proportion of particles desired to be adsorbed and floated by TBAC. Yet, higher pH will promote loss of metallic values to the float.

Summing up, particles expected to have a negative surface charge (at the natural pulp pH for instance) were probably neutral, or depressed by Ca^{2+} adsorption. This impeded TBAC adsorption and the pull was therefore not as high as expected. The lower pH possibly conditioned

all pulp particles to positive surface charges or generated more Ca^{2+} and this further depressed particles with negative surface charges. The calcium proportion in this sample was much higher than that of all the target elements (Table 6.1) to the extent that any effect due to calcium in the response to treatments can be overwhelming. The increase in pull at the more basic pH 10 shows the system responded to the basic projection of the TBAC conditioning scheme (higher negative surface potential with increasing pH), albeit very low. As observed, activity of Ca^{2+} remains a major suspect for the response being observed in this system. Being in such a high proportion, the conditioning could not subdue its effect. The overall performance indicates the peculiarities of a complex flotation system that this sample represents.

7.6 CALCIUM DESEMINATION IN THE PCB COMMINUTION FINES AND PRESENCE IN PROCESS WATER

As pointed out earlier, calcium ions appear culpable of the observed response of PCB CF to chemical conditioning. Hence, dissemination of calcium in the samples and its presence in the process water were investigated, as laid out in Section 4.7. Figure 7.5 shows a backscattered electron micrograph of dispersed unpolished particles of the sample, showing various particles contrasted based on the atomic number grayscales. The long cylindrical shapes of the glass fibres also serve as distinct contrast. The SEM-EDS spectra of some of the phases, as marked in Figure 7.5, are shown in Figure 7.6. The spectra confirmed calcium presence inside the glass fibres particles (P8). In addition, Ca was found in other particles, such as the titanium bearing particle P1. With calcium being constituent of the glass fibres and the high relative abundance of glass fibres in the sample, the high proportion of calcium in the sample chemical composition (see Table 5.4 and 6.1) can be understood.

For the process water analysis, only 25 of the 68 elements scanned were found in the process water (see Table A4.1 in Appendix IV). Of these, only the six indicated were in Table 7.7 were above 1 ppm concentration level. Although distilled water was always used for the experiments, a sample of the laboratory mains water supply was also analysed, as can be seen in the table. The result shows the presence of calcium in the process water. Other metals, such as sodium and potassium, also found in the water form soluble salts and would therefore not depress the way calcium would do. Given the high content of calcium in the sample, its equilibrium concentration

in solution will be easily maintained. Any reaction using up calcium from the solution would therefore be sustained remarkably. If calcium ion in the aqueous phase is forming an insoluble compound and causing depression in this system, such activity will be sustained by the large

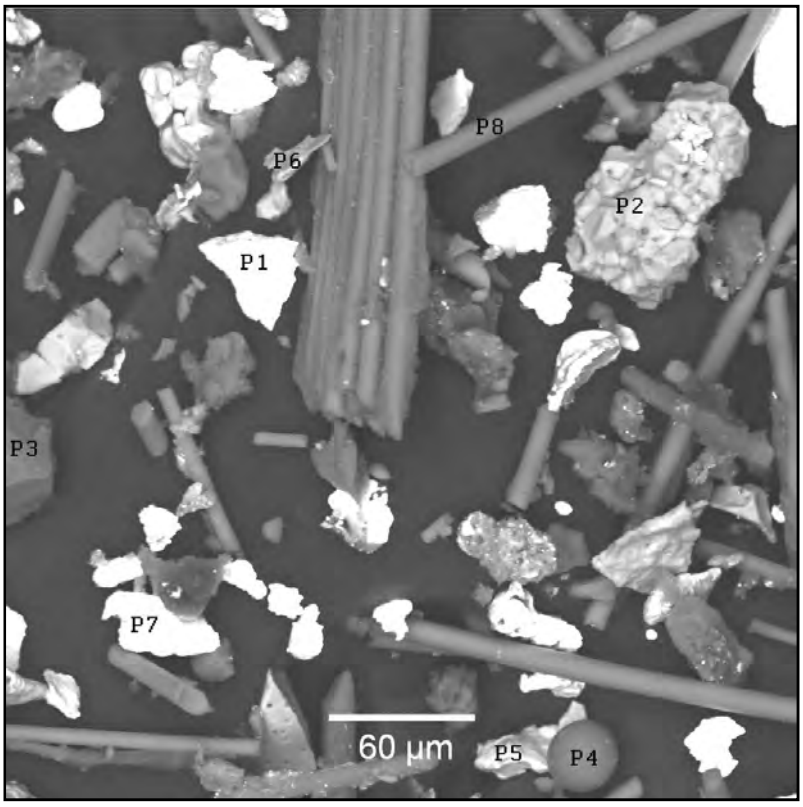

Figure 7.5: Backscattered electron SEM micrograph of dispersed particles of PCB CF
P1 – P8 correspond to particles whose EDS spectra are shown in Figure 7.6

Table 7.7: ICP-MS scan results for elements above 1 ppm concentration in PCB CF pulp filtrate

	Background	Lab Water (ppm)	PCB CF Filtrate (ppm)
Ca	<0.01	1.47	7.07
K	<0.01	0.78	6.84
Mg	<0.01	0.38	3.09
Na	<0.01	3.24	14.04
Si	<0.01	0.39	2.76
Zn	<0.01	0.01	1.28

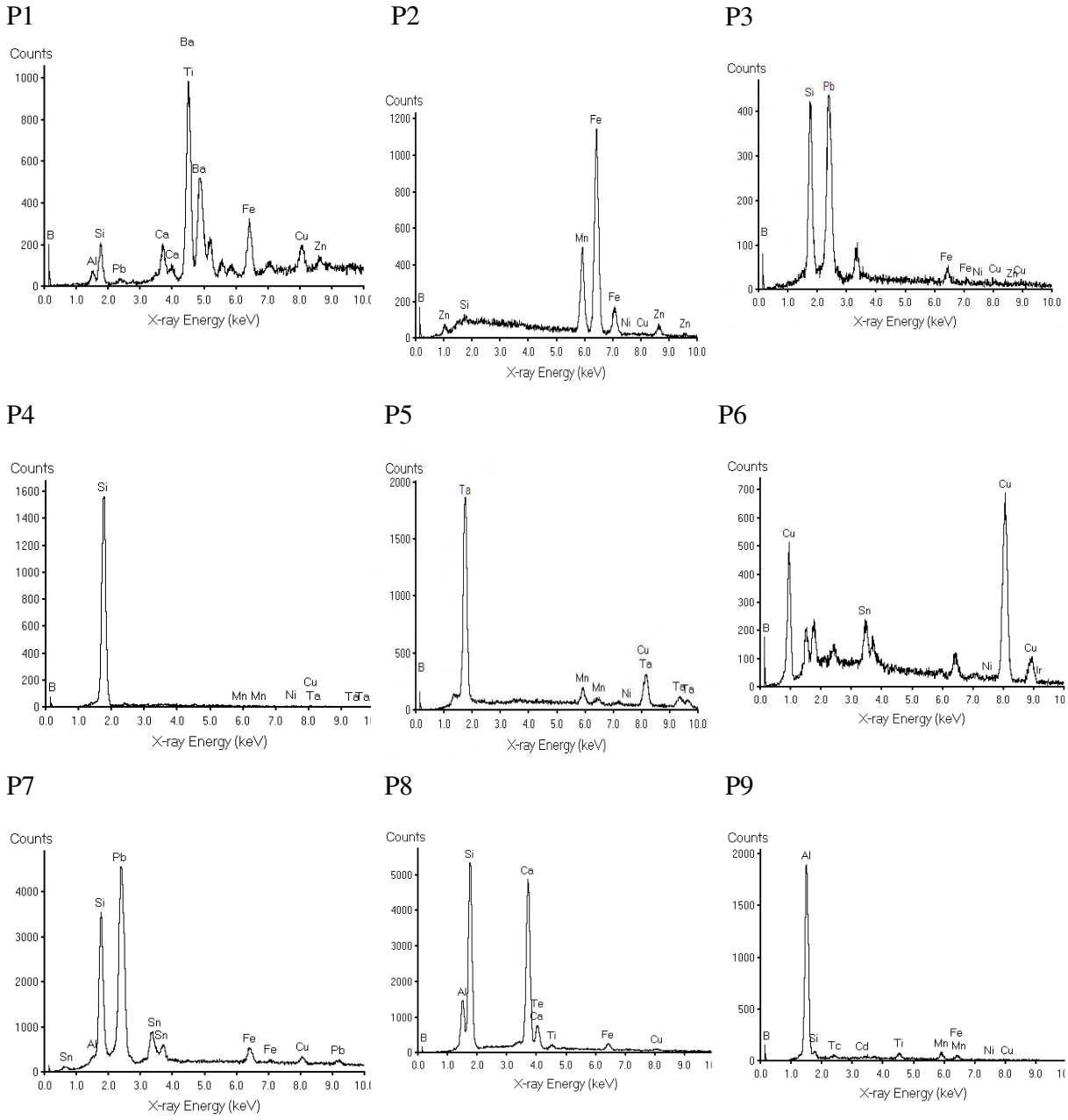

Figure 7.6: Sample EDS spectra of particles in the PCB CF.
(The label on each spectra corresponds to that of the respective particles it identifies in Figure 6.6, except for spectra P9 which is for an aluminum bearing particle from another micrograph which is not shown.)

calcium reserve in the sample. The depression will, therefore, be overwhelming. Since this reaction would have taken place well before a collector is introduced, it would be difficult for the

collector to displace the surface compound already formed. This most possibly explains the poor response to collector observed in this system.

7.7 SEM AND AES INVESTIGATION OF PARTICLE SURFACES

Another possibility mentioned for the observed level of response to chemical conditioning by PCB CF in the froth flotation investigations is the surface condition of the metallic particles themselves. Surface investigations were therefore carried out as detailed in Section 4.7.3. Observation of the copper traces in the FE SEM gave the micrograph shown in Figure 7.7. The 'log' in the figure is a micrograph of a bare copper trace particle about 25 µm in diameter. The micrograph gave an indication of a surface that is not purely metallic, indicated by the bright electron charging effect in the micrograph. This effect was observed at a voltage of 1 kV. Total blur was observed on some fibres at higher voltages. A normal metallic surface would be conducting and would therefore not accumulate charges at the positive polarity of the sample stage inside the microscope. This presupposes the presence of a non conducting layer. This can be an organic coating residue or an oxide layer.

Also looking at the micrograph, the narrow gully found across the length may indicate a soft-left over of the PCB resins on the trace copper particle. This would also hinder collector interaction. It was mentioned that such left-over resin, depending on the extent of surface coverage, could be responsible for such a particle reporting to float under the NHR scheme (see Section 6.2). However, the auger electron spectroscopy investigation was more informative regarding the actual make-up of this surface and other sample surfaces of the particles in the sample.

Figure 7.8 shows a secondary electron image (at 1 kV landing voltage of primary beam) of the particles on carbon tape, as presented for the Auger spectroscopy investigation (see the details in Section 4.7.3). Figures 7.9 to 7.12 shows the depth composition profiles on the surfaces of particle P1, P2 and F2, as well as stacks of kinetic energy spectrum at various depths from the surface on F5. More detailed data from the Auger electron spectroscopic investigation of the surfaces of various particles, as laid out in Section 4.7.3, are presented in Appendix 4.

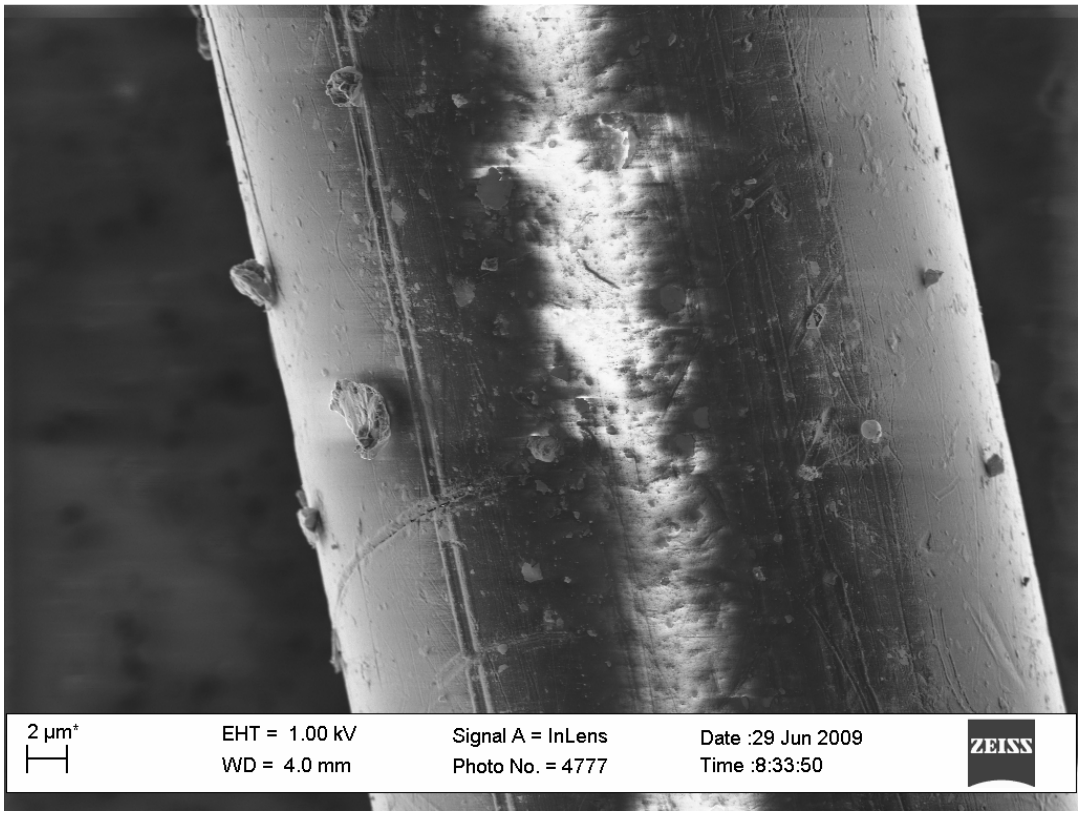

Figure 7.7: Field emission SEM micrograph of the surface of a PCB copper trace particle.

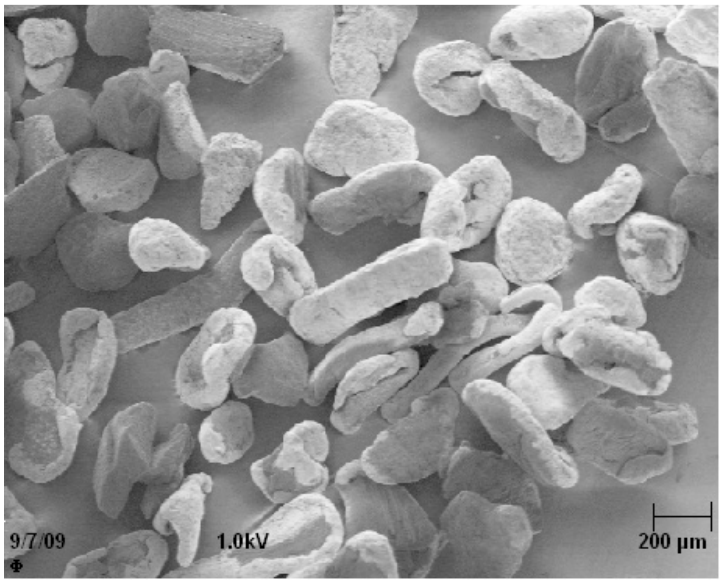

Figure 7.8: Secondary electron image of assorted metallic particles on carbon tape as presented for the auger electron spectroscopic investigation.

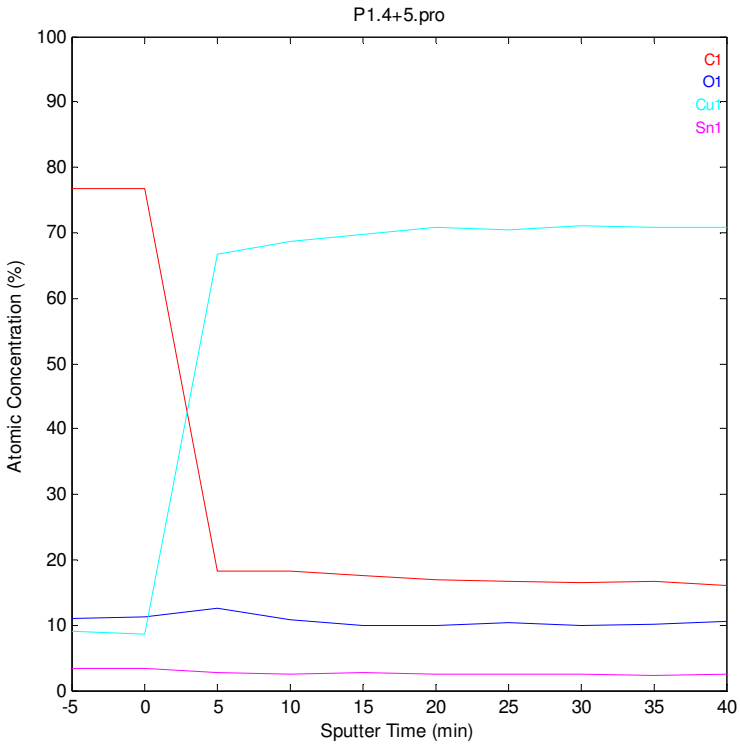

Figure 7.9: Depth concentration profile from AES surveys on the surface of particle P1 at various sputtering times indicative of depths from the surface.

In Figure 7.9, for P1, a high proportion of carbon (76.5 %) and oxygen (about 11.5 %) can be seen on the surface. After five minutes of sputtering, to a depth of about 42 nm (at about 85 Å /minute sputtering), the profile shows that the carbon proportion has reduced remarkably to around 18 %. This continued with a little drop down to about 340 nm (40 minutes of sputtering). Oxygen did not show much drop over this depth. A little representation of tin (about 3%) continued across the profile, while copper fraction increased from below 10% on the surface to above 70 % over this depth.

Interpreting this profile, the bulk particle is copper and the surface tin could be from solder vapor. The high carbon on the surface can be attributed to a huge contribution from the atmosphere, while the smaller fraction down the depth would represent a more tangible layer of organic material on the surface, which could even be up to a micron thick, when comparing depth impressions on Figure 7.7 for instance. The oxygen profile, at the surface, could be taken as a contribution from atmospheric adsorption and oxidation of the fraction of the metal on the surface. Into the surface, the metal concentration increases and so would be the fraction of

oxygen from metal oxidation. The slight increase in oxygen concentration when metallic fraction shot up at the fifth minute survey somehow shows this. Away from the surface, the oxidation shows a slight decrease, but the layer down to the end of the profile generally remains oxidized.

From this profile on P1, some explanation can already be presented for flotation responses obtained from copper in this sample. Since the surfaces can be coated by a fairly thick layer of organic matter, which can be hydrophobic, the more coated a particle is, the more the chances are that it can float under NHR, and the less the chances are that it will respond to chemical conditioning – with a range of middling behaviours in between. This can explain why copper recovery in the NHR reverse flotation concentrate is relatively low. The surface oxidation down to a depth above 300 nm would explain the poor response to the xanthate collector, which was slightly improved by sulfidation. That the response on sulfidation was not drastic may then be traced back to the process water ions, such as calcium, as previously discussed.

The profile of P2 is shown in Figure 7.10. This is similar to that of P1, except for some trace elements such as sulfur and chlorine found on the surface. As P2 was soaked in process water, these elements indicate that some process water ions interacted with the surface. It shows, as mentioned, that species from the sample in the pulp really interacted with the surfaces, and will bias the behavior of the surfaces. The fact that trace elements can be detected down to the depths profiled shows a possible ingress through porous surface matter such as organics.

The profile for P3 is shown in Figure 7.11. Particle P3 was soaked in distilled water and the profile does not show such elements from process water ions as found on P2. This profile can be compared to that of P1.The relatively higher tin may not be taken as P3 is a Cu-Sn alloy because Sn commenced continuous decay after five minutes of sputtering. Rather, the profile shows possibly how close this particle surface was to a soldered junction or via. In any case, the profile does show how the flotation response of a supposedly copper particle can be expected to vary due to deposition of another metal on the surface in the production process.

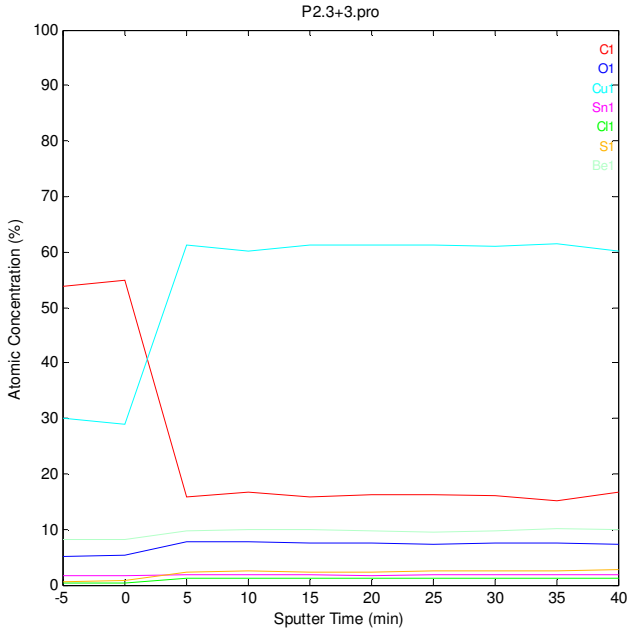

Figure 7.10: Depth concentration profile from AES surveys on the surface of particle P2 at various sputtering times indicative of depths from the surface.

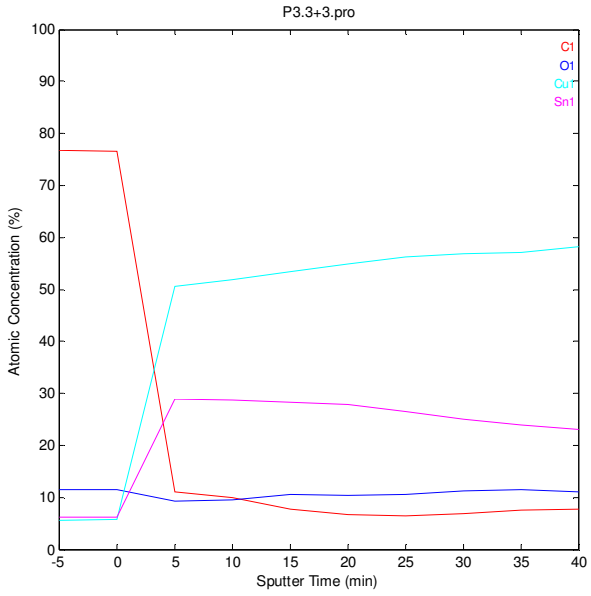

Figure 7.11: Depth concentration profile from AES surveys on the surface of particle P3 at various sputtering times indicative of depths from the surface.

Profiles on the surfaces of the fibre particles F1, F2, F3 and F4, are effectively alike (see Appendix 4) and the one for F3 is shown in Figure 7.12. The surfaces show carbon above 90%, oxygen and nitrogen, down through the depth profiled. The particles are from the actual copper trace wiring of the board which was right inside board resins. The presence of that much layer of organic on the surface is therefore understandable. Such a full organic surface coating would make such particles essentially hydrophobic. This explains the presence of such particles in the NHR float. The relative weight of the fibres, often being quite elongated, can also sever the attachment in the course of upward transport, such that such particles are also found in the NHR sink. The response of these trace particles could be expected to depend totally on these mechanisms – adsorption and detachment and to be totally isolated from reagent conditioning, as the surface compositions did not show any metallic fraction.

Figure 7.13 shows the profile of the whitish fibre particle F5. The profile shows this particle to be essentially a nickel-copper alloy with surface oxidation, as oxygen dropped from about 17% on the surface to around 6% at the final depth profiled. The high presence of calcium and silicon suggest the possible presence of glass fibre partially fused on this particle at this spot during comminution. Trace tin present is possibly from soldering. Some trace sulphur and nitrogen can also be seen, presenting the reality of a typical surface in an end use alloy. This type of particle will most likely report to the sink in NHR flotation, while its response to chemical conditioning can be difficult to predict.

This surface analysis has shed some light on the reality of the surfaces of metallic particles in the PCB CF. In pulp, the atmospheric carbon can be considered washed off, the remaining surfaces ranging from totally organic to totally oxide, with a series of middling coverage possible in between. The observed response chemical conditioning in most of the particles could be as being explained mostly due to relative inertness due to the surface being covered by an organic layer. Fractional oxide representation of the surface still makes some activation possible, as with sulfidation to xanthate, but this is not remarkable due to the high fraction of the surface that is inert. Ionic species in pulp can also be found to interact with the surface, leaving ions that can interfere with reagent activity.

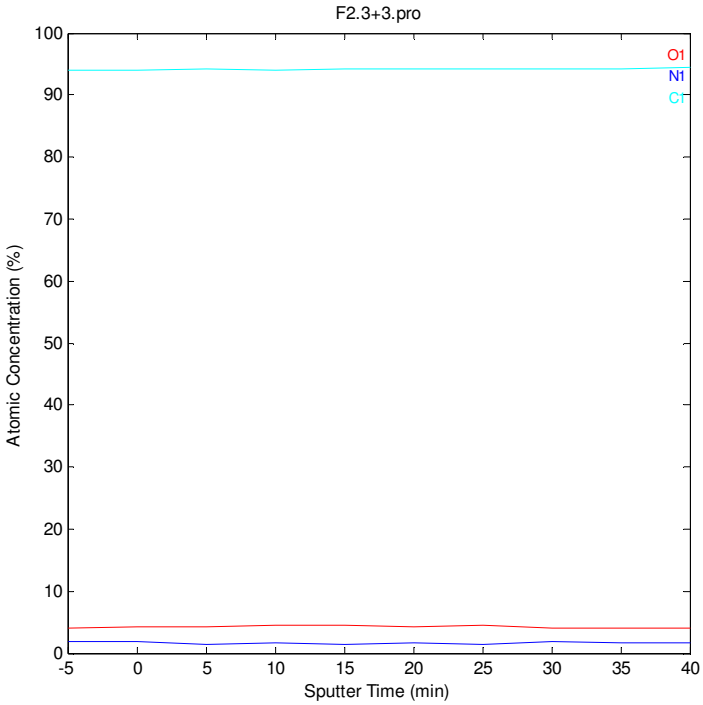

Figure 7.12: Depth concentration profile from AES surveys on the surface of particle F2 at various sputtering times, indicative of depths from the surface.

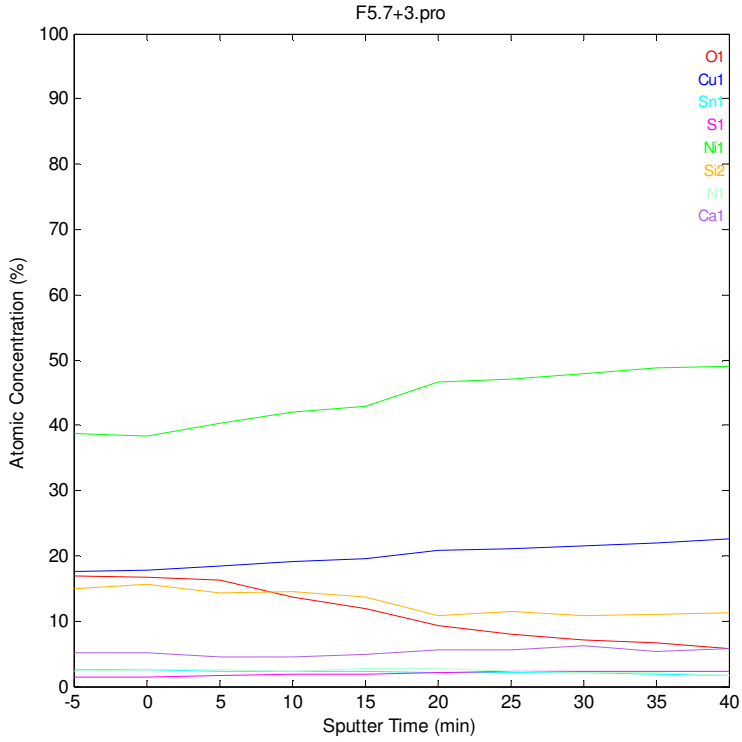

Figure 7.13: Depth concentration profile from AES surveys on the surface of particle F5 at various sputtering times indicative of depths from the surface.

7.8 CONCLUSION

Logical chemical conditioning schemes based on theoretical projections were investigated towards application of froth flotation for PCB comminution fines beneficiation. The results obtained will serve the purpose of providing insight into the response of PCB CF in flotation. Anionic and cationic collector schemes were used, as well as activation. Conditioning with PAX for a bulk collection of metallic particles, in line with native metal collection of xanthates, did not show a strong response. Dosages of up to about 400 g/ton were used to observe some recovery and enrichment in the float, with little further increase on sulfidation.

SMBT is a very selective collector for tarnished copper and lead minerals. It did not show such behavior with the PCB pulp particles. Performance of TBAC in this pulp toward further selective pull of non-metallic values after NHR pull has subsided appears promising. In consideration for depressant application, it is clear that CMC is not an effective depressant in this system, while gamma depression is more effective. Betamin 127A as a reagent for gamma depression can easily depress everything, except at dosages below 10 ppm.

Generally, the overall response obtained from the chemical condition is poor and a number of reasons can be advanced. A higher reagent (xanthate) dosage, for instance, shows the projected response exists, but the alloy surfaces may be relatively inert. Reactivity of minerals compared to end use alloy surfaces could be expected to differ. Engineering alloys have gone through definite finishing alloying treatment processes to make them stable materials that end-use applications demand. This would make the surface inert except to harsh environment which a flotation system may not represent. Oxidation of the metallic surface is another factor that could be responsible for the observed response. Oxides are generally expected on the surface of metallic particles, and the little improved response observed on sulfidation supports this.

Another strong reason that could be presented is the high calcium content of the sample. At about 7% content, far above all other target elements in this sample, any effect due to calcium in the response to the treatments would be overwhelming. Depression due to calcium is known in lime application for alkalinity regulation. It would be difficult to condition the system to respond in a manner opposite to the effect of this bulk constituent.

Follow up investigations on these probable causatives were informative. An ICP-MS trace element scan of the process water showed a calcium concentration in the process water of up to 7 ppm. This is equilibrium level in pulp. If any activity depletes it, it can be restored from the 7 wt. % reserve in the sample. SEM investigation of the particles showed calcium present in the glass fibres, which constitutes the bulk of the sample. Hence, if calcium is depressing anything, there would be sufficient supply to do this effectively.

Surface investigations, starting from FE-SEM showed surface of metallic particles to be charging under an electron beam, indicative of a non-conducting surface coating. This could be an inert organic layer, the presence of which would hinder reagent activity. Auger depth composition profiles on many particles of PCB comminution products further confirm this. The surface layers range from fully organic to metal oxides. None of the surface is pure alloy. Process water also leaves species that could interfere with reagent activity on the surfaces. This provides evidence for explaining the observed responses.

In summary, the prospect of chemical conditioning in PCB CF flotation has been investigated across logical froth flotation schemes. However, the flotation system that PCB CF presents is an interesting challenge to the versatility of froth flotation. The results gave indications of what may or may not work in this prospect. This provides a good basis for further investigation. Such investigation may first be for pure characteristics or phenomenological quest and not necessarily for functional scheme. A whole investigation can focus one specific reagent, thereby generating broader understanding of how the system behaves and its peculiarities. Upon such further understanding, more functional schemes may then be sought.

8.0 CONCLUSIONS

Recovery of material resource from end-of-life electronics, and the PCB in particularly, continues to be a major challenge for material sustainability of technological development in the face of dwindling natural reserves. This investigation was aimed at exploiting the versatility of froth flotation for beneficiation of the PCB comminution fines. The investigation approach was extensive, involving characterisation of the sample, investigation of various flotation schemes and many follow-up investigations.

Characterisation work shows the PCB comminution fines has loose bulk density lighter than water and a true material density of about 3 g/cm^3. This, coupled with surface hydrophobicity observed in the sample, necessitates that pulping must be done under water – a procedure that entails breaking a paste of the sample under water. Wet assaying of the sample was found to be highly dependent on the digestion condition. Absolute assays of a constituent element as for hazardous constituent analysis will require comparison of data from more than one digestion condition. Comparative assaying of samples from beneficiation treatments can however use aqua regia digestion. It gives a less hazardous procedure compared to hydrogen fluoride plus microwave and nitric acid treatment. It also provides analysis liquor from which all constituent elements can be analysed, compared to that from total digestion via sodium peroxide fusion. It implies that, for this sample, total digestion will not always give better results compared to partial digestion. It was also found that certain analytical techniques, such as thermogravimetric analysis, may not be recommended in PCB characterisation. It gave no distinct inflexion point to characterise any constituent. This is due to the diverse material constituents of the sample.

Particle liberation in the sample was found to be very high, but still not complete. An instance of the unliberated fraction at −75 µm gave about 5000 particles per million. The morphology of the metallic particles was highly diverse, with an average circularity shape factor of 0.63. This, coupled with the material diversity, posed a major constraint in sub-sieve particle size distribution analysis. The liberated particles themselves contain more than one chemical element, being alloys. Beneficiation operation therefore cannot attempt to separate such particles into

constituent elements; realistic schemes can aim only at achieving some bulk collection of metallic values into a concentrate.

Reverse flotation of metallic values based on natural hydrophobic response (NHR) was proposed and found to be successful in application to this sample. Microflotation indicated the favourable kinetic regime in implementing PCB comminution fines flotation would be low compared to conventional minerals. A study of the favorable kinetics under the scheme described as natural hydrophobic response gave about 500 rpm and 500 ml/min aeration rate, at 300 g sample in a 3.5 *l* Leeds cell. Without the use of a collector, natural hydrophobic response was observed. This also gave stable froth without the aid of a frother. The NHR froth was critically discussed purely as a fine particle stabilised froth and not surfactant stabilised. Au and Pd, which are the major economic drivers of PCB processing, were among the elements best enriched into the sink at an adjudged optimal 64% recovery for Au, at an enrichment ratio above three. Ti achieved an even better performance. Recovery loss of metal to the float was observed to increase with mass pull and not water recovery when results of flotation over varying PSDs were compared. Such loss will, therefore, be due more to carry-over under bulk upward mass transfer and entrapment in the froth. The flotation over narrower (coarser) PSD (+106 – 75 µm) also supports the fine particle stabilisation mechanism advanced for the NHR froth, as the dynamic froth stability height was very low compared to that of the finer fraction. It also indicated that the NHR scheme can be successfully applied at the coarser fraction.

The chemical conditioning of the PCB CF flotation system is quite challenging. Responses to the reagents were minimal. Potassium amyl xanthate did not condition the metallic particles for flotation remarkably as it does with native metals. Sulfidation showed a little improvement in response to PAX. SMBT – a selective collector for tarnished copper and lead minerals – did not show such selectivity in the PCB comminution fines pulp. Some cationic pull with TBAC toward further selective pull of non-metallic values after NHR pull had subsided was observed (although also very little). Macromolecular depression with CMC achieved virtually no depression of the natural hydrophobic response within practical dosages. Depression by lowering surface tension with Betamin 127A was effective, but still not very helpful for selective pull after chemical conditioning. Frothing and entrainment sets in within dosages required to suppress the NHR.

Surface oxidation of the metallic particles and generally low reactivity of end use alloy compared to natural mineral surfaces are probable causes for this poor response to reagent. The complex flotation system the pulp itself represents cannot be ruled out, pointing to calcium depression as another possible explanation for the overall depression observed in the system. The sample itself contains about 7 % calcium by mass. ICP-MS trace element analysis of the process water confirmed a calcium presence up to 7 ppm equilibrium concentration in the pulp water. Surface investigations, with field emission scanning electron microscope and auger electron spectroscopy composition depth-profiling, revealed the presence of organic layers on the surface of the metallic particles. The surfaces were also found to be oxidised down to about 340 nm depth profiled. None of the surface is pure alloy, occurring in forms that are relatively inert to reagents.

Summing up from all the analyses and results from these investigations, the complexity observed in the chemical conditioning of PCB CF, coupled with the difficulty of suppressing naturally floating particles, it can be submitted that the natural hydrophobic response remains the ideal scheme that can be recommended for PCB CF flotation. Recovery compromise is a major challenge to the NHR scheme when pulling too high. In a continuous system, provision for scavenging and cleaning will improve this. The very low impeller energy and aeration rate found to be favourable for PCB CF flotation will make the cleaning and scavenging inexpensive. Lastly, it must be noted that the NHR scheme operates at zero reagent cost (no collector, no frother). Optimisation of the performance of the scheme responds remarkably well to kinetic parameter variation. These are major scorecards which will keep campaigning for the natural hydrophobic response scheme in consideration of froth flotation for beneficiation of this peculiar material fraction.

REFERENCES

Adamson, A.W., 1990. *Physical chemistry of surfaces*, John Wiley, New York.

Allan, G.C. and Woodcock, J.T., 2001. A review of the flotation of native gold and electrum. *Minerals Engineering*, Vol. 14 (9), pp. 931-962.

Alter, H., 2005. The recovery of plastics from waste with reference to froth flotation. *Resources, Conservation and Recycling,* Vol. 43, 119 – 132.

ASTM Standards: http://www.astm.org/STORE/standardsearch.shtml

ASTM Volume 03.05, October, 2007. *Analytical chemistry for metals, ores, and related materials.* E 32.

ATSDR, 1993. *Agency for Toxic Substances and Disease Registry*. US Public Health Service, (1993): Lead.

ATSDR, 1999. *Agency for Toxic Substances and Disease Registry*. US Public Health Service: Top 20 Hazardous Substances: ATSDR/EPA Priority List for 1999.

Babara B. K., 2003. Preparation of samples for metal analysis', in: Somenath, M. (ed), *Sample preparation techniques in analytical chemistry, Chemical Analysis:* A series of monographs on analytical chemistry and its application, vol. 162.

Basilio, C.I., Kim, D.S., Yoon, R.H. and Nagaraj, D.R., 1992. Studies on the use of monothiophosphates for precious metals flotation, *Minerals Engineering,* 1992, Vol. 5/3-5, pp 397 – 409.

Betachem MSDS, 2007. Material safety data sheet for Betamin 127A and Betamin 65. Betachem (Pty) Ltd., Johannesburg, South Africa. http://www.bchem.co.za

Bikerman, J. J., 1973. *Foams.* Springer-Verlag New York.

Bindal, S.K., Sethumadhavan, A.D., Nikolov and Wasan, D. T., 2002. Foaming mechanisms in surfactant free particle suspensions, *AIChE Journal*, Vol. 48 (10), pp. 2307 – 2314.

Bradshaw, D. J. and O'Connor, C. T., 1996. Measurement of the sub-process of bubble loading in flotation. *Minerals Engineering*, Vol. 9/4, pp 443 – 448.

Bravo, S.V.C., Torem, M.L., Monte, M.B.M., Dutra, A.J.B. and Tondo, L.A., 2005. Influence of particle size and collector on the flotation of very low grade auriferous ore. *Minerals Engineering*, Vol. 18, pp 459 – 461.

Buchan, R and Yara, B, 1995. Recovering plastics for recycling by mineral processing techniques. *J. Miner. Met. Mater. Soc,* Vol. 47, pp 52 – 55.

Buckley, A.N. and Woods, R., 1991. Adsorption of ethyl xanthate on freshly exposed galena surfaces. *Colloids and Surfaces,* 53: 33 – 45.

Buckley, A.N. and Woods, R., 1990. X-ray photoelectron spectroscopic and electrochemical studies of the interaction of xanthate with galena in relation to the mechanism proposed by Page and Hazell. *International Journal of Mineral Processing*, 28(3-4): 301 – 311.

Bulatovic, S.M., 1999. Use of organic polymer in the flotation of polymetallic ores. *Minerals Engineering*, 12, 341 – 354.

Bulatovic, S.M., 2003. Evaluation of alternative reagent schemes for the flotation of platinum group minerals from various ores. *Minerals Engineering*, 16 (2003) 931 – 939.

Castro M. B., Remmerswaal J.A.M., Brezet, J.C., A. van Schaik, and Reuter, M.A., 2005. A simulation model of the comminution-liberation of recycling streams: Relationships between product design and the liberation of materials during recycling. *Int. J. Miner. Process*, v75, pp 255 – 281, 2005.

Coomb, Clyde F., 2001. *Printed Circuits Handbook*, 5 ed. Mc Graw Hill.

Crosbie R., Robertson C., Smit I. and Ser V., 2005. The benefits of Inter-particle comminution on floatation, Centenary of Flotation Symposium, Brisbane, QLD, pp. 823 – 828, 2005.

Crozier, R. D., and Klimpel, R.R., 1989. Frothers: plant practices. *Minerals Processing and Extractive Metall. Rev.*, Vol. 5, pp. 257 – 279.

CSAO, 2005: Synthetic Vitreous Fibers – Guidelines now available. *Construction Safety Magazine,* Spring.

Cui, J and Forssberg, E, 2003. Mechanical recycling of waste electric and electronic equipment: a review. *Journal of Hazardous Materials*, B99, 243-263.

Davydov, A. A., 1990. *Infrared Spectroscopy of Adsorbed Species on the Surface of Transition Metal Oxides*, Edited by Rochester, C.H., John Wiley & Sons, West Sussex, England.

Desco Electronic Recyclers. www.desco.co.za/process.htm

Directive 2002/95/EC of the European parliament and of the council on the restriction of the use of certain hazardous substances in electrical and electronic equipment; *Official Journal of the European Union* l37/19 EN 13.2.2003.

Duan, J., Fornasiero, D. and Ralston, J., 2003. Calculation of the flotation rate constant of chalcopyrite particles in an ore. *Int. J. Miner. Processing*, 2003, 72, 227-237.

Dunn, B. D. and Nicholas, D., 1998. Elemental distribution of parts and materials making up of electronic box. *Circuit World*, 24(2), 21 – 23.

Dodbiba G., Haruki N., Shibayam, A., Miyazaki, T. and Fujita T., 2002. Combination of sink-float separation and flotation technique for purification of shredded PET-bottle from PE or PP flakes. *Int. J. Miner. Process*, vol. 65, pp. 11 – 29.

Douglass G. Brookins, 1988. *Eh-pH Diagrams for Geochemistry*, Springer-Verlag, New York.

D'Silva K., 2004. Brominated organic micropollutants – igniting the flame retardants issue. *Critical Reviews in Environmental Sc. and Tech*, vol. 34, pp. 141 – 207.

Dymatron Inc, USA: http://www.dymatron.com/megapact.html

Elif, K. and Surendra, M.G., 2006. Disassembly to order system under uncertainty. *Omega*, vol. 34/6, pp. 550 – 562.

Ehrler, S., 2002. Properties of new printed circuit board based materials. *Circuit World*, vol. 28/4 pp 38 – 45, 2002.

ESR PATENT, 1994. *Bidirectional dense medium barrel*, US Patent 5,373,946 Dec 20.

E-Waste Guide: *Actors in South Africa recycling system*, www.ewaste.ch/case_study_southafrica/

Finlay, A., 2005: E-waste challenges in developing countries, South Africa case study. *Association for Progressive Communication,* Issue Papers, November 2005.

Furter Lee, 2004. E-waste has dawned, *Résource*, May 2004, pp 8 – 11.

Feldmann, K. and Scheller, H., 1995. The printed circuit board - a challenge for automated disassembly and for the design of recyclable interconnect devices. *CONCEPT – Conf. on Clean Electronics Products and Technology*, October. IEE Conference Publication #415, pp. 186-190.

Forrest, K., Yan, D., and Dunne., R., 2001. Optimization of gold recovery by selective gold flotation for copper-gold-pyrite ores. *Minerals Engineering*, Vol. 14/2, pp 227-241.

Fraunholcz, N. and Dalmijn, W.L., 1997a. Wetting mechanisms in the flotation of plastics. Proceedings: *XX International Mineral Processing Congress*, Aachen, Germany, Vol 5, pp. 329 – 349. Clausthal-Zellerfeld, Germany: GMDB Gesellschaft fur Bergbau, Metallurgie, Rohstoff- und Umwelttechnick.

Fraunholcz N., 1997b. *Plastics flotation*. Ph.D. Thesis, Delft University of Technology, The Netherlands.

Fuerstenau, D.W., 1982. Mineral-Water Interfaces and the Electrical Double Layer, in: King, R.P. (ed.), *Principles of Flotation,* SAIMM, Johannesburg, pp. 17 – 30.

Fuerstenau, M.C., 1982. Sulphide mineral flotation, in: *Principles of Flotation,* King, R. P. (ed.) SAIMM, Johannesburg.

Fuerstenau, D. W. and Fuerstenau, M.C., 1982. The flotation of oxide and Silicate Minerals, in: *Principles of Flotation*, King, R.P. (ed.), SAIMM, Johannesburg, pp. 17 – 30.

Fuerstenau, D.W. and Healy, T.W., 1972. *Adsorptive Bubble Separation Techniques.* Edited by R Lemlich. Academic Press, New York, Chapter 6.

Fuerstenau, D.W. and Raghavan, S., 1986. Surface chemistry properties of oxide copper minerals, in: *Advances in Mineral Processing*, Somasundaran, P. (ed.), Chap. 23. SME Inc, Littleton, 395.

Galbraith, P. and Devereux, J. L., 2002: Beneficiation of printed wiring board with gravity concentration. *IEEE International Symposium on Electronics and the Environment.*

George, P., Nguyen, A.V. and Jameson, G.J. Assessment of true flotation and entrainment in the flotation of submicron particles by fine bubbles. *Minerals Engineering*, v17, pp. 847 – 853, 2004.

Gold, S. and Dietz, K., 2003. VOGT electronic FUBA makes its own rules, VOGT press, viewed 30 June 2009: <http://www.circuitree.com/Articles/Feature_Article/3c2624ce3dfe7010VgnVCM100000f932a8c0____>

Goosey, M. and Kellner, R., 2003. Recycling technologies for the treatment of end of life printed circuit boards (PCBs). *Circuit World*, v. 29, pp. 33 – 37, 2003.

Goosey M. and Kellner R., 2002. A scoping study: End-of –life printed circuit boards. *Department of Trade and Investment*, Shipley Europe Limited.

Gomez, C. O., Strickler, D. W. and Austin, L. G., 1984. An iodized mounting medium for coal particles. *J. of Electron Microscopy Tehnnique*, vol. 1, pp. 285-287.

Guern, C. L. Conil, P. and Houot, R., 1997. Physical-Chemical separation (floatation) of plastics waste before recycling. Proceedings: *XX International Mineral Processing Congress*, Aachen, Germany, vol. 5, pp. 319 – 327, 1997. Clausthal-Zellerfeld, Germany: GMDB Gesellschaft fur Bergbau, Metallurgie, Rohstoff- und Umwelttechnik.

Gupta, A., Yan, D.S., 2006. *Minerals Processing Design and Operation: An Introduction* (Chapter 16), Elsevier.

Hamos GmbH, Germany. <http://hamos.com/en/products/plants/scrap.htm> Assessed, June 2009.

Harris, P.J., 1982. Frothing phenomena and frother. In *Principles of Flotation*, ed. R. P. King, SAIMM, Johannesburg, pp. 17 – 30.

Henryk Matusiewicz, 2003. Wet Digestion Methods. *Comprehensive Analytical Chemistry*, Vol. 41, pp. 193-233.

Holm Eirik, 2001. What is a PCB? Accessed June 30, 2009, <http://www.tomshardware.com >

Higashiyama, Y. and Asano, K., 1998. Recent progress in electrostatic separation technology. *Particulate Science and Technology*, Vol. 16, pp. 77 – 90.

Iji, M. and Yokoyama, S., 1997. Recycling of printed wiring boards with mounted electronic components. *Circuit World*, Vol 23/3, pp. 10 – 15.

ISO 71.040.40, 2009. ISO Standards in Chemical Analysis, Including Analysis of Gases and Surface Chemical Analysis, published and under review (Accessed, January 2009).

Iuga, A., Neamtu, V., Suarasan, I., Morar, R., Dascalescu, L., 1998. Optimal high-voltage energization of corona-electrostatic separators. *IEEE Transaction on Industry Applications,* Vol. 34, pp. 286-293.

Jirang, C., 2005. Mechanical Recycling of Consumer Electronic Scrap. *Licentiate thesis,* Department of Chemical Engineering and Geosciences, Mineral Processing Division, Lulea University of Technology, LTU-LIC – 05/36, Sweden.

Khalafalla, S. E., 1973. Separating non-ferrous metals in incinerator residue using magnetic fluids. *Separation Science*, Vol. 8, pp. 161 – 178.

Khalafalla, S. E., 1976. Magnetic separation of the second kind: magnetogravimetric, magnetohydrostatic, and magnetohydrodynamic separation. *IEEE Transactions on Magnetics*, Vol. MAG-12, No. 5.

Kang Hai-Yong and Schoenung J. M., 2005. Electronic waste recyling: A review of US infrastructure and technology options. *Resources, Conservation and Recycling*, Vol. 45, pp. 368 – 400.

Kellerwessel, H., 1993. Concentration with air applications – process, equipment, options, limits. *Aufbereitungs – Technik* Vol. 34(3), pp. 144-150.

Kelly, G. E. and Spottiswood, D. J., 1989. *Introduction to Mineral Processing.* John Willey & Sons, Australia.

Kravchenko, N.D., Dubinskii, Y. M. and Krichevskii, V.I., 1983. Processing scrap of radio-electronic equipment. *The Soviet Journal of Non-ferrous Metals (Tsvetnye Metally)* Vol. 24, pp. 100-101.

Kim, B., Lee, J., Seo, S., Park, Y. and Sohn, H., 2004. A process for extracting precious metals from spent printed circuit boards and automobile catalysts, *JOM*, Vol. 56, No. 12, pp. 55-58.

Kotz, J.C. and Treichel, P., 1999. *Chemistry and Chemical Reactivity.* Fourth Ed., Saunders College Publishing, Florida, USA.

Kung, H. H., 1989. *Transition Metals Oxides: Surface Chemistry and Catalysis*. Elsevier Science Publishing Inc., New York, USA.

Laskowski, J.S., Liu, Q and O'Connor C.T., 2007. Current understanding of the mechanisms of polysaccharide adsorption at the mineral/aqueous solution interface. *International Journal of Mineral Processing*, 84 (2007) 59 - 68.

Laurie, J. Flynn, 2005. Poor nations are littered with old PC's, *New York Times*, Oct. 24, 2005.

Lee Ching-Hwa, Chang-Tang Chang, Kuo-Shuh Fan and Tien-Chin Chang, 2004. An overview of recycling and treatment of scrap computers. *J. Hazardous Matls.*, B114, pp. 93 – 100.

Lee Ching-Hwa, Ssu-Li Chang, King-Min Wang and Lih-Chyi Wen, 2000. Management of scrap computer recycling in Taiwan. *J. of Hazardous Matls.*, Vol. A73, pp. 209 - 220.

Lee, K., Archibald, D., McLean, J. and Reuter, M. A., 2009. Flotation of mixed copper oxide and sulphide minerals with xanthates and hydroxamate collectors. *Minerals Engineering,* Vol. 22, pp. 395 – 401.

Lee, J. S., Nagaraj, D. R. and Coe, J. E., 1998. Practical aspect of oxide copper recovery by alkyl hydroaxamates. *Minerals Engineering*, Vol. 11, No. 10, pp. 929 – 939.

Legarth, J. B., Alting, L., Danzer, B., Tartler, D., Brodersen, K., Scheller, H. and Feldmann, K., 1995. A new strategy in the recycling of printed circuit boards. *Circuit World*, Vol. 21, No. 3, pp. 10–15.

Lekki, K. and Laskowski, J., 1975. A new concept of frothing in flotation system and general classification of flotation frothers. In *Proc. 11th International Minerals Processing Congress,* Cagliari, 1975, pp. 427 – 448.

Lenahan, W. C., and Murray-Smith, R. de L., 1986. Assay and Analytical Practice in the South African Mining Industry, *SAIMM Monograph,* Series M6, Johannesburg.

Leon Kruger, 2006. *Personal Communication.* DeBeers Group, South Africa.

Lewis, F. M., Coburn, J. L., and Bhappu, R. B., 1976. Comminution: a guide to size reduction system design. *Mining Engineering*, Vol. 28.

Li Jihanzi, Puneet S, Zong G, Hong-Chao Z., 2004. Printed circuit board recycling: a state of the art survey. *IEEE Transaction on Electronics Packaging Manufacturing*, Vol. 27/1, pp. 33 – 42.

Lins, F. F. and Adamian, R., 1993. The influence of some physical variables on gold flotation. *Minerals Engineering*, Vol. 6, No. 3, 1993. pp. 267-277.

Lungu, M., 2005. Separation of small non-ferrous particles using an angular rotary drum eddy current separator with permanent magnets. *Int. J. of Mineral Processing*, Vol. 78, pp. 22 – 30.

Mackay, T., 2004. Where do PCs go to die? *PC Format*, August, pp. 16 – 20.

Martinovic, J., Bradshaw D.J. and Harris P.J., 2004. Investigation of surface properties of gangue minerals in platinum bearing ores. *International Platinum Conference 'Platinum Adding Value'* South African Institute of Mining and Metallurgy.

MatWeb: http://www.matweb.com/search/SearchProperty.asp

Miller, J.D., Kappes, R., Simmons, G.L., LeVier K.M., 2006. Pyrite activation in amyl xanthate flotation with nitrogen. *Mineral Engineering*, Vol. 19 (6-8), pp. 659-665.

Moltke, T., 2009. Head, Industrial Metals and Minerals Research Institute, University of Pretoria, South Africa. *Personal Communication*, June 2009.

Mauerer, O., 2005. New reactive halogen-free flame retardant system for epoxy resins. *Polymer Degradation and Stability*, Vol. 88, pp. 70 – 73.

Murphy, D. B., 2001. *Fundamentals of Light Microscopy and Electronic Imaging*. Wiley-Liss, New York.

Nagaraj, D.R., Brinen, J., Farinato, R. and Lee, J., 1991. A study of interactions of dicresyl monothiophosphate with noble metals by electrochemical and spectroscopic methods. *SME Annual. Meeting,* Denver, Colorado.

Nagaraj, D.R., Brinen, J.S., Farinato, R.S. and Lee, J., 1992. A study of interaction of Di-*p*-cresyl monothiophosphate with noble metals using electrochemical, wetting and spectroscopic methods. *Langmuir*, Vol. 8(8), pp. 1943 – 1949.

NIH, 2009. NIH, Image J – Image processing and analysis in Java. National Health Institutes, USA. <http://rsbweb.nih.gov/ij/> Accessed: July 2009.

Niro Analytical Services, 2009. Powder bulk density, A2a, viewed 31 July, 2009, < http://www.niro.com/niro/cmsdoc.nsf/WebDoc/ndkw6u9atz>

Nourreddine M., Björkman B., Zhang S. and Forssberg E., 1998. Thermodynamic conditions for the formation of dioxin during the recycling of non-ferrous metals from electric and elelctronic scrap. *Proceedings: EPC Congress*, Edited by B. Mishra, The Minerals, Metals and Materials Society.

Numata, Y., Takahashi, K., Liangi, R., and Wakamatsu, T., 1998. Adsorption of 2-mercaptobenzothiazole on pyrite. *International Journal of Mineral Processing*, Vol. 53, pp. 75 – 86.

O'Connor, C. T., Dunne, R. C. and Duncan, R. B., 1987. Comparison of performance of various laboratory flotation cells, *Trans. Institution of Mining & Metall.*, Section C, 96, 168-170.

Ogunniyi, I.O., Log book, PCB physical processing investigations, 2006. University of Pretoria, Pretoria, South Africa.

Patent Application, WO 6006/013568 A3, 2006. Recovery of precious metals scrap by hydrometallurgical processing, February.

Pease, J.D., Curry, D.C. and Young, M.F., 2005. Designing flotation circuits for high fines recovery. In *Centenary of Flotation Symposium*, Brisbane, QLD, 6-9 June, 2005, pp. 905 - 912.

Polat, M., Chander, S., First order flotation kinetics models and methods for estimation of the true distribution of flotation rate constants. *Int. J. Mineral Processing*, 2000, 58, 145 – 166.

Pugh, R. J., 2007. The physics and chemistry of frothers. In: Fuerstenau, M.C., Jameson, G., Yoon, R.H. (Eds.), *Froth Flotation: A century of Innovation*. SME, pp. 259 – 282.

Pyke, B., Fornasiero, D. and Ralston, J., Bubble particle heterocoagulation under turbulent conditions. *Journal of Colloid and Interface Sc*., 2003, 265, 141-151.

Rame-Hart Inc, 1999. Automated contact angle goniometer. *RHI 2001 imaging software instruction manual.* Rame-Hart Inc, Mountain Lakes, NJ 07046.

Rao, S. R.: *Xanthates and Related Compounds*. Marcel Dekker, Inc., New York, 1971.

Rawle, A., Malvern Instruments Ltd. *Basic principles of particles size analysis.* Malvern, Worcestershire, WR14 1XZ, UK. Accessed, 30 June 2009, <www.selectscience.downloads/articles/5470_Basic_principles_of_particle_size_analysis_MRK034-low_res.pdf >

Restch GmbH and Co., 2005. Size reduction with rotor mills, accessed 30 June, 2009, <http://www.retsch.de/downloads/brochure_rotor_mills_en.pdf>

Roesch, M., and Ehrler S., 1997. Introduction of thermount reinforced materials into printed circuit board manufacturing. *HP Electronic Packaging and Manufacturing Conference*, San Diego, California. March 12 – 14. 1997.

Rosenqvist, T., 1988. *Principles of extractive metallurgy.* 2 ed. Mc Graw Hill, Auckland.

Sander, S., Schubert, G., Jackel, H.-G., 2004. The fundamentals of the comminution of metals in shredders of the swing-hammer type. *Int. J. Miner. Processing,* Vol. 74S, 385-393.

Schwarz, S. and Alexander, D., 2006. Gas dispersion measurements in industrial flotation cells. *Minerals Engineering*, Vol. 19, pp. 554-560.

Shent H., Pugh, R.J. and Forssberg, E., 1999. A review of plastics waste recycling and the flotation of plastics. *Resources, Conservation and Recycling, Vol.* 25, 85 – 109.

Shen, H., Forssberg, E. and Pugh, R.J., 2002. Selective flotation separation of plastics by chemical conditioning with methyl cellulose. *Resources, Conservation and Recycling*, Vol. 35, pp. 229 – 241.

Shibata, J., Matsumoto, S., Yamamoto, H., Kusak, E. and Pradip, 1996. Flotation separation of plastics using selective depressants. *International Journal of Minerals Processing,* Vol. 48, pp. 127 – 134.

Shuey, S.A., Vildal, E.E. and Taylor, P.R., 2006. Pyrometallurgical processing of electronic waste', *SME Annual Meeting*, March 2006, St. Louis, MO.

Shchukarev, A.V., Kravets, I.M., Buckley, A.N. and Woods, R., 1994. Submonolayer adsorption of alkyl xanthates on galena. *Int. J. of Mineral Processing*, Vol. 41 (1-2), pp. 99 – 114.

Somenath Mitra, 2003. *Sample preparation techniques in analytical chemistry*. Chemical Analysis: a series of monographs on analytical chemistry and its applications, Edited by J. D. Winefordner; Wiley-Interscience, New Jersey.

Stennett, A.D., Whalley, D.C., 1999. Novel techniques for electronic component removal. *Soldering and Surface Mount Technology* 11/2, pp 7 – 11.

Sum, E. Y. L., 1991. The recovery of metals from electronic scrap, *Journal of the Minerals Metals and Materials Society*, Vol. 43/4, pp. 53 – 60.

Svarosky L., 1987. *Powder Testing Guide: Methods of Measuring the Physical Properties of Bulk Powders*, Elsevier, Essex.

Svoboda, J., 2000. Separation in magnetic fluids: time to meet technological needs. *In Proceedings: MINPREX Congress*, Melbourne, Australia, pp. 297 – 300.

Taylor, B., 2002. Searching for solutions – Recycling electronic scrap. *Recycling Today.* Vol. 40/6, pp. 56, 58-60, 62.

Thomasnet.com, 2002. Restch, GmbH Ultra Centrifugal Mills ZM100. Accessed, 30 June 2009, <http://news.thomasnet.com/fullstory/16888>

Thompson, D. W. and Collins, I. R., 1992. Electrical properties of the gold-aqueous solution interface. *Journal of Colloid and Interface Science*, Vol. 152 (1), pp. 197 – 204.

United States Patent 5513809, 1996: Cryogenic Vibratory Mill Apparatus, http://www.freepatentsonline.com/5513809.html

Vera, M. A., Franzidis, J. P. and Manlapig, E. V., 1999. The JKMRC high bubble surface area flux flotation cell. *Minerals Engineering*, Vol. 12, No. 5, pp. 477 – 484.

Veslind, P.A., Rimer, A.E., 1981. *Unit operations in resource recovery engineering.* Prentice Hall, New Jersey.

Vinod Kataria and Sanjay Singh Sansanwal, 2005: 'Printed Circuit Boards, India: EMS makers boost demand', ECN Asia. http://www.ecnasiamag.com/article.asp?id=1600

Weigel, R.L., 1975. Liberation in magnetite iron formations. *Trans. AIME/SME*, Vol. 258, pp. 247 – 256.

Wen, X., Duan, C., Jiao, H., Zhao, Y., Zhou, X. and Song, S., 2005. Study on metal recovery from discarded printed circuit boards by physical methods. *In Proceeding: IEEE International Symposium on Electronics and the Environment.*

Willard, Horbart H., Merritt, L. L., Dean, J.A., and Settle, Frank A., 1988. *Instrumental methods of analysis.* Seventh Ed., Wardsworth Inc, California.

Wills, B. A., 1997. *Mineral processing technology*. Sixth Ed., Pergamon Press, UK.

Wikkipedia Free Encyclopaedia: Printed Circuit Board: http://en.wikipedia.org/wiki/Printed_circuit_board#column-one (Assessed: 30 June 2009).

Woods, R, 1996. Chemisorption of thiols on metals and metals sulfides. *Modern Aspects of Electrochemistry*, No. 29, Edited by John O'M. Bockris *et al.*, Plenum Press New York, 1996.

Xuefeng, W., Yuemin, Z., Chenlong, D., Xiaohua, Z., Hongguang, J., and Shulei, S., 2005. Study of metal recovery from discarded printed circuit boards by physical methods. *IEEE Int. Symposium on Electronics and the Environment.*

Xiao, C., Allen III, L. and Biddle, M.B., 1999. Electrostatic separation and recovery of mixed plastics. *Society of Plastic Engineers Annual Recycling Conference.*

Yokoyama, S. and Iji M., 1997. Recycling of printed circuit board with mounted electronic part, *IEEE International Symposiums on Electronics and the Environment,* San Francisco, pp. 109 – 114.

Zhao, Y., Wen, X., Li, B., and Tao, D., 2004. Recovery of copper from printed circuit boards', *Minerals and Metall. Processing*, Vol. 21, No. 2, pp. 99 – 102.

Zhan, M. and Shenton, K. E., 1980. Magnetic Fluid Bibliography, IEEE Transactions on Magnetics, v16, no. 2, March 1980.

Zhang, S. and Forssberg, E., 1999. Intelligent liberation and classification of electronic scrap. *Powder Technology*, v105, pp. 295 – 301.

Zhang, S., Forssberg, E., Arvidson, B. and Moss, W., 1998. Aluminum recovery from electronic scrap by high force eddy current separator. *Resources, Conservation and Recyling*, Vol. 23, pp. 225 – 241.

Zhang, S. and Forssberg, E., 1997. Mechanical Separation-oriented characterization of electronic scrap. *Resource, Conservation and Recycling,* Vol. 21, pp. 247 – 269.

Zhang, S., Forssberg, E., Menad, N. and Bjorkman, B., 1998. Metal recycling by air table separation - theory and application. *EPD Congress*, The Minerals Metals and Materials Society, pp 497 - 515.

Zhang, S. and Forssberg, E., 1997. Electronic scrap characterizaton for materials recycling. *J. of Waste Management and Resource Recovery*, Vol. 3, pp. 157 – 167.

Zheng, X., Franzidis, J.P. and Johnson, N.W., 2006. An evaluation of different models of water recovery in flotation. *Minerals Engineering*, Vol. 19, pp. 871 – 882.

Zisman, W.A., 1964. Relation of equilibrium contact angle to liquid and solid constitution. *Advances in Chemistry*. No 43, Washington DC: American Chemical Society, pp. 1 – 51.

APPENDIX I Experimentation Documentary – Equipment and Procedure

A1.1 Sample Generation Documentary

A documentary of the sample generation operations that follows presents the sample PCBs used, a pictorial flow of the comminution stages, PCB fines health hazard and PPE, and a capture of PCB -75 µm fines sample (as generated).

I. Representative PCBs

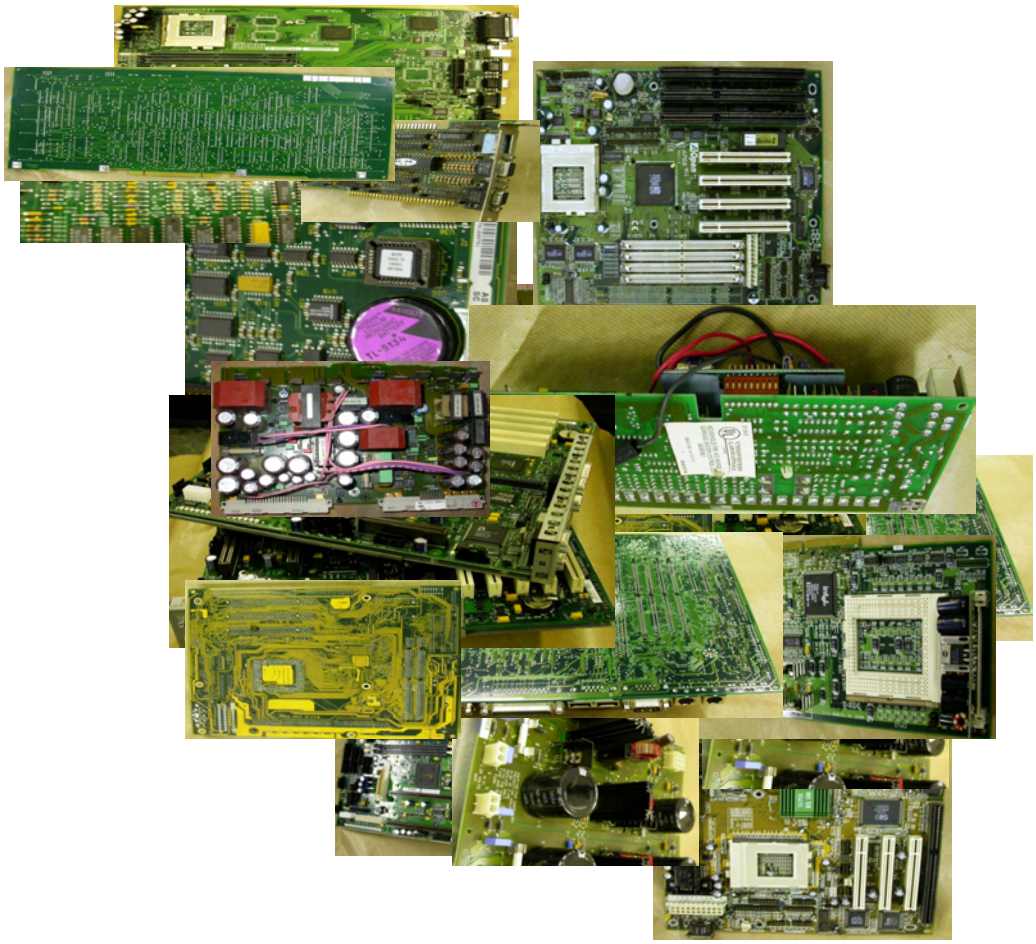

Figure A1.1: Representative PCB samples.

II. Comminution Stages

Pictorial summary of the comminution stages is shown in Figure A1.2

Figure A1.2: Pictorial flow of the comminution stages:

Hazardous components first removed from the boards; boards guillotined into fragments; closed hammer mill fine crushing; liberated metallic pieces separated from beaten bare boards; final closed hammer mill grinding of bare boards in stages and the final -75 µm fraction screened from the last −2 mm grinding.

III. PCB Fines Health Hazards and PPE

Health hazards associated with PCB comminution derive mostly from glass fiber particles. Inhaling or ingestion of various types of particles from PCB constituents is a general occupational hazard for comminution operation. Particles containing hazardous constituents and elements (such as mercury, polyvinyl chloride, cadmium, cobalt, lead, arsenic, selenium, brominated flame retardants, antimony trioxide flame retardant, etc.) can be air-borne and be ingested or inhaled. Possible effects of these constituents in the human biosystem include: severe skin irritation, respiratory problems, insomnia, memory loss, high blood pressure, cognitive functional loss, psychomotor skill and spatial skill loss, disruption of the endocrine system, increase risk of cancer in the digestive and the lymph system and neurological disorders. The recommended PPE for exposure to glass fiber fines (CSAO, 2005) which cover respiratory and skin protection, were used during the comminution work (as shown in Figure A1.3).

Figure A1.3: Picture showing full PPE gear employed during hammer mill comminution of PCB. The gear includes: N95 respirator, eye shield, laboratory coat and trousers, disposable hooded outer overall, safety shoe and ankle length PVC gloves with fabric inner lining.

A1.2 Equipment for Flotation Investigation

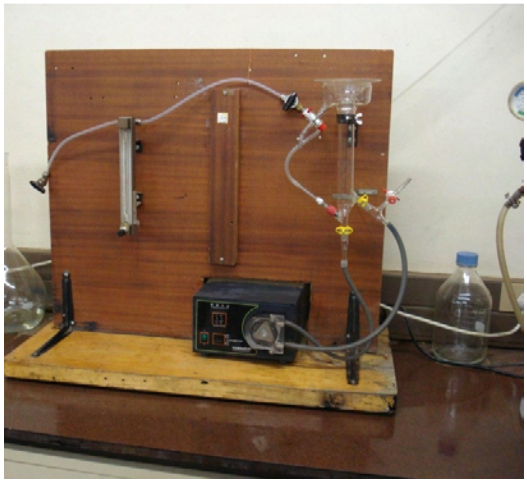

Figure A1.4: Cell used for the microflotation experiments

Figure A1.5: University of Cape Town Leeds flotation cell

Figure A1.6: Betachem Modified Bikerman froth stability test rig

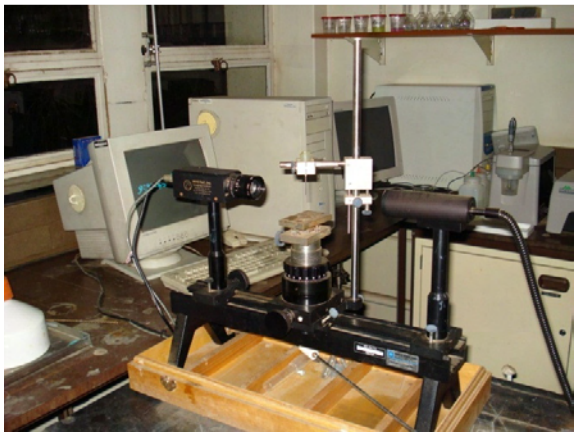

Figure A1.7: Goniometer stand

A1.3 Procedures

A1.3.1 Derivation of conversion factors for leach solution assay to actual sample assay

To ensure representative sampling, varying masses of sample were taken for digestion from different fractions; higher mass of sample from fractions with higher total mass. For every 50 g

mass of flotation fraction, a 2 g sample was taken for digestion. In small fractions, much lesser than 10 g, 1 g was taken.

Final leach solutions were always made up to 250 cm^3.

Given leach solution assay = y ppm = y mg/l:

→ y mg of the element is contained in one liter of such leach solution.

∴ 250 cm^3 contains y/4 mg, which is the total amount digested from the X g of sample.

∴ Actual assay, % = (y/4000x)*100

→ For x = 1 g, actual assay, % = y/40.

That is, y divided by a factor of 40 gives the assay in percentage.

For X =1, 2, 4, and 6, the factors follow as 40, 80, 160 and 240 respectively. For E12A, for instance, all the float fractions were between 10 – 50 g, hence 2 g samples were taken for digestion. The sink masses were between 100 and 150, and 6 g sample was taken. The conversion factor for the leach solutions for all the float fractions from E12A will therefore be 80, while for the sinks it will be 240, as in Table A3.2.

A1.3.2 Water Recovery Data and Collection Procedure

Water recovery in batch flotation can be determined as a fraction of the total water in the cell that is recovered into a float fraction (Zheng *et al.*, 2006). Data for this can be obtained by determining the amount water of added to the cell to replace the water recovered into the float fraction. A procedure considered more direct to determine water recovered into a fraction was used in the investigation by obtaining the mass difference between the wet float fraction and the sample recovered after drying. To do this, the following data were collected for each float fraction:

RW1 = Initial mass of bottle with rinse water

RW2 = Mass of bottle with rinse water after rinsing all the float fraction from the tip of the cell into the collection pan and from there into drying pan

RW = Mass of rinse water used = RW1 – RW2

A = Mass of all of wet float fraction, rinse water and drying pan

PS = Mass of pan and flotation fraction sample after drying

Hence:

Water Pull into a fraction (W_P, g) = A – PS – RW

With cell total water content regularly topped to approximately 3500 ml level for each fraction, then:

Water Recovery (W_{rec}, %) = W_P/35

This procedure is considered more accurate, as the actual amount of water recovered with the sample is used, compared to the assumption that the top-up water is the amount of water recovered into the sample. Topping-up exactly to a marked level under a heavily frothing pulp in a dynamic batch flotation may not be precisely done always. For example, it is easy to top-up to return the water level to 3490 ml total volume instead of 3500 ml, and the level will still be almost the same, given the relatively wide cross-sectional area of the cell. Assuming the actual drop was down to 3450 ml level, then recovered water will be determined as 40 ml instead of 50 ml, based on top-up water volume. Water recovery, in %, will then be computed as 40/35 instead of 50/35. Whereas, if the actual value of 50 ml is used, but the initial water volume is taken as 3500 ml instead of a possible 3490 ml (due to top-up error), the water recovery, in %, will be calculated as 50/35 instead of 50/34.9. The error in this latter approach is obviously quite minimal compared to the former.

APPENDIX 2: Results and Analysis – I

A2.1 Characterization

Table A2.1 Density values determination data

	Loose Bulk Density (g/cm^3)		Tapped Bulk Density (g/cm^3)		True Density (g/cm^3)	
	Constant Vol (ml).	Loose mass to fill (g)	Vol (cm^3) after tapping 200x	Tapped Density	Sample Mass (g)	Displaced Vol (cm^3)
Test I	100	53.33	57	0.94	20	7
Test II	100	54.88	58	0.95	20	7
Test III	100	53.98	57	0.95	30	10
Density	0.54 (δ_R = 1.4%)		0.94 (δ_R = 0.7%)		2.9 (δ_R = 2.3%)	

δ_R = relative standard deviation of the averaged data.

Table A2.2: PCB CF particle size distribution data

Sieve Aperture Diameter, µm	Cumulative Undersize, %	Rel. St. Dev., % (10 data)
75	98.6	0.4
53	85.1	0.9
38	66.7	1.6
0	0	0

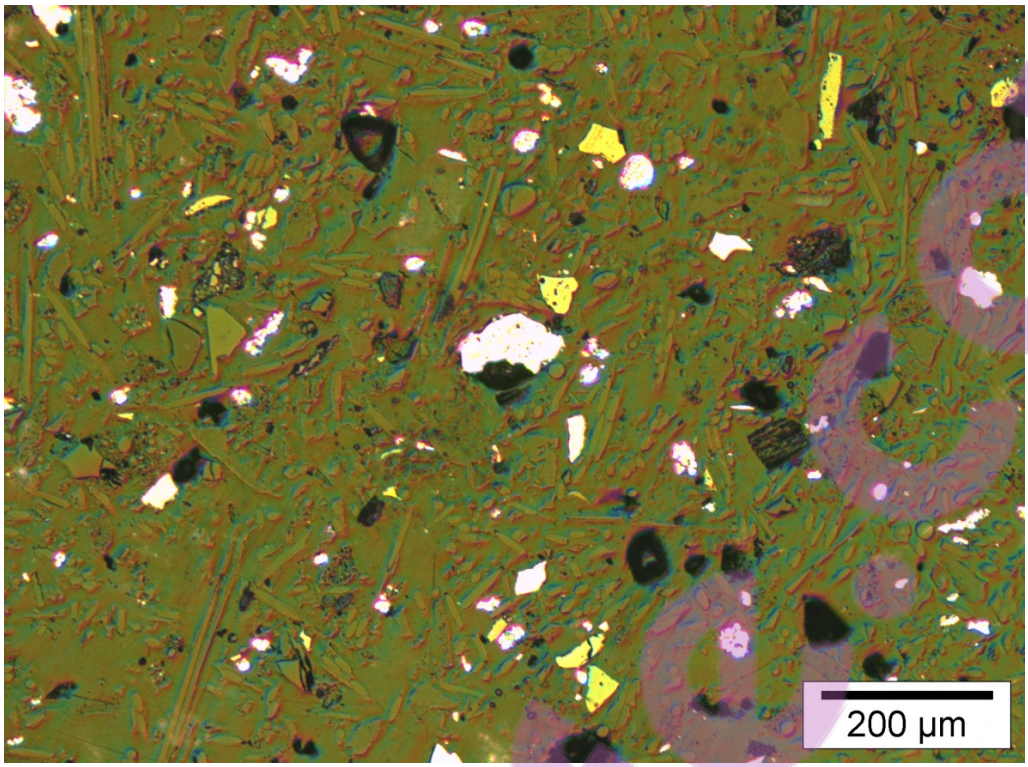

Figure A2.1: Optical micrograph of the binarised image of Figure 5.3 for circularity shape factor analysis of the metallic particles.

Table A2.3: ImageJ shape factor analysis data

#	Area	Circularity	Feret	%Area	FeretAngle	Solidity	#	Area	Circularity	Feret	%Area	FeretAngle	Solidity
1	18.18	0.87	6.64	100	149.04	0.89	59	851.62	0.52	56.55	100	77.78	0.88
2	181.49	0.86	17.55	100	144.25	0.93	60	225.65	0.37	27.62	100	21.8	0.65
3	376.3	0.7	29.73	100	167.83	0.87	61	48.05	0.71	10.1	100	16.39	0.84
4	23.7	0.66	7.94	100	21.04	0.8	62	687.66	0.5	45.52	100	124.29	0.84
5	79.87	0.69	15.34	100	164.93	0.9	63	104.87	0.44	21.66	100	153.43	0.8
6	1077.91	0.39	55.83	100	14.18	0.75	64	38.31	0.68	10.95	100	128.66	0.87
7	1380.18	0.24	99.56	100	84.75	0.79	65	28.25	0.58	11.06	100	11.89	0.89
8	84.74	0.5	15.04	100	155.38	0.79	66	21.75	0.5	10.27	100	33.69	0.75
9	86.69	0.59	15.4	100	51.01	0.82	67	31.82	0.7	9.28	100	100.62	0.87
10	569.8	0.51	37.47	100	61.88	0.76	68	53.9	0.89	9.95	100	156.37	0.91
11	371.75	0.47	35.54	100	131.1	0.79	69	121.43	0.73	14.81	100	112.62	0.89
12	124.67	0.44	17.99	100	169.05	0.73	70	36.04	0.84	8.7	100	148.39	0.9
13	28.57	0.6	8.68	100	23.2	0.76	71	110.71	0.54	21.45	100	106.99	0.86
14	1410.7	0.58	55.32	100	168.11	0.88	72	135.71	0.77	17.3	100	162.76	0.9
15	566.23	0.77	33.04	100	32.32	0.92	73	967.85	0.67	45.31	100	50.1	0.9
16	60.39	0.74	12.19	100	127.41	0.89	74	276.62	0.87	21.08	100	71.08	0.95
17	141.56	0.83	15.29	100	116.57	0.93	75	108.77	0.61	16.76	100	162.18	0.85
18	227.92	0.45	34.61	100	159.78	0.88	76	16.88	0.81	6.96	100	145.01	0.87
19	1257.13	0.79	45.54	100	58.3	0.95	77	80.19	0.65	13.01	100	28.81	0.82
20	173.05	0.74	18.86	100	25.02	0.9	78	614.61	0.25	64.16	100	19.72	0.69
21	75.32	0.69	15.04	100	142.7	0.9	79	60.39	0.7	11.75	100	22.83	0.83
22	119.48	0.6	18.66	100	77.66	0.84	80	18.18	0.59	7.92	100	59.74	0.77
23	212.34	0.61	20.65	100	65.56	0.85	81	102.92	0.48	18.86	100	154.98	0.81
24	110.06	0.91	13.54	100	157.75	0.95	82	168.51	0.74	18.39	100	73.81	0.89
25	46.43	0.61	12.8	100	147.72	0.81	83	173.7	0.81	18.24	100	14.47	0.93
26	390.58	0.3	54.78	100	18.81	0.76	84	938.63	0.66	52.53	100	49.4	0.92
27	251.95	0.66	25.95	100	70.77	0.9	85	45.45	0.82	10.75	100	122.01	0.92
28	295.45	0.34	32.39	100	39.29	0.72	86	113.64	0.75	16.84	100	23.96	0.89
29	167.53	0.87	16.94	100	109.65	0.94	87	24.03	0.84	7.43	100	147.53	0.89
30	36.36	0.67	9.74	100	20.56	0.82	88	157.47	0.78	18.87	100	118.89	0.92
31	896.75	0.6	50.97	100	174.23	0.83	89	272.73	0.7	23.05	100	81.47	0.86
32	237.66	0.68	21.08	100	108.92	0.88	90	78.25	0.72	14.29	100	23.5	0.88
33	281.17	0.73	26.35	100	21.57	0.92	91	312.98	0.57	29.3	100	13.5	0.86
34	20.45	0.61	9.01	100	108.43	0.85	92	190.58	0.52	23.42	100	18.43	0.84
35	289.93	0.83	24.47	100	12.09	0.94	93	827.59	0.35	43.93	100	9.71	0.78
36	33.12	0.73	9.97	100	30.96	0.86	94	299.35	0.61	28.03	100	153.43	0.85
37	20.13	0.43	9.7	100	49.76	0.6	95	90.26	0.78	13.7	100	135	0.87
38	31.17	0.46	11.75	100	104.04	0.76	96	84.41	0.82	12.09	100	171.87	0.91
39	56.49	0.74	13.01	100	151.19	0.88	97	992.52	0.68	42.98	100	96.09	0.89
40	1615.9	0.66	54.71	100	125.68	0.9	98	133.77	0.49	23.97	100	108	0.8
41	23.38	0.88	7.75	100	143.97	0.94	99	240.26	0.48	28.3	100	64.98	0.79
42	1233.43	0.48	55.73	100	127.1	0.83	100	250	0.7	24.51	100	162.41	0.89
43	256.17	0.44	35.99	100	156.68	0.82	101	653.89	0.55	43.62	100	23.89	0.82
44	544.8	0.49	38.7	100	76.37	0.84	102	38.64	0.78	9.97	100	30.96	0.87
45	600.64	0.45	35.57	100	58.09	0.8	103	48.38	0.63	12.5	100	24.23	0.85
46	101.3	0.63	14.7	100	125.54	0.83	104	112.99	0.6	19.9	100	113.63	0.83
47	40.58	0.79	9.69	100	151.93	0.89	105	175.32	0.77	17.67	100	159.23	0.89
48	770.12	0.25	61.75	100	48.37	0.69	106	1104.86	0.47	53.71	100	85.74	0.89
49	5467.49	0.46	125.01	100	3.4	0.82	107	168.51	0.83	19.15	100	120.38	0.94
50	375.65	0.33	33.79	100	174.19	0.67	108	55.19	0.69	12.99	100	15.26	0.92
51	28.57	0.8	8.06	100	8.13	0.88	109	14637.87	0.46	251.92	100	162.22	0.79
52	390.58	0.57	26.56	100	35.39	0.89	110	42.21	0.89	8.7	100	121.61	0.91
53	21.43	0.93	6.16	100	146.31	0.9	111	49.03	0.72	11.06	100	168.11	0.87
54	272.08	0.56	24.99	100	24.23	0.86	112	61.36	0.8	11.54	100	110.22	0.93
55	309.09	0.6	24.97	100	152.85	0.9	113	266.88	0.83	24.26	100	99.46	0.97
56	104.22	0.37	27.45	100	175.24	0.89	114	266.88	0.83	24.26	100	99.46	0.97
57	30.84	0.35	15.34	100	21.8	0.79	115	105.84	0.54	19.35	100	13.63	0.82
58	76.62	0.55	17.18	100	5.71	0.89	116	68.83	0.67	15.04	100	37.3	0.89

A2.2 NHR Froth and Mass Pull: Figures and Data

Figure A2.2: Natural hydrophobic froth build up under E21A condition in the first minute of aeration.

Figure A2.3: E21A at 30 minutes still showing froth loading

Figure A2.4: E21C at 28 min of flotation showing clean white unloaded froth
A 59 seconds movie clip showing this froth bursting readily as they are not longer loaded is here.

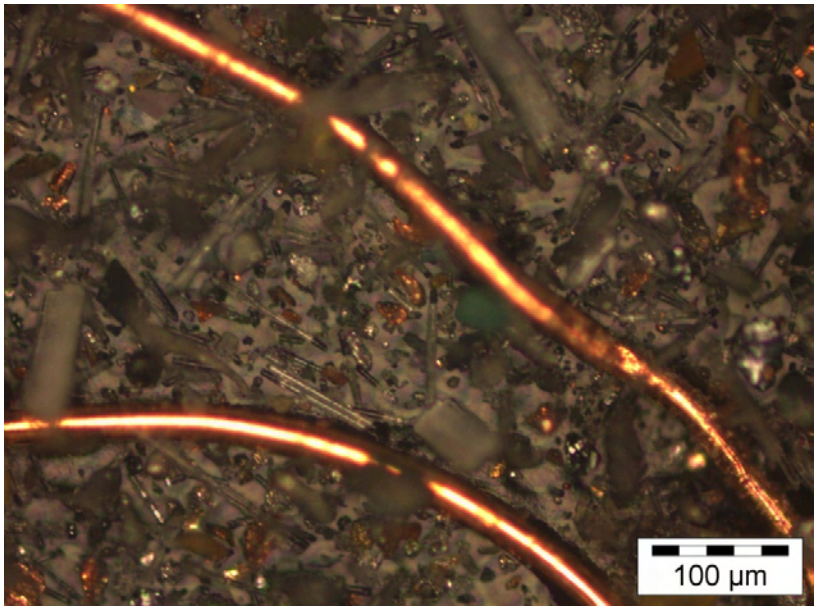

Figure A2.5: Optical micrograph of a PCB CF reverse flotation concentrate sample showing printed wiring board copper traces.

Table A2.4: Mass pull with time for flotation under the NHR scheme at varying kinetic conditions
(The experimental designations in Table 4.1 were given extra notations 1 and 2 representing duplicate investigations)

Experiment	Mass Pull (g)					CMP (g)	Sink (g)	CMP + Sink (g)
	1 min	4 min	10 min	18 min	30 min			
E11A	18.7	23.9	78.8	74.9	69.2	265.5	332.3	597.8
E21A1	11.7	24.9	47.1	43.7	35.6	163.0	135.4	298.4
E21A2	11.8	26.3	45.3	40.9	32.3	156.6	140.7	297.3
E21B1	24.1	67	90.3	35.2	6.8	223.4	76.4	299.8
E21B2	23.8	66.6	90.4	34.6	7.8	223.2	74.7	297.9
E21C1	32.2	105.3	90	14.6	1.6	243.7	55.7	299.4
E21C2	34.0	98.7	87.7	17.8	1.9	240.1	57.2	297.3
E22A1	18.9	36.3	56.9	42.8	27.5	182.4	116.9	299.3
E22A2	17.1	33.8	55.7	40.8	26.8	174.2	124.7	298.9
E22B1	44.4	115.3	72.9	5.7	0	238.3	60.4	298.7
E22B2	43.0	102.1	77.8	9.5	0	232.4	65.6	298.0
E22C1	79.3	145.5	34.1	0	0	258.9	40.7	299.6
E22C2	75.7	141.6	37.8	0	0	255.1	44.0	299.1

Table A2.5a: Cumulative Mass Pull data, % (from normalized mass pull, with CMP + Sink as 100%)

Experiment	1 min	4 mins	10 mins	18 mins	30 mins
E11A	3.13	7.13	20.31	32.84	44.41
E21A1	3.92	12.27	28.05	42.69	54.62
E21A2	3.97	12.82	28.05	41.81	52.67
E21B1	8.04	30.39	60.51	72.25	74.52
E21B2	7.99	30.35	60.69	72.31	74.92
E21C1	10.75	45.93	75.99	80.86	81.40
E21C2	11.44	44.64	74.13	80.12	80.76
E22A1	6.31	18.44	37.45	51.75	60.94
E22A2	5.72	17.03	35.66	49.31	58.28
E22B1	14.86	53.47	77.87	79.78	79.78
E22B2	14.43	48.69	74.80	77.99	77.99
E22C1	26.47	75.03	86.42	86.42	86.42
E22C2	25.31	72.65	85.29	85.29	85.29

Table A2.5b: Averaged cumulative Mass Pull data, % (as plotted in Figure 6.4)

- from normalized mass pull (CMP + Sink = 100%)

Experiment	0 min	1 min	4 min	10 min	18 min	30 min
E11A	0	3.13	7.13	20.31	32.84	44.41
E21A	0	3.95	12.54	28.05	42.25	53.65
E21B	0	8.01	30.36	60.59	72.28	74.72
E21C	0	11.09	45.28	75.06	80.49	81.08
E22A	0	6.02	17.74	36.56	50.53	59.61
E22B	0	14.65	51.08	76.34	78.88	78.88
E22C	0	25.89	73.85	85.86	85.86	85.86

Table A2.5c: Standard error of the means for each data point in Table A2.5a.

- Data used for error bars in Figure 6.4.

Experiment	0 min	1 min	4 min	10 min	18 min	30 min
E21A	0	0.024	0.275	0.001	0.442	0.975
E21B	0	0.025	0.021	0.092	0.029	0.204
E21C	0	0.341	0.645	0.926	0.370	0.318
E22A	0	0.297	0.707	0.895	1.220	1.331
E22B	0	0.217	2.387	1.536	0.896	0.896
E22C	0	0.580	1.191	0.563	0.563	0.563

- Standard error of mean, ε, related to standard deviation, δ, and sample size, n, as

$$\varepsilon = {}^{\delta}/_{\sqrt{n}} \quad . \quad . \quad . \quad . \quad . \quad . \quad \text{A2.1}$$

Table A2.6: First order fitting data of the cumulative mass pull for the plot in Figure 6.5 (ln Rm/(Rm-R) at each time, t)

Experiment	0 min	1 min	4 min	10 min	18 min
E11A	0	0.07	0.17	0.61	1.34
E21A	0	0.08	0.27	0.74	1.55
E21B	0	0.11	0.52	1.67	3.42
E21C	0	0.15	0.82	2.60	4.93
E22A	0	0.11	0.35	0.95	1.88
E22B	0	0.21	1.04	3.43	-
E22C	0	0.36	1.97	-	-

- For E22B, E22C regimes the responses are fully defined with fewer points. The first order expression becomes undefined before 30 minutes elapsed, as R continues to be equal to Rm after mass pull has stabilized.

A2.3. NHR Digestion Residue Analysis

F1, F2, F3, F4 and F5 pertain to float fractions collected at 1, 4, 10, 18 and 30 minutes respectively.

Table A2.7: Fraction of float fractions digested in hot aqua regia, % (indicative of metallic assay)

Experiment	F1	F2	F3	F4	F5	SINK
E11A	4.80	9.85	14.03	13.44	11.40	25.65
E21A	16.07	11.56	9.00	9.70	10.06	22.50
E21B	15.74	12.45	11.36	12.83	11.37	38.26
E21C	17.96	14.80	15.55	17.06	17.34	42.20
E22A	16.61	13.24	12.74	12.46	12.45	30.57
E22B	16.27	14.17	14.29	13.48	0.00	37.99
E22C	16.32	12.18	15.39	0.00	0.00	43.11

From fraction digested multiplied by mass of each flotation fraction, distribution of total metallic contents expressed as percentage was computed for each fraction. This is indicative of recoveries to each fraction.

Table A2.8: Distribution of total metallic content, %

Experiment	F1	F2	F3	F4	F5	SINK
E11A	0.77	2.00	9.41	8.57	6.71	72.54
E21A	3.95	6.22	8.74	8.62	7.19	65.28
E21B	6.73	13.69	18.36	8.02	1.49	51.73
E21C	9.62	24.46	22.38	4.47	0.49	38.58
E22A	4.96	7.69	11.89	8.64	5.60	61.22
E22B	12.21	26.44	18.49	1.75	0.00	41.11
E22C	23.46	32.42	10.26	0.00	0.00	33.86

Table A2.9: Digestion residue analysis data indicative of sink assay and recovery, with sink's mass percentage of feed, as plotted in Figure 6.6.

	Assay, %	Recovery,%	Conc Mass %
E11A	25.65	72.54	55.38
E21A	22.50	65.28	46.02
E21B	38.26	51.73	25.18
E21C	42.20	38.58	18.82
E22A	30.57	61.22	40.27
E22B	37.99	41.11	21.00
E22C	43.11	33.86	14.12

- Assay and Recovery extracted from Tables A2.7 and A2.8.
- Concentrate mass % is percentage of feed left in the final sink; percentage complement of cumulative mass pull after 30 mins in Table A2.5b.

A2.4 NHR ICPOES: Data and Analysis

See Appendix 3.

A2.5 Indication of bubble sizes at various kinetic regimes

a. d.

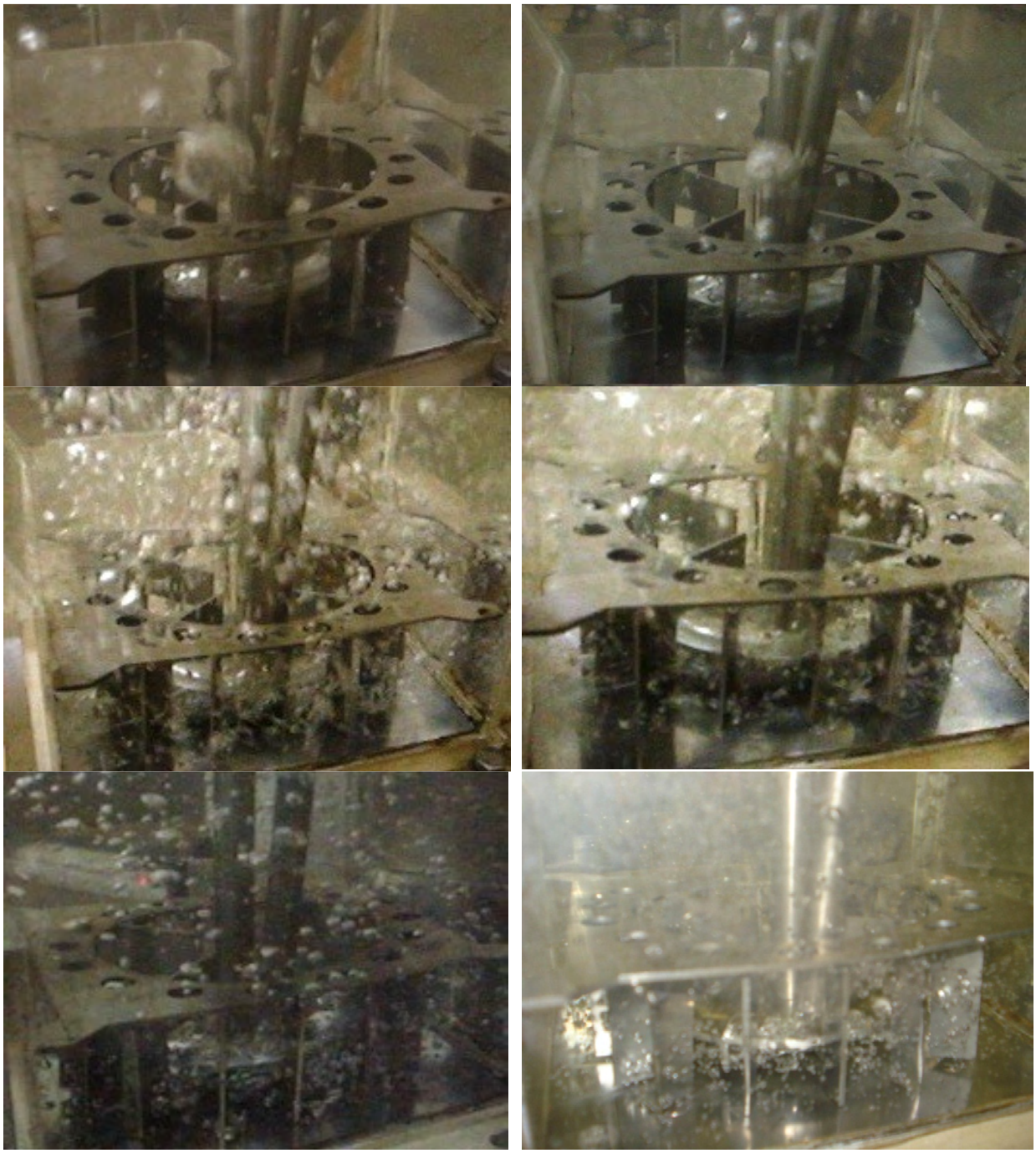

c. f.

Figure A2.6: Frozen frames showing variation of bubble sizes with impeller speed and aeration rate at: 1000 mlpm aeration and (a) 300 rpm (b) 400 rpm, (c) 500 rpm; and at 500 mlpm aeration and (d) 300 rpm, (e) 400 rpm, (f) 500 rpm.

A2.6 Estimation of Sb and Jg under E21C and E22B kinetic regimes

S_b bubble surface area flux is related to J_g, superficial surface area velocy and d_b, diameter of gas bubble in a flotation system as

$$S_b = 6J_g/d_b$$

while,

$$J_g = Q/A$$

where Q is the aeration rate, and A is the cell cross-section area.

By doubling Q (from 500 mlpm to 1000 mlpm) at constant A, Jg doubles in moving from E21C regime to E22B. That is,

$$J_{g\ E22B} / J_{g\ E21C} = (1000/A)/(500/A) = 2$$

An estimate of d_b follows from the operation of the impeller system. 8 stator bars breaks the air flow at the exist pipe per revolution to give the bubble sizes. Agitation speeds of 500 rpm and 400 rpm in E21C and E22B gives 4000 and 3200 stator breakages of air flow per minute in each regime respectively. All things beings equal, as a rough estimate, in E21C, 500 ml is broken into 4000 bubbles per minute. This gives 1/8 ml sized bubbles. Under E22B, 1000 ml air is broken into 3200 bubbles per minute, giving 5/16 ml sized bubbles. Estimate bubble size ratio under E22B to E21C therefore gives

$$d_{b\ E22B} / d_{b\ E21C} = (5/16) / (1/8) = 2.5$$

Estimating Sb with these parameter ratios

$$S_{b\ E21C} / S_{b\ E22B} = (6J_{g\ E21C} / d_{b\ E21C}) / (6J_{g\ E22B} / d_{b\ E22B})$$
$$= (J_{g\ E21C} / J_{g\ E22B}) * (d_{b\ E22B}/d_{b\ E21C})$$
$$= ½ * 2.5 = 1.25$$

A2.7 NHR Improvement

a. **b.**

Figure A2.7: Frozen frames showing bubble sizes at 300 rpm impeller speed and 500 aeration rate (a) before and (b) after modification of the Leeds cell impeller system.

Figure A2.8: NHR froth for the -75+38 µm size fraction. Low froth height is obvious compared to Figure A2.2

Table A2.10: Mass pull data after impeller modification – XNHR condition (Data for Table 6.4)

Mass Pull, g			
Experiment	18 min	30 min	48 min
XNHR1	62.3	15.8	8
XNHR2	58.7	18.4	8.8
XNHR3	63.9	16.3	6.5
Cumulative Mass Pull, %			
Experiment	18 min	30 min	48 min
XNHR1	41.6	52.1	57.5
XNHR2	39.3	51.6	57.5
XNHR3	42.9	53.8	58.1
Averaged Cumulative Mass Pull, % with standard errors of the mean			
XNHR	41.2	52.5	57.7
Standard Deviation	1.8	1.2	0.4
Standard Error of the means	1.1	0.7	0.2

Table A2.11: ICPOES scan assays of select elements in aqua regia leach solution of size classified PCB CF samples

Element	Assay, %	
	75-38 µm	-38 µm
Al	2.19	2.56
Ca	5.38	6.16
Cu	2.11	1.71
Fe	1.69	1.37
Mg	0.42	0.39
Mn	0.22	0.32
Ni	0.5	0.45
Zn	0.77	0.59

Table A2.12: Relative standard deviation (δ_R, %) of duplicate CMP data under varying reagent dosages for gamma depression.

Experiment	1 min	4min	10min	18min	30min
NHR	3.07	1.42	1.23	0.46	0.39
20 ppm	2.95	2.77	1.12	0.96	0.96
60 ppm	10.28	4.50	0.57	0.16	0.16
100 ppm	5.70	2.77	2.24	1.32	1.32
150 ppm	1.74	1.16	1.03	0.05	1.65

APPENDIX III Results and Analysis II – NHR ICPOES

Table A3.1: ICPOES raw assays (in ppm) of leach solution from flotation fractions of E21A1 and E21A2 (repeat) kinetic regimes

Fraction	Ag	Al	Au	Ca	Cu	Fe	Mg	Ni	Pb	Pd	Pt	Si	Sn	Ti	V	Zn
E21A1 F1	5.4	283	0.8	614	179	243.0	16.7	9.3	124.0	0.55	<0.05	3.5	204.0	9.3	0.3	23.8
E21A1 F2	5.4	271	0.6	597	181	185.0	16.1	8.3	112.0	0.53	<0.05	2.9	182.0	7.7	0.2	24.0
E21A1 F3	5.1	274	0.6	596	179	154.0	16.2	7.8	101.0	0.51	<0.05	4.1	162.0	7.5	0.2	23.4
E21A1 F3	5.1	271	0.6	589	176	153.0	16.0	7.7	99.5	0.50	<0.05	4.0	162.0	7.4	0.2	23.1
E21A1 F4	5.1	278	0.6	608	180	135.0	16.2	7.6	94.8	0.49	<0.05	3.4	154.0	6.8	0.2	24.5
E21A1 F5	5.2	289	0.5	632	178	127.0	17.2	7.5	90.3	0.50	<0.05	3.3	145.0	7.0	0.2	24.7
E21A1 S	17.0	828	8.2	1570	1250	914.0	47.8	89.8	1010.0	6.93	0.1	9.1	1380.0	122.0	1.0	229.0
E21A2 F1	5.3	273	0.8	604	182	246.0	15.9	9.2	126.0	0.51	<0.05	3.5	207.0	8.8	0.3	23.8
E21A2 F2	5.5	275	0.7	603	187	203.0	16.3	8.7	117.0	0.50	<0.05	3.7	189.0	8.8	0.2	24.4
E21A2 F3	5.3	280	0.6	612	185	160.0	16.5	8.1	104.0	0.48	<0.05	2.5	169.0	8.1	0.2	24.0
E21A2 F4	5.0	296	0.6	642	180	137.0	17.6	7.6	94.9	0.45	<0.05	2.9	153.0	8.1	0.2	24.2
E21A2 F5	5.0	294	0.5	640	174	127.0	17.4	7.4	89.1	0.45	<0.05	3.9	143.0	7.6	0.2	24.0
E21A2 S	9.9	818	7.6	1560	1220	864.0	46.6	85.2	965.0	6.72	0.0	5.0	1330.0	111.0	0.9	220.0

A3.1 Sink Assay, Reconstituted Feed Assay and Enrichment Ratio

Table A3.2: Matrix of conversion factors for calculating actual assay for each flotation fraction in E21A1 and E21A2 (obtained as explained in Section A1.3.1).

Fraction	Ag	Al	Au	Ca	Cu	Fe	Mg	Ni	Pb	Pd	Pt	Si	Sn	Ti	V	Zn
E21A1 F1	80	80	80	80	80	80	80	80	80	80	80	80	80	80	80	80
E21A1 F2	80	80	80	80	80	80	80	80	80	80	80	80	80	80	80	80
E21A1 F3	80	80	80	80	80	80	80	80	80	80	80	80	80	80	80	80
E21A1 F3	80	80	80	80	80	80	80	80	80	80	80	80	80	80	80	80
E21A1 F4	80	80	80	80	80	80	80	80	80	80	80	80	80	80	80	80
E21A1 F5	80	80	80	80	80	80	80	80	80	80	80	80	80	80	80	80
E21A1 S	240	240	240	240	240	240	240	240	240	240	240	240	240	240	240	240
E21A2 F1D	80	80	80	80	80	80	80	80	80	80	80	80	80	80	80	80
E21A2 F2D	80	80	80	80	80	80	80	80	80	80	80	80	80	80	80	80
E21A2 F3D	80	80	80	80	80	80	80	80	80	80	80	80	80	80	80	80
E21A2 F4D	80	80	80	80	80	80	80	80	80	80	80	80	80	80	80	80
E21A2 F5D	80	80	80	80	80	80	80	80	80	80	80	80	80	80	80	80
E21A2 SD	240	240	240	240	240	240	240	240	240	240	240	240	240	240	240	240

Table A3.3: Calculated actual assay (%) for flotation fractions from E21A1 and E21A2 (Each factor in Table A3.1 divided by corresponding data in Table A3.2).

Fraction	Ag	Al	Au	Ca	Cu	Fe	Mg	Ni	Pb	Pd	Si	Sn	Ti	V	Zn
E21A1 F1	0.0669	3.5375	0.0098	7.6750	2.2375	3.0375	0.2088	0.1163	1.5500	0.0068	0.0438	2.5500	0.1161	0.0033	0.2975
E21A1 F2	0.0680	3.3875	0.0080	7.4625	2.2625	2.3125	0.2013	0.1041	1.4000	0.0066	0.0356	2.2750	0.0959	0.0030	0.3000
E21A1 F3	0.0638	3.4063	0.0071	7.4063	2.2188	1.9188	0.2013	0.0963	1.2531	0.0063	0.0504	2.0250	0.0933	0.0028	0.2906
E21A1 F4	0.0641	3.4750	0.0069	7.6000	2.2500	1.6875	0.2025	0.0948	1.1850	0.0062	0.0428	1.9250	0.0851	0.0028	0.3063
E21A1 F5	0.0649	3.6125	0.0068	7.9000	2.2250	1.5875	0.2150	0.0935	1.1288	0.0062	0.0414	1.8125	0.0875	0.0029	0.3088
E21A1 S	0.0708	3.4500	0.0342	6.5417	5.2083	3.8083	0.1992	0.3742	4.2083	0.0289	0.0379	5.7500	0.5083	0.0041	0.9542
E21A2 F1	0.0661	3.4125	0.0094	7.5500	2.2750	3.0750	0.1988	0.1146	1.5750	0.0064	0.0431	2.5875	0.1095	0.0032	0.2975
E21A2 F2	0.0688	3.4375	0.0082	7.5375	2.3375	2.5375	0.2038	0.1084	1.4625	0.0062	0.0461	2.3625	0.1105	0.0031	0.3050
E21A2 F3	0.0668	3.5000	0.0078	7.6500	2.3125	2.0000	0.2063	0.1009	1.3000	0.0060	0.0313	2.1125	0.1016	0.0029	0.3000
E21A2 F4	0.0629	3.7000	0.0069	8.0250	2.2500	1.7125	0.2200	0.0954	1.1863	0.0056	0.0365	1.9125	0.1010	0.0029	0.3025
E21A2 F5	0.0619	3.6750	0.0068	8.0000	2.1750	1.5875	0.2175	0.0925	1.1138	0.0057	0.0489	1.7875	0.0951	0.0029	0.3000
E21A2 S	0.0411	3.4083	0.0316	6.5000	5.0833	3.6000	0.1942	0.3550	4.0208	0.0280	0.0208	5.5417	0.4625	0.0038	0.9167

Deportment of each element to each float fraction obtained by multiplying assay (%) in each fraction with mass of the fraction (g). With a factor of 1000, this gives the deportment in mg. For E21A, E21A1 and E21A2 rows in Table A3.3 operated on respective parts of the column data in Table A2.4 to give Table A3.4:

Table A3.4: Deportment of selected elements to each flotation fraction, mg

Fraction	Ag	Al	Au	Ca	Cu	Fe	Mg	Ni	Pb	Pd	Si	Sn	Ti	V	Zn
E21A1 F1	7.8	413.9	1.1	898.0	261.8	355.4	24.4	13.6	181.4	0.8	5.1	298.4	13.6	0.4	34.8
E21A1 F2	16.9	843.5	2.0	1858.2	563.4	575.8	50.1	25.9	348.6	1.6	8.9	566.5	23.9	0.7	74.7
E21A1 F3	30.1	1604.3	3.4	3488.3	1045.0	903.7	94.8	45.4	590.2	3.0	23.8	953.8	43.9	1.3	136.9
E21A1 F4	28.0	1518.6	3.0	3321.2	983.3	737.4	88.5	41.4	517.8	2.7	18.7	841.2	37.2	1.2	133.8
E21A1 F5	23.1	1286.1	2.4	2812.4	792.1	565.2	76.5	33.3	401.8	2.2	14.7	645.3	31.2	1.0	109.9
E21A1 S	95.9	4671.3	46.3	8857.4	7052.1	5156.5	269.7	506.6	5698.1	39.1	51.3	7785.5	688.3	5.5	1291.9
E21A2 F1	7.8	402.7	1.1	890.9	268.5	362.9	23.5	13.5	185.9	0.8	5.1	305.3	12.9	0.4	35.1
E21A2 F2	18.1	904.1	2.1	1982.4	614.8	667.4	53.6	28.5	384.6	1.6	12.1	621.3	29.1	0.8	80.2
E21A2 F3	30.2	1585.5	3.5	3465.5	1047.6	906.0	93.4	45.7	588.9	2.7	14.2	957.0	46.0	1.3	135.9
E21A2 F4	25.7	1513.3	2.8	3282.2	920.2	700.4	90.0	39.0	485.2	2.3	14.9	782.2	41.3	1.2	123.7
E21A2 F5	20.0	1187.0	2.2	2584.0	702.5	512.8	70.3	29.9	359.7	1.8	15.8	577.4	30.7	0.9	96.9
E21A2 S	57.8	4795.5	44.4	9145.5	7152.3	5065.2	273.2	499.5	5657.3	39.4	29.3	7797.1	650.7	5.3	1289.8

The elemental assay of each batch feed was reconstituted as deportment to all fractions divided by total mass of all the fractions, multiplied by 10^6, to give the assay in ppm. Sink elemental assays was computed as average of the two repeats as in Table A3.3, converted to ppm. Enrichment ratio calculated as sink assay divided by feed assay. This is gives the data in Table A3.5 for E21A, which contains enrichment ratio data for E21A in Table 6.3.

Table A3.5: Sink and reconstituted feed assays (ppm) and enrichment ratio (ER) under E21A kinetic regime

	Ag	Al	Au	Ca	Cu	Fe	Mg	Ni	Pb	Pd	Si	Sn	Ti	V	Zn
Sink	559.6	34291.7	329.0	65208.3	51458.3	37041.7	1966.7	3645.8	41145.8	284.4	293.5	56458.3	4854.2	39.3	9354.2
Feed	602.4	34542.9	190.8	70976.6	35672.4	27514.3	2013.2	2203.8	25665.9	163.4	356.4	36884.8	2748.0	33.7	5906.1
ER	0.93	0.99	1.72	0.92	1.44	1.35	0.98	1.65	1.60	1.74	0.82	1.53	1.77	1.17	1.58

A3.2 Recovery of elements to sink over time

Recovery in percentage of elements to sink over time was computed as the quotient of (i) deportment to all fractions for the specific element less deportment to float fractions up to corresponding time and (ii) total deportment to all fractions for the specific element. The result was express in percentage as in Table A3.6. Data for each replicates were averaged for each regime as in Table A2.8 for E21A, where the recovery at 30 minutes equals final recovery for E21A shown in Table 6.3.

Table A3.6: Recovery (%) of elements to sink over time for E21A1

Time, min	Ag	Al	Au	Ca	Cu	Fe	Mg	Ni	Pb	Pd	Si	Sn	Ti	V	Zn
0	100.00	100.00	100.00	100.00	100.00	100.00	100.00	100.00	100.00	100.00	100.00	100.00	100.00	100.00	100.00
1	96.12	96.00	98.04	95.77	97.55	95.72	95.96	97.96	97.66	98.39	95.82	97.31	98.38	96.20	98.05
4	87.73	87.84	94.63	87.02	92.29	88.77	87.66	94.07	93.15	95.05	88.57	92.20	95.53	88.97	93.86
10	72.84	72.32	88.87	70.59	82.52	77.88	71.97	87.26	85.52	89.03	69.17	83.60	90.29	75.92	86.17
18	58.96	57.63	83.67	54.95	73.33	68.99	57.32	81.04	78.83	83.58	53.91	76.02	85.85	63.87	78.66
30	47.52	45.19	79.53	41.71	65.92	62.17	44.65	76.05	73.64	79.12	41.88	70.20	82.13	53.83	72.50

Table A3.7: Recovery (%) of elements to sink over time E21A2

Time, min	Ag	Al	Au	Ca	Cu	Fe	Mg	Ni	Pb	Pd	Si	Sn	Ti	V	Zn
0	100.00	100.00	100.00	100.00	100.00	100.00	100.00	100.00	100.00	100.00	100.00	100.00	100.00	100.00	100.00
1	95.11	96.12	98.03	95.83	97.49	95.58	96.12	97.94	97.57	98.45	94.43	97.23	98.41	96.23	98.01
4	83.78	87.42	94.21	86.54	91.75	87.46	87.24	93.59	92.55	95.09	81.16	91.61	94.82	88.08	93.45
10	64.84	72.16	87.95	70.31	81.97	76.43	71.77	86.63	84.87	89.52	65.67	82.94	89.14	74.85	85.74
18	48.73	57.59	82.93	54.94	73.37	67.90	56.87	80.68	78.54	84.80	49.34	75.85	84.05	62.85	78.72
30	36.21	46.16	79.05	42.84	66.81	61.66	45.24	76.13	73.84	81.04	32.07	70.62	80.26	53.41	73.22

Table A3.8: Recovery (%) of elements to sink over time E21A (Average for E21A1 and E21A2)

Time, min	**Ag**	**Al**	**Au**	**Ca**	**Cu**	**Fe**	**Mg**	**Ni**	**Pb**	**Pd**	**Si**	**Sn**	**Ti**	**V**	**Zn**
0	100	100	100	100	100	100	100	100	100	100	100	100	100	100	100
1	96	96	98	96	98	96	96	98	98	98	95	97	98	96	98
4	86	88	94	87	92	88	87	94	93	95	85	92	95	89	94
10	69	72	88	70	82	77	72	87	85	89	67	83	90	75	86
18	54	58	83	55	73	68	57	81	79	84	52	76	85	63	79
30	42	46	79	42	66	62	45	76	74	80	37	70	81	54	73

A3.3 Assay of elements in sink over time

Assay of element in sink over time was computed as 10^6 x quotient of (i) total deportment in all fractions less deportment in all mass pull up to corresponding times and (ii) total mass of all fractions less mass pull up to corresponding times.

Table A3.9: Assay (ppm) of elements in sink over time for E21A1

Time, min	Ag	Al	Au	Ca	Cu	Fe	Mg	Ni	Pb	Pd	Si	Sn	Ti	V	Zn
0	672.8	34458.8	194.1	70785.0	35658.7	27646.7	2013.4	2220.7	25793.1	164.7	408.1	36968.6	2793.4	34.0	5940.3
1	676.7	34613.7	199.1	70936.6	36399.8	27689.6	2021.6	2276.3	26357.1	169.6	409.2	37642.9	2875.6	34.2	6094.4
4	676.4	34684.0	210.5	70585.8	37709.9	28123.8	2022.5	2393.7	27532.4	179.4	414.2	39059.4	3057.9	34.7	6388.7
10	684.8	34820.3	241.1	69823.1	41115.2	30084.2	2024.7	2707.6	30823.3	204.9	394.5	43185.7	3524.1	36.1	7152.7
18	695.9	34838.3	285.0	68244.5	45872.4	33459.8	2024.6	3157.4	35672.0	241.5	386.0	49302.6	4207.2	38.1	8198.0
30	708.3	34500.0	342.1	65416.7	52083.3	38083.3	1991.7	3741.7	42083.3	288.8	378.8	57500.0	5083.3	40.5	9541.7

Table A3.10: Assay (ppm) of elements in sink over time for E21A2

Time, min	Ag	Al	Au	Ca	Cu	Fe	Mg	Ni	Pb	Pd	Si	Sn	Ti	V	Zn
0	532.1	34627.0	187.4	71168.1	35686.0	27382.0	2013.0	2187.0	25538.7	162.0	304.7	36801.1	2702.6	33.4	5872.0
1	531.8	34975.2	193.0	71662.1	36558.1	27501.7	2033.1	2250.7	26184.8	167.6	302.3	37600.7	2794.6	33.7	6047.2
4	516.0	35036.1	204.3	71285.4	37895.8	27717.5	2032.6	2369.1	27357.8	178.3	286.2	39018.8	2966.1	34.0	6351.4
10	483.9	35043.7	231.1	70181.0	41024.0	29351.9	2026.3	2657.2	30398.5	203.5	280.6	42808.3	3379.0	35.0	7061.1
18	449.7	34581.2	269.5	67800.6	45403.3	32242.6	1985.2	3059.9	34780.7	238.3	260.7	48407.4	3939.1	36.4	8015.3
30	410.8	34083.3	315.8	65000.0	50833.3	36000.0	1941.7	3550.0	40208.3	280.0	208.3	55416.7	4625.0	38.0	9166.7

Table A3.11: Assay (ppm) of elements in sink over time for E21A (Average for E21A2 and E21A2)

Time	Ag	Al	Au	Ca	Cu	Fe	Mg	Ni	Pb	Pd	Pt	Si	Sn	Ti	V	Zn
0	602.4	34542.9	190.8	70976.6	35672.4	27514.3	2013.2	2203.8	25665.9	163.4	1.1	356.4	36884.8	2748.0	33.7	5906.1
1	604.3	34794.5	196.1	71299.4	36479.0	27595.7	2027.4	2263.5	26271.0	168.6	1.2	355.8	37621.8	2835.1	34.0	6070.8
4	596.2	34860.0	207.4	70935.6	37802.9	27920.6	2027.6	2381.4	27445.1	178.9	1.3	350.2	39039.1	3012.0	34.3	6370.1
10	584.3	34932.0	236.1	70002.1	41069.6	29718.0	2025.5	2682.4	30610.9	204.2	1.6	337.6	42997.0	3451.6	35.5	7106.9
18	572.8	34709.8	277.2	68022.6	45637.9	32851.2	2004.9	3108.6	35226.3	239.9	1.9	323.4	48855.0	4073.2	37.2	8106.7
30	559.6	34291.7	329.0	65208.3	51458.3	37041.7	1966.7	3645.8	41145.8	284.4	2.4	293.5	56458.3	4854.2	39.3	9354.2

A3.4 Enrichment Ratio versus Recovery to sink for each element over time

Computations such as in A3.1 – A3.3 done for each kinetic regime gave data for recoveries versus assays over time for the elements for each regime as shown in Table A3.12 below for Au.

Table A3.12: Sink's Au recovery (%) versus assay (ppm) over time for the various kinetic regimes.

E21A		E21B		E21C		E22A		E22B		E22C	
Au-Rec	Au-Assay	Au-Rec	Au-Assay	Au-Rec	Au-Assay	Au-Rec	Au-Assay	Au-Rec	Au-Assay	Au-Rec	Au-Assay
100	190.8	100	203.4	100	203.5	100	201.1	100	221.5	100	209.4
98	196.1	95	211.7	92	211.1	97	207.5	91	236.4	79	224.9
94	207.4	86	251.3	70	276.5	92	225.3	76	345.3	59	471.4
88	236.1	74	381.5	61	499.6	85	269.9	66	618.4	51	763.1
83	277.2	69	507.3	61	611.1	80	325.2	64	676.6	51	763.1
79	329.0	68	547.8	58	626.6	77	382.7	64	676.6	51	763.1

For uniformity of effect assessment, the assay scale was converted to enrichment ratios taking the assay at time zero as the feed assay of the batch sample used for each regime. For Au, this gives Table A3.13, which is the data for Figure 6.7.

Table A3.13: Enrichment ratio (ER) versus recovery (Rec, %) for Au in sinks under varying kinetic regimes.

E21A		E21B		E21C		E22A		E22B		E22C	
Au-Rec	Au-ER	Au-Rec	Au-ER	Au-Rec	Au-ER	Au-Rec	Au-ER	Au-Rec	Au-ER	Au-Rec	Au-ER
100	1	100	1	100	1	100	1	100	1	100	1
98	1.03	95	1.04	92	1.04	97	1.03	91	1.07	79	1.07
94	1.09	86	1.24	70	1.36	92	1.12	76	1.56	59	2.25
88	1.24	74	1.88	60	2.45	85	1.34	66	2.79	51	3.65
83	1.45	69	2.49	60	3.00	80	1.62	64	3.05	51	3.65
79	1.72	68	2.69	57	3.08	77	1.90	64	3.05	51	3.65

Data for other elements for the plots in Figure 6.8 – 6.13 extracted from the analysis for all the regimes are presented in Tables following.

Table A3.14: Enrichment ratio (ER) versus recovery (Rec, %) for Pd in sinks under varying kinetic regimes.

E21A		E21B		E21C		E22A		E22B		E22C	
Pd-Rec	Pd ER	Pd-Rec	Pd ER	Pd-Rec	Pd ER	Pd-Rec	Pd ER	Pd-Rec	Pd ER	Pd-Rec	Pd ER
100	1	100	1	100	1	100	1	100	1	100	1
98	1.03	96	1.05	94	1.06	97	1.04	92	1.08	85	1.15
95	1.09	85	1.23	67	1.36	92	1.13	72	1.49	54	2.06
89	1.25	70	1.79	55	2.22	85	1.35	59	2.51	46	3.23
84	1.47	65	2.35	53	2.67	80	1.62	58	2.76	46	3.23
80	1.74	64	2.53	52	2.74	77	1.91	58	2.76	46	3.23

Table A3.15: Enrichment ratio (ER) versus recovery (Rec, %) for Ti in sinks under varying kinetic regimes.

E21A		E21B		E21C		E22A		E22B		E22C	
Ti-Rec	Ti-ER	Ti-Rec	Ti-ER	Ti-Rec	Ti-ER	Ti-Rec	Ti-ER	Ti-Rec	Ti-ER	Ti-Rec	Ti-ER
100	1	100	1	100	1	100	1	100	1	100	1
98	1.03	97	1.06	95	1.08	97	1.04	94	1.10	88	1.19
95	1.10	88	1.27	77	1.50	93	1.14	79	1.63	68	2.59
90	1.26	77	1.96	69	2.78	87	1.37	68	2.92	61	4.31
85	1.48	73	2.63	68	3.43	82	1.67	67	3.21		
81	1.77	72	2.85	66	3.52	79	1.96				

Table A3.16: Enrichment ratio (ER) versus recovery (Rec, %) for Pb in sinks under varying kinetic regimes.

E21A		E21B		E21C		E22A		E22B		E22C	
Pb-Rec	Pb ER	Pb-Rec	Pb ER	Pb-Rec	Pb ER	Pb-Rec	Pb ER	Pb-Rec	Pb ER	Pb-Rec	Pb ER
100	1	100	1	100	1	100	1	100	1	100	1
98	1.02	95	1.03	92	1.04	96	1.02	88	1.04	78	1.06
93	1.07	80	1.16	61	1.26	89	1.08	63	1.30	43	1.63
85	1.19	63	1.60	48	1.95	79	1.24	48	2.04	34	2.40
79	1.37	57	2.05	47	2.31	72	1.46	46	2.20		
74	1.60	55	2.20	45	2.37	67	1.68				

Table A3.17: Enrichment ratio (ER) versus recovery (Rec, %) for Cu in sinks under varying kinetic regimes.

E21A		E21B		E21C		E22A		E22B		E22C	
Cu-Rec	Cu-ER	Cu-Rec	Cu-ER	Cu-Rec	Cu-ER	Cu-Rec	Cu-ER	Cu-Rec	Cu-ER	Cu-Rec	Cu-ER
100	1	100	1	100	1	100	1	100	1	100	1
98	1.02	95	1.03	92	1.04	96	1.03	89	1.05	80	1.09
92	1.06	79	1.14	57	1.24	88	1.08	62	1.27	42	1.59
82	1.15	57	1.45	43	1.75	76	1.20	42	1.80	31	2.21
73	1.28	49	1.77	40	2.00	67	1.36	41	1.93		
66	1.44	47	1.88	38	2.04	61	1.53				

Table A3.18: Enrichment ratio (ER) versus recovery (Rec, %) for Fe in sinks under varying kinetic regimes

E21A		E21B		E21C		E22A		E22B		E22C	
Fe-Rec	Fe-ER	Fe-Rec	Fe-ER	Fe-Rec	Fe-ER	Fe-Rec	Fe-ER	Fe-Rec	Fe-ER	Fe-Rec	Fe-ER
100	1	100	1	100	1	100	1	100	1	100	1
96	1.00	90	0.98	86	0.97	93	0.99	80	0.95	70	0.94
88	1.01	70	1.01	50	1.04	83	1.01	52	1.08	37	1.40
77	1.08	51	1.30	37	1.51	70	1.11	37	1.56	27	1.93
68	1.19	44	1.59	36	1.73	61	1.24	35	1.65		
62	1.35	42	1.69	33	1.76	56	1.38				

Table A3.19: Enrichment ratio (ER) versus recovery (Rec, %) for Ca in sinks under varying kinetic regimes

E21A		E21B		E21C		E22A		E22B		E22C	
Ca-Rec	Ca-ER	Ca-Rec	Ca-ER	Ca-Rec	Ca-ER	Ca-Rec	Ca-ER	Ca-Rec	Ca-ER	Ca-Rec	Ca-ER
100	1	100	1	100	1	100	1	100	1	100	1
96	1.00	92	1.00	88	1.00	94	1.00	85	1.00	73	0.99
87	1.00	68	0.99	37	0.96	81	0.99	47	0.96	23	0.89
70	0.99	35	0.89	20	0.79	61	0.97	18	0.77	10	0.67
55	0.96	22	0.78	14	0.68	46	0.92	15	0.72		
42	0.92	19	0.74	12	0.66	35	0.87				

APPENDIX IV **Process Water and Particle Surface Investigations**

Table A4.1: Trace element levels in PCB CF flotation process water (ppm)

Element	Background	Lab Water	PCB CF	Element	Background	Lab Water	PCB CF
Ag	<0.01	<0.01	<0.01	**Na**	<0.01	3.24	14.04
Al	<0.01	<0.01	0.65	**Nb**	<0.01	<0.01	<0.01
As	<0.01	<0.01	<0.01	**Nd**	<0.01	<0.01	<0.01
Au	<0.01	<0.01	<0.01	**Ni**	<0.01	<0.01	0.07
B	<0.01	0.07	0.69	**Os**	<0.01	<0.01	<0.01
Ba	<0.01	0.08	0.56	**P**	<0.8	0.01	0.06
Be	<0.01	<0.01	<0.01	**Pb**	<0.01	<0.01	0.29
Bi	<0.01	<0.01	<0.01	**Pd**	<0.01	<0.01	<0.01
Ca	<0.01	1.47	7.07	**Pr**	<0.01	<0.01	<0.01
Cd	<0.01	<0.01	<0.01	**Pt**	<0.01	<0.01	<0.01
Ce	<0.01	<0.01	<0.01	**Rb**	<0.01	<0.01	0.01
Co	<0.01	<0.01	0.01	**Re**	<0.01	<0.01	<0.01
Cr	<0.01	<0.01	0.01	**Ru**	<0.01	<0.01	<0.01
Cs	<0.01	<0.01	<0.01	**Sb**	<0.01	0.00	0.08
Cu	<0.01	<0.01	0.25	**Sc**	<0.01	<0.01	<0.01
Dy	<0.01	<0.01	<0.01	**Se**	<0.01	<0.01	<0.01
Er	<0.01	<0.01	<0.01	**Si**	<0.01	0.39	2.76
Eu	<0.01	<0.01	<0.01	**Sm**	<0.01	<0.01	<0.01
Fe	<0.01	0.01	0.53	**Sn**	<0.01	<0.01	0.16
Ga	<0.01	<0.01	<0.01	**Sr**	<0.01	0.01	0.05
Gd	<0.01	<0.01	<0.01	**Ta**	<0.01	<0.01	<0.01
Ge	<0.01	<0.01	<0.01	**Tb**	<0.01	<0.01	<0.01
Hf	<0.01	<0.01	<0.01	**Te**	<0.01	<0.01	<0.01
Hg	<0.01	<0.01	<0.01	**Th**	<0.01	<0.01	<0.01
Ho	<0.01	<0.01	<0.01	**Ti**	<0.01	<0.01	0.05
In	<0.01	<0.01	<0.01	**Tl**	<0.01	<0.01	<0.01
Ir	<0.01	<0.01	<0.01	**Tm**	<0.01	<0.01	<0.01
K	<0.01	0.78	6.84	**U**	<0.01	<0.01	<0.01
La	<0.01	<0.01	<0.01	**V**	<0.01	<0.01	<0.01
Li	<0.01	<0.01	0.09	**W**	<0.01	<0.01	<0.01
Lu	<0.01	<0.01	<0.01	**Y**	<0.01	<0.01	<0.01
Mg	<0.01	0.38	3.09	**Yb**	<0.01	<0.01	<0.01
Mn	<0.01	<0.01	0.09	**Zn**	<0.01	0.01	1.28
Mo	<0.01	<0.01	<0.01	**Zr**	<0.01	<0.01	0.01

Particles – P1

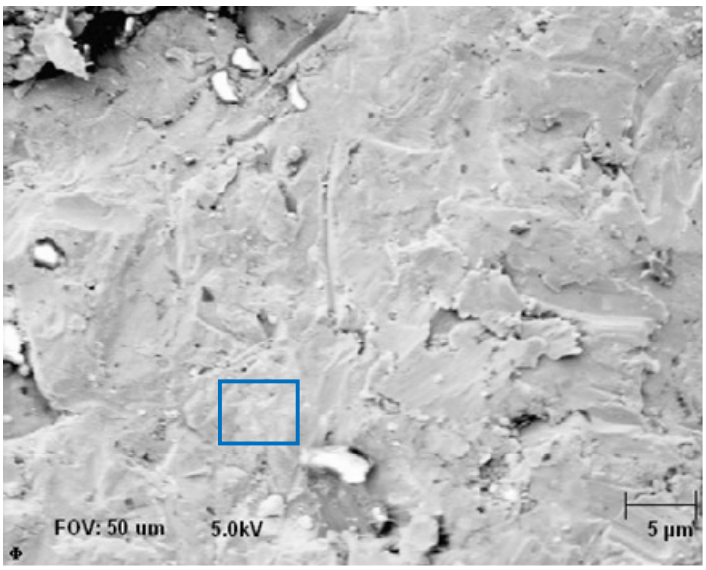

Figure A4.1: Secondary electron image on particle P1. Blue square indicates area of Auger electron spectroscopic analysis.

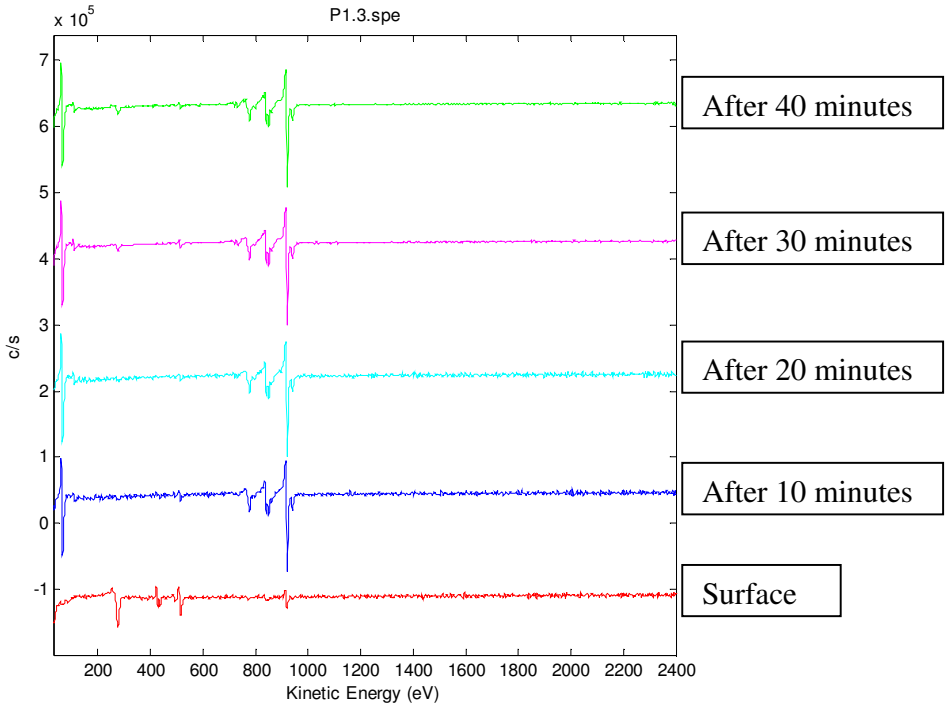

Figure A4.2: Comparison of AES survey spectra at various sputtering times on (indicative of depths from) the surface of particle P1.

Particles – P2

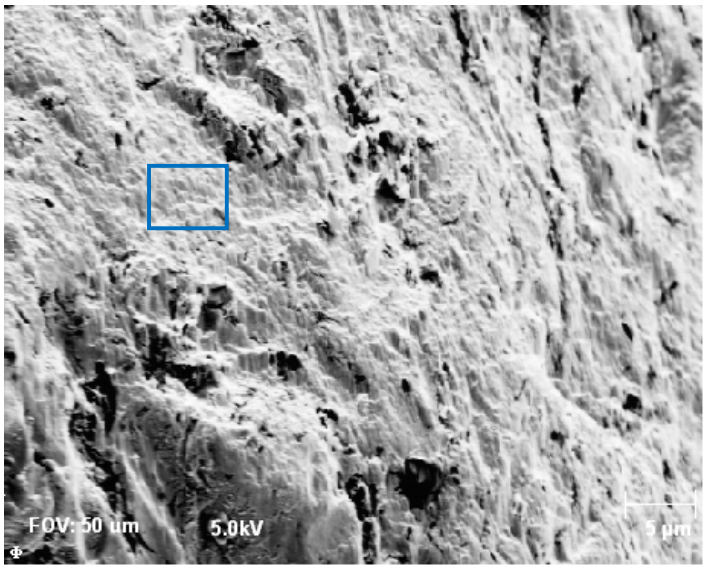

Figure A4.3: SEM secondary electron image on Particle P2 at 5 kV 10 nA primary beam current: Blue square indicates area of analysis.

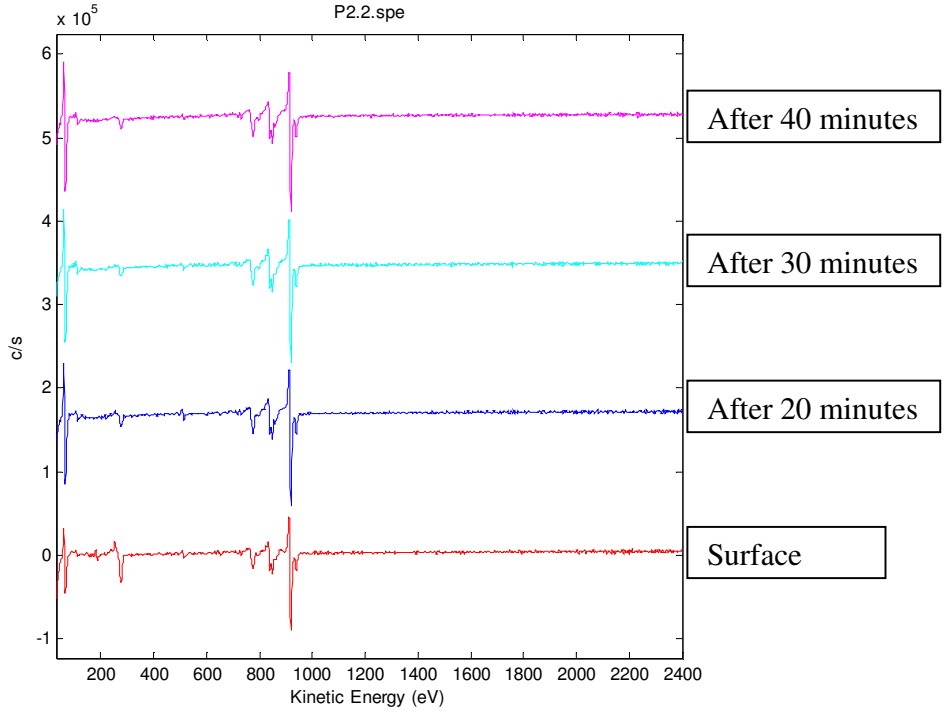

Figure A4.4: Comparison of AES survey spectra at various sputtering times on (indicative of depths from) the surface of particle P2.

Fiber Particle – F2

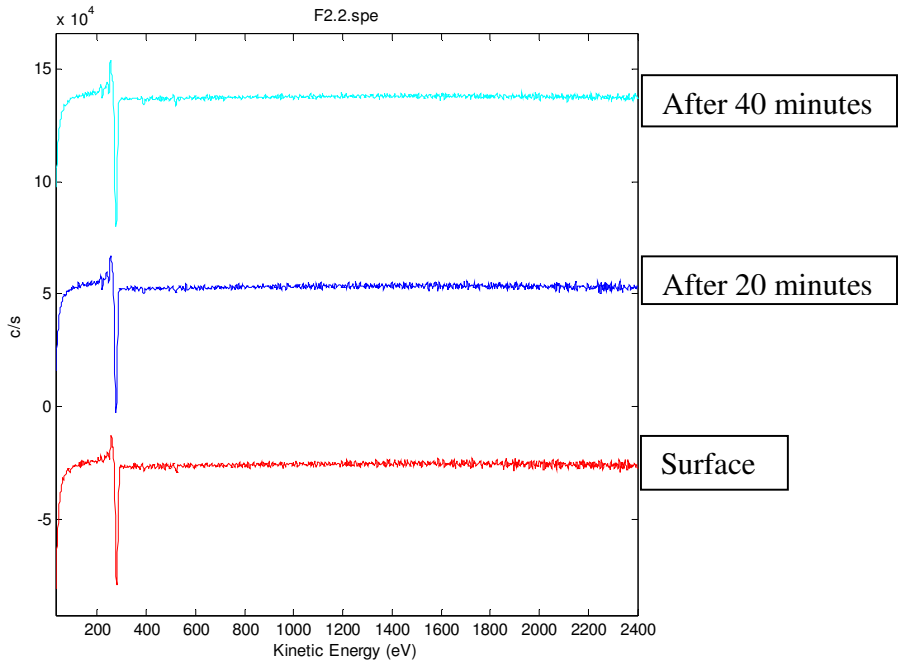

Figure A4.5: Comparison of AES survey spectra at various sputtering times on (indicative of depths from) the surface of fiber particle F2.

Fibres Particle F3:

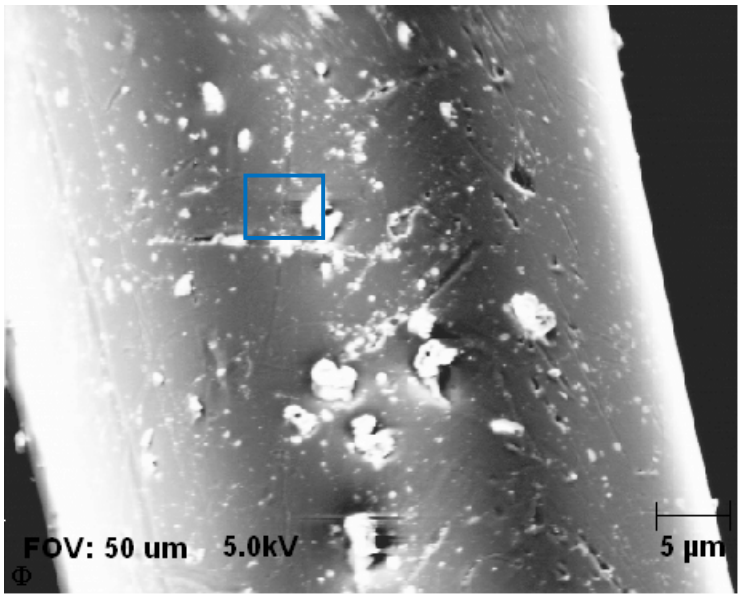

Figure A4.6: Secondary electron image on fiber particle F3 at 5 kV 10 nA primary beam current: Blue square indicates area of Auger electron spectroscopic analysis.

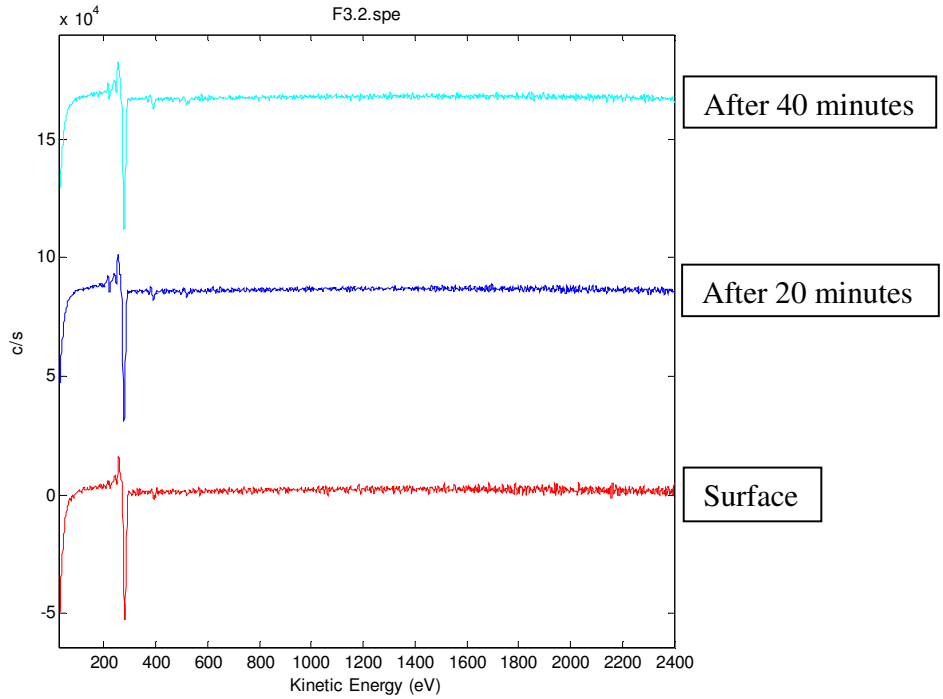

Figure A4. 7: Comparison of AES survey spectra at various sputtering times on (indicative of depths from) the surface of fiber particle F3.

FIBER PARTICLE F4

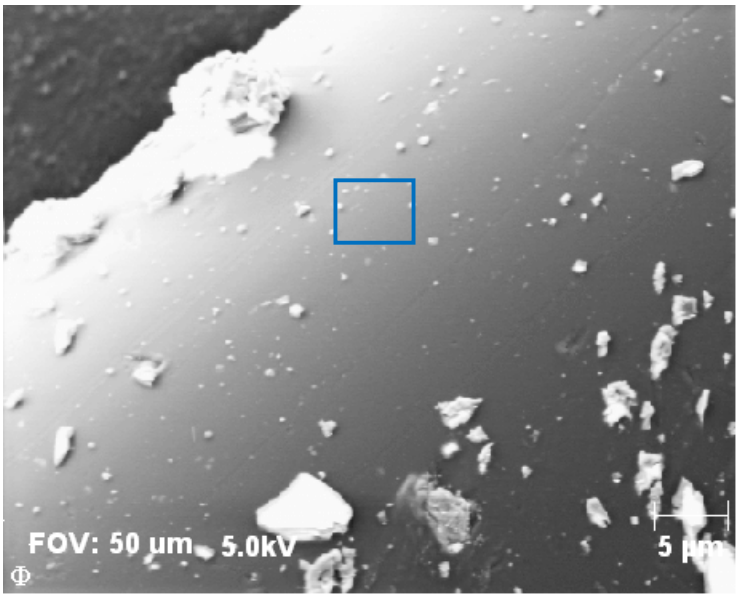

Figure A4.8: Secondary electron image on fiber particle F4. Blue square indicates area of Auger electron spectroscopic analysis.

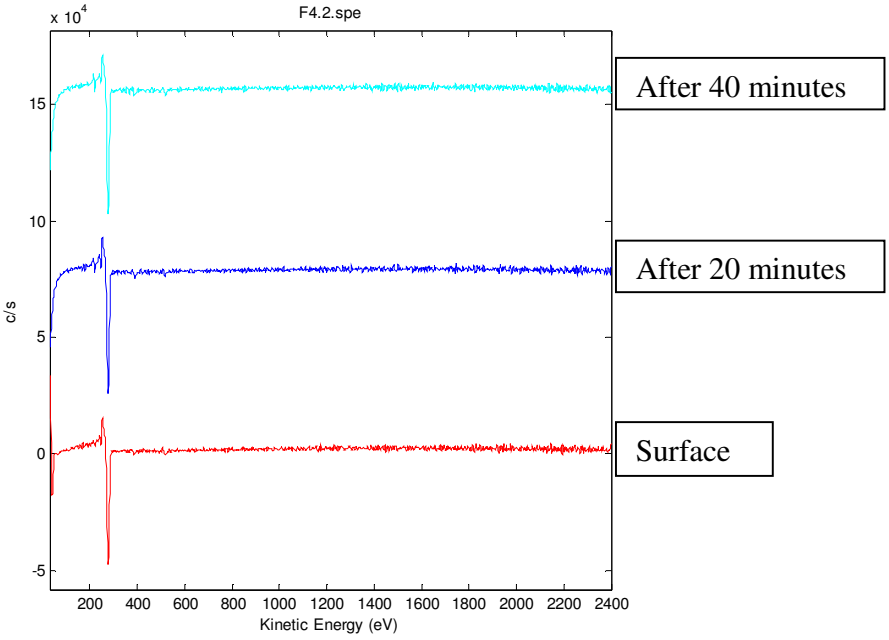

Figure A4.9: Comparison of AES survey spectra at various sputtering times on (indicative of depths from) the surface of fiber particle F4.

Fiber Particle F5

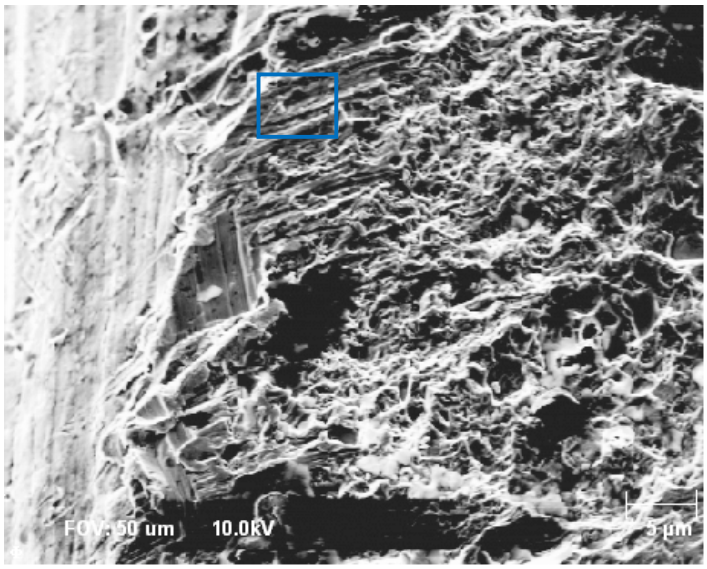

Figure A4.10: Secondary electron image on fiber particle F4. Blue square indicates area of Auger electron spectroscopic analysis.

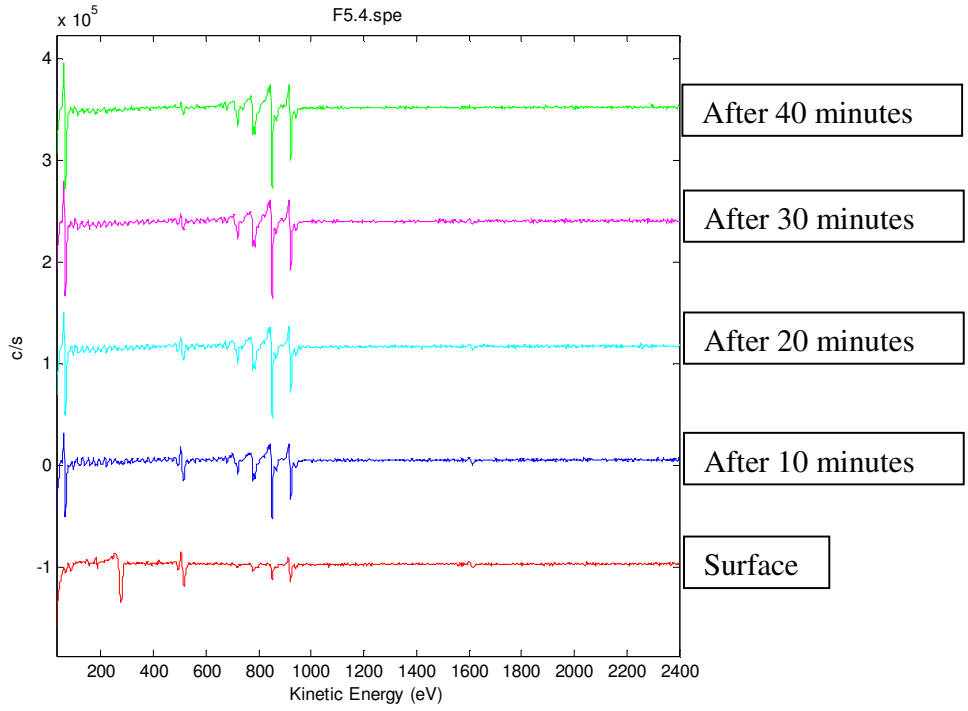

Figure A4.11: Comparison of AES survey spectra at various sputtering times on (indicative of depths from) the surface of fiber particle F5.

APPENDIX V PUBLICATIONS

1. Ogunniyi, I. O., Vermaak, M.K.G. and Groot, D. R., 2009. Chemical composition and liberation characterization of printed circuit board comminution fines for beneficiation investigations. *Waste Management,* Vol. 29, pp 2140 – 2146, 2009. http://dx.doi.org/10.1016/j.wasman.2009.03.004

2. Ogunniyi, I. O. and Vermaak, M.K.G., 2009. Froth flotation for beneficiation of printed circuit board comminution fines: an overview". *Minerals Processing and Extractive Metallurgy Review*, Vol. 30 (2), pp. 101 – 121. http://dx.doi.org/10.1080/08827500802333123

3. Ogunniyi, I. O. and Vermaak, M.K.G., 2009: "Application of froth flotation for beneficiation of printed circuit board comminution fines." *Mineral Engineering*, Vol. 22, pp. 378-385. http://dx.doi.org/10.1016/j.mineng.2008.10.007

4. Ogunniyi, I. O. & Vermaak, M. K. G., 2008: 'Froth flotation in e-waste processing'. *Mineral Processing 2008 (SAIMM), Aug. 7 & 8, Cape Town, South Africa, Book of Abstracts, pp OR 25.*

5. Ogunniyi, I. O. & Vermaak, M. K. G., 2007. 'Improving printed circuit board physical processing – An overview', *Proceedings of European Metallurgical Conference – EMC 2007, June 11 – 14, Dusseldorf, Germany, pp 1645 – 1656.*